Signalling mechanisms in epilepsy and synaptic scaling

Mariella Hurtado Silva

BMedSc (Hons Class 1)

A thesis submitted to fulfil requirements for the degree of Doctor of Philosophy

Sydney Medical School

Faculty of Medicine and Health

The University of Sydney

February 2023

To the Hurtado Clan.

Juan (Dad), Inge (Mum), Michael,
Christian and Keira

And mi abuelo Guido Silva

Statement of originality

This is to certify that to the best of my knowledge, the content of this thesis is my own work. This thesis has not been submitted for any degree or other purposes.

I certify that the intellectual content of this thesis is the product of my own work and that all the assistance received in preparing this thesis and sources have been acknowledged.

Signature:

Mariella Hurtado Silva

28th February 2023

Table of Contents

Acknowledgements

Getting to the point of being able to submit a thesis is not something that I thought possible at many points in my PhD. I thank you God for giving me this opportunity and supplying me with the grace to make it through. I know that if it was not also for the people around me, encouraging and supporting me at almost every single point of the way. I would not have made it.

Thank you to my collaborators. From the University of Bonn in Germany and the Anggono Lab at the Queensland brain institute. I have never met many of you, but without your help, this thesis would never have been possible!

A special thank you to Dr. Ignatius Pang and Dr. Ashley Waardenberg for helping me with my data analysis.

To my lead supervisor, Dr. Mark Graham. You have been so patient with me over these last four years. Thank you for always being understanding and kind. I appreciate how you have always been ready to listen to my problems, concerns and struggles. You were always there to help me when I have needed it (on more than a couple of occasions). I know that there is no way I would have made it to this point, without your support and guidance.

To my supervisor, Assoc. Prof. Wendy Gold and the members of the Molecular neurobiology group. Thank you for adopting me into your lab group! I know proteomics is a foreign language to many, but you were always so enthusiastic to hear my weekly updates. I cannot thank you enough for always being so willing to help me with my experiments and support me in any capacity you could.

Thank you to my many lab colleagues past and present. Dr. Jing Xue, Prof. Phillip Robinson, Frederikke Koch and Philip Zhong. For making the lab a better place to work and for always being willing to lend a hand.

To Jesse Wark, for the tremendous guidance you provided at the start of my project and for being a great colleague.

To Vickie Chan, I think you understand why I single you out. You have been a great friend to me over these last four years. I know, four years. Thank you for talking me through all my TC problems. For helping me and just being a constant source of encouragement. I am so grateful that you have tolerated me so much and laughed with me (and at me) along the way. Thank you.

To my amazing church family. I am beyond grateful for how everyone has encouraged me along the way. To those of you who patiently listened to my problems, prayed for me, messaged me to see how I was going. I am a debtor. Thank you for displaying the love of God to me. I particularly want to thank Renee, Anthony, Bronwyn, Lucy, Brett, Carmen, Patricio, Nicky, Frances, Rejoice, Genesis, Vinny, Daniel, Guy and my fellow other numerous co-labourers. Thank you for showing me how to look away from myself and always pointing me to the cross.

To my wonderful family. I know my many failings as a daughter and a sister, so I know that this wasn't easy for you. Thank you for helping me. For never letting me feel sorry for myself and pushing to keep going. Mum and Dad, I am so grateful that I was gifted with parents like you. I know that I cannot ever repay you for what you have given me. Michael, thank you for your willingness to serve always. Christian, thank you for being an amazing role model. Keira, thank you for being a great friend. And Spartacus, who requires no elaboration. I thank God for each you and for this challenging experience. .

Thank you again, to everyone who I have and have not mentioned. I know my words will fail to express the gratitude I have.

Publications

Publications related to this thesis:

- Hanafy, A. S., Steinlein, P., Pitsch, J., ***Hurtado Silva, M.***, Vana, N., Becker, A. J., Graham, M. E., Schoch, S., Lamprecht, A. & Dietrich, D. Subcellular analysis of blood-brain barrier function by micro-impalement of vessels in acute brain slices. *Nature communications* **14**, 481, doi:10.1038/s41467-023-36070-6 (2023).
- Royero, P., Quatraccioni, A., Frungel, R., ***Hurtado Silva, M.***, Bast, A., Ulas, T., Beyer, M., Opitz, T., Schultze, J. L., Graham, M. E., Oberlaender, M., Becker, A., Schoch, S. & Beck, H. Circuit-selective cell-autonomous regulation of inhibition in pyramidal neurons by Ste20-like kinase. *Cell reports* **41**, 111757, doi:10.1016/j.celrep.2022.111757 (2022).

Publications under review:

- ***Hurtado Silva, M.***, Waardenberg, A. J., Schoch, S., Dietrich, D. & Graham, M. E. Multiomic analysis of early epileptogenesis in mice reveals phosphorylation and dephosphorylation directed growth and synaptic weakening. *Cell reports* **Submitted 26th of November 2022**, Manuscript number: CELL-REPORTS-D-22-05669

Authorship attribution statement

1. **Chapter 3, Section 3.1, pages: 92-143** of this thesis is under review at cell reports as:

   Hurtado Silva, M., Waardenberg, A. J., Schoch, S., Dietrich, D. & Graham, M. E. Multiomic analysis of early epileptogenesis in mice reveals phosphorylation and dephosphorylation directed growth and synaptic weakening. *Cell reports* **Submitted 26th of November 2022**, Manuscript number: CELL-REPORTS-D-22-05669

DD performed the mouse model experimentation and tissue extraction. I (MHS) performed the proteomics-relevant sample preparation and mass spectrometry analysis. AJW processed the raw mass spectrometry data and performed statistical analysis. SS, DD and MEG conceived and designed the study. MHS, MEG and AJW analysed the data and created the figures. All authors contributed to the writing and editing of the manuscript.

2. For **Chapter 3**, **Section 3.8, pages: 148-153**

   I cultured neurons for both MEA and western blotting. I treated the neuronal cultures with stimulants and kinase inhibitors. I performed the western blotting experiments.

3. This thesis contains material published in:

"Royero, P. *et al.* Circuit-selective cell-autonomous regulation of inhibition in pyramidal neurons by Ste20-like kinase. *Cell reports* **41**, 111757, doi:10.1016/j.celrep.2022.111757 (2022).).

This is **Chapter 3, Section 3.6**, **pages: 144-146**. This includes data for Figure 3.9, **page: 146** I performed the mass-spectrometry experiments. MEG performed the mass-spectrometry data analysis.

4. **Chapter 5.**

Jocelyn Widagdo prepared cultured neurons for mass spectrometry. I performed the mass spectrometry experiments. Ignatius Pang processed the MaxQuant output into highly curated tables and statistics. I performed all subsequent gene ontology enrichment and generated all figures.

5. Throughout this thesis, my supervisor Mark Graham made suggestions to the improve the text and figures.

Authorship attribution attestation

In addition to the statements above, in cases where I am not the corresponding author of a published item, permission to include the published material has been granted by the corresponding author.

Signature:

Mariella Hurtado Silva
28th February 2023

As supervisor for the candidature upon which this thesis is based, I can confirm that the authorship attribution statements above are correct.

Signature:

Dr. Mark Graham
28th February 2023

Abbreviations

2D-PAGE	Two-dimensional polyacrylamide gel electrophoresis
ABC	ATP-binding cassette
AGAP	Arf-GAP with GTPase, ANK repeat and PH domain-containing protein
AKAP	A-kinase anchor protein
AKT1	Protein kinase B
AMPA	α-amino-3-hydroxy-5-methyl-4-isoxazole propionate
AMPAR	α-amino-3-hydroxy-5-methyl-4-isoxazole propionate receptor
AMPK	5'AMP-dependent protein kinase
APV	2-amino-5-phosphonopentanoic acid
Arc	Activity regulated cytoskeleton
ARFGAPs	ADP-ribosylation factor GTPase-activating protein family
ARHGAPs	Rho GTPase-activating protein family
ASD	Antiseizure drug
BDNf	Brain derived neurotrophic factor
Bic	Bicuculline
BLOC-1	biogenesis of lysosome-related organelles complex-1
BONCAT	bio-orthogonal non-canonical amino acid tagging
BRSK	Serine/threonine-protein kinase
BSA	Bovine serum albumin
CA	Cornu ammonis
CaM	Calmodulin
CaMK2	Ca^{2+}/calmodulin-dependent protein kinase II
cAMP	Cyclic adenosine monophosphate
CDK	Cyclin dependent kinase
CK2α	Casein kinase 2 α
CNQX	6-Cyano-7-nitroquinoxaline-2,3-dione
CNS	Central nervous system
COX	Cyclooxygenase
CREB	cAMP response element binding protein

DG	Dentate gyrus
DGC	DG granule cells
DIV	Days *invitro*
DLGAP	Disks large-associated protein
DM	Dissection media
DMSO	Dimethyl sulfoxide
DNaseI	Deoxyribonuclease I
DYRK1A	Dual specificity tyrosine-phosphorylation-regulated kinase 1A
EDTA	Ethylenediaminetetraacetic acid
EEG	Electroencephalogram
EGTA	Ethylene glycol-bis(β-aminoethyl ether)-N,N,N0,N0-tetraacetic acid
EPSP	Excitatory postsynaptic potential
ERK	extracellular signal-regulated kinase
ESI	Electrospray ionisation
EvLS	Everolimus
FBS	Foetal bovine serum
GABA	γ-aminobutyric acid
$GABA_A$	Ionotropic GABA receptor
$GABA_B$	Metabotropic GABA receptor
GO	Gene Ontology
GRIP1	Glutamate receptor-interacting protein 1
GSK3	Glycogen synthase kinase-3
HBSS	Hank's balanced salt solution
HCl	Hydrochloric Acid
HEPES	4-[2-hydroxyethyl]-1-piperazineethanesulfonic acid
HILIC	Hydrophilic interaction liquid chromatography
HPLC	High performance liquid chromatography
HS	Hippocampal sclerosis
IEG	Immediate early gene
IGF	Insulin-like growth factor

iGluR	Ionotropic glutamate receptor
IL	Interleukin
ILAE	International League Against Epilepsy
IMAC	Immobilised metal affinity chromatography
IPSP	Inhibitory postsynaptic potential
JNK	c-Jun N-terminal kinase
KA	Kainic acid
KD	Knockdown
KEGG	Kyoto encyclopedia of genes and genomes
KO	Knock out
LC	Liquid chromatography
LC-MS/MS	LC tandem mass spectrometry
LTD	Long-term depression
LTP	Long-term potentiation
LysC	Lysyl Endopeptidase®
m/z	mass to charge
MAP	Microtubule associated protein
MAPK	Mitogen-activated protein kinases
MC	Hilar mossy cells
MEA	Microelectrode array
MeCP	Methyl-CpG-binding protein
mEPSC	Miniature excitatory postsynaptic current
MFS	Mossy fibre sprouting
mGluR	Metabotropic glutamate receptor
MK2	MAPKAPK2
MQW	Double distilled, type 1 ultrapure Milli-Q water
MS	Mass spectrometry
MSK1	Mitogen and stress response kinase 1
mTLE	Mesial temporal lobe epilepsy
mTLE-HS	Mesial temporal lobe epilepsy with hippocampal sclerosis

MTOR	Mammalian target of rapamycin
MTORC	mTOR complex
NES	Non-epileptic seizure
Ngef	Neuronal guanine nucleotide exchange factor
NM	Neurobasal media
NMDA	N-methyl-D-aspartate
NMDAR	N-methyl-D-aspartate receptor
NMJ	Neuromuscular junction
nTLE	Neocortical temporal lobe epilepsy
Ntrk3	Neurotrophic receptor tyrosine kinase 3
PBS	Phosphate buffered saline
PBST	PBS solution with 0.1% Tween-20
PCA	Principle component analysis
PDL	Poly-D-Lysine
Pen/Strep	Penicillin-Streptomycin
PhTx	Philanthotoxin
PI3K	Phosphoinositide 3-kinases
Pilo	Pilocarpine
PKG	Protein Kinase G
Plk2	Polo-like kinase 2
PMSF	Phenylmethylsulfonyl fluoride
PNS	Peripheral nervous system
PP2B	Protein phosphatase 2B
PRM	Parallel reaction monitoring
PSD	Postsynaptic density
PSD95	Postsynaptic density protein 95
PTEN	Phosphatase and tensin homologue deleted on chromosome 10
PTM	Posttranslational Modification
PVP-40	Polyvinylpyrrolidone 40 kDa polymer
RIM	Rab3-interacting molecule

RPLC	Reverse phase liquid chromatography
RPTPα	Receptor-type tyrosine protein phosphatase alpha
RRP	Ready releasable pool
RSK1	Ribosomal S6 kinase 1
RT	Chromatographic retention time
RUV	Remove unwanted variation
S6K	P70 RSK
SDS	Sodium dodecyl sulfate
SDS-PAGE	Sodium dodecyl sulfate polyacrylamide gel electrophoresis
SE	Status epilepticus
Ser	Serine
SIMAC	Sequential elution from immobilised metal affinity chromatography
SLK	Ste20-like kinase
SNAP25	synaptosomal-associated protein of 25 kDa
Snapin	SNAP associated protein
SNARE	Soluble N-ethylmaleimide-sensitive factor activating protein receptor
SRM	Selected reaction monitoring
synGAP	Synaptic Ras GTPase-activating protein
TARPs	Transmembrane AMPA receptor regulatory proteins
TCEP	Tris(2-carboxyethyl) phosphine
TEAB	triethylammonium bicarbonate
TFA	Trifluoroacetic acid
TGF-β	Transforming growth factor beta
Thr	Threonine
TiO_2	Titanium dioxide
TiSH	Titanium dioxide-SIMAC-HILIC
TLE	Temporal lobe epilepsy
TNF-α	Tumour necrosis factor alpha
Tris	Tris(hydroxymethyl)aminomethane
TSC	Tuberous sclerosis complex

TTX	Tetrodotoxin
Tyr	Tyrosine
VGCC	Voltage-gated calcium channels
WT	Wild type

Abstract

Background: Neuroplasticity enables the brain to change its electrophysiological activity depending on stimuli. Neuroplasticity mechanisms often intersect with disease mechanisms. One type of plasticity is Hebbian plasticity, which is a positive feedback mechanism serving to strengthen or weaken synaptic transmission and is central to learning and memory [1]. Another type of plasticity is synaptic scaling, which is a negative feedback mechanism that adjusts Hebbian plasticity modification to ensure that net neuronal activity remains at a homeostatic set point [2]. Synaptic scaling is triggered by either excessive or reduced neuronal activity and these activity states induce downscaling or upscaling of synaptic strength to revert back to the activity set point [2]. Synaptic scaling mechanisms have not yet been fully revealed. However, scaling is likely to be highly relevant to disease since malfunction would result in neuronal activity that is excessive or inhibited. Epilepsy is characterised by excessive neuronal activity [3]. In theory, seizures arising from excessive excitation should invoke synaptic downscaling and so the question arises as to whether a malfunctioning downscaling mechanism is involved. Epilepsy develops over time in a process known as epileptogenesis but mechanistic information is lacking to understand which biological processes are most relevant.

Aims: The aims of this thesis were to *(i)* perform a deep phosphoproteomic and proteomic analysis of an early epileptogenesis mouse model, *(ii)* define the temporal changes to the phosphoproteome and proteome in a model of synaptic downscaling, and *(iii)* compare the results of the epileptogenesis and downscaling studies to determine features specific to each model.

Method: With our capacity to explore the phosphoproteome and proteome in-depth using mass spectrometry, the key phospho-signalling and protein expression events that drive synaptic downscaling and epileptogenesis were determined. Bioinformatic analysis was used to identify

key biological pathways and protein kinases. Validation was performed using targeted mass spectrometry. A preliminary follow-up analysis was performed using multi-electrode array and western blotting.

Findings: Comparing the phosphoproteomic and proteomic data from both the early epileptogenesis and synaptic downscaling screens we found that down-regulation of synaptic proteins to induce synaptic weakening occurred in both models, with subtle differences. In epileptogenesis, dephosphorylation of the postsynaptic density was highly layer-specific. However, in contrast to downscaling, presynaptic proteins were not major targets of regulation. Major differences were related to broader phosphorylation of posttranscriptional regulatory proteins in early epileptogenesis, likely driven by activation of additional protein kinases. Additional processes were specific to epileptogenesis; for example, an increased expression of proteins related to proteostasis.

Conclusions: Overall, this thesis serves as a valuable neuroscience resource, particularly for future epilepsy and synaptic scaling studies. This work provides evidence that kinase activity in the pilocarpine epileptogenesis model and Bicuculline synaptic downscaling model are distinct, provides evidence for the involvement of posttranscriptional regulation, evidence for wide spread dephosphorylation of synaptic proteins and identifies many potential drug targets and biomarkers.

Chapter 1. Literature Review

1.1. Introduction

The brain is a complex organ comprised of billions of neurons charged with performing specialised tasks or life sustaining functions. These functions require communication between neurons, which takes place at synapses. The strength of synaptic transmission is dynamically adjusted in a process known as synaptic plasticity. One such process is long-term potentiation (LTP). LTP increases synaptic strength through positive feedback of electrical activity/action potentials and is vital for learning and memory [4]. In contrast, homeostatic plasticity counteracts extreme positive feedback by a scaling mechanism that maintains overall brain activity at a setpoint, whilst allowing localised changes in synaptic strength [4]. As the brain operates in a window between extremes of high and low activity, a tight balancing act is required by the positive and negative feedback mechanisms of synaptic strengthening and homeostasis [5]. Epilepsy, which involves extreme and synchronised activity, is suspected to intersect with these plasticity mechanisms [6]. Genes involved in synaptic plasticity and neurological disease have been identified; however, there is a lack of understanding of the molecular mechanisms involved [7-9]. Knowledge of these molecular mechanisms may reveal new pathways to target in treatments for neurological diseases [10,11].

1.2. Synaptic Transmission

Transmission, processing and subsequent storage of information in the brain is facilitated by communication between neurons at synapses [12,13]. Synaptic transmission is a movement of ions and/or other molecular intermediaries to continue the propagation of an electrical impulse

generated from an external stimulus [11,14]. To sustain the impulse, the resting membrane potential must be disrupted in a process known as depolarisation (Figure 1.1). For neurons this resting potential normally sits between -45 to -75 mV [14]. For depolarisation to occur, the neuronal membrane potential must rise above the threshold value of approximately -55 mV (Figure 1.1) [14]. The action potential can also be disrupted by opposing signals working to hyperpolarise the membrane and prevent signal transmission (Figure 1.1) [14]. Overall, the ability for synaptic transmission to occur between neurons is dependent on the generation of action potentials which are governed by the flow of ions in and out of the neuron. Synaptic transmission between neurons can occur chemically or electrically [15,16]. Chemical transmission is the main form of synaptic transmission in the central nervous system (CNS) [17]. Chemical transmission begins following the generation of an action potential in the neuron with ions mobilising the resulting electrical impulse [12,13].

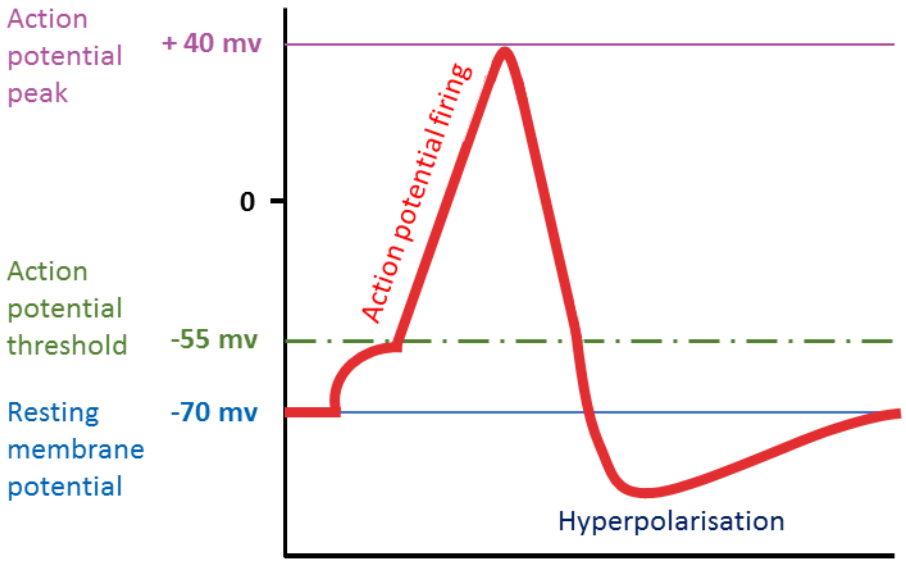

Figure 1.1. Graphical representation of action potential firing in neurons. For the neuron to depolarise and fire an action potential, the resting membrane potential (dark blue line) must increase to meet the threshold value (Green dotted line). This is accomplished with opening of

voltage-gated Na^+ channels allowing positively charged Na^+ ions to enter and depolarise the cell. Once the action potential has fired, voltage-gated Na^+ channels close and Na^+ ions stop entering. At the peak of the action potential (purple line) K^+ channels finally open to repolarise the membrane potential with the loss of positively charged K^+ ions [14]. K^+ ions continue leaving the cell making the membrane more negatively charged. The K^+ channels will close slowly, staying open a little longer than required causing the membrane to become hyperpolarised (labelled above). Once the K^+ channels finally close, the cell membrane can repolarise at the resting membrane potential [14].

The electrical impulse activates voltage-gated ion channels and is sustained down the length of the nerve axon by the high influx of Na^+ ions and slow efflux of K^+ ions resulting in membrane depolarisation of the presynaptic axon terminal (Figure 1.2A) [12,13]. Voltage-gated Ca^{2+} channels are also activated with depolarisation from the impulse [11]. The entrance of Ca^{2+} ions through these open channels rapidly triggers synaptic vesicle fusion and neurotransmitter release [11]. Neurotransmitters then bind to a corresponding postsynaptic receptor (ligand-gated ion channel) to open a channel and enable the entrance of ions into the postsynaptic terminal [12,13]. Activation of these receptors enables the postsynaptic neuron to become depolarised in milliseconds and continue the propagation of the action potential (Figure 1.2B) [12,13]. Thus neurotransmission is inextricably reliant on ion channels, neurotransmitter release, and receptor detection [18].

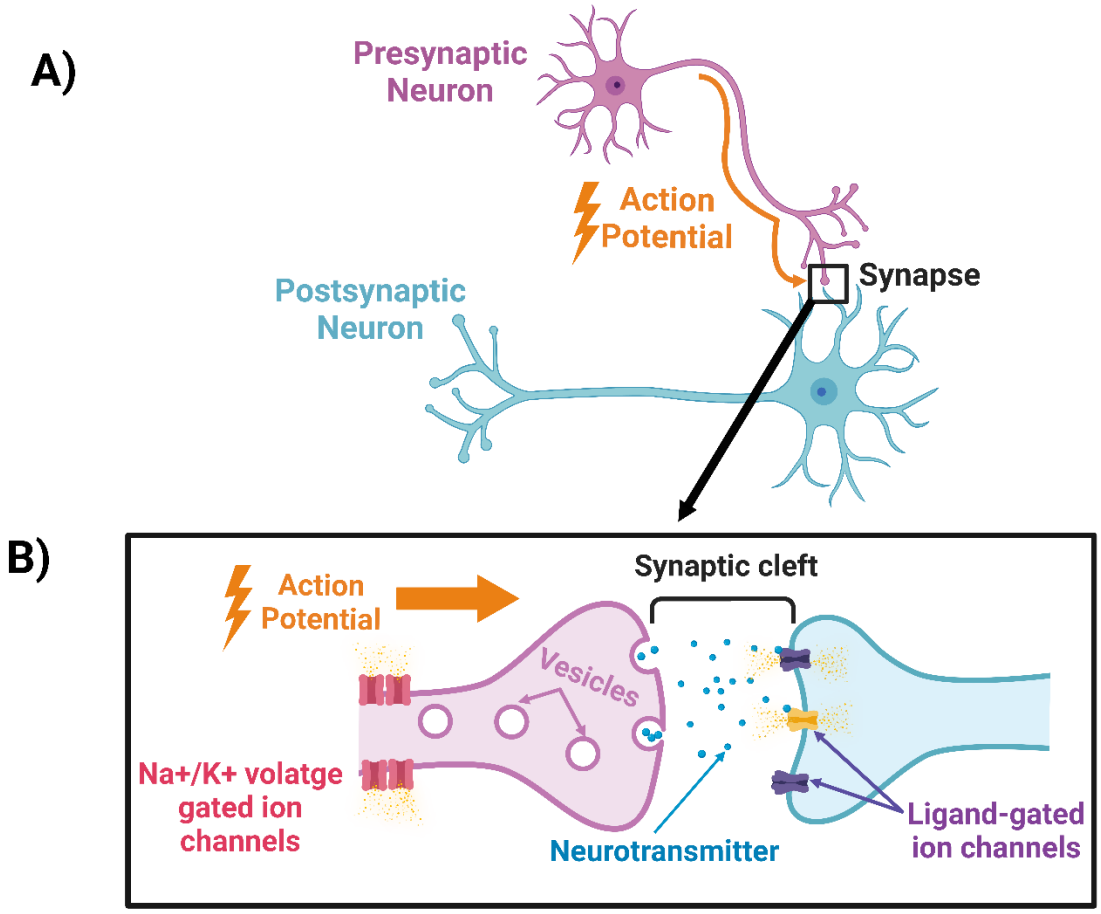

Figure 1.2. Signal transmission between neurons. A) Signal transmission begins with action potential generation from an external stimulus. In turn, the cell is depolarised enabling voltage-gated Na^+ channels (illustrated in pink above) to open, causing a rush of Na^+ ions into the cell [14]. K^+ ions are slowly leaked out of the cell through open K^+ channels (illustrated in pink above), however the Na^+ ions flood in at a greater rate and sustain the depolarisation along the length of the axon. B) Once the action potential reaches the axon terminal, voltage gated Ca^{2+} channels are opened and enable Ca^{2+} ions to flood into the cell [11]. The Ca^{2+} ion influx triggers the release of neurotransmitter filled vesicles from the presynaptic terminal. Vesicles release this neurotransmitter into the synaptic cleft to bind to neurotransmitter specific receptors (pictured: Ligand-gated ion channels) on the postsynaptic terminal. Receptors on the postsynaptic terminal open to allow influx of ions (ligand-gated ion channels) or activate second messengers responses (G-protein coupled receptors) to trigger depolarisation and/or molecular changes to the postsynaptic neuron [11]. Figure created with BioRender.com.

1.2.1. Neurotransmitters and their receptors

Chemical signalling across the synapse is facilitated by various neurotransmitters mediating different cellular responses in both the CNS and peripheral nervous systems (PNS) [18]. Neurons are either excitatory or inhibitory depending on the type of response generated in the postsynaptic neuron resulting from neurotransmitter-receptor binding. The two main neurotransmitters responsible for transmission in the central nervous system are glutamate and γ-aminobutyric acid (GABA), the main excitatory and inhibitory neurotransmitters [19]. Other neurotransmitters, e.g. acetylcholine and dopamine, in both the CNS and PNS, can have excitatory or inhibitory effects in synaptic transmission [18].

Here, the focus will remain on the two main neurotransmitters of the CNS, GABA and glutamate. GABA binding receptors are either ionotropic ($GABA_A$) or metabotropic ($GABA_B$; activate G-protein signalling) and are responsible for mediating inhibitory responses in the CNS [19,20]. Inhibition is achieved by hyperpolarising the membrane and disrupting the progression of the action potential. Binding of GABA to the $GABA_A$ receptor causes an influx of Cl^- ions and hyperpolarisation, resulting in the prevention of signal propagation [20]. This action is known as the inhibitory postsynaptic potential (IPSP) and is completed on a shorter timeframe by the $GABA_A$ receptor than the slower metabotropic $GABA_B$ receptor [20]. Glutamate receptors also have both ionotropic (iGluRs) and metabotropic (mGluRs) receptor types to facilitate excitatory neuronal transmission [19,21,22]. Excitatory transmission will have the opposite effect to inhibition in that depolarisation and action potential propagation is the main effect of receptor binding. The binding of glutamate to iGluRs allows K^+ ions to slowly leave the cell, whilst Na^+ and Ca^{2+} ions can now enter [23]. The net of effect of this ion movement is the depolarisation of the cellular membrane, promoting signal propagation [23]. This response of iGluRs and mGluRs binding is known as the excitatory postsynaptic potential (EPSP) [23].

Like GABA receptors, this response is quicker in the ionotropic than the metabotropic receptor. Despite differences in timed responses, the ionotropic and metabotropic receptors of both glutamate and GABA have important roles in regulating synaptic transmission [19].

Changing synaptic transmission between neurons will often involve changing the type or number of neurotransmitter receptors present on the postsynaptic terminal [19]. Both GABA and glutamate receptors are subjected to regulation via both movement along the neuronal membrane and recycling, in a process known as receptor trafficking [19]. Neurotransmitter receptor type is also altered by an exchange of the protein subunits which form these receptors. As a result, there are four iGluR groups, the two main types AMPA (α-amino-3-hydroxy-5-methyl-4-isoxazole propionate) and NMDA (N-methyl-D-aspartate) are present on most synapses [23]. AMPA is mainly the facilitator of Na^+ influx, whilst NMDA will enable Ca^{2+} entry in addition to the other cations [23]. Whilst the AMPA receptor (AMPAR) only requires glutamate binding for the channel to open, the NMDA receptor (NMDAR) is also blocked by an extracellular magnesium ion requiring a strong depolarisation to stop the blockade in addition to glutamate binding [23]. Importantly, the Ca^{2+} ions supplied by NMDAR activation trigger signalling cascades which may alter the number of receptors available on the postsynaptic terminal [21,23]. The population of receptors on the postsynaptic terminal determines the strength of synaptic transmission.

1.3. Synaptic plasticity

Molecular and structural modification of synapses causes either an increase or decrease to the strength of synaptic transmission and is known as synaptic plasticity (Figure 1.3) [19,21,22]. The most well studied form of synaptic plasticity, Hebbian plasticity, is a positive feedback mechanism [1]. Hebbian plasticity changes result in either a weakening or a strengthening of

synaptic transmission. Consistently high frequency synaptic transmission can strengthen synaptic transmission between neurons in a process known as LTP (Figure 1.3)[1,24]. Long-term depression (LTD) is the reverse effect from infrequent signal transmission weakening synaptic connections between neurons (Figure 1.3) [1,24]. Modifying synaptic transmission is accomplished by morphological or protein machinery changes to the presynaptic or postsynaptic terminal. These changes can consist of; changes to dendritic spine morphology, membrane excitability, receptor localisation, and number of vesicles released during transmission [24-26]. The most common Hebbian plasticity change for LTD and LTP processes is the modification of the number and types of receptors present on the postsynaptic terminal. The two main iGluRs types AMPAR and NMDAR are most often subject to modifications in receptor number on the post synaptic terminal to reflect the LTP or LTD change (Figure 1.3) [27]. In effect, any structural or molecular modifications that encompass Hebbian plasticity underlie the learning and memory process and knowledge of these processes is pivotal to understanding brain function.

Hebbian plasticity is the most well-studied form of synaptic plasticity, due to extensive research aimed at determining the main mechanisms behind learning and memory. Whilst Hebbian plasticity is essential for modifying synaptic transmission to facilitate learning processes, there is an inherent problem with maintaining synaptic strength via positive feedback. For instance, continued pre- or postsynaptic stimulation by neuronal firing strengthens the synapse by lowering the activation threshold, resulting in more firing and further LTP [2,4]. The result is a continuous positive feedback loop, enabling a theoretical exponential growth that could spread throughout the brain [2,4]. Clearly neuronal transmission requires Hebbian plasticity for learning and memory functions but there appears to be an infinite capacity for LTP/LTD modification if left unrestrained [2,4].

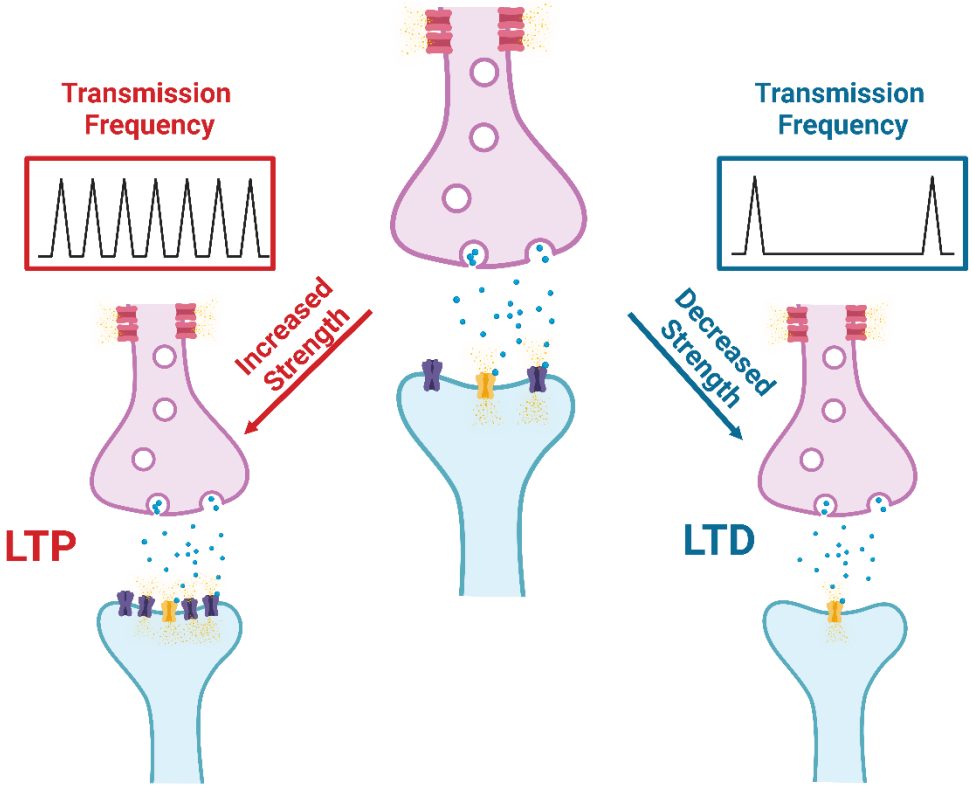

Figure 1.3. Hebbian form of synaptic plasticity. Signal transmission strength can be modified through processes of Hebbian plasticity [1]. Increased transmission (left) results in LTP via an increase in the number of receptors or amount of neurotransmitter released. Decreased transmission (right) has the opposite effect, resulting in LTD via a decrease in receptor numbers and released neurotransmitters. Figure created with BioRender.com.

The Hebbian activity disturbances, outlined above, have been documented to revert to a homeostatic set point by negative feedback mechanisms, collectively known as homeostatic plasticity [24,28]. In comparison to Hebbian plasticity, homeostatic plasticity has not benefitted from such extensive examination with little known about the driving mechanisms involved. Although various studies have implicated abnormal homeostatic regulation with impaired neurological function and several neurological pathologies [5,29-31]. This work will involve an

exploration of the proteins and signalling participating in homeostatic plasticity and identification of the homeostatic plasticity pathways involved in epilepsy.

1.4. Homeostatic plasticity

Any process which maintains synaptic transmission in equilibrium is defined as homeostatic and thus there are a range of different mechanisms that fall into this type of plasticity [27,32-34]. Homeostatic mechanisms can be employed at the pre and postsynaptic terminal at either a global or synapse specific level [32]. One of the most well studied forms of homeostatic plasticity is synaptic scaling, where either all excitatory or inhibitory synaptic inputs on a neuron are scaled up or down in response to perturbed synaptic transmission (Figure 1.4) [27,32,35]. To bring activity back to the homeostatic set point in excessive or prolonged inhibitory and stimulatory conditions, the machinery at a neuronal synapse is adjusted to up or downscale transmission and reverted to the set point [27,32]. Up and downscaling is achieved by changes to synaptic protein machinery as a result of various signalling mechanisms, which will be discussed in greater detail.

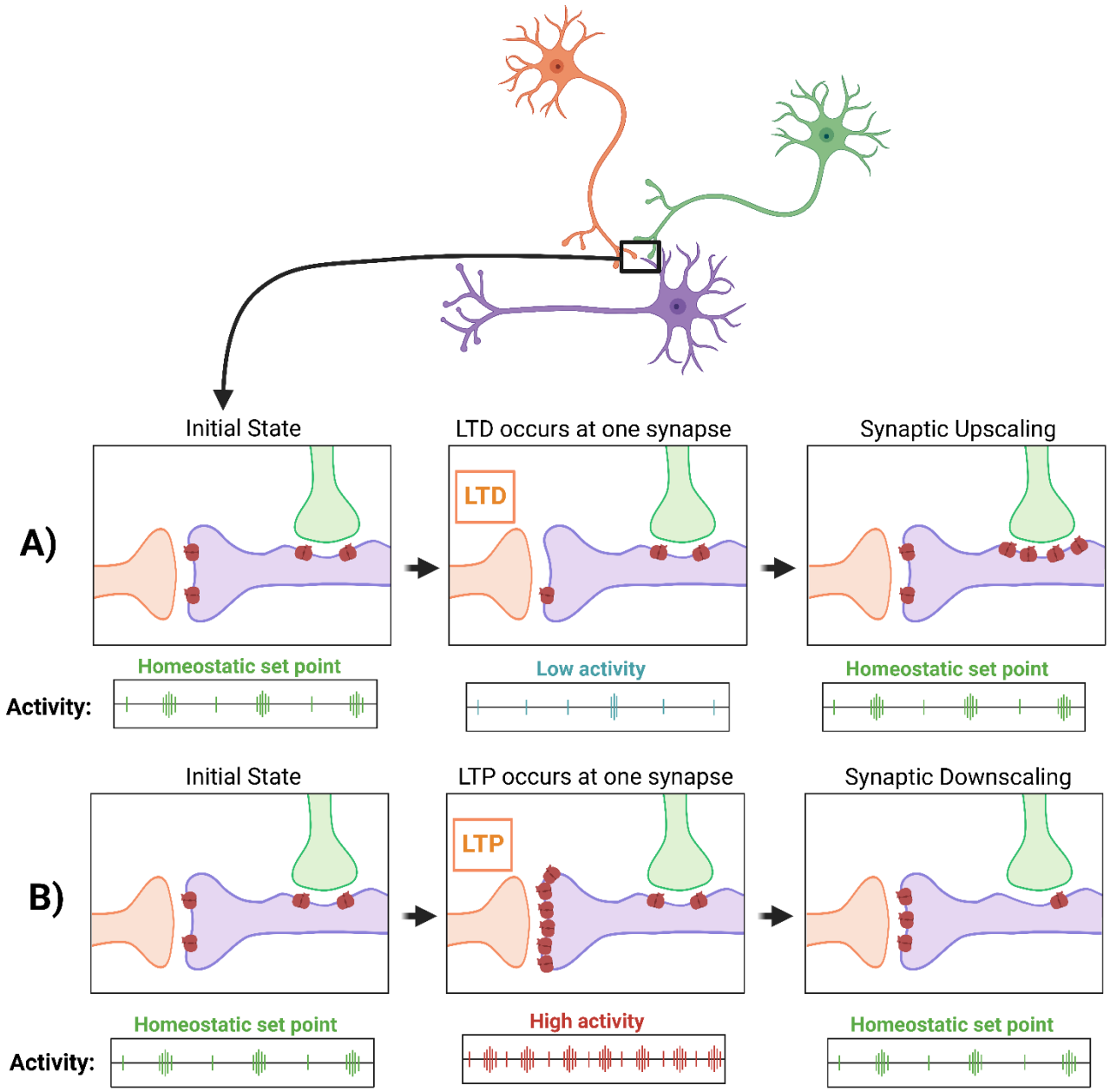

Figure 1.4. Illustration of synaptic scaling. Synaptic scaling is a form of homeostatic plasticity in which all excitatory synaptic outputs on a neuron (purple neuron in figure above) are up or downscaled to maintain stable neuronal activity. At the initial state, neuronal activity is at the homeostatic set point and receptors (dark red above) from each of the excitatory inputs (orange and green neurons above) are in a 1:1 ratio. A) As the orange/purple synapse undergoes LTD the number of receptors decreases from 2 to 1 on the orange/purple neuronal synapse and thus the ratio between the excitatory inputs shifts from 1:1 to 2:1. This decrease lowers the network activity past the homeostatic set point and triggers the activation of plasticity mechanisms. To restore activity back to the homeostatic set point, the number of receptors from each of the synaptic inputs are scaled up, but maintained in the new 2:1 ratio, to reflect

the change in individual synapse strength. B) In like manner, synaptic downscaling is the homeostatic response to an increased neuronal activity. Homeostatic mechanisms again restore the set point by scaling down the number of receptors in accordance with the new 3:1 ratio, to reflect the change in synapse strength. Figure adapted from Turrigiano [4] and created with BioRender.com.

1.4.1. Synaptic scaling

In the homeostatic transition process of synaptic scaling, different signalling pathways are engaged to modify synaptic machinery at both terminals and cause neurotransmission to up- or downscale respectively (Figure 1.4.) [4]. Early studies by both the Turrigiano, et al. [2] and O'Brien, et al. [36] groups, found that synaptic scaling engaged signalling mechanisms to affect postsynaptic receptor localisation. In the study by Turrigiano, et al. [2], bicuculline (Bic) a $GABA_A$ receptor antagonist and stimulant was used to downscale rat visual cortical cultures. To upscale the cultures, tetrodotoxin (TTX) a voltage-gated Na^+ channel antagonist, 2-amino-5-phosphonopentanoic acid (APV) an NMDAR antagonist and 6-Cyano-7-nitroquinoxaline-2,3-dione (CNQX) a kainate receptor and AMPAR antagonist were used to block excitatory transmission [2]. The TTX and CNQX treatments had initially diminished neuronal firing, however, at 48 h the miniature excitatory postsynaptic current (mEPSC) amplitudes dramatically increased to a respective 192% and 195% of the control mEPSC values [2]. The Bic treated cultures began at a high firing rate of about 265% of control mEPSC values, declining at 48 h to 70% of control values [2]. In contrast, APV treated cultures had no significant mEPSC recordings [2]. Turrigiano, et al. [2] concluded that the plasticity alterations were slow and progressive, as mEPSC changes occurred at 48 h, and that modifications regulating synaptic machinery involved mechanisms distinct from NMDAR signalling typically involved in LTP and LTD plasticity, as the APV treatment had no significant change. AMPAR localisation and involvement in synaptic scaling was later explored by the O'Brien, et al. [36] group, using APV,

CNQX, Picrotoxin ($GABA_A$ receptor antagonist) and Strychnine (Glycine receptor antagonist) to respectively up and down scale spinal cultures. O'Brien, et al. [36] used immunofluorescence of AMPAR subunits (GluR1-3), to quantitatively show that a prolonged decrease in excitatory synaptic activity results in an increased accumulation of AMPARs at the postsynaptic terminal and the opposite response for prolonged increased excitatory synaptic activity [36]. Both studies provided evidence of a delayed homeostatic response to perturbed neuronal transmission but lacked molecular evidence to implicate signalling pathways responsible for the synaptic modification.

To this end Schanzenbacher, et al. [37] performed a proteomic profile of homeostatic changes at 24 h to gain an appreciation of the various biological processes involved in synaptic scaling. In their study, Schanzenbacher, et al. [37] performed an analysis of Bic and TTX treated rat hippocampal neurons at 24 h, using a specialised metabolic labelling technique (BONCAT: bio-orthogonal non-canonical amino acid tagging) that tags newly synthesised proteins in order to distinguish proteins that are synthesised in response to synaptic scaling. The Schanzenbacher, et al. [37] group, first confirmed that new proteins are required to establish homeostatic changes by treating the cultures with either Bic or TTX and inhibiting protein synthesis with anisomycin for 12 h. The group found that at 12 h, control mEPSCs were not significantly different from the TTX and Bic plus anisomycin treated mEPSCs, indicating that protein synthesis is required to enact homeostatic modifications [37]. Following this result, neuron cultures were treated with azidohomoalanine (BONCAT reagent) for 24 h with either no additional treatment (control) or drugged with Bic or TTX [37]. Overall, the group detected 5,940 AHA proteins, with approximately 5,100 proteins generated in each experimental condition (Bic, TTX or untreated) In analysing the approximate 300 differentially regulated up and downscaled proteins, the group found that a large proportion were ubiquitin-proteasome type proteins, kinases, and phosphatases, underscoring an important role for posttranslational

protein modifications in the context of homeostatic mechanisms [37]. The other differentially regulated proteins were categorically functional proteins relating to ion channels, neurotransmitters, translation and transcription or structural proteins [37]. In a follow up study, the same group investigated changes in newly synthesised proteins at the 2-hour time point under the same up and downscaled conditions [38]. The group only found about 100 differentially regulated proteins at the early time point, with most of these proteins performing posttranslational functions like ubiquitin-proteasome type proteins, kinases, and phosphatases [38]. Indicating that synaptic scaling targets are actively regulated, either being signalled for degradation (ubiquitin-proteasome) or phosphorylated in an energy efficient means of homeostatic modification [38]. During the course of my investigation, a phosphoproteomic study was also completed by the Desch, et al. [39] group, finding that synaptic scaling targets of phosphorylation signalling are localised at the synapse. This study will be examined in Chapter 5 of this thesis.

1.5. Synaptic scaling and disease

Failure to homeostatically maintain neuronal activity has been postulated to influence seizure like states of activity in the neuronal network in disorders like epilepsy [8]. As many targets and signalling pathways of homeostatic regulation are also genetically associated with many neurological conditions (Table 1.1), relationships between these diseases and failed homeostatic regulation are currently being explored [8]. Schanzenbacher, et al. [37] in their original study, compared proteins which were regulated during pharmaceutically induced scaling with genes associated with common neurological conditions (e.g., schizophrenia, epilepsy, and autism), finding 166 genes associated with one or multiple disorders. Table 1.1 provides a summary of a few known signalling molecules involved in synaptic scaling at the pre- and

postsynaptic terminal, and includes a summary of molecular function, connected signalling pathways, and potential relationship between the signalling molecule and neurological disease. Notably, many of the synaptic scaling proteins that are involved with phospho-signalling are also implicated in various neurological disorders (Table 1.1 see synGAP, CaMKII, CDK5, MTORC1, BDNF). To this end, direction of this review will shift to remain on potential associations between phosphorylation in homeostatic plasticity and epilepsy.

Table 1.1. Known mediators of homeostatic plasticity

Signalling molecule | Receptor	Signalling pathway involvement / Function	Synaptic upscaling/ downscaling	Animal Model	Connection to neurological conditions	References
Tumor necrosis factor alpha (TNF-α)	Proinflammatory cytokine secreted by glia. Known involvement in signal transduction pathways (e.g. Jun N-terminal kinase, caspase, etc.)	Upscaling in response to low activity. Connected to AMPAR trafficking	Hippocampus and glia cells (Mouse) visual cortex (Rat and Mouse)	Neurological disorders involving injury, infection, or damage (e.g., Ischemia, dementia, epilepsy, traumatic brain injury)[40,41]	Stellwagen and Malenka [42] Steinmetz and Turrigiano [43] Kaneko, et al. [44]
Voltage gated Calcium channel $Ca_v2.1$ (Cacna1c)	Presynaptic voltage gated ion channel and part of the active zone. Involved with vesicle release.	Upscaling. Involved in presynaptic vesicle release in a retrograde homeostatic signalling mechanism	*Drosophila* NMJ	Familial hemiplegic migraine type 1, episodic ataxia type 2, (symptomatic epilepsy, developmental delay, migraine, etc.) [45]	Frank, et al. [46] Frank, et al. [47]
Homer 1a/ group 1 mGluR signalling	The IEG Homer 1a is activated by downstream signalling of group I mGluRs.	Downscaling. Homer 1a binds to mGluR during high activity states to activate mGluR signalling. This signalling promotes GluA2 phosphorylation to prevent AMPAR localisation	Cortex (Mouse) Prefrontal cortex (Mouse)	Group 1 mGluRs are targets of diseases like fragile X mental retardation syndrome, schizophrenia, and Alzheimer's disease	Hu, et al. [48] Diering, et al. [49]

Table 1.1. Continued

Signalling molecule | Receptor	Signalling pathway involvement / Function	Synaptic upscaling/ downscaling	Animal Model	Connection to neurological conditions	References
Snapin (SNAP associated protein)/ Dysbindin	Component of the biogenesis of lysosome-related organelles complex-1 (BLOC-1). Involved with vesicle release in conjunction with Dysbindin and synaptosomal-associated protein of 25 kDa (SNAP25)	Upscaling. Ca^{2+} dependent presynaptic vesicle release is coordinated with Snapin/dysbindin downstream of presynaptic $Ca_v2.1$ channels	*Drosophila* NMJ	Dysbindin is associated with Schizophrenia[50].	Dickman, et al. [51] Dickman and Davis [30]
MTOR (mammalian target of rapamycin)/ MTOR complex (MTORC) 1	MTORC1 is a protein complex component of the MTOR pathway. MTOR is a serine/threonine kinase that regulates cellular processes like growth, proliferation, and protein translation through phospho-signalling	Upscaling. Chronic activity blockade requires localised protein synthesis driven by MTORC1. Brain-derived neurotrophic factor (BDNF) is synthesised downstream of MTORC1 activation.	Hippocampus (Rat)	Tuberous sclerosis, epilepsy, and autism spectrum disorder[52]	Henry, et al. [53] Henry, et al. [54]
Calcium/ calmodulin-dependent protein kinase (CaMK) II	CaMKII is a Ca^{2+} /Calmodulin complex dependant enzyme present in two isoforms αCaMKII and. CaMKII is involved in gene regulation, synaptic plasticity	βCaMKII expression increases with excessive synaptic inactivity. Whilst αCaMKII is expressed with excessive synaptic activity. βCaMKII expression increases GluR1 AMPA subunit surface localisation.	Hippocampus CA1-CA3 (Rat)	CaMKII is related to various neurological disorders including epilepsy, schizophrenia, Parkinson's and neurodevelopmental disorders (e.g. Angelman syndrome)[55]	Thiagarajan, et al. [56] Groth, et al. [57]

Table 1.1. Continued

Signalling molecule | Receptor	Signalling pathway involvement / Function	Synaptic upscaling/ downscaling	Animal Model	Connection to neurological conditions	References
CaMKIV	CAMKIV is involved in various regulatory roles including plasticity, cell cycle control, memory, inflammation, etc. Phosphorylates transcription factor cyclic adenosine monophosphate (cAMP) response element binding protein (CREB)	Bidirectional regulation. To upscale, low levels of activated nuclear CaMKIV triggers gene transcription and AMPA accumulation. In downscaling, activated CaMKIV reduces excitatory synaptic strength and intrinsic neuronal excitability.	Neocortex (Rat) Visual cortex (Rat)	Not clear. Potential link to cognitive and neurodevelopmental disorders[58]	Ibata, et al. [59] Joseph and Turrigiano [35]
BDNF	BDNF is the most abundant neurotrophin in the brain. Neurotrophins promote development, modulate synaptic function, and serve in critical synaptic plasticity roles. BDNF is involved in many pathways including Mitogen-activated protein kinase (MAPK) and tropomyosin receptor kinase B (TrkB)	Upscaling for pyramidal neurons, through AMPAR surface trafficking. Downscaling in nucleus accumbens neurons after prolonged excessive activity by decreasing AMPAR surface expression	Visual cortex (Rat) Nucleus accumbens (Rat and Mouse) Prefrontal cortex (Mouse)	Reduced BDNF levels are associated with various neuropathies including bipolar disorder, schizophrenia, Alzheimer's, Parkinson's, etc. High levels of BDNF in the brain are associated with epilepsy. [60]	Rutherford, et al. [61] Rutherford, et al. [62] Reimers, et al. [63]
Integrin beta 3 (Itgb3)	Cell adhesion molecule in the CNS. Integrin beta 3 facilitates binding of different ion channels and receptors to the postsynaptic density	Upscaling. Increases excitatory quantal size and content in organotypic hippocampal slices. Integrin beta 3 is required for GluR2 AMPAR localisation.	Hippocampus (mouse)	Potential contribution to epilepsy, Alzheimer's disease, schizophrenia, cognitive impairments and related conditions.[64]	Cingolani and Goda [65] Cingolani, et al. [66]

Table 1.1. Continued

Signalling molecule | Receptor	Signalling pathway involvement / Function	Synaptic upscaling/ downscaling	Animal Model	Connection to neurological conditions	References
Cyclin-dependent kinase (CDK) 5/ Calcineurin	CDK5 is a kinase activated when bound to cyclin associated with gene expression regulation, cell differentiation and survival and angiogenesis. Calcineurin is a serine/threonine phosphatase (also known as protein phosphatase 2B (PP2B)) that regulates calcium homeostasis and is dependent on Ca^{2+} /CaM activity.	Upscaling. Reduction of CDK5 increases releasable presynaptic vesicle pool size. The alpha calcineurin isoform is necessary for presynaptic vesicle exocytosis and regulates Ca^{2+} influx.	Hippocampus (Rat)	Both CDK5 and Calcineurin have been linked to the same neurodegenerative conditions such as Alzheimer's disease, Huntington's disease, epilepsy, Amyotrophic lateral sclerosis, etc. [67-69]	Kim and Ryan [70] Kim and Ryan [71]
Nova-2	Nova RNA binding proteins are neuron specific and regulate alternative splicing. Nova-2 is known to interact within Ca^{2+} signalling cascades and with CaMKII	Upscaling. Phosphorylation of Nova-2 by CaMKII enables phosphorylated Nova-2 to alternatively splice Ca^{2+} activated potassium channels to broaden action potential duration	Cortex (Rat and Mouse)	Paraneoplastic opsoclonus-myoclonus ataxia[72]	Li, et al. [73]
Methyl-CpG-binding protein (MeCP) 2	MeCP2 is involved in various cellular functions such as regulation of gene expression via methylated DNA binding	Bidirectional regulation, MeCP2 absence prevents synaptic scaling. MeCP2 activity is required to downregulate GluR2 for downscaling and for the AMPAR enhancement required to upscale synapses	Hippocampus and Cortex (Rat)	Rett syndrome, X-linked neurodevelopmental disorder with comorbidities that include seizures, breathing difficulties, gait disturbances, etc. [74]	Qiu, et al. [75] Blackman, et al. [76]

Table 1.1. Continued

Signalling molecule | Receptor	Signalling pathway involvement / Function	Synaptic upscaling/ downscaling	Animal Model	Connection to neurological conditions	References
Synaptic Ras GTPase-activating protein (synGAP)	SynGAP is a postsynaptic density (PSD) protein physically associated with the NMDAR and other PSDs like PSD95. synGAP is phosphorylated by various kinases including CaMKII, polo-like kinase 2 (Plk2) and CDK5.	Upscaling. Acute activity blockade requires synGAP mediated local protein synthesis possibly through exerting control of the MTOR and extracellular signal-regulated kinase (ERK) signalling pathways exact mechanism of action and protein targets require elucidation	Cortex (Rat and Mouse)	Mutations to the synGAP gene (*SYNGAP1*) are associated with schizophrenia, neurodevelopmental and cognitive disorders like autism spectrum disorder. Epileptic seizures are a comorbidity[77]	Wang, et al. [78]
Retinoic acid	Retinoic acid signalling is involved in neurogenesis, gene transcription and neuronal differentiation. Retinoic acid interacts with various pathways (e.g. Ras/MAPK and MTOR, etc.)	Upscaling in response to low activity. Interacts with AMPAR-trafficking pathway	Hippocampus (Rat and Mouse)	Alzheimer's disease, Schizophrenia, Depression[79]	Aoto, et al. [80] Sarti, et al. [81] Chen and Napoli [82] Arendt, et al. [83]
Activity regulated cytoskeletal (Arc) or Arg3.1	Immediate early gene (IEG). Arc is known to interact with proteins involved in the endocytic pathway (dynamin and endophilin). Arc regulates AMPAR endocytosis through the endocytic pathway.	Bidirectional regulation of GluR1 containing AMPAR in an activity dependent way. Arc over expression decreases GluR1 containing AMPAR. Knock out (KO) of Arc has the opposite effect.	Hippocampus and cortex (Rat and Mouse)	Potential connection to neurological diseases affecting cognitive function (Angelman syndrome[8]). Arc KO mice are hyperexcitable and experience periodic seizures[84].	Shepherd, et al. [85] Gao, et al. [86]

1.6. Phospho-signalling

Transfer of phosphate groups by means of phosphorylation and dephosphorylation are rapid protein modifications that have been found to regulate all known biological processes [87]. On any target molecule, the main sites of phosphorylation are on the amino acid residues serine (Ser), threonine (Thr) and tyrosine (Tyr) [87]. Phosphorylation modifications are incredibly complex and fine-tuned especially considering that multiple phosphorylation sites can be present on any protein target, which can be targeted by a single protein kinase or separate kinases at different sites [88]. Controlled phosphorylation at any of these different sites on the target molecule enables the select protein to perform inhibitory, stimulatory, or dual functions [88]. The molecular targets of individual phosphorylation pathways can also meet to either prevent or promote the propagation of a converging signalling pathway, indicating that phospho-signalling is a versatile and controlled process [88]. Therefore, analysing these protein targets and their phosphorylation sites can give indications of how signalling interactions are accomplished and how these interactions influence mechanisms of synaptic plasticity.

1.6.1. Phosphorylation, synaptic plasticity, and neurological disorders

Whilst the involvement of phosphorylation in all biological processes is well established, only 3% of discovered human phosphosites have a known function [87]. Concerning synaptic plasticity, some studies have elucidated that the phosphorylation of sites on target molecules perform vital roles regulating the synapse and mediating Hebbian and homeostatic plasticity. For example, phosphorylation of S295 on PSD-95 is known to promote the accumulation of AMPAR at the synapse and is downregulated during chronic elevated synaptic activity and LTD [89]. Broadly speaking, understanding how the phosphorylation of different sites on target

molecules modifies their physiological function does not only illuminate the dynamics of synaptic plasticity but also has great implications in understanding neurological disease and developing potential treatments. For instance, the Tao, et al. [90] group were interested in performing a functional analysis of the S80 phosphorylation site on MeCP2 because this phosphorylation site was conserved in mice, rats, and humans and the protein has clinical significance for the neurological disorder Rett syndrome. Tao, et al. [90] found that the S80 site was phosphorylated in an activity-dependent fashion by western blot analysis of both *in vivo* seizure stimulated and non-stimulated brain samples (mouse) and confirmed this result with a western blot analysis of TTX (inhibitory) and KCl (depolarising) stimulated mouse cortical neuron cultures. The group later found that the S80 site was phosphorylated by CaMKIV through use of kinase inhibitor and western blot analysis, although it remains unclear if S80 is a substrate of only CaMKIV. To complement the study, the group generated a mouse model with a knock-in mutation at $S80^{A}$ (serine to alanine), which prevented the phosphorylation of MeCP2 at S80, finding that the $S80^{A}$ mice displayed reduced locomotion compared to control mice, which is a phenotypic characteristic of Rett patients [90]. Whilst more work would be required to functionally validate the S80 site, the clinical significance of having a kinase to target pharmaceutically offers treatment alternatives for patients and provides clarity with respect to understanding disease development.

Targeting of kinases as disease treatments is currently being implemented in diseases like cancer, where phospho-signalling is known to promote the perturbed cell growth and proliferation that characterises the condition [91]. In epilepsy, receptors of voltage gated ion channels and neurotransmitter receptors are frequently targeted as drug treatments, however, these treatments are ineffective for approximately one third of patients [92,93]. Recently, groups have begun targeting kinases as potential treatments in epilepsy like the BDNF receptor TrkB, with success in producing an antiseizure effect in seizure-induced mice [94]. However, an

understanding of the disease mechanisms and how these signalling pathways are engaged in epilepsy are still in their infancy. To date no large scale phosphoproteomics study has been completed in epilepsy models, which may illuminate kinases and substrates involved in disease signalling [95].

1.6.2. Phosphopeptide enrichment strategies

Mass spectrometry (MS) based detection techniques are an essential element of large scale proteomic and phosphoproteomic sample analysis [87,96,97]. An important consideration for phosphoproteomic analysis is the fact that phosphorylation modification results in substoichiometric amounts of phosphorylated proteins at a given moment [87,97]. Due to the nature of data dependant acquisition methods frequently used in MS, the lower abundance phosphorylated peptides are easily overlooked during analysis because of an overwhelming background signal from higher abundance non-phosphopeptides [97]. In reducing the sample complexity by separating non-phosphorylated peptides from a given sample, the detection of phosphorylated peptides is improved during analysis, thus phosphopeptides are frequently enriched prior to MS [87,97]. Two of the most implemented enrichment techniques involve metal affinity chromatography with the phosphopeptide binding through either metal oxide affinity (commonly with titanium dioxide (TiO_2)) or an immobilised metal [97-99]. For immobilised metal affinity chromatography (IMAC), immobilised chelated metal ions (either Fe^{3+} or Ga^{3+}) from the IMAC column bind to the negatively charged phosphate groups on the peptides to form a phosphate-metal ion complex. The loading buffer solution allows non-phosphorylated peptides, with a weaker affinity for the metal ions to elute from the column [98]. The bound and purified phosphopeptides can then be eluted from the column by washing with free phosphate ions or increasing the pH [98]. Enrichment of phosphopeptides by TiO_2 works using the same

principle of phosphopeptide binding selectively to the metal oxide and separating from an unbound non-phosphorylated peptide fraction [99].

Subsequent improvements to phosphopeptide enrichment strategies have involved optimisation of buffer solutions to decrease the relative metal affinity of non-phosphopeptides [100] and incorporate a multi-step enrichment process that has since been adapted for large-scale phosphoproteome analyses. To increase the yield of phosphorylated peptides from tissue samples, sequential elution steps were added to the IMAC protocol with different elution buffers (SIMAC: sequential elution from IMAC) to separate mono-phosphorylated peptides from multi-phosphorylated peptides [101]. Briefly, SIMAC implements a first round TiO_2 isolation of phosphorylated peptides, as TiO_2 is more effective in phosphopeptide enrichment than IMAC [101]. The phosphopeptides are then separated by IMAC with an acid wash to elute mono-phosphorylated peptides and a basic wash to isolate the multi-phosphorylated fraction [101]. Later, an additional step was added to the protocol combining SIMAC with hydrophilic interaction liquid chromatography (HILIC) (coined TiSH) to isolate the multi-phosphorylated peptide fraction and further fractionate mono-phosphorylated peptides with high performance liquid chromatography (HPLC) [102,103]. The HILIC separation step (water solvent elution) is suited to hydrophilic phosphopeptides and is orthogonal to the subsequent reversed phase (RP HPLC) separation (acetonitrile solvent elution) implemented prior to MS/MS [102,103]. Using the TiSH protocol, groups have reported obtaining around 10,000 to 40,000 phosphopeptides from samples [95,104]. Alternatively, other groups using a high pH RPLC for fractionation instead of HILIC are reporting numbers of >30,000 identified phosphopeptides [105,106], and the Sharma, et al. [107] group report a deep phosphoproteome analysis of >50,000 phosphopeptides using strong cation exchange chromatography for sample fractionation. Presently, fractionation strategies combined with phosphopeptide enrichment provide a great phosphoproteomic depth but are labour-intensive and consume large quantities of MS instrument time [97]. There is a progression

towards techniques that implement simpler phosphopeptide enrichments without fractionation, that are reproducible and use less instrument time, however, these methods currently do not provide the same phosphoproteomic coverage as the enrichment plus fractionation strategies [97]. Therefore, to generate a deep phosphoproteomic profile of an epilepsy model, an enrichment plus fractionation strategy will be employed for the phosphoproteomic analysis.

1.7. Epilepsy

Epilepsy is a common neurological disease affecting 39.9 to 54.6 million people worldwide [108]. In approximately 50% of these cases, the underlying trigger of epilepsy will not be identified and have an unknown cause [109,110]. Epilepsy manifests in seizures that are the result of excessive or highly synchronised neuronal activity [3,111]. The physical and psychological consequences of seizures have a severe impact on living standards and overall quality of life [110]. In excess of 20 antiseizure drugs (ASDs) are available and are being implemented to treat seizure symptoms [109]. Approximately 27% of epilepsy patients will have drug-resistant epilepsy, whereby two ASD schedules (either combination or monotherapies) will fail to achieve continued seizure freedom [93,112]. Interestingly, patients with particular epilepsy types e.g. temporal lobe epilepsy (TLE), tend to be the most resistant to ASDs highlighting the need to deduce underlying mechanisms of the disease [93,113,114]. A recent study by Oliver, et al. [115] has identified over 900 genes that cause a monogenic epilepsy disorder when mutated. A separate study by Wang, et al. [7] identifies 84 genes known to primarily cause epilepsy or an epilepsy syndrome when mutated, of which genes encoding ion channels and receptors were the most prevalent (28/84) [7]. When mutated, these primary epilepsy genes are responsible for mild to severe epilepsy conditions including Dravet syndrome (*SCN1A*) and Juvenile myoclonic epilepsy (*GABRA1*) [7]. The large range of epilepsy associated genes indicates large

genetic diversity in epilepsy aetiology and implicates the involvement of a variety of biological pathways [7,109,116,117]. Despite this wealth of genetic information, clinically available treatment is still limited to symptom management with ASDs [92]. As knowledge of epileptogenic mechanisms is still in its infancy, more work using omics approaches could help progress our current understanding and elucidate key epilepsy causing molecular players and pathways [116,117]. The current translational aim of epilepsy research is to target key molecular agents specific to disease causing mechanisms and develop therapies that can halt or modify epilepsy development, potentially benefiting a greater range of epilepsy patients worldwide.

1.7.1.1. Temporal lobe epilepsy

Focal epilepsy is the most prevalent form of epilepsy, accounting for 60% of all epilepsy [109]. TLE is a common form of focal epilepsy which can be broadly characterised by the occurrence of focal seizures in the temporal lobe region of the brain, on either the right or left hemisphere [118]. Mesial TLE (mTLE) is attributed to at least 80% of TLE cases and commonly afflicts adults [119,120]. mTLE is associated with seizures arising mainly in the hippocampus but broadly in the mesial region of the temporal lobe (i.e. hippocampus, amygdala and entorhinal cortex) [118,120]. A common pathological feature of mTLE is hippocampal sclerosis (mTLE-HS), in fact many cases of mTLE have hippocampal seizure involvement leading to reduced size, loss of principle neurons and lesion development [93,118]. Therefore, seizure control of patients with mTLE is paramount to prevent further neuronal damage and epileptogenic network remodelling. However, individuals with mTLE-HS are regularly affected by ASD resistance usually requiring surgical intervention for seizure control [93,118]. As mTLE is a common form of focal epilepsy, many individuals will potentially be resistant to ASDs requiring better drug

treatments for seizure control and to prevent further neuronal damage and epileptogenic network remodelling.

1.7.1.1.1. Hippocampal sclerosis in temporal lobe epilepsy

The hippocampus, apart from being an important structure in learning, emotions and memory, is considered an important structure in epilepsy pathology [121,122]. The hippocampal formation itself consists of the parahippocampal gyrus (Entorhinal Cortex), subiculum, dentate gyrus (DG) and hippocampus proper (Cornu Ammonis; CA) (Figure 1.5.) [123]. The CA is divided into four regions (CA1-CA4) to form a curved bean structure which ends with the CA4 field (hilar region) enclosed in the dark U-shaped grey matter of the DG (Figure 1.5)[121,124]. CA1-3 regions have a predominant pyramidal principal neuron population and a small interneuron population (Figure 1.5)[121]. These pyramidal neurons will largely form excitatory synapses whilst interneurons will form inhibitory synapses [121]. Interneurons are crucial in preventing seizure-like activity by acting as modulators of excitatory activity in the hippocampus [121]. The DG contains two types of glutamatergic neurons, granule cells (DGCs) and hilar mossy cells (MC) the latter of which is the principal cell of the CA4 region [125,126]. DGCs project unmyelinated axons, known as mossy fibres, that connect the entorhinal cortex to the hippocampus CA3 region to form excitatory synapses with pyramidal neurons [121,125,127].

In an epilepsy context, DGCs forming new axonal connections to the inner molecular layer of the DG, is observed as mossy fibre sprouting (MFS) [127,128]. MFS was thought to promote the development of epileptogenic excitatory circuits causing an imbalance between inhibitory and excitatory inputs [121]. However, the importance of MFS was undermined when different studies demonstrated that a lack of MFS or prevention of MFS did not result in an absence of epileptogenesis [122,129-131].

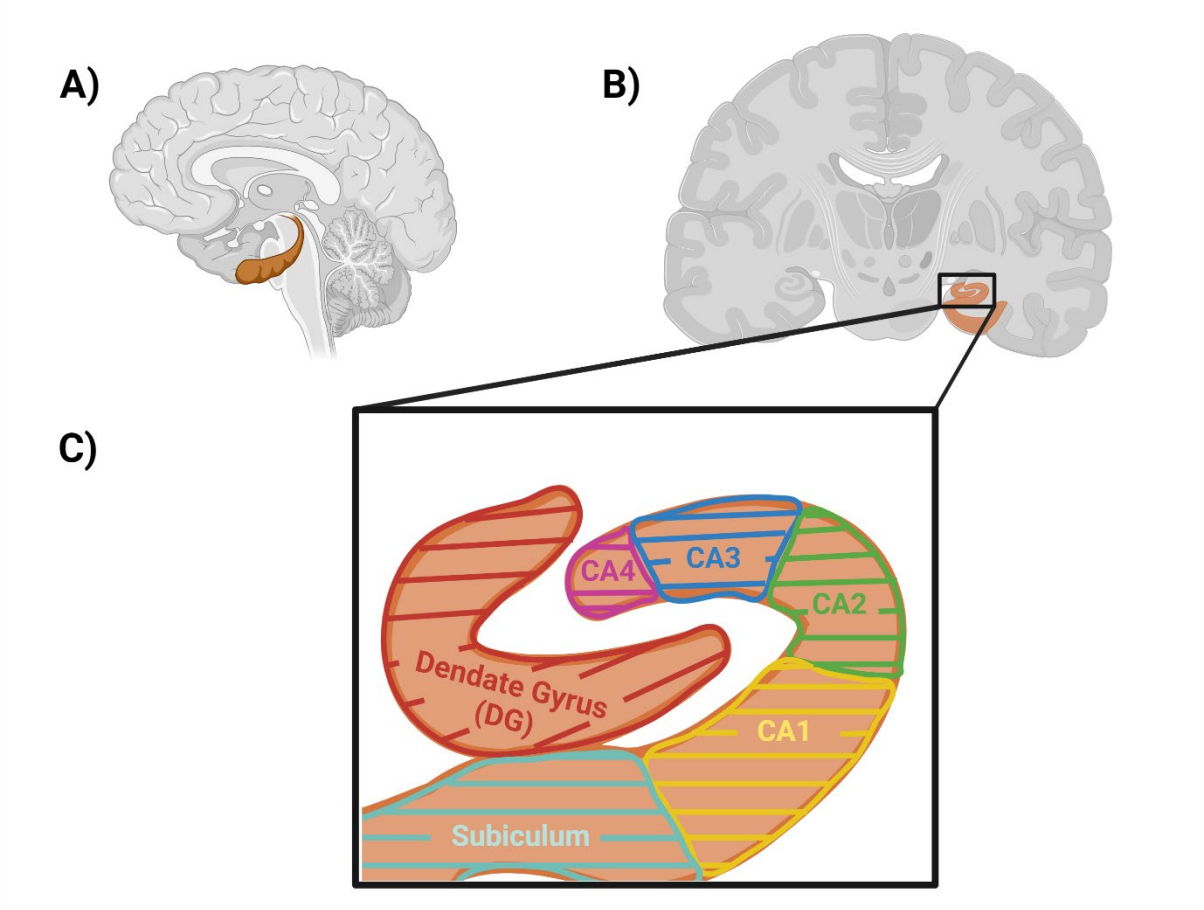

Figure 1.5. Hippocampus: diagram and labelled anatomy. A) Midsagittal view of the human brain with the hippocampus highlighted in orange. B) Coronal view at the thalamus with hippocampal formation highlighted in orange. C) Hippocampal formation enlarged and labelled. The DG (red) and subiculum (light blue) have been coloured as indicated, whilst the regions of the CA have been coloured to their approximate locations (CA1: yellow, CA2: green, CA3: blue, CA4: pink).

It has been theorised that the epileptogenic effect of excitatory mossy fibre circuits might only be exhibited under conditions where factors that reduce GABAergic inhibition are elevated, such as during stress or sleep deprivation [122]. Whilst MFS is currently considered more of a pathological phenomenon than a causal factor for epilepsy, the remodelling of neuronal networks demonstrated by sprouting, remains an important concept for understanding epileptogenesis [122]. Other changes which contribute to the epileptogenic state and are

characteristic to hippocampal sclerosis (HS) are the selective loss of pyramidal neurons, propagation of interneurons and reactive gliosis [121,124]. Briefly, gliosis in HS is the physiological and biochemical alteration of glial cells in response to seizure insults [132]. Reactive glia (generally astrocytes and microglia) are involved in the release of chemokines, growth factors and other molecules to direct the inflammatory response, clearing cellular debris and inducing synaptic plasticity and tissue remodelling [132]. Pathological damage arises when glial cells exceed their neuronal support role and begin to exert detrimental activity in the brain [133]. Harmful gliosis results in the detrimental alteration of neuronal tissue and synaptic modifications [132,133]. As not all gliosis is necessarily harmful, isolation of signalling pathways or molecules that promote destructive modifications should prevent neurological tissue from becoming epileptogenic [132].

1.7.2. Epileptogenesis

Epilepsy is a progressive disorder whereby the experience of an epileptic seizure can induce changes to the brain that place it in an epileptogenic state. This process begins with the development of tissue capable of producing spontaneous seizures and involves the expansion of this tissue to result in either the development of an epilepsy disorder or a progression of the epileptic condition [134]. This development of epilepsy is known as epileptogenesis. Epileptogenesis coincides with progressive neuronal degeneration and has been well documented from mild to chronic forms of TLE, where recurrent seizures cause cell loss and damage to neuronal networks [135-137]. Since epilepsy is progressive, there is a possibility that the disease course might be halted or modified in patients with prophylactic treatments [138]. Many studies have explored epileptogenesis in the context of disease prevention and modification, to develop alternative treatments distinct from current ASDs medications. The primary aim of

ASDs is to prevent seizure generation (ictogenesis) and not necessarily prevent epileptogenesis or modify the disease course [139,140]. For this reason, it is suspected that current ASDs may not be antiepileptogenic or disease modifying treatments. In contrast, antiepileptogenic treatments are those taken after the initial brain insult to counter epileptogenesis, which include preventative or seizure modifying effects [134,141]. The development of antiepileptogenic and disease modifying treatments will require an understanding of activated pathways and mechanisms that contribute to the epileptogenic process. Whilst no current antiepileptogenic treatment exists, several drugs and drug targets have been discovered requiring clinical validation [141].

1.7.2.1. Epileptogenesis progression

Originally, it had been understood that epileptogenesis progressed in three distinct phases. The initial insult, latency (silent), and chronic epilepsy phase characterised by distinct physiological and molecular changes which predisposes individuals to epileptic seizures (Figure 1.6)[142]. However, limitations in the old epileptogenesis model became evident against data from both animal models and patient records [143,144]. For instance, the old model implies that once chronic epilepsy is developed, the condition cannot deteriorate further which has substantial implications for the utility of antiepileptogenic treatments [143,144]. However, there is a large amount of data and animal models that support progressive epilepsy deterioration including chronic epilepsy patient records with patterns of progressive uncontrolled seizures and the animal kindling model (repeated seizure insults to establish epilepsy in animals) [143,144]. Other data indicated that the latent period is not necessary for seizure development and that inconspicuous seizure manifestation is preventing early seizure detection [143,144]. Presently, the new model of epileptogenesis views molecular and physiological changes as progressive in

nature, so that once the brain is epileptogenic from the initial insult, subsequent seizure activity will exacerbate the epilepsy and prompt further seizure activity (i.e. *seizures beget seizures* [145]) [146].

The first occurrence of a brain insult triggers the start of epileptogenesis [142]. In the initial phase, the insult/seizure may be precipitated by an inherited condition (i.e., genetic), the result of physical trauma (e.g., traumatic brain injury, stroke, brain infection) or have an idiopathic manifestation [142]. This initial insult will trigger the activation of signalling pathways and mechanisms resulting in changes to synaptic signalling, structural protein expression, the transcription of immediate early genes (IEGs) and translation of transcription factors (Figure 1.6) [146,147]. Over the course of days to weeks during the latent phase there are modifications that occur resulting from the initial round of signalling such as neurodegeneration, depending on seizure severity, through neuronal apoptosis and changes in synaptic plasticity including the rewiring of synaptic connections, axonal sprouting, and neurogenesis [146,148]. The remodelled neuronal network increases in synchronised brain activity and forms hyperexcitable connections to replace neuronal connections lost in the initial injury [141]. At this point, various epileptogenic modifications have taken place to predispose the individual to seizure activity. Once the first clinical seizure is identified, the latent period is over, and the individual is diagnosed with an epilepsy disorder [122,146]. Subsequent seizure activity will continue to initiate new cycles of epileptogenic modifications eventually resulting in a brain that is prone to epileptic seizure activity (Figure 1.6 B). Consequently, identifying the signalling pathways and molecules involved in epileptogenic modifications has become a priority, in developing antiepileptogenic treatments and stopping the cycle of epileptogenesis.

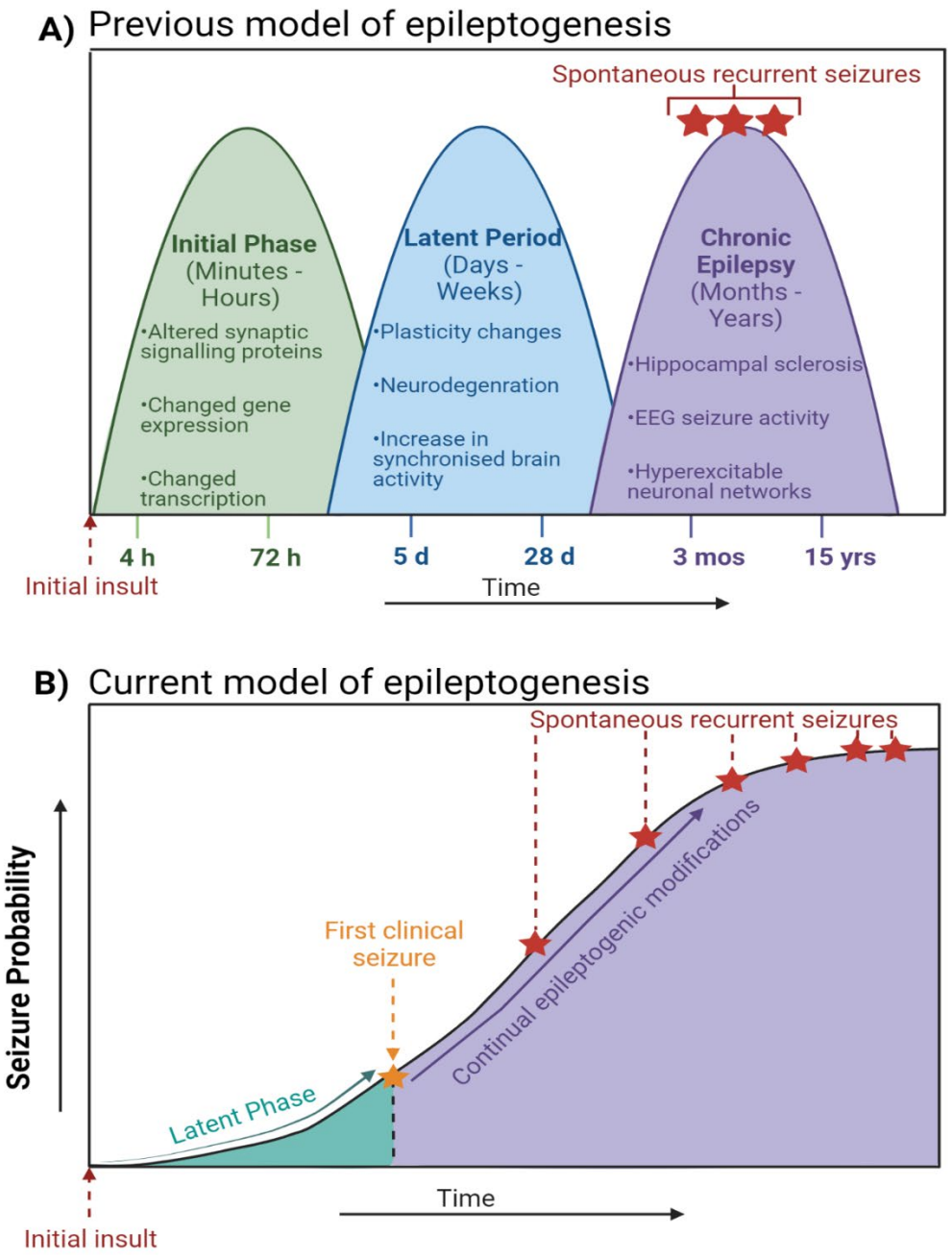

Figure 1.6 Phases of epileptogenesis. A) Originally epileptogenesis was theorised to occur in three distinct phases beginning with an initial insult, followed by a silent latent period and culminates in an epilepsy disorder [122,146]. The phases added chronology and a timescale to the events underlying epileptogenesis. For instance, the activation of different signalling pathways to alter transcriptomic and proteomic expression occurs within seconds of the initial insult, whilst the epileptogenic changes in synaptic plasticity and organisation may take weeks to years from latent period to the chronic phase[149]. However, this understanding overlooked continued epileptogenic modifications occurring because of seizure activity and suggests that the latent period was free of seizure activity [122,146]. B) The current view of epileptogenesis

acknowledges that molecular and pathophysiological changes are triggered following an initial insult. This model acknowledges that seizure activity can occur undetected during the latent period before the first seizure diagnosis. Adapted from Scharfman [122], Younus and Reddy [150] and Pitkanen, et al. [146]. Figure created with Biorender.com.

1.7.3. Molecular mechanisms of epileptogenesis

Current epilepsy research is largely completed on animal models, namely rodents, which have been designed to mimic the pathological damage, behavioural manifestation, and electrical activity associated with epileptic seizures [109,113]. Both genetic and acquired forms of epilepsy have been modelled in rodents to explore epileptogenic mechanisms, disease progression, biomarkers, drug targets and other aspects of epilepsy research which is limited by clinical studies and human epilepsy tissue analysis (sourced post-mortem or from resective surgery) [109,151]. Acquired epilepsy models are produced through chemoconvulsants, electrical stimulation, kindling (repeated stimulation through either a chemoconvulsant or electrical stimulus), and brain injury to simulate the epilepsy aetiology responsible for the pathology [109,151,152]. The most extensively applied models in epilepsy research are the pilocarpine (Pilo) and kainic acid (KA) chemoconvulsant models, which replicate the HS damage observed in mTLE patients and generates spontaneous recurrent seizure activity [113,151]. Apart from *in vivo* models, *in vitro* models derived from dissociated neuron cultures, organotypic brain slice preparations and induced pluripotent stem cells have also been adopted to research epileptogenic mechanisms such as neuronal network excitability and ictogenesis [153-156]. Whilst all data generated from these epileptogenesis models needs to be clinically validated, these models provide a foundation for exploring and understanding epilepsy disease mechanisms.

Given the accessibility of microarray and sequencing technologies, large amounts of genomic and transcriptomic expression during epileptogenesis have been documented across various epileptogenesis models [146]. Initial proteomic studies of epileptogenesis have lacked the depth, since they used mainly two-dimensional polyacrylamide gel electrophoresis (2D-PAGE) with mass spectrometry (MS) [157-164]. Improving proteomic methodologies and advances in technologies like liquid chromatography tandem MS (LC-MS/MS), have enabled more recent proteomic studies to produce greater data depth with some studies identifying hundreds to thousands of proteins across different brain tissues, types of epileptogenesis models and timepoints [165-169]. Despite the wealth of information generated, more investigation is required to understand epileptogenic signalling as mechanisms governing epileptogenic modifications remains poorly understood [170]. To date 'Omics' studies have provided minor agreement on significantly regulated proteins or changes to gene and transcript expression [146,171]. Some major reasons for this are methodological variations, the limited timepoints explored and the epileptogenesis model employed, as different models can elicit distinct physiological responses of varying strength due to the type of stimulus used, brain region affected and the intensity of tissue damaged induced [146,171]. Mechanisms involved in epileptogenesis are understood to involve a dynamic and complex interaction of different physiological responses, requiring more data to understand the timing patterns of molecular biological processes to distinguish pathophysiological modifications.

A key issue in defining epileptogenic mechanisms is distinguishing between neuroprotective, epileptogenic, and damaging but non-epileptogenic signalling responses following seizure activity [122,144,146]. Collectively, Omics studies have helped implicate the involvement of various signalling pathways and molecules, including but not limited to mammalian target of rapamycin (MTOR), interleukin (IL)-1β, IL-6, tumour necrosis factor alpha (TNF-α), cyclooxygenase-2 (COX-2), transforming growth factor β (TGF-β), insulin-like growth factor

1 (IGF-1) and p38 mitogen-activated protein kinases (MAPK) [146,171-174]. How these pathways and molecules interact to promote an epileptogenic state remains to be defined mechanistically. Currently there is emerging research exploring the overlap between synaptic plasticity and epileptogenesis in relation to these identified pathways and molecules. For instance, tuberous sclerosis complex (TSC) is a genetic disorder characterised by non-malignant tumour formation caused by mutations to the *TSC1* and *TSC2* genes [8]. TSC has been associated with seizures and *TSC1* and *TSC2* encode proteins that inhibit MTOR activity [8]. MTOR forms two complexes, MTOR complex 1 (MTORC1) and 2 (MTORC2), and is involved in cellular metabolism, cell survival, localised protein synthesis and synaptic growth when activated [170]. Of particular interest is the homeostatic plasticity mechanism associated with MTORC1, whereby loss of excitatory AMPAR activity drives a compensatory presynaptic enhancement through brain derived neurotrophic factor (BDNF) retrograde signalling, which is mediated by MTORC1 activity [53,175,176]. Wondolowski and Dickman [8] have proposed that hyperactive MTORC1 could potentially promote hyperexcitability and may be connected to epileptogenesis. Therefore, defining synaptic plasticity modifications and investigating these mechanisms in the context of epileptogenesis may enable a better understanding of how an epileptogenic state is established following brain insults.

1.8. Thesis aims

As the brain operates in a narrow activity window between an epileptic and comatose state, a tight balancing act of maintaining brain activity levels is required by negative feedback mechanisms such as synaptic scaling [5]. Epilepsy is characterised by excessive or highly synchronised neuronal activity and has been speculated to involve a weakened or failed homeostatic signalling response [111,177]. Currently, the mechanisms governing epileptogenesis

remain poorly understood, however, there are homeostatic signalling genes/proteins either involved or downstream targets of identified epileptogenic genes or molecules, such as MTOR, SCN1A, CACNA1A and KCNMA1[7,73,176,178]. Thus, current understanding of epilepsy disease mechanisms could benefit from an in-depth analysis of homeostatic plasticity pathways and synaptic scaling events.

With our current capacity to explore the phosphoproteome in-depth, there is the opportunity to discover the key phospho-signalling events that drive homeostatic regulation and epileptic seizures. Bioinformatic analysis also has the capacity to enable the identification of key signalling pathways and protein kinases involved in both epilepsy and homeostatic plasticity.

My hypothesis is that epilepsy and synaptic downscaling have shared signalling mechanisms which can be elucidated using phosphoproteomics and proteomics analyses. The hypothesis will be tested with the following aims:

1) Perform a deep phosphoproteomic and proteomic analysis of an early epileptogenesis mouse model

2) Define the temporal changes to the phosphoproteome and proteome in a model of synaptic downscaling.

3) Compare the results of the epileptogenesis and downscaling studies to determine features specific to each model

Chapter 2. Materials and Methods

Note that the methods related to a submitted manuscript in chapter 3 are not presented here. All other methods are presented here.

2.1 Materials

Unless otherwise indicated, all stock solutions were prepared with reverse osmosis double distilled, 18 MΩ water obtained from the Millipore Milli-Q® Direct Water Purification System (MQW) [Darmstadt, Germany].

2.1.1 Mammalian tissue culture

Consumable plasticware for tissue culture was sourced from Falcon® [Corning, NY]. Neurobasal Media (NM), trypsin, sodium-pyruvate, Hank's balanced salt solution (HBSS), B-27 supplement, GlutaMAX™-1 supplement, Poly-D-Lysine, B27™ supplement, foetal bovine serum (FBS), TrypLE™ Select Enzyme and Penicillin-Streptomycin (Pen/Strep) were from Gibco™ [Waltham, MA]. Deoxyribonuclease I (DNaseI), 4-[2-hydroxyethyl]-1-piperazineethanesulfonic acid (HEPES), and 45% glucose solution were from Sigma-Aldrich® [Darmstadt, Germany]. Cell strainers (100 μM, Sterile) was from Thermo Fisher Scientific™ [Waltham, MA]. Minisart® 0.22 μM Syringe Filter was from Sartorius [Göttingen, Germany]. 250 mL Nalgene™ Rapid-Flow™ Sterile 0.22 μM Filter Units were from Thermo Fisher Scientific™ [Waltham, MA]. MQW, 1.5 mL Eppendorf tubes [Hamburg, Germany] and plugged and unplugged glass Pasteur pipettes were autoclaved for sterilisation prior to use in tissue culture.

2.1.1.1 Drugs and other chemical reagents

Everolimus (EvLS) was from Selleck Chemicals [Houston, TX]. Sterile dimethyl sulfoxide (DMSO), HEPES, ethylene glycol-bis(β-aminoethyl ether)-N,N,N0,N0-tetraacetic acid

(EGTA), ethylenediaminetetraacetic acid (EDTA) and Phenylmethylsulfonyl fluoride (PMSF) were from Sigma-Aldrich® [Darmstadt, Germany]. The cOmplete™, EDTA-free Protease Inhibitor Cocktail and PhosSTOP™ were from Roche [Darmstadt, Germany]. Bic was from Tocris [Bristol, UK]. Sodium dodecyl sulfate (SDS) solution was from Bio-Rad [Hercules, CA]. Tergazyme was from Alconox® [NY, NY]. All chemicals and reagents, except where otherwise indicated, were of high purity (≥ 98%).

2.1.2 Protein Biochemistry

Low protein bind tubes (0.6 mL, 1.7 mL and 2 mL) and 10 µL pipette tips were used for all proteomics work and were from Axygen® [Corning, NY]. Trifluoroacetic acid (TFA), anhydrous acetonitrile, 50 % hydroxylamine solution, iodoacetamide, triethylammonium bicarbonate (TEAB), HEPES, TrypZean, PHOS-Select™ Iron Affinity Gel, tris(2-carboxyethyl) phosphine (TCEP) were from Sigma-Aldrich® [Darmstadt, Germany]. Methanol was from Honeywell [Charlotte, NC]. Glycolic acid and acetonitrile were from Fluka [The TMTpro™-16 plex Label Reagent Sets and TMTpro™ 18 plex label reagents were from Thermo Fisher Scientific™ [Waltham, MA]. Lysyl Endopeptidase® (Lys-C) was from FUJIFILM Wako Pure Chemical Corporation [Osaka, Japan]. Titansphere TiO_2 5 µM powder was from GL Sciences [Tokyo, Japan]. ReproSil Gold C18 1.9 µm resin was from Dr Maisch [Ammerbuch, Germany]. Formic acid was from VWR international [Radnor, PA]. Sep-Pak tC18 3cc Vac cartridges (200 mg sorbent) were from Waters [Milford, MA]. Urea was from Astral Scientific [Taren Point, Australia]. Chloroform was from ChemSupply [Port Adelaide, Australia]. All chemicals and reagents except where otherwise indicated, were MS grade or of high purity.

2.1.2.1 Antibodies, gels, and western blot membranes

All secondary horseradish peroxidase-conjugated antibodies were from DAKO [Santa Clara, CA]. The primary anti-β-actin horseradish peroxidase-conjugated antibody was from Sigma-Aldrich® [Darmstadt, Germany]. The primary antibodies anti-p70 S6 kinase and anti-phospho-p70 S6 kinase (T421/S424) were from Cell Signalling Technology® [Danvers, MA]. Precast Mini-PROTEAN® TGX™ gels, SDS Powder, bromophenol blue, Trans-Blot® Turbo™ 0.2 µM nitrocellulose membranes, Tris(hydroxymethyl)aminomethane (Tris), Precision Plus Protein™ all blue standards and 10x Tris/Glycine/SDS buffer were from Bio-Rad [Hercules, CA]. Phosphate buffered saline (PBS) tablets and 2-mercaptoethanol were from MP biomedicals [Irvine, CA]. Glycerol was from ChemSupply [Gillman, Australia]. Acetic acid (glacial) was from Merk [Darmstadt, Germany]. Hydrochloric acid 32% (HCl) was from RCI Labscan [Bangkok, Thailand]. Tween-20 detergent, Ponceau S stain, bovine serum albumin (BSA) and Polyvinylpyrrolidone 40 kDa polymer (PVP-40) was from Sigma-Aldrich® [Darmstadt, Germany]. SuperSignal® West Pico PLUS chemiluminescent substrate kit was from Thermo Fisher Scientific™ [Waltham, MA].

2.2 Animal ethics declaration

All utilised animals were handled in accordance with the approved procedures and guidelines of the relevant governing animal ethics committees. The animal experiments involved in the phosphoproteomics of Bic stimulated *in vitro* mouse primary hippocampal cells (Chapter 5) were conducted with approval from the University of Queensland, Anatomical Biosciences Ethics Committee. All other noted in-house *in vitro* experiments were conducted according to authorised procedures and with ethics approval from the Children's Medical Research Institute/Children's Hospital at Westmead Animal Ethics Committee (projects C377 and C396).

2.3 Experimental overview

The general experimental workflow used for the studies in this thesis is presented below in Figure 2.1. The specific experimental methods sections have been annotated in the Figure.

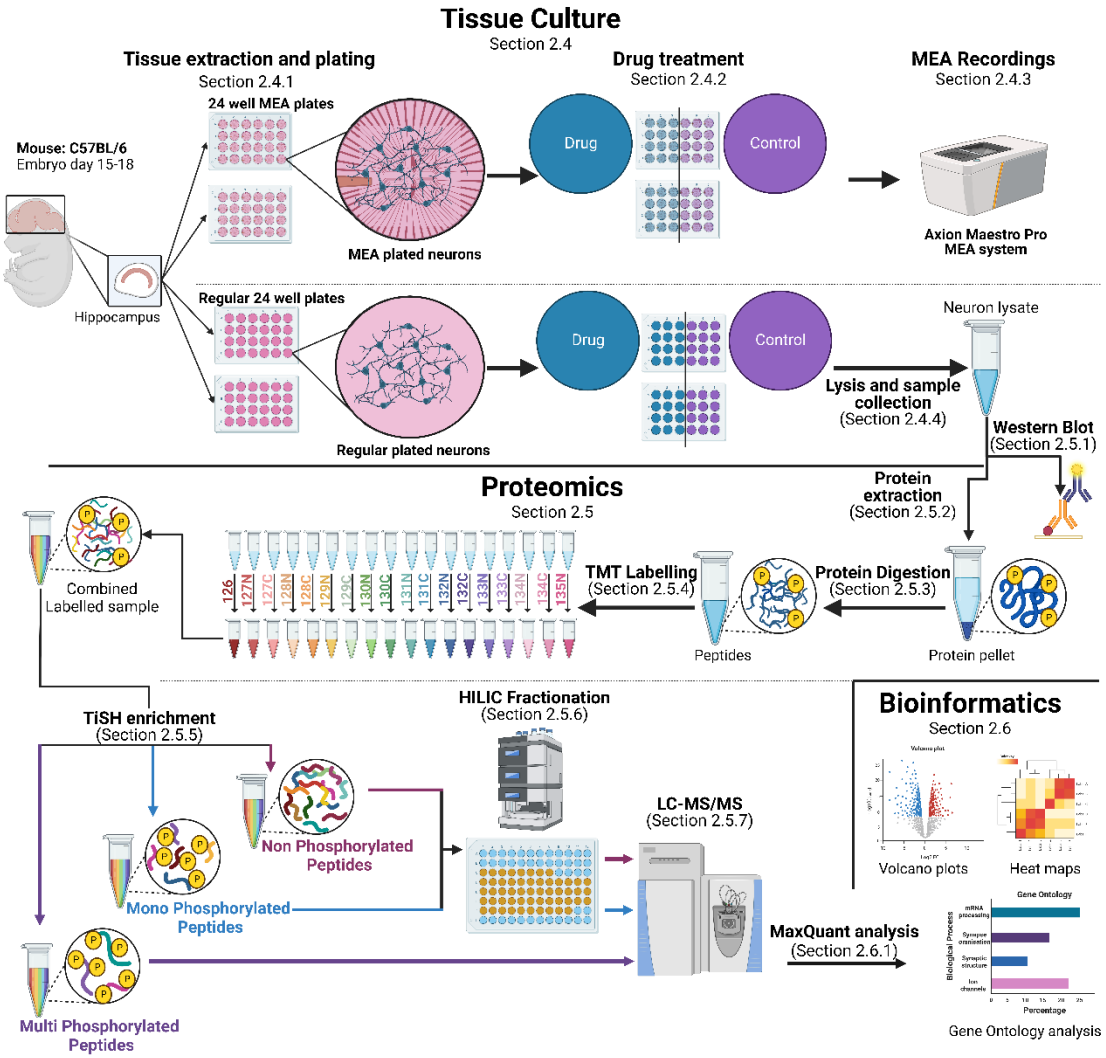

Figure 2.1 Experimental workflow. Figure created with BioRender.com

2.4 Mammalian tissue culture

2.4.1 Primary hippocampal cell culture

Prior to commencing tissue culture work, the following media solutions and materials were prepared. To triturate hippocampal tissue, 9 inch Paster pipettes were plugged with cotton and fire-polished as described by Fath, et al. [179], to form pipettes with three different size openings (wide, intermediate, narrow) which were autoclaved for sterilisation prior to use. To prevent contamination, all media was filter sterilised through a 0.2 μM filter (small volumes required Minisart™ filters, stock solutions required Nalgene™ units). Dissection media (DM) was HBSS (5.3 mM potassium chloride, 0.4 mM potassium phosphate monobasic, 137.9 mM sodium chloride, 0.3 mM sodium phosphate dibasic, 5.6 mM D-glucose, no Ca^{2+} or Mg^{2+}), 100 U/mL Pen/Strep, 1 mM sodium-pyruvate, 20 mM HEPES pH 7.2-7.5, 25 mM glucose. NM5 media was 5% (vol/vol) heat inactivated FBS, 100 U/mL Pen/Strep and 4 mM GlutaMAX™-1 supplement in NM media. NM0 media was 100 U/mL Pen/Strep and 2 mM GlutaMAX™-1 supplement in NM media. Before adding media to neurons, a working solution of NM5 or NM0 was made in a tissue culture flask with 2% (vol/vol) B27™ supplement (to form NM5/B27 and NM0/B27 respectively) and placed in an incubator (37 °C, humidified, 5% CO_2) to gently heat and equilibrate gases for at least 2 hours. Before plating hippocampal cells (Section 2.4.1.1), 24 well MEA plates from Axion Biosystems (CytoView, M384-tMEA-24W or BioCircuit, M384-BIO-24) [Atlanta, GA] were coated with 500 μL Poly-D-Lysine (0.1 mg/mL) and regular 24 well plates were coated with 300 μL Poly-D-Lysine (0.1 mg/mL) and left in an incubator overnight. The following day, coated plates were washed three times with 1 mL sterilised MQW and 500 μL NM5 was dispensed into plate wells before returning the plates back to the incubator. The plates were used within 7 days of preparation and incubation with NM5 media.

2.4.1.1 Hippocampal isolation, plating, and cell maintenance

The hippocampal culture procedure is a method adapted from the Fath, et al. [179] group with minor alterations. The method of culturing hippocampal neurons was primarily the same for the Chapter 5 synaptic downscaling discovery screen and the Chapter 3 *in vitro* epileptogenesis follow up study. The differences were as follows: Chapter 5 neurons were grown in 12 well plates and cells were seeded at a density of approximately 200-250,000 cells per well.

Time-mated C57/Bl/6 mice were bred inhouse to obtain embryos of age E15.5 to E18.5. For 1 dame, 30 mL of NM5/B27 media was prepared 2 h prior to commencing hippocampal isolation. The laminar flow hood, stereoscopic microscope with bottom illumination (Leica WILD M3Z Type S from Leica Microsystems [Wetzlar, Germany]) and surgical equipment (two no. 7 curved Dumont forceps, two no. 5/45 Dumont forceps and one no. 5 straight Dumont forceps from WPI [Sarasota, FL], medium toothed tissue forceps and fine tissue forceps from Aesculap [Tuttlingen, Germany], and two fine scissors from Met-App [Huntingdale, Australia]) were wiped with 70% ethanol (vol/vol) and UV sterilised for at least 20 mins prior to use. The dame was euthanised via CO_2 inhalation and transferred to the sterilised laminar flow hood to remove embryos via caesarean section with fine scissors and both types of tissue forceps as described by Fath, et al. [179]. Keeping the embryos in a 10 cm cold DM filled dish, embryos were decapitated and heads transferred to a 6 cm DM filled dish over ice using fine scissors and fine tissue forceps. The brains were subsequently extracted from heads and transferred to a 6 cm DM filled dish over ice using fine scissors and no. 7. The hippocampus was isolated in a 6 cm DM filled dish over ice using the microscope, no. 5 and 5/45 Dumont forceps. As the hippocampi were collected the tissue was placed into a 50 mL Falcon tube filled with 1.8 mL of DM and kept cold on ice. Once all the hippocampi were harvested, TrypLE was added (diluted 10X to 1X) and the solution was warmed at 37 °C for 30 minutes to aid tissue dissociation. After the 30 min TrypLE incubation, 50 µL DNaseI (10 mg/mL) was added for

30 s to digest DNA and prevent tissue clumping. The tissue was rinsed three times with 2 mL heated NM5/B27 media to remove DNase and TrypLE solution. The hippocampi were then gently triturated in 2 mL NM5/B27 media by slowly pipetting up and down 10 times with each fire polished pipette size, beginning with the widest opening and finishing with the fine opening pipette to obtain a homogenised solution. The homogenised hippocampal cell solution was strained through a 100 µM cell strainer and the strainer rinsed with 1 mL NM5/B27. A 10 µL volume was removed from hippocampal cell solution to count cells with a hemacytometer. Each well was seeded with 70,000 cells in 500 µL NM5/B27 (both MEA and regular plates) and left overnight in incubator. The following day, NM5/B27 media was aspirated and replaced with 1 mL of prepared NM0/B27 media. No media changes occurred until days *in vitro* (DIV) had reached 6, following DIV6, 50% of the media volume was changed for fresh NM0/B27 twice a week until required. When working with multiple plates, the media from plates was exchanged one at a time, leaving plates outside the incubator for the minimal time necessary.

MEA plates were re-used no more than ten times and cleaned in between using a combination of 0.5 % Trypsin-EDTA solution, 10 mg/mL Tergazyme solution and 70% ethanol.

2.4.2 Drug treatments

The drug stock solutions were prepared in advanced at 1,000 times the required concentration, aliquoted, and stored in accordance with manufacturer's recommendations. Bic was dissolved in DMSO and stored as a 20 mM stock, EvLS was dissolved in DMSO and stored as a 50 µM stock. For the Chapter 5 Synaptic downscaling discovery screen Bic was dissolved in MQW and stored as a 20 mM stock.

The day before a chemical stimulation, on DIV13-14, half of the media was changed, and the plated neurons were allowed to adjust to the new media overnight. The following day, drugs

were injected directly into the equilibrated media to perform a 1,000 fold dilution and achieve the desired concentration. For Bic stimulations, 20 mM stock was diluted to 20 µM in 0.2% DMSO. EvLS was diluted to 50 nM. Combined Bic and EvLS treatments were diluted to 20 µM and 50 nM, respectively in 0.2% DMSO. DMSO controls were diluted to a media concentration of 0.2 %. For the Chapter 5 Synaptic downscaling discovery screen MQW served as the Bic control.

MEA recordings were taken as required (Section 2.4.3). No further media changes were performed following drug stimulation. All other drug treatments were performed in like manner to achieve desired final concentrations from the working stock concentration.

2.4.3 MEA recordings

Neuron mEPSCs were measured using the Maestro Pro (Maestro-316) MEA system with AxIS BioCore version 4B and AxIS version 3.6.1.14 from Axion BioSystems [Atlanta, GA]. Plates were kept at 37 °C and 5% CO_2 with the built-in incubator during recordings. No electrical stimulation was applied to the plate at any time. The default configured processing settings for neural network detection were implemented, using the neural spikes analog mode setting, a 3 kHz Kaiser window digital low pass filter, 200 Hz IIR digital high pass filter, a -5.48 E^{-8} V/sample voltage scale, 12.5 kHz sampling frequency and median referencing method. The spike detector settings used was the adaptive threshold crossing method using a spike threshold set to 6, threshold status was variable, pre-spike duration was 0.84 ms, post-spike duration was 2.16 ms, coincident event filter was default (well), coincidence occurrence threshold was 4 electrodes, coincidence event window was 160 µs, sample overlap was not allowed and the spike count interval was 1 s. The burst detector settings used was the inter-spike interval threshold burst detection algorithm, 100 ms maximum inter-spike interval, minimum number of spikes was 5, synchrony window was 20 ms and network burst detection was not enabled.

The statistics compiler settings were default using 18 kΩ minimum covered resistance and a minimum spike rate for active electrode of 5 spikes/minute.

The software generated advanced statistics compiler output, which included the electrode burst lists, spike counts, and network burst lists, was used for MEA data analysis.

2.4.3.1 Data collection and analysis for MEA recordings

The mean firing rate and the average number of bursts was recorded for the eight wells corresponding to the respective treatment group prior to and following stimulation at the designated timepoints (Figure 3.10A). The mean firing rate and number of bursts was averaged for a baseline reading for all wells prior to stimulation and designated the "average plate pre-stim value". The mean firing rate and number of bursts was also averaged for a baseline reading for the eight wells allocated to each treatment prior to stimulation and designated the "average pre-stim treatment value" for the control, Bic and Bic/EvLS treatments, respectively. The mean firing rate and burst MEA data was collected for each timepoint following stimulation. To normalise the MEA readings for each plate recording, the raw pre- and post-stim values for each timepoint was divided by the average pre-stim treatment value for the respective condition. This value was subsequently multiplied by the average plate pre-stim value. This process was repeated to obtain a normalised pre- and post-stim value for each treatment at every timepoint.

These data processing steps were completed using MS excel and Graph Pad Prism version 9.2.0 for figure generation.

2.4.4 Neuron lysis and sample collection

At the designated timepoint, media was vacuum aspirated from the required well and neuron samples were collected with the addition of 100 µL neuron lysis buffer (2% SDS, 50 mM HEPES at pH 7.4, 2 mM EGTA, 2 mM EDTA, cOmplete™ EDTA-free Protease Inhibitor Cocktail, 2 mM PMSF, and PhosSTOP). Wells were scraped on each axis and the lysates were collected and stored at -20 °C until required.

2.5 Protein Biochemistry

2.5.1 Western Blot

2.5.1.1 SDS-polyacrylamide gel electrophoresis

Protein lysates were split into two samples. Eighty percent of the sample was used for proteomics analysis (section 2.5.2) and the remaining twenty percent was reserved for western blotting (section 2.5.1). Prior to western blotting or SDS-polyacrylamide gel electrophoresis (SDS-PAGE), the protein concentration of the original lysate was determined during proteomics analysis through UV absorbance at 280 nm (section 2.5.3). The UV absorbance at 280 nm was used to determine the amount of protein in the western blot samples.

Frozen protein lysates were slowly thawed on ice and centrifuged at 13,000 rpm and 4 °C for 10-15 mins, to remove insoluble cell debris. The desired amount of protein was then removed from the samples and into a separate tube for mixing with Laemmli sample buffer (0.375 M Tris pH 6.8, 4 mg/ml Bromophenol blue, 10 % glycerol, 2 mM EGTA and 8 % 2-mercaptoethanol) for SDS-PAGE separation. Samples were then boiled in buffer for 5 min at 85 °C and quickly spun down on a benchtop centrifuge prior to loading in wells. Precast Mini-PROTEAN® TGX™ gels of either 10% or 12% acrylamide, depending on proteins of interest

and resolution required, were used for the SDS-PAGE separation. The precast gels were loaded into a Mini PROTEAN® Tetra Cell tank from Bio-Rad [Hercules, CA] and filled with 50 mM Tris pH 8.3 in the lower reservoir and 25 mM Tris pH 8.3, 190 mM glycine, 0.1 % SDS in the upper reservoir. Samples were loaded in to designated wells and bookended with 4 µL and 2 µL of prestained protein molecular weight markers (Precision Plus Protein™ all blue standards). Gels were run at 150 V for approximately an 1 h or until sufficiently resolved as judged by the dye front and markers.

2.5.1.2 Membrane transfer

Proteins were transferred from the SDS-PAGE gel to a Mini Trans-Blot® Turbo™ 0.2 µm nitrocellulose membrane using the Trans-Blot® Turbo™ Transfer System (Bio-Rad [Hercules, CA]). Following the packaging directions, the gel was sandwiched horizontally between the "bottom" and "top" Mini Trans-Blot sections and placed directly on the Turbo transfer cassette. A small roller was used to gently push out air bubbles caught between the layers before closing the cassette and placing into the system. The default "Mixed MW" and "Mini" setting was used for a mini membrane transfer of the proteins to the membrane. When the transfer had finished, the membrane was stained with Ponceau S red stain (0.5 % Ponceau S powder in 1 % Acetic acid) for 10 min and rinsed with water to verify successful protein transfer. To prepare for antibody probing, the nitrocellulose membrane was incubated on an orbital shaker at 4 °C overnight in blocking buffer (5% (w/v) BSA, 0.5% (w/v) PVP-40 in PBS solution with 0.1% Tween-20 (PBST)).

2.5.1.3 Antibody probing

The primary antibodies were used in the following concentrations: anti-Rabbit secondary antibody, 1:10 000; anti-β-actin primary antibody, 1:50,000; anti-p70 S6 kinase primary

antibody, 1:250; anti-phospho-p70 S6 kinase (T421/S424) primary antibody, 1:250. The antibody solutions were prepared to the appropriate concentration in PBST.

After membranes had blocked overnight in blocking buffer, the buffer solution was discarded. Depending on the molecular weight of the target protein, the membrane could be cut in half to probe for both the low molecular weight housekeeping protein (β-actin, 43 kDa) and a higher molecular weight protein of interest (e.g. p70 S6 kinase, 70 kDa), using the bookending protein ladders to guide the cut. The primary antibody PBST solution was added to the membrane and incubated at 25 °C with orbital rotation and shaking for 1 h. Following primary antibody incubation, the membrane was rinsed three times with 25 mL PBST for 5 min intervals with orbital rotation. The rinsed anti-β-actin antibody incubated membrane was then incubated with 10 mL ECL reagent (1:1, Peroxide: Luminol solution from the SuperSignal® West Pico PLUS chemiluminescent substrate kit) for 5 min. Other membranes were then incubated with the anti-Rabbit secondary antibody solution and incubated at 25 °C with orbital rotation and shaking for 1 h. The membrane was rinsed three times with 25 mL PBST for 5 min intervals with orbital rotation followed by a 5 min incubation with 10 mL of ECL reagent. After ECL incubation, the blot was shielded from light in a sealed non-transparent container. The blot was read by exposure in the ChemiDoc™ Touch Imaging System from Bio-Rad [Hercules, CA], at multiple exposure times to optimise chemiluminescent signal.

2.5.1.4 Densitometry and normalisation of relative protein expression

Analysis of the western blot images was performed on the Image lab v6.1 software by Bio-Rad [Hercules, CA]. To perform densitometry analysis, the volume tool in the Image lab analysis tool box was implemented. For each protein blot, the DMSO control band was used as the reference sample and the Bic and Bic/EvLS bands were the unknown bands. The software then

generated a relative expression value for the Bic and Bic/EvLS treatments using the DMSO as the point of reference.

The output was then processed using MS excel for data normalisation. To normalise the relative protein expression values against actin, the relative expression value was averaged for all treatments in a replicate for both the p70 S6 kinase protein and phospho-protein respectively, denoted "average replicate protein expression". The raw relative expression for either phospho- or p70 S6 kinase protein was then divided against the raw actin relative expression for the respective treatment and multiplied by the corresponding average replicate protein expression, denoted the "actin adjusted value". The actin adjusted value for the Bic and Bic/EvLS treatments were then divided by the control actin adjusted value in each replicate for a normalised value.

The normalised p70 S6 kinase protein and phospho-protein values were tested for significance using an unpaired, two-tailed t-test with welch correction. The statistical analysis and subsequent figure generation was performed using Graph Pad Prism version 9.2.0.

2.5.2 Protein Extraction

2.5.2.1 Reduction and Alkylation

For the Chapter 5 MS experiments, neuronal lysate samples from drug treated cultured neurons, as described in section 2.4.2 were reduced in 10 mM TCEP at 85 °C for 10 min with mixing at 1200 rpm on a ThermoMixer® C from Eppendorf [Hamburg, Germany]. Samples were returned to room temperature on ice and subsequently alkylated with 25 mM iodoacetamide at 22 °C for 30 minutes in the dark with mixing at 1200 rpm on a ThermoMixer® C.

2.5.2.2 Chloroform-methanol protein precipitation

Following reduction and alkylation, proteins were precipitated from samples using chloroform-methanol extraction as described by Wessel and Flugge [180]. Isolated protein precipitates were air dried on a ThermoMixer® C at 37 °C for about 1 to 2 hours with no mixing.

2.5.3 Protein digestion

Protein precipitates were dissolved in a 20 µL urea buffer solution (7.8 M urea, 50 mM TEAB). As approximately 100 µg of protein is expected from each well on a 12 well plate, and the cell lysate from 3 wells was combined to form one sample, 138 µg of Lys-C was incorporated into the urea buffer solution to digest the protein content from 46 samples. The samples were digested for 8 hours at 25 °C with mixing at 900 rpm on a ThermoMixer® C. Samples were diluted with 140 µL buffered solution (100 mM HEPES at pH 8) along with TrypZean at an estimated ratio of 1 ug per 100 ug protein. The samples were subsequently digested at 37 °C with mixing at 900 rpm on a ThermoMixer® C. The trypsin digestion was repeated with an additional 10 µL buffered solution (100 mM HEPES at pH 8) along with TrypZean using the same amount as above and was incubated for 8 hours under the same conditions. The peptide concentration was estimated by absorption at 280 nm on a N60 Nanophotometer® from Implen [München,Germany].

2.5.4 TMT Labelling

2.5.4.1 TMT Labelling for Chapter 5 bicuculline samples

Based on the protein concentration estimates, 300 µg of peptide was aliquoted into new tubes and volumes were adjusted to 100 µL with MQW. After activating two TMTpro-16 plex™ Label Reagent Sets and two TMTpro-17 plex™ label reagents with anhydrous acetonitrile, 20 µL of a dissolved TMT reagent vial was used to label 300 µg of sample and incubated at 25 °C for 2 h with mixing at 900 rpm. Samples were labelled in accordance with the schemes

described below. To ensure completeness of labelling, 0.3 µL was taken from samples and tested by short LC-MS/MS analysis to confirm labelling was > 98%. Excess TMT reagent in samples was quenched with 8 µL of 5% hydroxylamine solution for 15 minutes at 25 °C with mixing at 1200 rpm. Samples were then pooled into one of two designated group for a 17-plex experiment using two TMT 17-plex reagent sets, as described below. The pooled samples were acidified with 100% formic acid to pH < 3 and the volume was reduced to 150 µL under vacuum centrifugation with an EZ2 GeneVac® evaporator (Genevac Ltd [Ipswich, United Kingdom]). The samples were diluted to 2 mL with 0.1% trifluoracetic acid and desalted using one Sep-Pak tC18 3cc Vac cartridge per sample.

A 17-plex TMT labelling scheme was used for the Bic samples (Table 2). A 600 µg reference sample was made by combining 37.5 µg of protein sample from the eight timepoints from two replicates. This reference sample was labelled with two 134C TMT tags, mixed thoroughly and split in half between the group 1 and 2 TMT 17-plexes. The group 1 TMT 17-plex consisted of replicates one and two which were labelled in accordance with the scheme outlined in Table 2. The group 2 TMT 17-plex consisted of replicates three and four which were labelled in accordance with the scheme outlined in Table 2.The TMT kit lot numbers were XC344112 and XD345167.

Table 2. TMT 17-plex labelling scheme for Chapter 5 synaptic downscaling samples

Replicate ID	Control / Bic	Timepoint	TMT Pro label	Group number
Bio-replicate 1	Control (untreated)	0 min	126	Group 1
Bio-replicate 1	Bic	5 min	127**N**	Group 1
Bio-replicate 1	Bic	30 min	127**C**	Group 1
Bio-replicate 1	Bic	1 h	128**N**	Group 1
Bio-replicate 1	Bic	2 h	128**C**	Group 1
Bio-replicate 1	Bic	6 h	129**N**	Group 1
Bio-replicate 1	Bic	24 h	129**C**	Group 1
Bio-replicate 1	Bic	48 h	130**N**	Group 1
Bio-replicate 2	Control (untreated)	0 min	130**C**	Group 1

Bio-replicate 2	Bic	5 min	131**N**	Group 1
Bio-replicate 2	Bic	30 min	131**C**	Group 1
Bio-replicate 2	Bic	1 h	132**N**	Group 1
Bio-replicate 2	Bic	2 h	132**C**	Group 1
Bio-replicate 2	Bic	6 h	133**N**	Group 1
Bio-replicate 2	Bic	24 h	133**C**	Group 1
Bio-replicate 2	Bic	48 h	134**N**	Group 1
Bio-replicate 3	Control (untreated)	0 min	126	Group 2
Bio-replicate 3	Bic	5 min	127**N**	Group 2
Bio-replicate 3	Bic	30 min	127**C**	Group 2
Bio-replicate 3	Bic	1 h	128**N**	Group 2
Bio-replicate 3	Bic	2 h	128**C**	Group 2
Bio-replicate 3	Bic	6 h	129**N**	Group 2
Bio-replicate 3	Bic	24 h	129**C**	Group 2
Bio-replicate 3	Bic	48 h	130**N**	Group 2
Bio-replicate 4	Control (untreated)	0 min	130**C**	Group 2
Bio-replicate 4	Bic	5 min	131**N**	Group 2
Bio-replicate 4	Bic	30 min	131**C**	Group 2
Bio-replicate 4	Bic	1 h	132**N**	Group 2
Bio-replicate 4	Bic	2 h	132**C**	Group 2
Bio-replicate 4	Bic	6 h	133**N**	Group 2
Bio-replicate 4	Bic	24 h	133**C**	Group 2
Bio-replicate 4	Bic	48 h	134**N**	Group 2
Reference Sample	-	-	134**C**	Group 1
Reference Sample	-	-	134**C**	Group 2

2.5.5 TiSH phosphopeptide enrichment

To obtain fractions enriched in non-, mono- and multi-phosphorylated peptides from each timepoint, the samples were applied to the "TiSH" method of phosphopeptide enrichment as described in Engholm-Keller and Larsen [103]. All recovered multi- and mono-phosphorylated peptides were desalted, with multi-phosphorylated samples ready for liquid chromatography tandem mass spectrometry (LC-MS/MS) analysis (Section 2.5.7). Mono-phosphorylated peptides were subjected to hydrophilic interaction chromatography (HILIC) (Section 2.5.6) for further fractionation prior to LC-MS/MS analysis. The non-phosphorylated peptides which do

not bind to titanium dioxide were collected from the first TiSH wash step. From each pooled non-phosphorylated peptide group, 150 µg of sample was desalted and fractionated by HILIC prior to LC-MS/MS analysis. There were a total of 24 mono- and non-phosphorylated HILIC fractions selected for analysed.

2.5.6 HILIC Fractionation

HILIC sample fractionation was completed using a Dionex UltiMate 3000 HPLC system (Thermo Fisher Scientific™ [Waltham, MA]) with a TSKgel Amide-80 1 mm inside diameter x 250 mm long column (Tosoh Bioscience [Tokyo, Japan]). All desalted non- and mono-phosphorylated samples were prepared to 150 µL in 90% acetonitrile, 9.9% water, 0.1% trifluoracetic acid (HILIC Buffer A) for the HILIC fractionation. Each non- and mono-phosphorylated sample was fractionated separately. Samples were injected at a flow rate of 60 µL/min with buffer A at 100% for 10 min. The gradient was from 100% HILIC buffer A to 40 % HILIC buffer B (99.9% water and 0.1% trifluoracetic acid) for 35 minutes at a flow rate of 50 µL/min, then to 80% buffer B for 3 minutes then back to 100% buffer A for 12 minutes. Sample fractions were collected in 30 s intervals into a 96 well plate using a Probot by LC Packings (Dionex™ [Waltham, MA]) controlled by µCarrier 2.0. Individual and pooled fractions were chosen for LC-MS/MS analysis based on the intensity of the ultraviolet (UV) signal at 214 nm. The 96 well plates were dried under vacuum centrifugation and the 24 chosen wells were dissolved in 5.5 µL 0.1% formic acid for LC-MS/MS analysis.

2.5.7 Mass Spectrometry

LC-MS/MS for all samples was completed with a Dionex UltiMate 3000 RSLC nano system and Q Exactive Plus hybrid quadrupole-orbitrap mass spectrometer (Thermo Fisher

Scientific™ [Waltham, MA]). The enriched multi-phosphorylated sample and the sample content of the enriched non- and mono-phosphorylated HILIC fractions were loaded directly onto an in-house 300 × 0.075 mm column packed with ReproSil Gold C18 1.9 µm resin [Dr Maisch, Germany]. A column oven (PRSO-V1, Sonation lab solutions [Biberach, Germany]) combined to the nano flex ion source maintained the column at 50 °C with an electrospray operating at 2.3 kV. The S lens radio frequency level was 50 and capillary temperature was 250 °C. For MS analysis, 5 µL from all samples were injected into a 20 µL loop and loaded onto the column. The sample content was eluted from the column using a reverse phase gradient with reversed phase buffer A (0.1% formic acid in water) and buffer B (0.1% formic acid, 90% acetonitrile, 9.9% water). There were two gradient variations used for MS acquisition. Briefly, all mono- and multi phosphorylation enriched samples were subjected to a 120 min gradient beginning with 99% buffer A and 1% buffer B separation for 25 min at 300 nL/min. The flowrate was then reduced to 250 nL/min and the gradient was shifted from 95% buffer A to 75% buffer A in 74 min to 65% buffer A in 8 min, to 1% buffer A in 1 min and held for 2 min, the gradient shifted to 99% buffer A in 1 min and held for 8 min, the flow rate was increased to 300 nL/min for equilibration at the end of the run. The non-phosphorylated fractions were subjected to a 140 min gradient beginning with 99% buffer A and 1% buffer B separation for 18.5 min at 300 nL/min. The flow rate was then reduced to 250 nL/min and the gradient was shifted from 94% buffer A to 72% buffer A in 101.5 min, to 65% buffer A in 8 min, to 1% buffer A in 1 min and held for 2 min, the gradient shifted to 99% buffer A in 1 min and held for 8 min, the flow rate was increased to 300 nL/min for equilibration at the end of the run. MS acquisition was performed throughout the 120 min and 140 min analyses.

Data-dependant acquisition LC-MS/MS was performed on all samples. In both the 120 min and 140 min methods, MS scans were at a resolution of 70,000 with an automatic gain control target of 1,000,000 for a maximum ion time of 100 ms from m/z 375 to 1500. The MS/MS

scans were at a resolution of 35,000 with an automatic gain control target of 200,000. The maximum ion time was 115 ms for the 120 min method and 100 ms for the 140 min method. For both methods, the loop count was 12 and the first mass was fixed at m/z 120. For the 120 min method the isolation window was 1.2 m/z, and the normalized collision energy was 34. For the 140 min method the isolation window was 1.1 m/z, and the normalized collision energy was 31. Singly charged ions and those with charge >8 were excluded from MS/MS and dynamic exclusion was for 35 s in the 120 min method and 37 s in the 140 min method.

2.5.8 Targeted mass spectrometry analysis of SLK phosphorylation and protein levels

These experimental steps follow the tryptic digestion of protein outlined in Chapter 3 Methods section "Sample processing for proteomics analysis". Approximately 600 ug each from the sixteen mock and pilocarpine samples (mock and pilo 4 and 24h) were purified by solid phase extraction (Oasis 30 mg sorbent, Waters) and enriched for phosphopeptides using titanium dioxide enrichment as previously described [103] and as above, without enriching for multi-phosphorylated peptides. The unbound peptide was collected and used to target non-phosphorylated peptides.

One third of the enriched phosphopeptides in each sample was injected in 5 µL into a Dionex UltiMate 3000 RSLC nano system and analysed by a Q Exactive Plus hybrid quadrupole-orbitrap mass spectrometer (Thermo Fisher Scientific). The column was 300 × 0.075 mm fused silica with a pulled tip and packed with ReproSil Pur C18 AQ 1.9 µm resin [Dr Maisch, Germany]. The electrospray gradient was the same 120 min method described in Section 2.5.7. Parallel reaction monitoring MS was performed for 120 min. The MS/MS resolution was 70,000, the automatic gain control target was 3,000,000, the maximum ion time was 220 ms,

the isolation window was 0.7 m/z and the normalised collision energy was 30. Approximately 2500 ng of non-phosphopeptide in 3.5 µL was injected using a different gradient for analysis. The sample loading was in 99% A for 17.5 min at 300 nL/min, then the gradient was to 6% B in 1 min at 250 nL/min, to 28% B in 101.5 min, and then the gradient continued the same as for phosphopeptides to a total length 140 min. The parallel reaction monitoring MS settings were the same as for phosphopeptides.

SLK peptides were selected based results from the discovery screen in Chapter 3 section 3.3, prior screens in the laboratory and from the SRMAtlas library[181]. The final target list of SLK peptides and phosphopeptides were chosen based on favourable peptide charge, intensity and length[182]. As phosphorylation is a highly dynamic post translational modification, non-SLK control peptides with stable levels of phosphorylation were required for data normalisation[183]. These were phosphorylated peptides with low level absolute $\log_2$ fold changes pulled from the data using the "getSPS()" function from the PhosR package[184]. Two peptides from non-phosphorylated proteins tubulin alpha-4A chain and cytoplasmic dynein 1 heavy chain 1 were also included as loading controls to determine SLK protein level.

Trial analyses were performed to optimise RT windows and undetectable or low-quality peptides were removed from the target list.

Each peptide was targeted within a 12 min or wider retention time window. All MS files were searched using MaxQuant 1.6.7.0 to create a library of search results as evidence of correct identification and retention time. Within MaxQuant, the *Mus musculus* reference proteome with 55,315 entries, downloaded from UniProt on August 11 2022, was used, as well as the in-built contaminants fasta file. Oxidation of Met, acetylation of N-terminal residues, phosphorylation of Ser/Thr/Tyr and deamidation of Asn/Gln were variable modifications and carbamidomethylation of Cys was a fixed modification. Minimum peptide length was 6,

trypsin/P was used for enzyme specificity with a maximum of 2 missed cleavages. All other MaxQuant settings were default. The MaxQuant msms.txt output file and the raw files were examined in Skyline 20.1.0.76. Five or more fragment ions and a maximum of 2 ppm mass accuracy was required for each peptide. The quantitative values for each peptide were exported to Excel and the peptide intensities were normalised to the loading controls. The data was then exported to Prism 9.0.2 for statistical analysis. Multiple unpaired t-tests were performed and the P value was adjusted with a false discovery rate of 5%. All data with an adjusted P value < 0.05 was considered significant. Proteomic data including skyline analysis files and raw MS files are publicly available at PanoramaWeb, ProteomeXchange ID: PXD036547.

2.6 Data analysis for Chapter 5 synaptic downscaling discovery screen

2.6.1 MaxQuant protein data search

The raw LC-MS/MS data was processed with MaxQuant v1.6.7 (Tyanova, et al. [185]) using the following settings. Variable modifications were oxidation of Met, acetylation of protein N-terminus, deamidation of Asn/Gln and phosphorylation of Ser/Thr/Tyr. Carbamidomethyl of Cys was a fixed modification. Digestion was set to Trypsin/P with a maximum of 3 missed cleavages. The *Mus musculus* reference proteome with 63,667 entries of canonical and isoform sequences downloaded July 29 2022 was used as well as the inbuilt contaminants file. Minimum peptide length was 6 and maximum peptide mass was 6000 Da. Second peptides and dependent peptides searches were enabled. Peptide spectrum matching and protein false discovery rates were set to 0.01. Minimum score for modified peptides was 40. Modified peptides and counterpart non-modified peptides were excluded from protein quantification. All other parameters were default.

2.6.2 Differential abundance analysis of proteins

2.6.2.1 Data cleaning

The "proteinGroups.txt" output file from MaxQuant were processed. Each protein group must have at least one unique peptide. Any proteins were removed from further analysis if they match any entries in the contaminants or the reverse sequence decoy databases, in which the protein accession starts with CON__ or REV__ prefixes respectively. The "reporter intensity corrected" column were used for further analysis. Proteins with any missing values were removed from the analysis.

2.6.2.2 Identifying a representative UniProt accession for each protein group

The following rules from Engholm-Keller, et al. [95]were used to identify a representative UniProt accession for each protein group.

1. For proteins that mapped to multiple UniProtKB protein accessions, the accession with the highest "protein existence (PE)" value was kept as the best evidence (http://www.uniprot.org/help/protein_existence). Where the protein accession was an isoform (therefore lacking PE information), the PE value was taken from the parent protein.

2. When the PE value was equal, a Swiss-Prot (sp) entry was taken over a TrEMBL (tr) entry.

3. If both entries were Swiss-Prot, the non-isoform was selected.

4. If both entries were isoforms, the longest isoform was selected.

2.6.2.3 Data normalisation

First, samples were $\log_2$ transformed and between sample normalization were performed using the "scaled" normalization from the 'limma' R package. Second, to remove the batch effects from biological data, the remove unwanted variation (RUV) R package [186] was used to remove batch effects. The method relies on having a set of endogenous negative control proteins, which are proteins with little changes in protein abundances between different cell types or experimental treatments. For this study, a set of 500 empirical negative control proteins with little or no change in protein expression across samples (q-value < 0.05) were identified from an initial ANOVA test. The RUVIII method [187] was used to remove the unwanted variations across the samples and six unwanted components (k = 6) were removed by the tool. The RUVIII method requires the experiment design matrix, a matrix describing the replicates for each treatment condition, and the list of negative control proteins. Differential abundance analysis of proteins was performed using the adjusted abundance matrix. The results from this differential abundance analysis were then used for all analyses.

2.6.2.4 Differential phosphopeptide abundance analysis

Differential abundance analysis of phosphopeptides were performed by comparing each time point with time zero. The statistical analysis was similar to that of the quantitative proteomics analysis above, in which the 'limma' R package[188], linear modelling and empirical Bayes methods was used to calculate the moderated p-values for pairwise comparison of time point. The false discovery rate correction was applied using q-values[189]. Significant differentially expressed phosphopeptides were defined as those with q-values less than 0.05.

2.6.2.5 Normalisation of the phosphosite log fold-change by the host protein's log fold-change

For host protein normalization of the phosphopeptide, the host protein's log_2 fold change was subtracted from the log_2 fold change of the phosphopeptide. The host protein normalized phosphopeptide log_2 fold changes were used for all subsequent analysis.

The statistical significance of the phosphopeptide is also normalised by the host protein's p-value using the Fisher's method to calculate a combined significance q-score[190]. It is not technically a q-value due to less adherence to statistical assumptions and therefore it is a q-score. If the phosphopeptide and protein are changing in the same direction, it means that change in abundance of the phosphopeptide could at least be partially explained by the change in protein abundance. Thus, additional conditions were imposed to lessen the significance of the q-score.

If the direction of the fold change for the phosphopeptide and the direction of the fold change of the protein were the same, the q-value of the phosphopeptide and the q-value of the protein were used directly for normalization using the Fisher's method. This would result in a less statistically significant q-score for the phosphopeptide. If the direction of the log fold change was opposite between phosphopeptide (s) and protein, then 1 minus the protein q-value and the original phosphopeptide q-value were used for normalization using the Fisher's method. This would result in a more significant q-score for the phosphopeptide.

2.6.2.6 KinSwingR

The 'KinSwingR' R library [95] was used to perform kinase-substrate enrichment to infer upstream kinases with up- or down-regulated activities in the experiment. To de-duplicate multi-phosphorylated peptides containing common phosphorylation sites, the highest magnitude log_2 fold change of the phosphorylation site across all phosphopeptides (with

duplicated sites) and the corresponding q-value were kept for KinSwingR analysis. Known kinase-substrate interactions from all mammalian species (from PhosphositePlus version DB5) was used to train kinase-specific scoring matrices. The KinSwingR analysis was then proceeded with default parameters as described in Engholm-Keller, et al. [95].

2.6.3 Analysis of data from Desch et al. 2021

The analysis of data from Desch, et al. [39] were similar to the Chapter 5 Synaptic downscaling, as described above in Section 2.6. The main differences were that the Desch et al. dataset included technical replicates and that the dataset contained missing values which required missing values imputation. The MaxQuant result files were downloaded from the PRIDE repository [191] (PRIDE: PXD021834). Between samples imputations were performed on all biological and technical replicate samples using the cyclic loess normalization as implemented in limma. There were three technical replicate samples for each biological replicate sample. For each protein, the label fee quantification (LFQ) values of the two or three technical replicates of each biological replicate sample were averaged. The single value was used if only one replicate was available. Otherwise, the protein would harbour a missing value for that biological replicate sample. Phosphopeptides with data for all four biological replicates for at least two groups were included for further analysis and missing values imputation using the PhosR library [183]. For site- and condition specific imputation, values were imputed by sampling from empirical normal distribution and estimated based on the mean and standard deviation within each biological replicates group. When not enough data were present within a group for condition specific imputation, global tail-based imputation was used to sample values from the empirical normal distribution with downshifted mean and variance. To remove unwanted variation from the proteomics data, the number of negative control proteins were 500 and the number of unwanted factors removed was 10 (k=10). For the removal of unwanted variation from the phosphoproteomics data, the number of negative control proteins were 500 and the

number of unwanted factors removed was 13 (k=13). After the calculation of $\log_2$ fold-change and statistical significance (q-value) between a pair of time-points, proteins with missing values in any of the biological replicates in any of the two time points were removed from further analysis. All other calculations were similar to the calculations performed for the Chapter 5 synaptic downscaling, as described above in Section 2.6.

2.6.4 Gene ontology enrichment

The following analysis is similar to the gene ontology enrichment described in Chapter 3 Section 3.5.

The significantly regulated phosphopeptides for the seven comparisons designated 5 min, 30 min, 1 h, 2 h, 6 h, 24 h and 48 h were divided into up and down-regulated groups, resulting in fourteen sets. The phosphopeptides were ranked from most significant to least significant and then from largest to smallest quantitative value. The significance ranking value and quantitative ranking value was summed for each phosphopeptide to produce a final combined rank. The gene for each phosphopeptide was extracted to produce a ranked gene list. Redundant gene names were discarded, retaining the highest ranked gene name for each phosphopeptide. The ranked gene lists were submitted as separate up- and down- regulated groups to gProfiler [192] using the 'multi-query' and 'ordered query' options. Note that an ordered query is an iterative process that may not use the entire ranked gene list to obtain significance [192], weighting the output toward the higher ranking genes. The organism was set to *Mus musculus* (version: GRCm39). A custom background was used which consisted of all the genes represented by the proteins detected in both the proteomics and phosphoproteomics. Genes without annotation were included in the background. The significance threshold was $P < 0.05$ and using the gProfiler algorithm for adjustment of multiple hypotheses [193]. The following data sources and

version were used: GO Molecular Function release July 1 2022, GO cellular component release July 1 2022, GO Biological Process release July 1 2022, KEGG release September 5 2022, Reactome annotations Biomart classes September 15 2022 and WikiPathways version September 10 2022.

Significant protein values were also divided into up and down-regulated groups and ranked by both significance and by the magnitude of the quantitative values. For protein groups mapping to multiple genes, the first listed gene was kept and the remaining genes discarded. Redundant genes were also removed before submission. All fourteen up- and down- regulated sets were submitted to gProfiler using the same settings as for phosphopeptides. The full output from gProfiler is supplied in supplementary Appendix 23.

Chapter 3. Proteomic and phosphoproteomic study of early epileptogenesis in a pilocarpine mouse model

3.1 Background

Epileptogenesis is the process by which a normal brain is altered through structural and/or molecular changes to neuronal networks, to generate spontaneous seizures [109,146]. During the process of epileptogenesis, the affected brain becomes increasingly susceptible to seizure activity and can result in the development of chronic epilepsy [109,146]. Plasticity modifications to the neuronal network induced by epileptic seizure activity is suspected to be a major contributor to the pathological state and has been implicated from various epileptogenesis models [194]. Furthermore, the chronically high activity induced by seizures is predicted to trigger the activation of homeostatic mechanisms to revert activity back to the set point, but experimental evidence has been lacking [177]. Many mediators of synaptic scaling have been found to overlap with known epilepsy genes [7], including *CACNA1A*, *MECP2* and *SYNGAP1*. *CACNA1A* encodes a pore forming subunit of a P/Q type calcium channel involved in presynaptic homeostatic plasticity[195]. *MECP2* causes bidirectional synaptic scaling through affecting the activity of AMPAR [75,76]. *SYNGAP1* mediates localised protein synthesis required for synaptic upscaling [78]. However, the connection between epileptogenesis and dysregulated homeostatic plasticity mechanisms remains superficial as relatively little is known about epileptogenic mechanisms, warranting further investigation [177].

Status epilepticus has been defined as an abnormally prolonged seizure resulting from the failed activation of seizure termination mechanisms which can have severe neurological consequences such as neuronal injury and death [196]. Status epilepticus is typically more severe than most seizures experienced by human patients, although the definition has changed over

time [196,197]. In the pilocarpine experimental animal model of epileptogenesis, status epilepticus is chemically induced as the precipitating injury, resulting in chronic epilepsy after a latent period. The pilocarpine model replicates the hippocampal sclerosis damage seen in mesial temporal lobe epilepsy (mTLE) patients [113,151]. For this study, the hippocampus from pilocarpine stimulated mice was removed at 4 and 24h following induced seizure activity. Proteins from the hippocampus were subsequently isolated to perform a phosphoproteomic and proteomic discovery screen of epileptogenesis.

To validate the results of the phosphoproteomic and proteomic discovery screen, a parallel reaction monitoring (PRM) assay was used. PRM, is a type of targeted MS that can be used for a peptide assay. PRM detects user defined peptides, typically identified from a non-targeted MS data acquisition [182,198,199]. PRM is based on the selected reaction monitoring (SRM) assay. Both assays require knowledge of the mass to charge (m/z) ratio and chromatographic retention times (RT) from target-specific peptides (precursor ions) [182,198,199]. SRM also requires the m/z of the product ions [182,198,199] to specifically isolate target ions for fragmentation and detection [182,198,199]. In SRM, 'triple' quadrupoles or quadrupole-ion trap mass spectrometers are used[182]. In PRM, the second mass analyser is replaced with a high-resolution orbitrap mass analyser and a full scan is collected rather than only specific product ions[198,199]. The high-resolution mass analyser enables the PRM assay to obtain high ion specificity and monitor product ions in parallel without prior definition[198,199].

Ste20-like kinase (SLK) peptides were targeted by PRM analysis. SLK, an enzyme involved in dendritic tree development and facilitating inhibitory activity in neuronal networks[200], has been reported to have a decreased expression in human epileptogenic brain lesions [200]. The aim was to explore SLK phosphorylation and protein expression during early epileptogenesis through PRM and provide validation of the quantitative results obtained from the phosphoproteomic and proteomic discovery screen.

Presented as an article manuscript submitted to Cell Reports with minor alterations for integration in thesis:

- Heading and subheadings are numbered in accordance with the style used in thesis.
    - Figure numbering includes chapter number (e.g., Fig 10 in manuscript is Figure 3.10 in thesis)
    - Figure legends are provided below corresponding figure.
- Supplementary materials are presented in the appendix and are referenced as "appendix" and numbered in thesis order of appearance (e.g., Fig S1 in manuscript is Appendix 1 in thesis)
- SLK PRM analysis is presented following the study (Section 3.6-3.8 and Figure 3.9) and is not part of the manuscript submission.
    - The SLK PRM analysis is material published in Royero, P., et al. Circuit-selective cell-autonomous regulation of inhibition in pyramidal neurons by Ste20-like kinase. *Cell reports* **41**, 111757, doi:10.1016/j.celrep.2022.111757 (2022)
    - Only the analysis which validates this study appears below.

3.2 Multiomic analysis of early epileptogenesis in mice reveals phosphorylation and dephosphorylation directed growth and synaptic weakening

Mariella Hurtado Silva[1], Ashley J. van Waardenberg[2], Susanne Schoch[3], Dirk Dietrich[4], Mark E. Graham[1,*]

[1] Synapse Proteomics, Children's Medical Research Institute, The University of Sydney, Westmead, New South Wales, 2145, Australia.

[2] i-Synapse, Cairns, Queensland, 4870, Australia.

[3] Department of Neuropathology, University Hospital Bonn, Section for Translational Epilepsy Research, Bonn, North Rhine-Westphalia, 53127, Germany.

[4] Department of Neurosurgery, University Hospital Bonn, Bonn, North Rhine-Westphalia, 53127, Germany.

[*] Corresponding author: mgraham@cmri.org.au

3.2.1 Abstract

To investigate the phosphorylation-based signalling and protein changes occurring early in epileptogenesis, the hippocampi of mice treated with pilocarpine were examined by quantitative mass spectrometry at 4 and 24 h post-status epilepticus at vast depth. Hundreds of posttranscriptional regulatory proteins were the major early targets of increased phosphorylation. At 24 h, many protein level changes were detected and the phosphoproteome continued to be perturbed. The major targets of decreased phosphorylation at 4 h and 24 h were a subset of postsynaptic density scaffold proteins, ion channels and neurotransmitter receptors.

Many proteins targeted by dephosphorylation at 4 h also had decreased protein abundance at 24 h, indicating a phosphatase-mediated weakening of synapses. Increased translation was indicated by protein changes at 24 h. These observations, and many additional indicators within this multiomic resource, suggest that early epileptogenesis is characterized by signalling that stimulates both growth and a homeostatic response that weakens excitability.

Key words

Epilepsy, epileptogenesis, phosphoproteome, proteome, signalling, posttranscriptional, homeostatic plasticity, postsynaptic density, MTOR

3.3 Introduction

Epileptogenesis constitutes the process by which brain tissue becomes capable of generating spontaneous recurrent seizures [146] and is triggered by genetic factors or a precipitating insult, followed by a latent period before the first observation of a clinical seizure. In experimental animal models of epileptogenesis, induction of status epilepticus (SE) results in chronic recurring seizures after a latent period [201]. Currently, there are no clinically available anti-epileptogenic drugs [146]. The identification of factors involved in the development of chronic epilepsy may lead to new anti-epileptogenesis drugs.

A persistent hypothesis is that epileptic activity arises from excessive positive electrophysiological feedback on excitatory synapses. An imbalance towards excitation may arise from a reduction in inhibitory input or excess of excitatory input. Loss or damage to inhibitory synapses [202] and growth or sprouting that results in new synapses [203,204] may cause positive feedback. However, many neurobiological processes are implicated in epileptogenesis and a focus on excitatory/inhibitory imbalance may be limiting [201]. Inflammation and the

immune response, cell growth, plasticity, oxidative stress and epigenetic reprogramming are all implicated in epileptogenesis and lead to reorganization of circuits via synapse loss, neurite outgrowth, altered synaptic strength, reorganization of the extracellular matrix, damage to the blood-brain barrier, recruitment of inflammatory cells and gliosis [109,171]. Despite this knowledge, the molecular mechanisms and timing of events in epileptogenesis are not clear. Thus, a broad and unbiased view of the protein and signalling landscape is important for further understanding.

Early proteomic studies in animal models were low-depth using two-dimensional electrophoresis [157,160,163]. Using LC-MS/MS, multiple studies have been performed in animal models but were either limited in depth or were only focused on later stages of epileptogenesis [166,167,205]. Using patient samples, a 2020 study identified greater than one hundred differentially expressed proteins in the dentate gyrus [206] and a recent study found hundreds of changes in the hippocampus and cortex of patients [207]. Changes to the transcriptome in animal models [208-213] or in patient samples [214,215] have often been examined because of the ease of access to transcriptomics technology. There has been only limited agreement on changes in gene expression between each study [146,171]. One way forward is to gain a greater understanding of the entire process of epileptogenesis, which includes the early phospho-signalling that is driving mechanisms that lead to changes in protein expression. The same channels and receptors involved in monogenic epilepsy are well known to be functionally regulated by phosphorylation. However, phosphorylation has not been a focus in epilepsy research. Neither has large-scale phosphoproteomics been applied to any stage of epileptogenesis, to our knowledge.

Stimulus-dependent phospho-signalling occurs faster than transcriptomic and proteome changes, is dynamic and can persist to produce a new phosphoproteome status, potentially perpetuating epileptogenic states. Surveying the phosphoproteome can also identify key

protein kinases involved in signalling through modelling of observed changes to phosphorylation sites that conform to kinase motifs [95]. Here, we present a large-scale phosphoproteomics study of hippocampal tissues from the pilocarpine mouse model of epileptogenesis. In addition to pilocarpine-induced signalling, we also identify the signalling induced by diazepam, which was primarily used to terminate behavioural seizures [216,217]. Data analysis revealed, firstly, that SE induced early phosphorylation of proteins involved in posttranscriptional regulation. Secondly, SE induced dephosphorylation of synaptic proteins. These two major themes extended to related protein level changes that supported both growth via translation and synaptic weakening. Through modelling of kinase activity, we predicted activated protein kinases and protein kinase substrates more affected by phosphatase activity. We found evidence for activation of mitogen-activated protein kinase (MAPK) pathways and mammalian target of rapamycin (MTOR), which are both involved in translation. Also, CDK5 and CAMK2 substrates, involved in plasticity, were dephosphorylated. The depth of this resource ensures a comprehensive foundation to explore new mechanistic leads that might explain protective or detrimental processes occurring in epileptogenesis.

3.4 Results

3.4.1 Study Design

Status epilepticus (SE) was induced in adult mice by application of pilocarpine and terminated 40 min later by injection of diazepam (Figure. 3.1A). A second group of mice received a mock treatment, including diazepam (Figure. 3.1A). The hippocampus was dissected at 4 and 24 h after the induction of SE. The samples for each time point were lysed, digested and tagged using the TMT11plex system (Figure. 3.1B, Appendix 1A). Phosphopeptides were enriched and fractionated prior to LC-MS/MS analysis. The phosphopeptide-depleted sample was also fractionated and analysed by LC-MS/MS to determine changes to the proteome (Figure. 3.1B).

Principle component analysis (PCA) indicated the similarities of the replicates and differences between conditions. In general, replicates for each condition were clustered and phosphoproteome changes were more pronounced than protein changes, particularly at 4 h after SE (Appendix 1B-E). The TMT reporter ion intensities were $\log_2$ transformed prior to statistical analysis. The $\log_2$ fold change was calculated as shown in Figure. 3.1B and abbreviated as Pilo4h and Pilo24h. The processed phosphoproteome and proteome data is provided as tables within Appendix 2 and 3.

3.4.2 Deep phosphoproteome analysis of post-status epilepticus signalling

We obtained 23,306 unique phosphopeptides with quantitative information from the 4 h TMT11plex set and 22,940 phosphopeptides from the 24 h TMT11plex set (Figure. 3.1B and Appendix 1A). The combined data consisted of 28,119 unique phosphopeptides intersecting on 18,127 phosphopeptides for both the 4 and 24 h timepoints (Appendix 2).

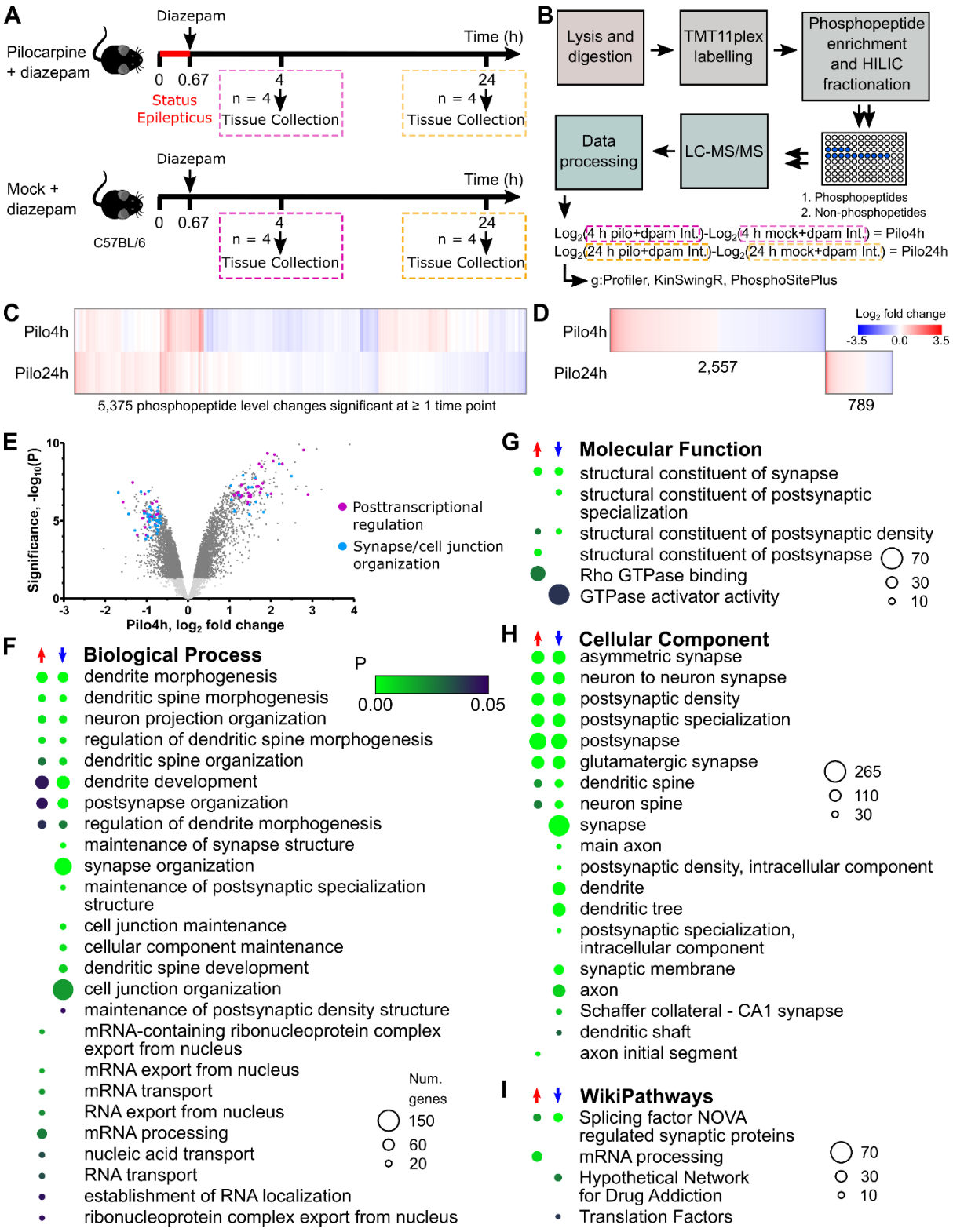

Figure 3.1. The pilocarpine induced phosphoproteome and GO terms at 4 h after SE. (A) Status epilepticus was induced in mice by pilocarpine and followed by diazepam injection at 40 min. Control mice received a mock treatment and diazepam. Mice were euthanised at 4 and 24 h and the hippocampus was dissected. (B) The hippocampus was homogenized, lysed and

digested with trypsin. Tryptic peptides were labelled with TMT11plex reagents. Phosphopeptides were enriched and fractionated using the TiSH method prior to LC-MS/MS analysis. The phosphopeptide-depleted sample was also fractionated and analysed by LC-MS/MS to determine changes to the proteome. The data was log2 transformed and specific comparisons were applied in multiple analyses. The grouped average data is presented for each timepoint. Heat maps of the hierarchically clustered log2 fold change values for (C) each phosphopeptide significant at one or more time points and (D) each phosphopeptide detected at only one timepoint. (E) Volcano plot for the significantly regulated phosphopeptides for the Pilo4h comparison. Light grey dots are values below the threshold for significance. Dots representing the top one hundred ranked phosphopeptides from proteins with the biological process terms synapse organization or cell junction organization or related to posttranscriptional regulation are coloured. Enriched (F) Biological Process, (G) Molecular Function, (H) Cellular Component and (I) WikiPathways terms for Pilo4h. A scale bar for probability is shown. The size of the circle represents the number of genes enriched.

Phosphopeptides with underlying protein level changes were discarded, rather than attempting to correct the phosphorylation level by subtraction of two poorly related values. Since we keep all protein changes, we lose no information at the gene level by discarding phospho-level changes from dynamic proteins. After discarding, there were 5,375 phosphopeptides with at least one significant change for either Pilo4h and Pilo24h (Figure. 3.1C). Some phosphopeptides were only detected for one time point. These included 2,557 significant phosphopeptides for Pilo4h and 789 for Pilo24h (Figure. 3.1D). There were 6,497 phosphopeptides significantly regulated for Pilo4h on 2,545 proteins and 3,472 phosphopeptides significantly regulated for Pilo24h on 1,801 proteins, which were used for subsequent analyses.

3.4.3 Gene ontology enrichment and general approach to data analysis

To understand how this vast level of phospho-signalling might be influencing specific cellular functions we devised an approach to extract useful information from gene ontology (GO) enrichment. We took a conservative approach by limiting the background gene set to only proteins we could detect by mass spectrometry (Appendix 4), rather than the entire mouse proteome, which would unhelpfully indicate hundreds of enriched terms. Independently for Pilo4h and Pilo24h, we separated up and down-regulated phosphorylation, which was similar in number for all phosphoproteome comparisons. Then we assigned the maximum positive and negative quantitative values for phospho-regulation to each protein and ranked the proteins using both quantitative value and significance of the maximal change (Appendix 2). We queried multiple data sources for enriched gene ontology terms using gProfiler [192], including Ensembl (biological process, molecular function and cellular component), WikiPathways, Kyoto encyclopedia of genes and genomes (KEGG) and Reactome (Appendix 5). Maximum $\log_2$ fold changes were not always representative of the overall phospho-regulation of the protein and so we also present the median $\log_2$ fold changes for selected proteins.

3.4.4 Pilocarpine increased phosphorylation of actin cytoskeleton-linked postsynaptic proteins at 4 h

Here, we focus first on phosphorylation site changes for Pilo4h, represented as a volcano plot in Figure. 3.1E and as enriched GO terms in Figure. 3.1F-I. There were multiple enriched biological process terms related to neuron projection or dendrite spine morphogenesis/organization with both increases and decreases in phosphorylation (Figure. 3.1F). This bi-directional phosphorylation was also observed for related molecular function and cellular component terms (Figure. 3.1G-H). After closely inspecting the highly ranked

proteins (Appendix 2) in this enriched set (Appendix 5) with bi-directional phosphorylation, it was apparent there was a subset of proteins with an overall increase in phosphorylation.

This subset of highly ranked proteins included cortactin, kalirin, microtubule associated protein 1A (MAP1A), MAP2, drebrin, homer 1/3 and SH3 and multiple ankyrin repeat domains protein 1-3 (SHANK1-3) (Figure. 3.2A-H and Appendix 6A-D). Cortactin had both increases and decreases in phosphorylation. Overall, cortactin was converted to a more multi-phosphorylated state, despite a near zero median $\log_2$ fold change (Figure. 3.2A). Median fold change might be most relevant to how phospho-signalling exerts influence on protein function. A 2.2-fold increase of MAP1A phosphorylation at S1898 (Figure. 3.2C) was ranked second of all proteins associated with enriched GO terms (Appendix 2). Sixty-eight MAP1A sites were regulated for Pilo4h and 82% of these were increased (Figure. 3.2C). The majority of 65 MAP2 sites had increased phosphorylation (Figure. 3.2D). The median drebrin phosphorylation was increased (Figure. 3.2E) and the largest increase was 1.6-fold for phosphorylated S241. Homer1 (Figure. 3.2F) and homer3 (Appendix 6A) had increased phosphorylation on multiple sites at 4 h after SE, whereas the two homer2 sites detected were regulated in opposing directions (Appendix 6E). Synaptic Ras GTPase-activating protein (synGAP) had many highly ranked phosphorylation sites (with GO terms, Appendix 2) and was overall up-regulated (Figure. 3.2G).

Apart from kalirin (Figure. 3.2B), there were at least forty-six proteins with up-regulated phosphorylation that contributed to the enrichment of the Rho GTPase binding molecular function term (Figure. 3.1G, Appendix 5). Many of these proteins promote actin binding, morphogenesis and/or neurite outgrowth. A notable activator of GTPases, signal-induced proliferation-associated 1-like protein 1, showed increased phosphorylation (Appendix 6D). Thus, pilocarpine-induced phosphorylation occurred on proteins with the potential to alter the cytoskeleton within synapses or sites of neurite outgrowth.

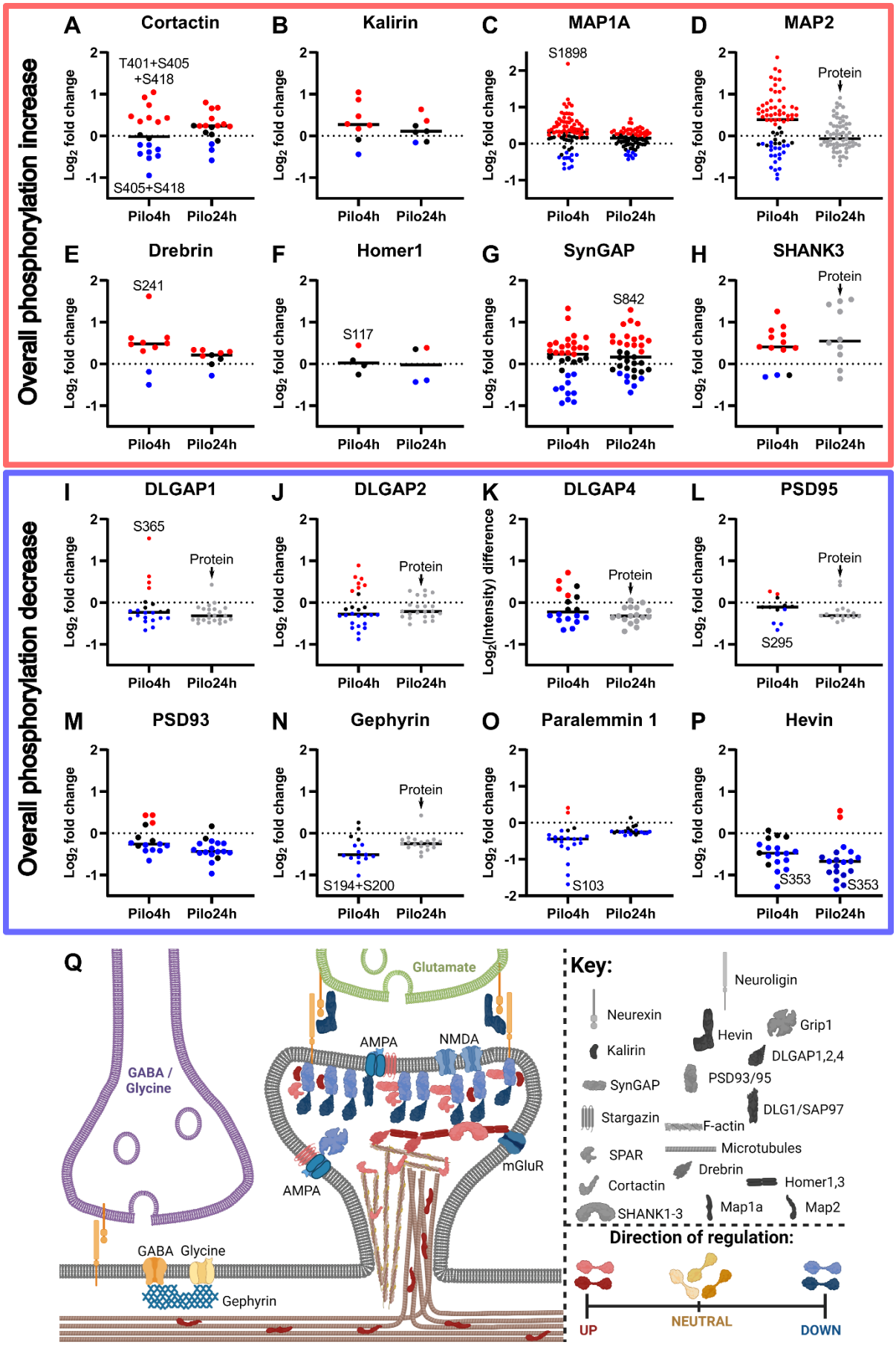
Overall phosphorylation increase
A Cortactin
T401+S405 +S418
S405+S418
B Kalirin
C MAP1A
S1898
D MAP2
Protein
E Drebrin
S241
F Homer1
S117
G SynGAP
S842
H SHANK3
Protein
Overall phosphorylation decrease
I DLGAP1
S365
Protein
J DLGAP2
Protein
K DLGAP4
Log2(Intensity) difference
Protein
L PSD95
Protein
S295
M PSD93
N Gephyrin
Protein
S194+S200
O Paralemmin 1
S103
P Hevin
S353
S353
Log2 fold change
Pilo4h
Pilo24h
Q
Glutamate
AMPA
NMDA
GABA / Glycine
AMPA
mGluR
GABA Glycine
Gephyrin
Key:
Neuroligin
Neurexin
Hevin
Grip1
Kalirin
DLGAP1,2,4
SynGAP
PSD93/95
Stargazin
F-actin
DLG1/SAP97
SPAR
Microtubules
Drebrin
Cortactin
Homer1,3
SHANK1-3
Map1a
Map2
Direction of regulation:
UP
NEUTRAL
DOWN

Figure 3.2. Phosphorylation trends for postsynaptic proteins. (A) Plots of phosphopeptide log_2 fold changes for proteins with overall increased or decreased phosphorylation. Shown are (A) cortactin, (B) kalirin (C) MAP1A, (D) MAP2, (E) drebrin, (F) homer1, (G) synGAP, (I) DLGAP1, (J) DLGAP2, (K) DLGAP4, (L) PSD95, (M) PSD93, (N) gephyrin (O) paralemmin 1 and (P) hevin. Phosphopeptide fold changes represented by black dots did not significantly change at that time point, but did change at the other time point. Phosphopeptide fold changes represented by grey dots had underlying changes in protein. The direction of the underlying protein change is shown by a grey arrow. (Q) Drawing of the postsynaptic compartment showing the PSD scaffold layers that had overall increased (red), neutral (yellow) or decreased (blue) phosphorylation. The key identifies each protein by shape. Created with BioRender.com

3.4.5 Proteins linked to neurotransmitter receptors and cell junctions were mainly dephosphorylated at 4 h

A group of biological process terms were significantly associated only with decreased phosphorylation (Figure. 3.1F). The terms synapse organization and cell junction organization encompassed most of these proteins. The top 100 ranked phosphopeptide signals associated with these terms are highlighted in Figure. 3.1E. Examining the higher ranked signals, we found that scaffolding proteins directly or indirectly linked to neurotransmitter receptors or cell junctions were prominent (Figure. 3.2I-P). For example, disks large-associated protein 1 (DLGAP1) had overall down-regulated phosphorylation sites (Figure. 3.2I). The down-regulated DLGAP1 site at S499 is conserved in all DLGAPs. DLGAP2 and 4 also had overall down-regulated phosphorylation (Figure. 3.2J-K) and DGLAP3 was overall close to neutral (Appendix 6F).

Postsynaptic density protein 95 (PSD95) was overall dephosphorylated (Figure. 3.2L), as were disks large family members PSD93 (Figure. 3.2M) and synapse associated protein 97 (Appendix 6G). The glutamate receptor-interacting protein 1 (GRIP1), which binds AMPA receptors had decreased phosphorylation at two sites (Appendix 6H). Most AMPA receptor

subunits, N-methyl D-aspartate (NMDA) receptor subunits and metabotropic glutamate receptors had overall decreased phosphorylation at 4 h after SE (Appendix 2). Ultrastructural data suggests that the postsynaptic density (PSD) is composed of interconnected scaffold layers [218]. In Figure. 3.2Q we show that most PSD proteins that are present in the first two scaffold layers beneath the plasma membrane and glutamate receptors were dephosphorylated at 4 h, whereas the lower scaffold proteins and MAPs had increased phosphorylation.

Gephyrin, the scaffolding protein for inhibitory γ-aminobutyric acid (GABA) and glycine receptors, also had decreased phosphorylation (Figure. 3.2N, Q), for example, S338. CAMK2α, which is present in the PSD of excitatory synapses, was overall dephosphorylated (Appendix 6I). In contrast, GABA receptor subunits had no clear overall phospho-signalling trend at 4 h (Appendix 2).

The terms “cell junction maintenance” and “cell junction organization” were associated with down-regulated phosphorylation for Pilo4h (Figure. 3.1F). The “cell junction organization” set included dephosphorylation of paralemmin 1 (encoded by *Palm*) at eighteen phosphorylation sites at 4 h (Figure. 3.2O). The extra cellular matrix protein, hevin (encoded by *Sparcl1*) showed an overall decrease in phosphorylation (Figure. 3.2P), particularly S353 (1-fold decrease).

3.4.6 Pilocarpine-induced phosphorylation of posttranscriptional regulatory proteins at 4 h

A group of biological process terms including “mRNA processing”, “mRNA transport”, “RNA export from nucleus” and the WikiPathways term “mRNA processing” were associated with increased phosphorylation for Pilo4h (Figure. 3.1F, I and Appendix 5). These terms describe sub-processes of the general process of posttranscriptional regulation and involved

approximately two hundred and forty such proteins. The top one hundred ranked phosphopeptide signals involved in posttranscriptional regulation are highlighted in Figure. 3.1E. The data includes RNA binding proteins that target the mRNA of neurotransmitter receptors, such as the proteins encoded by *Sfpq*, *Nova2*, *Celf4*, *Pum1*, *Pum2*, *Eif4enif1* and *Cpeb4* [219]. Taking the top fifty ranked phosphopeptides with enriched GO terms (Appendix 2), we found that twenty-seven were from proteins with posttranscriptional regulation terms (Figure. 3.3A). Although the RNA splicing term was not enriched at 4 h, many of the proteins with high magnitude increased phosphorylation were spliceosome components or function in RNA splicing (Figure. 3.3A). Although more synaptic proteins were perturbed by phospho-signalling at multiple sites (Figure. 3.1F-I, Figure. 3.2A-P), posttranscriptional regulation was the major status epilepticus-induced process at 4 h after SE, since proteins with this function had higher ranking and magnitude of phosphorylation (Figure. 3.1E).

3.4.7 Known regulatory phosphorylation mechanisms supported increased translation and cell differentiation, but not growth at 4 h

By extracting curated information on the known functions of phosphorylation sites we identified the processes with evidence for being either induced or inhibited by phosphorylation. Figure. 3.3B-C shows the magnitude of change for known functional phosphorylation sites at 4 h. The median fold change indicates there was dephosphorylation of sites known to induce cell growth and phosphorylation of sites that inhibit growth, indicating overall low growth. Translation was induced by phosphorylation (Figure. 3.3B). Greater than forty percent of all detected sites that are known to induce translation were perturbed (Figure. 3.3D) and none that inhibit translation were detected (Figure. 3.3E). However, sites regulating translation were few in our data set (Appendix 7) as they are rare in public databases [87].

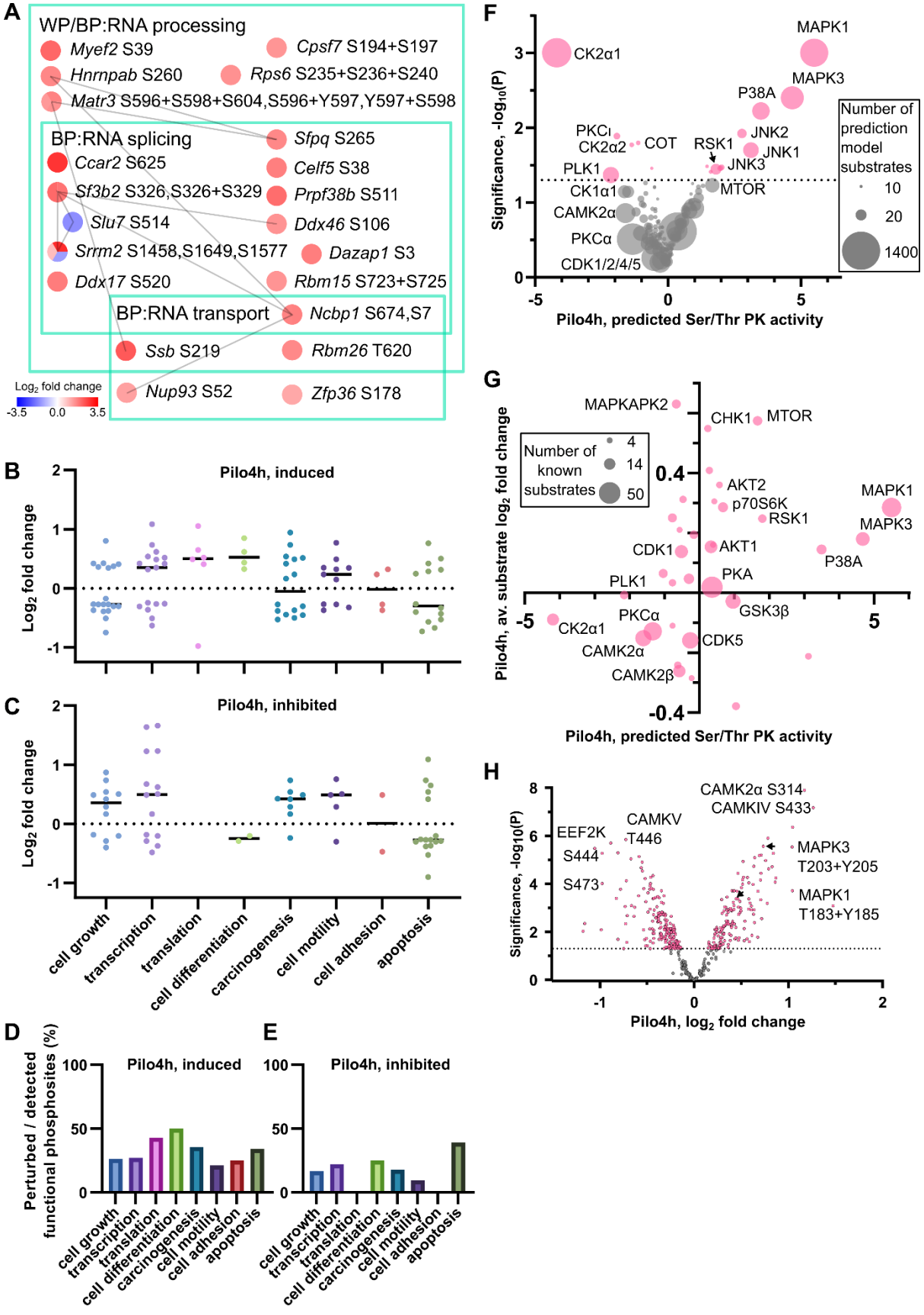
A
WP/BP:RNA processing
Myef2 S39
Cpsf7 S194+S197
Hnrnpab S260
Rps6 S235+S236+S240
Matr3 S596+S598+S604,S596+Y597,Y597+S598
BP:RNA splicing
Sfpq S265
Ccar2 S625
Celf5 S38
Sf3b2 S326,S326+S329
Prpf38b S511
Slu7 S514
Ddx46 S106
Srrm2 S1458,S1649,S1577
Dazap1 S3
Ddx17 S520
Rbm15 S723+S725
BP:RNA transport
Ncbp1 S674,S7
Ssb S219
Rbm26 T620
Nup93 S52
Zfp36 S178
Log2 fold change
-3.5
0.0
3.5
B
Pilo4h, induced
Log2 fold change
C
Pilo4h, inhibited
Log2 fold change
cell growth
transcription
translation
cell differentiation
carcinogenesis
cell motility
cell adhesion
apoptosis
D
Perturbed / detected functional phosphosites (%)
Pilo4h, induced
E
Pilo4h, inhibited
F
Significance, -log10(P)
CK2α1
MAPK1
MAPK3
P38A
PKCι
CK2α2
COT
RSK1
JNK2
JNK1
JNK3
PLK1
CK1α1
MTOR
CAMK2α
PKCα
CDK1/2/4/5
Number of prediction model substrates
10
20
1400
Pilo4h, predicted Ser/Thr PK activity
G
Pilo4h, av. substrate log2 fold change
MAPKAPK2
CHK1
MTOR
Number of known substrates
4
14
50
AKT2
p70S6K
RSK1
MAPK1
MAPK3
CDK1
AKT1
P38A
PLK1
PKA
GSK3β
PKCα
CK2α1
CDK5
CAMK2α
CAMK2β
Pilo4h, predicted Ser/Thr PK activity
H
Significance, -log10(P)
CAMK2α S314
CAMKIV S433
EEF2K
S444
S473
CAMKV
T446
MAPK3
T203+Y205
MAPK1
T183+Y185
Pilo4h, log2 fold change

Figure 3.3. Strongly responding phosphorylation of RNA processing proteins, functional phosphorylation sites and KinSwing predicted protein kinase activity. (A) Schematic of the phosphorylation sites of posttranscriptional regulatory proteins ranked in the top fifty by intensity and probability, at 4 h after SE. The overlapping membership of WikiPathways or Biological Process terms is shown. The colour of circles represents the log_2 fold change. Log_2 fold changes are shown for phosphorylation sites with known ability to (B) induce or (C) inhibit various functions at 4 h. The median value is shown for each function as a line. The functional phosphorylation sites detected as perturbed in the phosphoproteome data as a percentage of all detected phosphorylation sites is shown for (D) induced functions and (E) inhibited functions. (F) Volcano plot of KinSwing predicted activity of protein kinases induced by pilocarpine at 4 h. The size of each dot is scaled to the number of known substrates used to build the protein kinase consensus motif. (G) The average substrate log_2 fold change for known substrates of protein kinases perturbed by pilocarpine at 4 h versus the KinSwing predicted protein kinase activity. (H) Volcano plot of the log_2 fold changes for phosphopeptides occurring on Ser/Thr protein kinases at 4 h.

Cell motility and apoptosis also had mixed signals (Figure. 3.3B-C). Overall, there were indications that cell growth was prevented whilst translation and cell differentiation were promoted. There were also very few cell differentiation sites detected (Appendix 7); however, half of those detected were phosphorylated (Figure. 3.3D) and supported induction of cell differentiation (Figure. 3.3B). Many sites regulating transcription were detected (Appendix 7) but both induction and inhibition were promoted by phosphorylation (Figure. 3.3B-C).

3.4.8 Protein kinases and phosphatases activated at 4 h implicated MAPK pathways and neuronal plasticity

We used KinSwing, an algorithm we previously developed [95], to predict which protein kinases were involved in the induced signalling. KinSwing uses the quantitative phosphopeptide data to infer the activity of protein kinases with known substrate motifs (Figure. 3.3F and Appendix

8). We may only infer net kinase activity since the contribution from protein phosphatases on phosphosite levels is unknown. At 4 h, components of the MAPK signalling pathway, MAPK1, MAPK3, P38A, P38B, c-Jun N-terminal kinase 1 (JNK1), JNK2, JNK3 and ribosomal S6 kinase 1 (RSK1) were predicted from the phosphopeptides to be significantly activated. In contrast, casein kinase 2 α1 (CK2α1) and CK2α2 had decreased inferred activity (Figure. 3.3F). Since the detected phosphopeptides included known substrates of protein kinases [220], we compared the average significant $\log_2$ fold change of these known substrates to the KinSwing predicted activity (Figure. 3.3G). The known substrates of MAPK1, MAPK3, P38A, and RSK1 were up-regulated and CK2α1 substrates were down-regulated, validating KinSwing predictions. Increased MTOR activity was supported by known substrates in Figure. 3.3G despite the activity increase predicted by KinSwing not being statistically significant (Figure. 3.3F, P = 0.059).

Direct phosphorylation of protein kinases may cause a change in activity. The known MAPK1 T183+Y185 and MAPK3 T203+Y205 activation sites were phosphorylated at 4 h (shown via volcano plot in Figure. 3.3H), confirming the KinSwing prediction (Figure. 3.3F) and direction of substrate phosphorylation (Figure. 3.3H). Multiple phosphosites for CAMK family members were detected (Appendix 3), including several highly down-regulated phosphosites for the pseudo-kinase CAMKV. The up-regulated phosphorylation of CAMK2α at likely inhibitory site, S314 and the autonomous activity site of CAMK2α, T286, was down-regulated at 4 h (Appendix 6I). Even though the prediction for decreased activity of CAMK2α was not significant (Figure. 3.3F), CAMK2α substrates were overall dephosphorylated (Figure. 3.3G).

The phosphorylation status of several tyrosine protein kinases, like fibroblast growth factor receptor 3, epidermal growth factor receptor and neurotrophic receptor tyrosine kinase 2 were strongly regulated at 4 h (Appendix 9A).

Both alpha and beta catalytic subunits of protein phosphatase 2B (PP2B)/calcineurin were among the most significantly phosphorylated proteins at 4 h (Appendix 9B). The phosphatase 2A regulatory protein, biorientation of chromosomes in cell division protein 1-like 1, had multiple significantly regulated phosphosites (Appendix 9C). Extracellular leucine-rich repeat fibronectin containing 1 and 2 and cAMP regulated phosphoprotein 19 were phosphatase regulatory proteins that were significantly regulated by phosphorylation (Appendix 9C). Receptor-type tyrosine protein phosphatase alpha (RPTPα) exhibited highly significant up-regulated phosphorylation at 4 h, for example, a 1.1-fold increase at S176 (Appendix 9D). Overall, there was evidence at 4 h for activation of MAPK pathway kinases as well as altered activity of kinases and phosphatases that regulate neuronal plasticity.

3.4.9 A new phosphoproteome status at 24 h post-status epilepticus

Only 36% of the phosphopeptides regulated at 4 h were also regulated at 24 h, indicating that there was a new phosphoproteome status at 24 h after SE. A volcano plot of the 3,472 significantly changing phosphopeptides for Pilo24h is shown in Figure. 3.4A. GO enrichment was performed for the phosphoproteome at 24 h (Figure. 3.4B-F and Appendix 5). Very few biological process, molecular function, WikiPathways and Reactome terms were significantly enriched (Figure. 3.4B, D-F), indicating that many of the phosphorylation site changes were on proteins distributed equally in the foreground and background gene lists. This indicates a general stimulation of many biological processes. However, some important terms were at the forefront of changes.

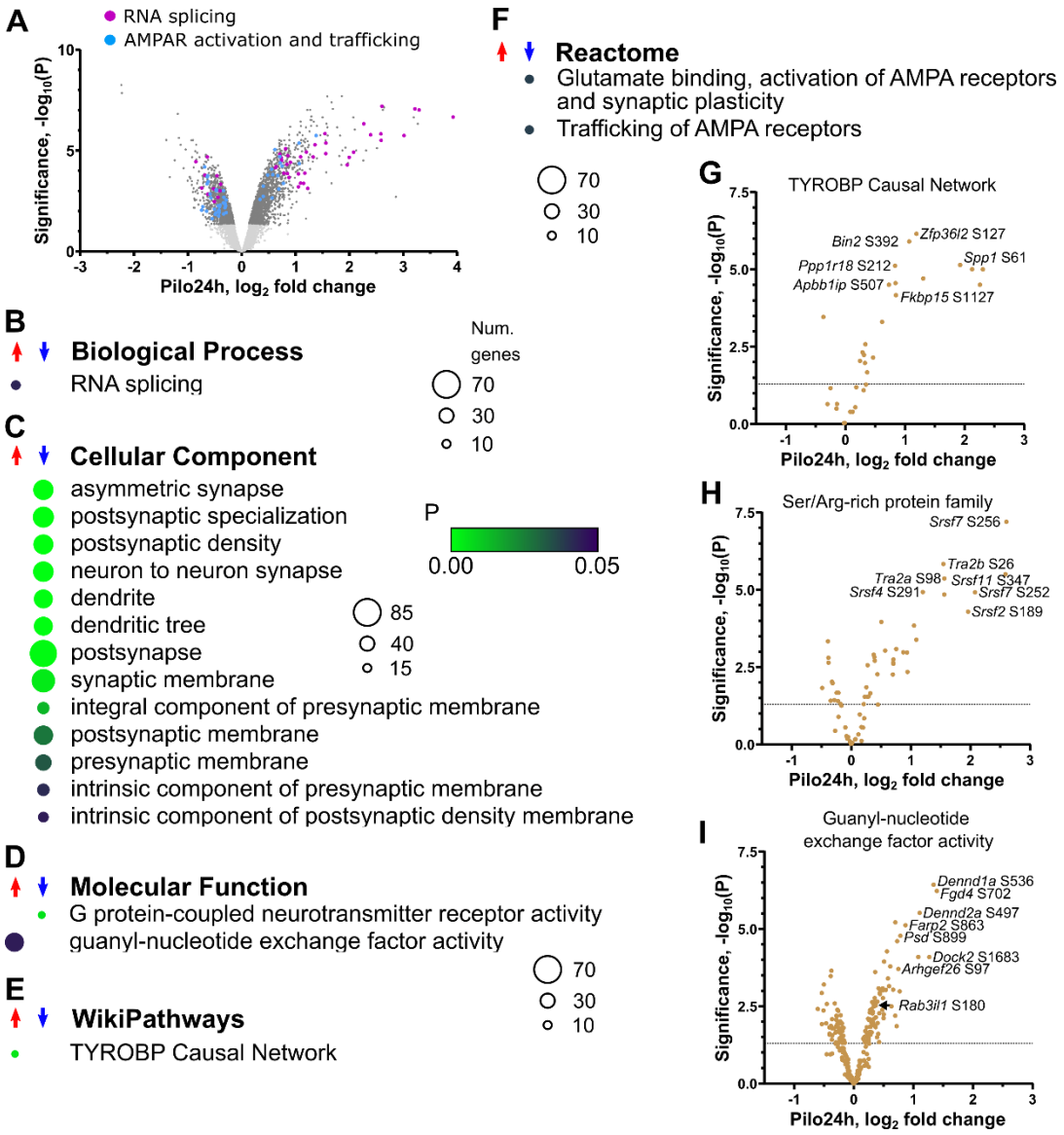

Figure 3.4. The phosphoproteome at 24 h after SE. (A) Volcano plot for the significantly regulated phosphopeptides at 24 h after SE. Light grey dots are values below the threshold for significance. Dots representing the top fifty ranked phosphopeptides from proteins with the biological process term RNA splicing and the Reactome terms related to AMPA receptor activation and trafficking are coloured. Enriched (B) Biological Process, (C) Cellular Component, (D) Molecular Function, (E) WikiPathways and (F) Reactome terms for Pilo24h. A scale bar for probability is shown. The size of the circle represents the number of genes enriched. Volcano plots are shown for phosphopeptides with membership of (G) the WikiPathways TYROBP Causal Network, (H) the UniProt curated splicing factor Ser/Arg-rich protein family and (I) the molecular function guanyl-nucleotide exchange factor activity term.

3.4.10 Microglia activation, RNA splicing and guanyl-nucleotide exchange factor activity were associated with increased phosphorylation at 24 h

The WikiPathways "TYROBP Causal Network" term was associated with increased phosphorylation at 24 h (Figure. 3.4E) and describes a microglia activation network [221], including seven proteins encoded by the genes *Spp1*, *Bin2*, *Ppp1r18*, *Samsn1*, *Fkbp15*, *Apbb1ip* (Figure. 3.4G). Some of these proteins had increased phosphorylation at 4 h, but with lower magnitude and probability. The "RNA splicing" biological process term was significantly enriched at 24 h for proteins with increased phosphorylation (Figure. 3.4A-B). These included proteins that were also phosphorylated at 4 h (Figure. 3.3A). However, at 24 h, a sub-group of proteins were highly ranked that included six members of the Ser/Arg-rich protein family of splicing factors (Figure. 3.4H). Another group with increased phosphorylation at 24 h were proteins with guanyl-nucleotide exchange factor activity (Figure. 3.4D and I).

3.4.11 Inhibitory and excitatory neurotransmitter receptors were dephosphorylated at 24 h

Down-regulated phosphorylation at 24 h was associated with the molecular function term "G protein-coupled neurotransmitter receptor activity" and the Reactome terms "glutamate binding, activation of AMPA receptors and synaptic plasticity" and "trafficking of AMPA receptors" (Figure. 3.4D and F). These terms included multiple receptor and ion channel subunits (Appendix 5) with an overall trend of decreased phosphorylation at 24 h (Figure. 3.4A, 3.5A-F). Some of the same proteins also had overall decreased phosphorylation at 4 h but the trend was more apparent at 24 h (see examples in Figure. 3.5G-N).

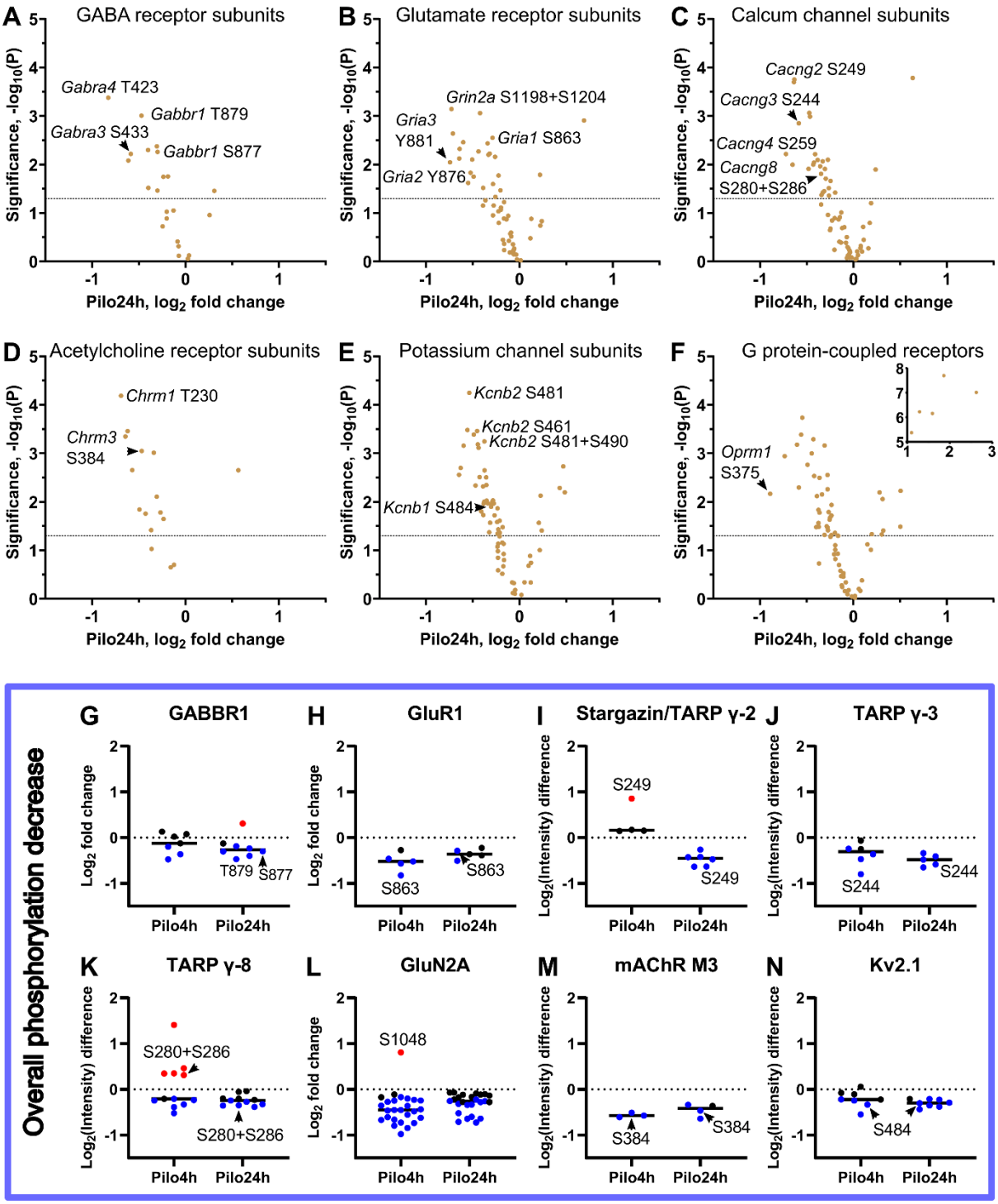

Figure 3.5. Phosphorylation trends for ion channels and neurotransmitter receptors at 24 h after SE. Volcano plots are shown for phosphopeptides with membership of the molecular function (A) GABA-A receptor activity, (B) glutamate receptor activity, (C) voltage-gated calcium channel activity, (D) acetylcholine receptor activity, (E) potassium channel activity and (F) G protein-coupled receptor activity. Plots of phosphopeptide $\log_2$ fold changes with overall decreased phosphorylation at 24 h for (G) gamma-aminobutyric acid type B receptor

subunit 1 (GABBR1) (H) glutamate receptor 1 (GluR1), (I) stargazing/transmembrane AMPA receptor regulatory protein γ-2 (TARP γ-2) (J) TARP γ-3, (K) TARP γ-8, (L) N-methyl-D-aspartate receptor subunit 2A (GluN2A), (M) muscarinic acetylcholine receptor M3 (mAChR M3) (N) potassium voltage-gated channel subfamily B member 1 (Kv2.1).

Pilocarpine induced dephosphorylation of the metabotropic γ-aminobutyric acid (GABA) B receptor 1 (GABBR1) and the ionotropic GABA A receptors 3 and 4, at 24 h after SE. Other GABA receptors with closer association to epilepsy were excluded from the phosphorylation analysis because of underlying changes in the protein level. Many glutamate receptor phosphorylation sites were dephosphorylated at 24 h, for example, the AMPA receptor subunit GluR1 (encoded by *Gria1*) dephosphorylation of S863. (Figure. 3.5B and H). The transmembrane AMPA receptor regulatory proteins (TARPs) were included in the significantly enriched Reactome terms (Figure. 3.4F) and had higher magnitude responses. Stargazin, encoded by *Cacng2*, had the most significant dephosphorylation at 24 h of all the TARPs at S249 (0.6-fold decrease, Figure. 3.5I). S249 is one of a group of dephosphorylated sites conserved in TARP γ-2, 3, 4 and 8 (Figure. 3.5C and I-J). N-methyl-D-aspartate receptors were not part of enriched Reactome terms (Figure. 3.4F) but were highly ranked and occurred in most of the enriched cellular component terms (Figure. 3.4C); The 2A subunit (GluN2A, encoded by *Grin2a*) had thirteen dephosphorylated sites at 24 h (Figure. 3.5B and L) indicating that dephosphorylation was not limited to AMPA receptors. Muscarinic acetylcholine receptors are G protein-coupled receptors and followed the trend of decreased phosphorylation at 24 h (Figure. 3.5D), for example, dephosphorylation of S384 of muscarinic acetylcholine receptor M3 (0.5-fold decrease, Figure. 3.5M). Since there are many types of G protein-coupled receptors, we asked whether they were all predominantly dephosphorylated at 24 h in our data. We found that, with exceptions, most receptor phosphorylation site changes were decreases (Figure. 3.5F). An example is the μ-opioid receptor (Figure. 3.5F).

3.4.12 Pilocarpine induced dephosphorylation of potassium channels at 24 h

Potassium channels were highly ranked in five of the cellular component terms associated with decreased phosphorylation (Figure. 3.4C). The delayed rectifiers Kv2.1 and Kv2.2 (encoded by *Kcnb1* and *Kcnb2*) had multiple down-regulated phosphorylation sites (Figure. 3.5E) and two sites were decreased for epilepsy-associated Kv2.1 (encoded by *Kcnb1*) (Figure. 3.5N).

3.4.13 Functional phosphorylation sites support cell growth, cell motility and inhibition of apoptosis at 24 hours

Using curated information on known functional phosphorylation sites, it became clear that cell motility was likely induced by phospho-regulation at 24 h after SE, without significant inhibition (Figure. 3.6A-D). Cell growth was induced, as was the associated process of carcinogenesis (Figure. 3.6A), although both were also simultaneously inhibited by a lesser number of functional phosphorylation sites (Figure. 3.7B). Phospho-regulated inhibition of apoptosis was also clearly supported at 24 h (Figure. 3.7B). Functional phosphorylation sites for apoptosis were well represented in the data (Figure. 3.6C-D), although the overall level of perturbed functional phosphorylation sites was decreased at 24 h relative to those at 4 h (Figure. 3.3D-E).

3.4.14 Protein kinase and phosphatase activity at 24 h implicates signalling involved with cell growth and chronic synaptic activity

At 24 h, multiple cyclin-dependent protein kinases (CDK) had decreased inferred activity, using KinSwing (Figure. 3.6E and Appendix 8). CDK1 and CDK5 substrates had the most evidence for decreased phosphorylation using the average fold change for known substrates (Figure. 3.6F).

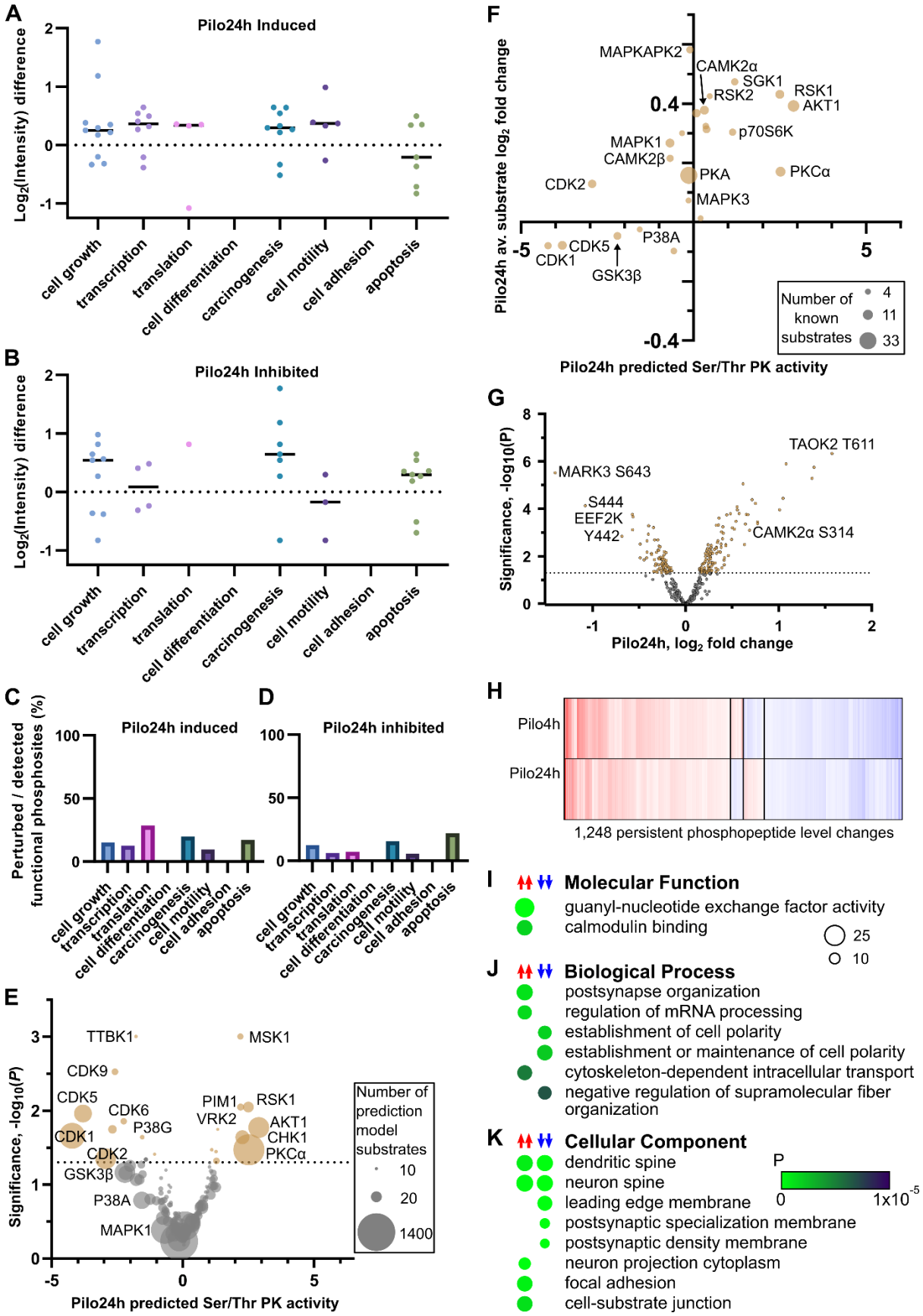
A
Pilo24h Induced
Log2(Intensity) difference
cell growth
transcription
translation
cell differentiation
carcinogenesis
cell motility
cell adhesion
apoptosis
B
Pilo24h Inhibited
C
Pilo24h induced
Perturbed / detected functional phosphosites (%)
D
Pilo24h inhibited
E
Significance, -log10(P)
TTBK1
MSK1
CDK9
CDK5
CDK6
P38G
CDK1
CDK2
GSK3β
P38A
MAPK1
PIM1
VRK2
RSK1
AKT1
CHK1
PKCα
Number of prediction model substrates
10
20
1400
Pilo24h predicted Ser/Thr PK activity
F
Pilo24h av. substrate log2 fold change
MAPKAPK2
CAMK2α
SGK1
RSK2
RSK1
AKT1
p70S6K
MAPK1
CAMK2β
PKA
PKCα
CDK2
MAPK3
P38A
CDK5
CDK1
GSK3β
Number of known substrates
4
11
33
Pilo24h predicted Ser/Thr PK activity
G
Significance, -log10(P)
TAOK2 T611
MARK3 S643
S444
EEF2K
Y442
CAMK2α S314
Pilo24h, log2 fold change
H
Pilo4h
Pilo24h
1,248 persistent phosphopeptide level changes
I
Molecular Function
guanyl-nucleotide exchange factor activity
calmodulin binding
25
10
J
Biological Process
postsynapse organization
regulation of mRNA processing
establishment of cell polarity
establishment or maintenance of cell polarity
cytoskeleton-dependent intracellular transport
negative regulation of supramolecular fiber organization
K
Cellular Component
dendritic spine
neuron spine
leading edge membrane
postsynaptic specialization membrane
postsynaptic density membrane
neuron projection cytoplasm
focal adhesion
cell-substrate junction
P
0
1x10-5

Figure 3.6. Functional phosphorylation, KinSwing predicted protein kinase activity at 24 h after SE and persistently regulated phosphorylation. Log_2 fold changes are shown for phosphorylation sites with known ability to (A) induce or (B) inhibit various functions at 24 h. The median value is shown for each function as a line. The functional phosphorylation sites detected as perturbed in the phosphoproteome data as a percentage of all detected phosphorylation sites is shown for (C) induced functions and (D) inhibited functions. (E) Volcano plot of KinSwing predicted activity of protein kinases induced by pilocarpine at 24 h. The size of each dot is scaled to the number of known substrates used to build the protein kinase consensus motif. (F) The average substrate log_2 fold change for known substrates of protein kinases perturbed by pilocarpine at 24 h versus the KinSwing predicted protein kinase activity. (G) Volcano plot of the log_2 fold changes for phosphopeptides occurring on Ser/Thr protein kinases at 24 h. (H) Heat map of phosphopeptides significantly and persistently perturbed at both 4 and 24 h. Enriched (I) Molecular Function (J) Biological Process and (K) Cellular Component terms for Pilo24h. A scale bar for probability is shown. The size of the circle represents the number of genes enriched.

Mitogen and stress response kinase 1 (RSK1) and protein kinase B (AKT1) were predicted to be up-regulated (Figure. 3.6E) and had known substrates with increased phosphorylation (Figure. 3.6F), implicating signalling pathways associated with the stress response and cell growth.

Direct phosphorylation of protein kinases at 24 h did not implicate many phosphorylation sites with known function. However, we observed CAMK2α inhibitory S314 phosphorylation at 24 h (0.7-fold increase, Figure. 3.6G), which was diminished relative to the phosphorylation level at 4 h (1.2-fold increase, Figure. 3.3H), and phosphorylation of ephrin type-A receptor 4 phosphorylation at Y779 (0.7-fold increase, Appendix 10A).

There were fewer phospho-regulated phosphatases at 24 h (Appendix 10B). Prominent proteins with altered phosphorylation level included the Ser/Thr phosphatase slingshot homolog 1 and 2 (Appendix 10B), the phosphatase regulator calmodulin (Appendix 10C) and the Tyr phosphatase RPTPζ (Appendix 10D).

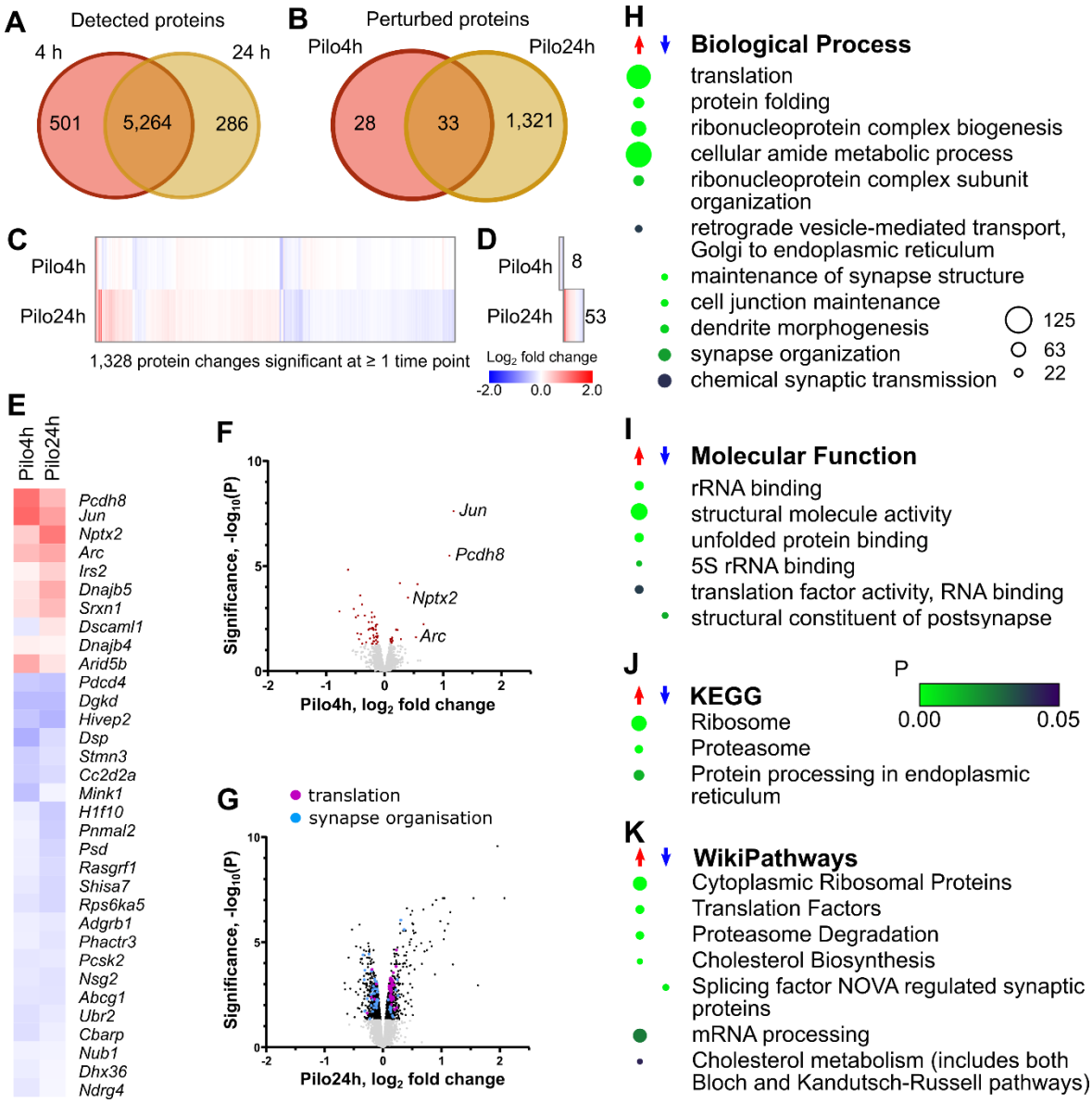

Figure 3.7. The proteome at 4 and 24 h after SE. Venn diagram of (A) proteins detected and (B) perturbed at each time point, resolved to non-redundant gene names. Heat maps of (C) hierarchically clustered $\log_2$ fold changes for each protein group with at least one significant change, (D) protein changes uniquely detected and (E) protein changes persistently detected at 4 and 24 h after SE. (E) Heat map of (B) Venn diagram of all proteins detected at 4 and 24 h. (F) Volcano plot for the significantly regulated proteins at 4 h. Light grey dots are below the threshold for significance. (G) Volcano plot for the significantly regulated proteins at 24 h. The top fifty ranked proteins with the biological process terms translation and synapse organisation are shown as coloured dots. Enriched (H) biological process, (I) molecular function, (J) KEGG and (K) WikiPathways terms for Pilo24h. A scale bar for probability is shown. The size of the circle represents the number of genes enriched.

3.4.15 Persistent signalling from 4 to 24 hours after status epilepticus supports main findings

There were 1,248 phosphopeptides significantly changed at both 4 and 24 h post-SE (Figure. 3.6H), which was too small to obtain sufficient enriched GO terms with the procedure used for the single time points. After relaxing the background to include the entire mouse proteome, we found that enriched terms (Figure. 3.6I-K, Appendix 5) were consistent with the main trends already identified. Persistent increase in phosphorylation was observed for proteins associated with the terms guanyl-nucleotide exchange factor activity, postsynapse organization, regulation of mRNA processing, and neuron projection cytoplasm (Figure. 3.6I-K). The proteins involved included a subset of those shown in Figure. 3.2A-H and Figure. 3.4H-I, as well as additional transport proteins such as kinesin-like proteins KIF1B and KIF3B. Persistent decrease in phosphorylation was observed for the proteins associated with terms such as establishment of cell polarity and post synaptic density membrane. The proteins involved included a subset of the postsynaptic proteins shown in Figure. 3.2I-P and Figure. 3.5A-N. Thus, the persistently phospho-regulated proteins were mainly those with guanyl-nucleotide exchange factor activity, involved in RNA processing or located at the postsynapse.

3.4.16 The proteome at 4 h after SE indicated MAPK pathway stimulated immediate early gene expression

The proteomic screen detected 6,277 protein groups (Appendix 3). Protein groups are made up of one or more proteins that have evidence for existence from the detected peptides. The 6,277 protein groups mapped to 6,051 non-redundant gene names. When phosphopeptide-based protein identifications were allowed in the count (requiring at least two phosphopeptides), the number of non-redundant genes increased to 7,553 (Appendix 4). After discarding proteins

mapping to the same gene, there were 5,765 and 5,550 proteins in the 4 h and 24 h TMT11plexes, respectively, which intersected on 5,264 proteins (Figure. 3.7A, Appendix 3). 1,328 proteins were significantly perturbed at one or more time points after SE (Figure. 3.7C). There were eight and thirty-three perturbed proteins uniquely detected at 4 and 24 h, respectively (Figure. 3.7D). Only 33 proteins were persistently significant at both 4 and 24 h after SE (Figure. 3.7E).

Sixty-one proteins had significant level changes 4 h post-pilocarpine treatment and most of these were down-regulated (Figure. 3.7F). The regulated proteins were analysed for GO enrichment after separation into sets of up and down-regulated proteins. Only the WikiPathways term "p38 MAPK signalling pathway" was significantly enriched at 4 h and was associated with decreased levels of three proteins (Appendix 11). These proteins included ribosomal protein S6 kinase α5, and its substrate, high mobility group nucleosome-binding domain-containing protein 1. The levels of two immediate early genes, Jun and Arc (Figure. 3.7F), were significantly up-regulated at 4h, with Jun being the most significantly up-regulated protein with a 1.2-fold increase. Further proteins linked to neuronal activity also had increased abundance, protocadherin 8 (encoded by *Pcdh8*) and neuronal pentraxin 2 (encoded by *Nptx2*) (Figure. 3.7F). Jun, Arc, protocadherin 8 and neuronal pentraxin 2 were also among ten persistently up-regulated proteins (Figure. 3.7E). There were more persistently down-regulated proteins, but our analyses did not associate any specific GO terms with this group of proteins.

3.4.17 The proteosome, ribosome proteins and translation factors had increased expression at 24 h

Approximately 25% of the detected proteome had significantly changed abundance 24 h after pilocarpine injection (Figure. 3.7B and G). The enriched gene ontology terms indicated that

proteins involved in translation were the main up-regulated proteins at 24 h (Figure. 3.7G-K, Appendix 11). At least seventy ribosomal proteins had increased expression, including more than half of the proteins required for the small and large ribosomal subunits (Appendix 11). At least twenty eukaryotic initiation factor subunits were up-regulated, including eight subunits of the initiation factor 3 complex (Appendix 11).

Also associated with up-regulation were the terms "protein folding" (Figure. 3.7H), "unfolded protein binding" (Figure. 3.7I) and "retrograde vesicle-mediated transport, Golgi to endoplasmic reticulum" (Figure. 3.7H), which might indicate an increased use of protein synthesis mechanisms. In contrast, there was an up-regulation of twenty components of the proteosome complex (Appendix 11) resulting in enrichment of the "Proteasome" KEGG term (Figure. 3.7J) and "proteosome degradation" WikiPathways term (Figure. 3.7K). Many Reactome and cellular component terms were enriched. Of these, the majority were related to translation and proteome degradation (Appendix 12A-B).

3.4.18 Direct evidence for alternative splicing in the proteome at 24 hours

Twelve alternatively spliced protein variants (encoded by *Camkk2*, *Cltb*, *Dlg1*, *Gfap*, *Mbp*, *Slc14a1*, *Pdcd6*, *Tmpo*, *Dnaja3*, *Tpm3*, *Gabrb2* and *Gabrg2*) were detected with altered abundance at 24 h (Appendix 3), which may be related to the increased phosphorylation of proteins involved in RNA splicing (Figure. 3.5D). Two short forms of GABA receptor subunits had a reduced abundance, suggesting either a loss of a population of inhibitory synapses or reduced splicing of these short forms to alter GABA receptor properties. However, most of these results rely on identification of a single isoform-specific peptide and require further validation.

3.4.19 Pilocarpine induced down-regulation of synaptic proteins at 24 h

Synaptic-related terms “chemical synaptic transmission”, “synapse organization”, “dendrite morphogenesis”, “cell junction maintenance”, “maintenance of synaptic structure” and “structural constituent of postsynapse” were associated with reduced protein abundance at 24 h (Figure. 3.7H-I). These proteins included glutamate receptor subunits GluN2B, GluR4 and metabotropic glutamate receptor 5. Down-regulated proteins included components of the postsynaptic density like PSD93, PSD95, DLG1/SAP97, DLGAP1/2/4, SH3 and multiple ankyrin repeat domains protein 1-3 (SHANKs 1-3) and homer 2, presynaptic proteins like synapsin 3 and piccolo, transsynaptic cell adhesion molecules, neurexin 1 and neuroligin 2 and 3, transporters, sodium/calcium exchanger 3, and cytoskeletal proteins like tau, alpha-adducin and microtubule-associated protein 2 (MAP2). Overall, similar to the changes in the phosphorylation status (Figure. 3.2I-Q), decreased postsynaptic density protein levels were mainly observed for the upper and middle layers of the PSD scaffold (Appendix 13).

Proteins specific to GABAergic neurons, including gephyrin, five GABA receptor subunits, glutamate decarboxylase 1 and 2, and the potassium-chloride cotransporter (encoded by *Slc12a5*) were also down-regulated at 24 h.

3.4.20 Diazepam induced phosphorylation of cytoskeletal and plasticity proteins whilst GABA receptor subunits were dephosphorylated

We used a group of mice that received no treatments or injections (“untreated”) as a control to investigate the specific effects of diazepam injection (Figure. 3.8A). We identified 503 and 541 phosphorylation level changes, respectively, at 4 h and 24 h post-mock injection that were induced by diazepam (Appendix 14A-B, Appendix 2). There were 754 phosphopeptide changes significant at one or more time points (Figure. 3.8B) and additional changes on

phosphopeptides detected at only one timepoint (Figure. 3.8C). Forty-one changes were significant at both time points (Figure. 3.8C). The term “negative regulation of protein depolymerization” was enriched and associated with increased phosphorylation at 4 h after diazepam treatment (Figure. 3.8E-F). This term included the cytoskeletal proteins MAP1A, MAP1B, MAP2, β-adducin and spectrin-α non-erythrocytic 1 (Appendix 5). Diazepam altered the phosphorylation of its target GABA receptor at 4 h, mainly with dephosphorylation, which contributed to enrichment of the “postsynapse” cellular component term (Figure. 3.8F). Phosphorylation was decreased on GABA B receptor 1 and 2 subunits at homologous sites on the C-terminal cytoplasmic domain and was also decreased on GABA A receptor 3 (Appendix 2). GABA B receptor 1 was also dephosphorylated at these C-terminal sites at 24 h (Figure. 3.8D). However, most synaptic proteins had up-regulated phosphorylation (Figure. 3.8F), including AMPA and NMDA receptor subunits, such as S863 on GluR1 (Figure. 3.8D). The presynaptic proteins piccolo, bassoon and Rab3-interacting molecule 1 (RIM1) also had up-regulated phosphorylation contributing to the enriched “synapse” term (Figure. 3.8F). Up-regulation of synaptic terms was also evident for phosphorylation at 24 h (Figure. 3.8G). Neurofilament heavy chain had increased phosphorylation at multiple sites, which was significant at both 4 and 24 h after diazepam (Figure. 3.8D) and contributed to enriched cellular component terms (Figure. 3.8E-F, Appendix 5).

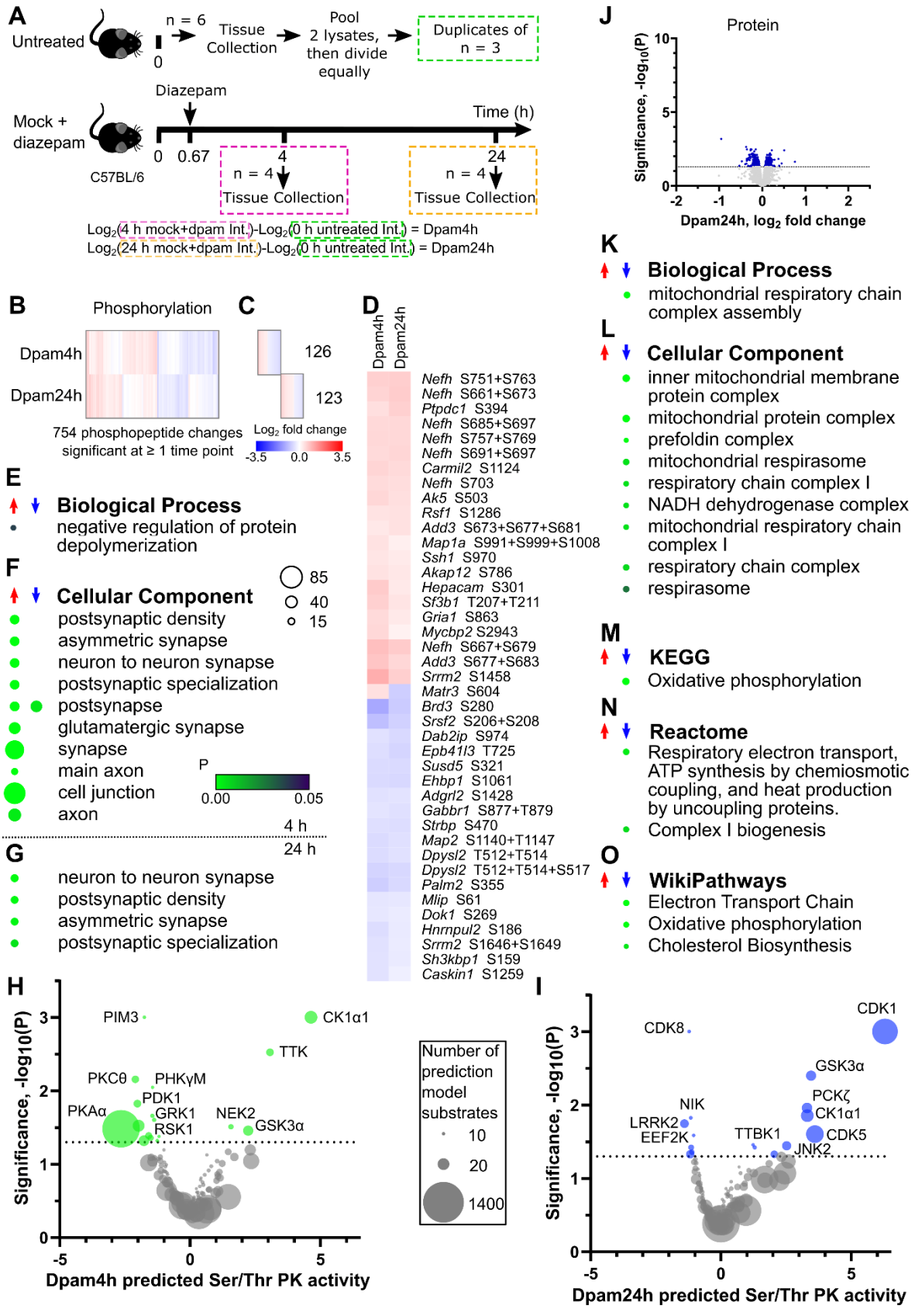

Figure 3.8. The phosphoproteome and proteome induced by diazepam at 4 and 24 h. (A) Mice receiving a mock injection followed by diazepam injection at 40 min were compared to

untreated mice. Heat maps of (B) hierarchically clustered log_2 fold changes for phosphopeptides with at least one significant change, (C) phosphopeptide changes uniquely detected 4 and 24 h after mock injection. Enriched (E) biological process terms at 4 h, (F) cellular component terms at 4 h and (G) cellular component terms at 24 h after mock injection. A scale bar for probability is shown. The size of the circle represents the number of genes enriched. Volcano plots of KinSwing predicted activity of protein kinases induced by pilocarpine at (H) 4 h and (I) 24 h. The size of each dot is scaled to the number of known substrates used to build the protein kinase consensus motif. (J) Volcano plot of the significantly regulated proteins at 24 h. Light grey dots are below the threshold for significance. Enriched (K) biological process (L) cellular component, (M) KEGG, (N) Reactome and (O) WikiPathways terms for protein changes at 24 h.

When we used KinSwing to investigate inferred protein kinase activity (Figure. 3.8H-I), we found that CK1α1 had the most inferred activity at 4 h (Figure. 3.8H). CDK5 had increased inferred activity at 24 h after diazepam (Figure. 3.8I). Also, a known substrate of CDK5, β-2-syntrophin S75 [222], had increased phosphorylation at 24 h after diazepam, supporting the prediction that CDK5 is affected by diazepam treatment.

3.4.21 Diazepam induced a decrease in mitochondrial respiratory chain proteins

Diazepam injection had no detectable effect on the proteome at 4 h. Approximately 3% of the detected proteome was affected 24 h after diazepam injection (Figure. 3.8J, Appendix 14C). The main class of proteins producing significantly enriched terms were mitochondrial respiratory chain proteins (Figure. 3.8K-O, Appendix 11), which were decreased. The WikiPathways term “Cholesterol biosynthesis” was also associated with decreased protein levels (Figure. 3.8O).

3.5 Discussion

SE triggers a large number of changes in the structural organization and cellular composition of the hippocampus as well as in the electrophysiological properties of the neuronal network which ultimately result in the manifestation of spontaneous self-recurring chronic seizures. Since neuronal activity impacts the cellular properties of brain cells, in particular of neurons, SE induces massive cellular signalling cascades that are causal for the changes underlying epileptogenesis. However, the signalling cascades that are triggered early after the initial insult have not been detailed, until this work. Here we find that early phospho-signalling is directed towards controlling posttranscriptional regulation and postsynaptic functions. Also, the earliest protein changes are supportive of translation but result in decreased postsynaptic proteins.

3.5.1 Reduced phosphorylation and protein expression of proteins involved in neuronal plasticity after SE

It is well established that neuronal networks aim to maintain their firing rate within a physiological target range by homeostatic regulation of synaptic strength [223]. Neurons experience strong pathophysiological activity during SE and the limited electrophysiological studies in rats [224,225] and mice [226] suggest that long-term potentiation (LTP) is impaired as an early compensatory mechanism opposing strong activity. Here, we have provided data that strongly supports a homeostatic synaptic response.

We find that phosphorylation level changes were strongly overrepresented in synaptic proteins, which persisted at both 4 and 24 h after SE. In particular, PSD proteins that play a role in regulating synaptic strength showed significant changes in their phosphorylation patterns. For example, the PSD95 phosphorylation site, S295, was dephosphorylated and is associated with long-term depression (LTD) [89]. PSD95 dephosphorylation may be indicative of a drive towards

synaptic weakening since we observed a general dephosphorylation of components of the PSD in the first two scaffold layers beneath the plasma membrane. Dephosphorylation was also observed in PSD membrane associated neurotransmitter receptors and cell junction proteins at both 4 and 24 h after SE. A PSD upper and middle layer-specific change in protein expression occurred at 24 h and included a decrease in the levels of neurotransmitter receptors and ion channels, indicating that dephosphorylation was followed by reduced protein abundance, indicative of synaptic weakening of excitatory synapses.

It is well established that the interplay of CAMK2α and PP2B controls the phosphorylation status of postsynaptic proteins and neurotransmitter receptors, thereby regulating synaptic strength during plasticity [227]. Our results also show that SE results in changes in the activity of these two proteins. Changes in the phosphorylation status of the CAMK2α autophosphorylation sites indicated that the kinase was deactivated at 4 and 24 h after SE and, fittingly, most predicted and known CAMK2α substrates were dephosphorylated at 4 h after SE. However, there were also examples indicative of prior hyperphosphorylation by CAMK2α, such as the increased phosphorylation of homers (homer1 S117 and homer3 S159) which are known to cause the dissolution of homer's interaction with metabotropic glutamate receptor 5 and circuit hyperexcitability [228]. In accordance with an overall decrease of CAMK2α activity, our data suggests that calcium-dependent phosphatases are active at 4h after SE. Both low and high frequency action potentials activate PP2B, which has a higher affinity for calmodulin than CAMK2 [229]. Supportive of this, we found that phosphorylation sites on PP2B which are known to inhibit PP2B activity were dephosphorylated in our model [230,231]. Furthermore, we observed dephosphorylation of known PP2B substrates. Kv2.1 was dephosphorylated at multiple known PP2B substrate sites, which are known to cause declustering and deactivation [232]. S863 on GluR1 was dephosphorylated, which is known to be mediated by PP2B and to cause receptor internalisation and LTD [233]. We observed TARP dephosphorylation, which is downstream of

PP2B and is associated with AMPA receptor trafficking and LTD [234]. Presynaptically, synaptic strength can be modulated by the interplay of CDK5 and PP2B [70]. Here, we observed dephosphorylation of known and predicted CDK5 substrates, particularly at 24 h, further implicating PP2B in SE induced signalling processes. Postsynaptic CDK5 function is less understood, but has some important substrates. For example, neurotrophic receptor tyrosine kinase 2 was dephosphorylated at a CDK5 substrate site which is required for activity-dependent structural plasticity associated with LTP [235]. There was evidence of synaptic down-scaling at 24 h, which included dephosphorylation of EEF2K substrates [236], dephosphorylation of DLGAP1 S499 [237,238], phosphorylation of synGAP S842 [239] and phosphorylation of ephrin type A receptor 4 Y779 [240]. The RNA splicing protein Nova2 was phosphorylated at T27 at 4 h after SE and is involved in the regulation of long-term potentiation and homeostatic plasticity via alternative splicing of synaptic proteins [73,241]. Taken together, our data suggests that an early response to SE is the activation of predominantly phosphatase-mediated regulation of postsynaptic receptor complexes, and other proteins broadly involved in neuronal plasticity, to alter synaptic strength, which suggests an early neuroprotective homeostatic response. Subsequent reduced abundance of the postsynaptic receptor complex is suggestive of weakened synaptic strength, synapse loss [242] or neuronal cell death [243].

3.5.2 SE triggers changes in the phosphorylation status of proteins associated with synaptic and neuronal reorganization

Pilocarpine-induced SE has been shown to result in dendritic spine loss [244]. Changes in the phosphorylation status of PSD scaffolding proteins and cytoskeletal proteins present in dendritic spines within our data might contribute to dendritic structural plasticity. For example, all SHANKs had increased phosphorylation at 4 h after SE. SHANK3 activity has been shown to regulate spine number and size [245]. Also, the phosphorylation status of multiple proteins

associated with the cytoskeleton, for example MAP2 and drebrin, was mainly increased early after SE. These postsynaptic scaffold components exist in a layer furthest from the membrane, which is a route of access to the PSD for CAMK2 [218] and it is striking that they have similar increased phosphorylation. Both increases and decreases in phosphorylation are likely to be relevant. PP2B activity has been shown to be relevant in controlling dendritic spine density, as when PP2B inhibitors were applied in epilepsy models, there was reduced loss of dendritic spines [244] and prevention of depolymerization of cytoskeletal proteins [246]. Considering our findings, PP2B should be revisited as a potential anti-epileptogenic target.

In addition, cell junction proteins such as paralemmin-1 and hevin were heavily dephosphorylated; however, the functions of the dephosphorylated sites are unknown. Hevin is implicated in epilepsy since it accumulates at excitatory synapses at 24 h in a rat pilocarpine seizure model [247] and phospho-regulation of paralemmin may influence its role in membrane remodelling and synapse formation [248]. Dysregulated cell junction proteins such as paralemmin-1 and hevin could contribute to synapse destabilization.

3.5.3 Evidence for MAPK pathway signalling potentially leading to posttranscriptional regulation and cell growth

Up-regulation of transcripts of immediate early genes, such as *Jun* and *Arc*, is a hallmark of early SE (Appendix 15). Our data supports the idea that the reported up-regulation of immediate early genes at the transcript level is translated to the protein level. We also found evidence of MAPK pathway signalling, including the extracellular signal-regulated kinase, P38, RSK and JNK families, at 4 h after SE. MAPK pathways are known to target transcription activators in response to stress, growth factors and neuronal activity [249]. MAPKs mainly activate transcription, but also the MTOR pathway, which is a known activator of translation

[170]. There is growing evidence that MAPKs and MTOR are implicated in epilepsy by phosphorylating and regulating RNA binding proteins, [170,219], for which our unbiased screen gives further support. MTOR inhibition has been shown to have favourable disease-modifying effects [141,170,250].

Strikingly, posttranscriptional regulatory proteins were the major targets of phosphorylation, at both 4 and 24 h after SE. The brain uses alternative splicing more than any other organ and has an expanded set of posttranscriptional regulatory mechanisms to match [219,251]. However, there have been few mechanistic studies of posttranscriptional regulatory proteins [87]. Our study revealed that posttranscriptional regulatory proteins that span the life cycle of an RNA molecule, including splicing, export, transport, translation and degradation [219] were major substrates of early signalling. We detected twelve isoform-specific changes in protein abundance at 24 h after pilocarpine stimulus leading to expression of protein isoforms that may affect synaptic transmission and supporting the idea that alternative splicing is regulated during epileptogenesis. A deeper proteogenomic analysis may define many more of these isoform-specific changes and improve our mechanistic understanding of phospho-signalling that drives RNA splicing.

The RNA binding proteins encoded by *Celf4* and *Sfpq* were also prominently phospho-regulated. *Sfpq* is important for axon survival and *Celf4* regulates neurotransmitter receptor abundance [219]. Since RNA binding proteins have cell-type specific functions that control neurotransmitter receptor abundance, their perturbation is likely to affect excitatory/inhibitory balance. The RNA binding protein, pumilio 2, was phospho-regulated in our data and has been implicated in epilepsy [252], but so far there are few such examples of RNA binding proteins related to epilepsy.

At 24 h, ribosomal proteins, translation initiation factors and proteins regulating folding had increased expression. Ribosome proteins can be locally synthesised and selectively bind to 3'-

untranslated regions creating specialized ribosomes for regulating the specificity and efficiency of local protein synthesis [219]. Increased levels of translation initiation factors increase efficiency of protein synthesis but have also been shown to selectively regulate the translation of neuronal mRNAs [253]. Thus, the up-regulated ribosomal and translation factor proteins at 24 h might be a continuation of the phospho-regulated posttranscriptional regulation first detected at 4 h after SE.

The detection of approximately twenty up-regulated proteosome components at 24 h post-status epilepticus suggests that protein degradation was highly activated. Previously it was found that status epilepticus inhibited proteosome activity and the effect was weaker in more vulnerable hippocampal regions [254]. At 4 h, we observed up-regulated phosphorylation of 26S proteasome non-ATPase regulatory subunit 1 (encoded by *Psmd1*) at T273 (Appendix 3), which inhibits the proteosome in human cells [255]. Thus, early phospho-signalling might mediate proteosome inhibition, but the observed up-regulation of proteosome components suggests that inhibition is temporary. Proteosome subunit levels and activity can be regulated by both phosphorylation and posttranscriptional regulation. Also, the proteosome is required for both apoptosis, to remove unwanted protein, and as a protein quality control mechanism in cell growth [256]. Thus, the exact role of up-regulated proteosome expression in epileptogenesis will require further investigation.

There were multiple additional indicators of cell growth. Protein kinases associated with growth signalling, such as MTOR and AKT1, had positive indicators for increased activity. MTOR is also known to contribute to an immune response. However, there was only minor evidence of microglia activation, beginning with a few relevant protein changes at 24 h. Thus, signals indicative of inflammation were present but relatively weak compared to indicators of growth.

Many Rho GTPase proteins had up-regulated phosphorylation at 4 h and guanyl-nucleotide exchange factors had persistently increased phosphorylation at both 4 and 24 h. Many of these proteins are known to mediate cytoskeletal functions which lead to morphogenesis or cell growth [257]. Also, there was increased phosphorylation of sites known to promote cell migration. The mechanisms for cell growth and migration are highly relevant to understanding epileptogenesis since growth or sprouting that might be necessary for repair may also lead to more excitatory synapses, causing positive feedback and more frequent seizures [203,204].

3.5.4 Duelling mechanisms of growth and synaptic weakening

Overall, the data supports a model of two major mechanisms that lead to opposing outcomes. These two processes are protein kinase-induced neuronal growth and phosphatase-induced synaptic weakening. Although transcription factors were targeted, the major conduit of growth signalling appeared to be posttranscriptional regulation. Localised translation adjacent to synapses [219] could be rapidly and persistently induced by seizure activity that dysregulates signalling pathways. Alternatively, enhanced translation might be a normal process of repair and adaptation that follows pathophysiological activation. The growth and translation regulator, MTOR, is a known target for inhibition that is considered anti-epileptogenic [170] and this work provides new context for the role of mTOR in epileptogenesis. At the same time that protein kinases are activated, seizure activity could over-activate phosphatases, induce synaptic weakening and reduce spine numbers, leading to synapse loss and cell death. SE is known to cause cell death, particularly of vulnerable interneurons, but this signalling might also be a homeostatic and neuroprotective response. We noted that some of the dysregulated proteins were homologs of human genes that are causal for epilepsy, although many were not. It is likely that epilepsy associated genes contribute to vulnerabilities in seizure pathways, but only a subset might be worth targeting and other worthy targets are not currently associated with

epilepsy. This work provides mechanistic leads that might explain a combination of protective and detrimental processes occurring in epileptogenesis and highlights the need to target more than one process or pathway.

3.5.5 Diazepam induced synaptic plasticity mechanisms and decreased expression of mitochondrial respiratory chain proteins

In the pilocarpine animal model of epileptogenesis, diazepam is used to allow mice to recover from SE due to activation of GABA receptors that inhibit excitatory synapse depolarization. Humans routinely use diazepam or homologous drugs to induce sleep. However, to our knowledge, there is limited understanding about the mechanistic effect of diazepam in the 24 h after administration. Surprisingly, we found that diazepam application on its own caused significant alterations in the hippocampal phosphoproteome. For example proteins involved in GABAergic signalling were phospho-regulated, GluR1 was phosphorylated at LTP-associated S863 [233,258] and there were phosphorylation changes on methyl-CpG-binding protein 2, a protein which regulates synaptic scaling [90]. The direction of phosphorylation change on GluR1, in particular, supports previous findings at the functional level that diazepam can induce synaptic up-scaling functionally similar to that induced by tetrodotoxin, [259,260]. Reduced abundance of proteins involved in the mitochondrial respiratory chain was the major protein change following diazepam at 24 h. Since diazepam suppresses brain activity, likely there was reduced energy metabolism. Our data calls for future studies investigating whether there are even longer-term effects (>24 h) following a single diazepam application and whether they might be related to the development of addictions.

3.5.6 Limitations

There are limitations to phosphoproteome data interpretation that have been detailed elsewhere [87]. In particular, most phosphorylation sites do not have a validated association with protein kinases or phosphatases and this affects the completeness of prediction methods. Only two time points were examined resulting in a lack of detail on the many time-dependent processes, which are likely occurring at once [146]. Combined with this is the problem that proteins from bulk tissue lose their cell type-dependent detail. Proteins can have a different response to stimuli in different brain regions, cell types or subcellular compartments. Additionally, findings from animal models do not always recapitulate the human condition.

3.5.7 Funding

MEG was funded by a National Health and Medical Research Project Grant (1079160). Our work was supported by the Deutsche Forschungsgemeinschaft (DFG) (SS: SFB1089, SCHO 820/4-1, SCHO 820/6-1, SCHO 820/7-1, SCHO 820/5-2, SPP1757; DD: SFB1089, SPP1757, INST1172 15, DI853/3-5&7, INST 217/785-1), the BONFOR program of the University of Bonn Medical Center (SS, DD).

3.5.8 Acknowledgements

We acknowledge the support of the Children's Medical Research Institute Biomedical Proteomics Facility. We would like to thank Annika Meyer, Pia Staussberg and Isabelle Paulussen for help with the pilocarpine animal model.

3.5.9 Author contributions

DD performed the mouse model experimentation and tissue extraction. MHS performed the proteomics-relevant sample preparation and mass spectrometry analysis. AJW processed the raw mass spectrometry data and performed statistical analysis. SS, DD and MEG conceived and designed the study. MHS, MEG and AJW analysed the data and created the figures. All authors contributed to the writing and editing of the manuscript.

3.5.10 Declaration of interests

The authors declare no competing interests.

3.6 Methods

3.6.1 Animals

All animal procedures were planned and performed to minimize pain and suffering and to reduce the number of used animals in accordance with the guidelines of the University Hospital Bonn, Animal-Care-Committee as well as the guidelines approved by the European Directive (2010/63/EU) on the protection of animals used for experimental purposes and ARRIVE guidelines. All mice were housed in a humidity (55 ± 10 %) and temperature (22 ± 2°C) controlled environment under a 12-h light–dark-cycle (light cycle 7 am to 7 pm) with water and food ad libitum and nesting material (Nestlets, Ancare, USA). Mice were allowed to adapt to the animal facility at least for seven days before any treatment.

3.6.2 Induction of chronic epilepsy by systemic pilocarpine injection

Male C57Bl6/N mice (Charles River; ~60 days old, weight ≥ 20 g) were injected subcutaneously with 335 mg/kg pilocarpine hydrochloride (Sigma) to induce Status

epilepticus, twenty minutes after pre-treatment with subcutaneous injection of 1 mg/kg scopolamine methyl nitrate (Sigma) as described previously [216,217]. Animals received an injection of diazepam (4 mg/kg, s.c.; Ratiopharm) forty minutes after SE onset. Control (non-SE) animals were treated identically but received saline instead of pilocarpine. Behavioural SE was clearly identified using a modified seizure scheme: sustained convulsions with postural loss designated as SE [216,217]. Among pilocarpine injected animals, only those that developed SE (SE-experienced) were further used for analysis.

3.6.3 Preparation of hippocampi lysates

4 h and 24 h post induction of SE hippocampi from both hemispheres were removed and immediately frozen on dry ice. Tissue was homogenized in 500 µl PBS (45 sec), before 125 µl lysis buffer was added consisting of 2% sodium dodecyl sulphate, 50 mM trisaminomethane/HCl pH 7.4, 2 mM ethylene glycol-bis(β-aminoethyl ether)-N,N,N0, N0-tetraacetic acid, 2 mM ethylenediaminetetraacetic acid, Complete Protease Inhibitor Cocktail (Roche), 2 mM phenylmethylsulfonyl (Sigma), 5 mM NaF (Sigma), 2 mM beta-glycerophosphate (Sigma), Phosphatase Inhibitor Cocktail 2 (1:1000) and PhosSTOP (Roche). Lysates were incubated at 85°C for 10 min and subsequently sonicated for 3 x 10 s. Samples were frozen on dry ice before being lyophilized for 60 h.

3.6.4 Sample processing for proteomics analysis

The freeze-dried samples were resuspended in a 100 µL solution of 10 mM tris(2-carboxyethyl) phosphine, reduced for 10 minutes at 85°C and subsequently alkylated in 25 mM iodoacetamide at 22 °C in the dark. Proteins were precipitated from the samples using chloroform-methanol extraction [180] and air dried. The precipitates were dissolved in 20 µL

solution containing 7.8 M urea, 50 mM triethylammonium bicarbonate and 5 µg of Lys-C (FUJIFILM Wako Pure Chemical Corporation) for an 8 h digestion at 25 °C. The samples were diluted with a solution containing 170 µL 100 mM 4-[2-hydroxyethyl]-1-piperazineethanesulfonic acid (HEPES) (pH 8) and 5 µg TrypZean trypsin (Sigma Life Sciences) for subsequent digestion at 37 °C for 4 h. The trypsin digestion was twice repeated with an additional 5 µg for 4 h at 37 °C. The peptide concentration was estimated by absorption at 280 nm (Implen Nanophotometer, Labgear).

Approximately 400 µg of peptide was aliquoted into new tubes of equal concentration, using 100 mM HEPES (pH 8) to adjust the volume. TMT11plex reagent sets (Thermo Fisher Scientific) were dissolved in anhydrous acetonitrile and applied to each of the twenty-two samples in a 1 h and 20 min incubation at 25 °C, using one reagent vial per 200 µg. To ensure completeness of labelling 0.6 µL from each sample was tested and were found to be > 98% labelled. Excess TMT reagent was quenched with 16 µL of a 5% hydroxylamine solution for 15 minutes at 25 °C. The 4 h and 24 h treatment samples were pooled separately according to their respective timepoints. The six control untreated replicates were then pooled together and thoroughly mixed before splitting the combined sample in half, to mix with the two timepoint treatments. The 4 h TMT sample set consisted of: control untreated bio-replicate 1, 126; control untreated bio-replicate 2, 127N; control untreated bio-replicate 3, 127C; 4 h mock treatment bio-replicate 1, 128N; 4 h mock treatment bio-replicate 2, 128C; 4 h mock treatment bio-replicate 3, 129N; 4 h mock treatment bio-replicate 4, 129C; 4 h pilocarpine treatment bio-replicate 1, 130N; 4 h pilocarpine treatment bio-replicate 2, 130C; 4 h pilocarpine treatment bio-replicate 3, 131N; 4 h pilocarpine treatment bio-replicate 4, 131C. The 24 h TMT sample set consisted of: control untreated bio-replicate 1, 126; control untreated bio-replicate 2, 127N; control untreated bio-replicate 3, 127C; 24 h pilocarpine treatment bio-replicate 4, 128N; 24 h pilocarpine treatment bio-replicate 3, 128C; 24 h pilocarpine treatment bio-replicate 2, 129N;

24 h pilocarpine treatment bio-replicate 1, 129C; 24 h mock treatment bio-replicate 4, 130N; 24 h mock treatment bio-replicate 3, 130C; 24 h mock treatment bio-replicate 2, 131N; 24 h mock treatment bio-replicate 1, 131C (lot numbers TB266076 and TA265136).

The two pooled samples were acidified with 100% formic acid to pH < 3 and the volume was reduced to 150 µL under vacuum centrifugation. The two samples were diluted to 2 mL with 0.1% trifluoracetic acid and desalted using a Sep-Pak tC18 3cc Vac cartridge (200 mg sorbent, Waters).

To obtain non-, mono- and multi-phosphorylated peptides from each timepoint, the samples were applied to the "TiSH" method of phosphopeptide enrichment as described in [103]. All recovered multi- and mono-phosphorylated peptides were desalted, with multi-phosphorylated samples ready for liquid chromatography tandem mass spectrometry (LC-MS/MS) analysis. Mono-phosphorylated peptides were subjected to hydrophilic interaction chromatography (HILIC) for further fractionation prior to LC-MS/MS analysis. The non-phosphorylated peptides which do not bind to titanium dioxide were collected from the first TiSH wash step. Approximately 3.5% of the 4 h and 24 h non-phosphorylated peptides were desalted and fractionated by HILIC prior to LC-MS/MS analysis.

HILIC sample fractionation was completed using a Dionex UltiMate 3000 HPLC system (Thermo Fisher Scientific) controlled by Chromeleon 6.8 software with a TSKgel Amide-80 1 mm inside diameter x 250 mm long column (Tosoh Bioscience). Samples were injected in 150 µL in 90% acetonitrile, 9.9% water, 0.1% trifluoracetic acid (HILIC Buffer A) at a flow rate of 60 µL/min with buffer A at 100% for 10 min. The gradient was from 100% HILIC buffer A 100% to 40 % HILIC buffer B (99.9% water and 0.1% trifluoracetic acid) for 35 minutes at a flow rate of 50 µL/min, then to 80% buffer B for 3 minutes then back to 100% buffer A for 12

minutes. Sample fractions were collected in 60 s intervals into a 96 well plate using a Probot (LC Packings) controlled by μCarrier 2.0. Selected fractions were pooled based on the intensity of the ultraviolet absorbance at 214 nm. The non-phosphorylated peptide HILIC fractionation was repeated and collected in 30 s fractions. Both 30 s and 60 s factions were analysed. The fractions were dried under vacuum centrifugation and dissolved in 5.5 μL 0.1% formic acid for LC-MS/MS analysis.

3.6.5 Mass Spectrometry

LC-MS/MS for all samples was completed with a Dionex UltiMate 3000 RSLC nano system and Q Exactive Plus hybrid quadrupole-orbitrap mass spectrometer (Thermo Fisher Scientific). The multi phosphorylated samples and HILIC fractions of the non- and mono-phosphorylated samples were loaded directly onto a 300 × 0.075 mm column packed with ReproSil Pur C18 AQ 1.9 μm resin (Dr Maisch, Germany). A column oven (PRSO-V1, Sonation lab solutions, Germany) integrated with the nano flex ion source (Thermo Fisher Scientific) maintained the column at 50 °C with an electrospray operating at 2.3 kV. The S lens radio frequency level was 50 and capillary temperature was 275 °C. For MS analysis, 5 μL from all samples was injected. The reversed phase buffers were: A (0.1% formic acid in water) and B (0.1% formic acid, 90% acetonitrile, 9.9% water). There were two gradient variations used for MS acquisition. All non- and mono phosphorylated fractions were subjected to a 110 min gradient beginning with sample loading at 99% buffer A and 1% buffer B separation for 25 min at 300 nL/min. The flow rate was then reduced to 250 nL/min in 30 s and the gradient was to 95% buffer A in 1 min, to 75% buffer A in 59 min, to 65% buffer A in 8 min, to 1% buffer A in 3 min and held at 1% buffer A for 2 mins before returning to 99% buffer A in 1 min and held for 10 min. For the multi phosphorylated samples the gradient was from 99% A to 95% buffer A in 6 min, to 72% buffer A in 116 min, to 65% buffer A in 10 min, to 1% buffer A in 3 min and held at 1%

buffer A for 3 mins before returning to 99% buffer A in 2 min and held for 10 min. MS acquisition was performed throughout the 110 min and 180 min analysis.

Data-dependant acquisition LC-MS/MS was performed on all samples. In both the 110 min and 180 min methods, MS scans were at a resolution of 70,000 with an automatic gain control target of 1,000,000 for a maximum ion time of 100 ms from m/z 375 to 1500. Both the 110 min and 180 min methods had MS/MS scan resolution at 35,000 with an automatic gain control target of 200,000. The maximum ion time was 110 ms for the 180 min method and 115 ms for the 110 min method. The loop count was 12 for the 110 min method and 13 for the 180 min method. For both methods the isolation window was 1.2 m/z, the first mass was fixed at m/z 120 and the normalized collision energy was 34. Singly charged ions and those with charge >8 were excluded from MS/MS and dynamic exclusion was for 25 s in the 110 min method and 30 s in the 180 min method.

The raw LC-MS/MS data was processed with MaxQuant v1.6.7.0 [185] using the following settings. Variable modifications were oxidation of Met, acetylation of protein N-terminus, deamidation of Asn/Gln and phosphorylation of Ser/Thr/Tyr. Carbamidomethyl of Cys was a fixed modification. Digestion was set to Trypsin/P with a maximum of 3 missed cleavages. The inbuilt contaminants file was used as well as the *Mus musculus* reference proteome with canonical and isoform sequences downloaded Feb 21 2020. Also, a fast file containing the sequence of immunoglobulin G-binding protein A (UniProt accession: A0A0H3K686) was included. TMT-labelled protein A was added to selected samples to assess TMT ratio compression. The accession exists in the MaxQuant output but was removed in the post-MaxQuant analysis of the data. Minimum peptide length was 6 and maximum peptide mass

was 6000 Da. Second peptides and dependent peptides searches were enabled. Peptide spectrum matching and protein false discovery rates were set to 0.01. Minimum score for modified peptides was 40. Modified peptides and counterpart non-modified peptides were excluded from protein quantification. Modified peptides or their non-modified counterparts were not used in the protein quantification. All other parameters were default. One razor plus unique peptide for proteins < 150 kDa and two razor plus unique peptides was required for proteins > 150 kDa for protein detection. The raw mass spectrometry files are available from the PRIDE repository and have the dataset identifier PXD038241.

3.6.6 Additional processing and statistical analysis of mass spectrometry data

The MaxQuant data was further processed using methods and 'best annotation' process described previously [95] with a modification to the phosphopeptides retained for further analysis that are multi-phosphorylated. Briefly, all sites are re-annotated against the fasta file used for MaxQuant searching, followed by median log2 transformation of duplicated sites. A difference to the previously described method is that all multi-phosphorylated peptides with a class 1 probability (primary phosphorylated site) above 0.5 were also retained if there was evidence of a class 1 site above 0.75 in at least one site in any experimental group. All replicates were quantile normalised [261] followed by imputation of missing data (each sample group was permitted 25% of missing data) using the knn nearest neighbour averaging method [262] and corrected for technical sources of variation by surrogate variable analysis [263]. After a first round analysis, the "MockInj_24_2" sample was removed as a significant outlier using the first 2 principle components of the normalised and corrected phosphorylation values (mahalanobis distance p-value = 0.0001) [264]. Data were then remapped as described above before further analysis. For differential phosphorylation and protein analysis, data were fit to a generalized linear model with Bayes shrinkage using limma version 3.36.5 (PMID: 25605792) comparing

Pilocarpine and Mock Injections for each matched timepoint and for each Mock Injection versus the pooled controls at 0 minutes and p-values were of the moderated t-test corrected for multiple comparisons using the Benjamini and Hochberg method[265] (Benjamini and Hochberg, 1995).

For all analyses, phosphopeptides that exhibited underlying changes in protein were excluded. Phosphopeptide data with no corresponding protein level data was kept, representing approximately one third of the detected phosphopeptides (Appendix 4). Volcano plots were produced by Prism 9.0.2 using data that contained at least one significant quantitative value resulting from any condition or time point for phosphopeptide or protein data. Quantitative values that were non-significant for all conditions were excluded. The same data was clustered using Morpheus (https://software.broadinstitute.org/morpheus/). Protein or phosphopeptide data was hierarchically clustered using Euclidian distance with a complete linkage method.

3.6.7 KinSwing

Protein kinase activity was predicted with KinSwingR version 1.1.4 (described here: [95] and implemented/available on R/BioConductor with additional implementation of significance scoring of kinase activity: http://bioconductor.org/packages/KinSwingR/). Briefly, KinSwing predicts kinase activity by first modelling kinase matches (position weight matrices of known mammalian kinase:substrate sequences) to each phosphorylated peptide. Kinase activity is then inferred using a network theoretic approach, where nodes represent kinases and edges represent modelled kinase:substrate interactions. Local network connectivity for each kinase is determined as the absolute proportion of positive and negative peptides that have significant fold changes ($p \leq 0.05$), weighted by the number of edges and number of substrate sequences

using to build the kinase model. Finally, the weighted kinase score is z-transformed to enable comparison between different conditions. In addition to these methods that are described in greater detail in [95], significance of the kinase activity score $swing_k$ is determined by permutating kinase node labels, K, to substrates, S, of the total network, M_{ks}. Thereby the probability of observing $swing_k$ is conditional on this permuted reference distribution, of size, N (1,000 permutations), and is computed for each tail of the distribution, positive and negative $swing_k$ scores.

The KinSwingR predictions of Ser/Thr activity were compared to the changes in phosphorylation status of known protein kinase substrates in the data by first downloading the known substrates from PhosphoSitePlus [220] (downloaded November 2 2020). For each protein kinase identified by KinSwingR, the average significant phosphopeptide intensity for all known substrates in our data was calculated. A minimum of four substrates was required. Kinase-substrate relationships from all mammals were allowed if the gene name and the sequence within four residues either side of the phosphorylation site was identical. All duplicate combinations of genes and sequence values from PhosphoSitePlus using these criteria were discarded. Multi-site phosphorylated peptides were not simplified or discarded but kept throughout all analyses. The first sequence window for the first phosphorylation site was assigned the quantitative value for the phosphopeptide in sequence analyses. In displaying data for Ser and Thr or Tyr protein kinases, those protein kinases with specificity for all three residues were repeated in each display. Kinase specificity was determined using the "Ser/Thr protein kinase activity" or "Tyr protein kinase activity" term from UniProt. Pseudo-kinases were allowed when displaying protein kinase $\log_2$ fold change data. Membership of various other enriched gene ontology terms was determined using QuickGO.

3.6.8 Gene ontology enrichment

The significantly regulated phosphopeptides for the four comparisons designated Pilo4h, Pilo24h, Dpam4h and Dpam24h were divided into up and down-regulated groups, resulting in eight sets. The phosphopeptides were ranked from most significant to least significant and then from largest to smallest quantitative value. The significance ranking value and quantitative ranking value was summed for each phosphopeptide to produce a final combined rank. The gene for each phosphopeptide was extracted to produce a ranked gene list. Redundant gene names were discarded, retaining the highest ranked gene name for each phosphopeptide. The ranked gene lists were submitted to gProfiler [192] using the 'multi-query' and 'ordered query' options. Note that an ordered query is an iterative process that may not use the entire ranked gene list to obtain significance [192], weighting the output toward the higher ranking genes. The organism was set to *Mus musculus* (version: GRCm38.p6). A custom background was used which consisted of all the genes represented by the proteins detected in both the proteomics and phosphoproteomics. Genes without annotation were included in the background. The significance threshold was $P < 0.05$ and using the gProfiler algorithm for adjustment of multiple hypotheses [193]. The following data sources and version were used: GO Molecular Function release June 1 2020, GO cellular component release June 1 2020, GO Biological Process release June 1 2020, KEGG release July 6 2020, Reactome annotations ensemble classes July 7 2020 and WikiPathways version June 10 2020.

Significant protein values were also divided into up and down-regulated groups and ranked by both significance and by the magnitude of the quantitative values. For protein groups mapping to multiple genes, the first gene was kept and the remaining genes discarded. Redundant genes were also removed before submission to submitted to gProfiler using the same settings as for

phosphopeptides. The list of significant terms was simplified using REVIGO [266]. The full output from gProfiler is supplied in Appendix 5 and 11.

In a separate analysis of persistently regulated phosphopeptides and proteins, the $\log_2$ fold change was required to be significant for both 4 and 24 h for inclusion. The same procedure for GO enrichment was followed except that the background was the subset of annotated genes in the *Mus musculus* genome (version GRCm39), the threshold for significance was set to 0.00001, the term size was limited to 400 genes and the data sources were newer. We used GO Molecular Function, GO cellular component and GO Biological Process released March 22 2022.

3.6.9 Phosphorylation site function analysis

The phosphorylation sites that are known to induce or inhibit a particular function were obtained from PhosphoSitePlus [220] (downloaded August 28 2020). We sequence matched the PhosphoSitePlus data to our data requiring an identical gene name and sequence within four residues either side of the phosphorylation site. Sequences from all mammals were allowed. Multi-site phosphopeptides were matched using the sequence window of the first phosphorylation site. If this caused a redundant match, the quantitative value with the largest magnitude was kept and the remainder discarded.

The following material is not part of the manuscript submission.

Whilst the following data appears also in Royero, et al. [267], only the analysis which validates this study is presented below.

Please refer to the Authorship attribution statement for author contribution.

3.7 Targeted analysis of Ste20-like kinase

3.7.1 Generating a target list for parallel reaction monitoring

To confirm the SLK phosphorylation and protein expression during epileptogenesis, as determined by the TMT method, a PRM assay was performed as described in Chapter 2, Section 2.5.8.

From a starting list of 16 SLK phosphosites we were able to detect and obtain quantitative data for seven SLK sites (Figure 3.9) and three stable non-SLK phosphorylation sites. Quantitative data was also obtained on five non-phosphorylated SLK target peptides and was used to represent the SLK protein fold change shown in Appendix 16.

3.7.2 Pilocarpine stimulation induces SLK phosphorylation

Phosphorylation is known to regulate SLK activity and SLK phosphorylation sites were perturbed in our TMT screen of pilocarpine treated mice. To validate this finding, we analysed SLK phosphorylation following pilocarpine treatment using PRM. Our targeted MS analysis of unlabelled hippocampal tissue yielded quantitative data for one ambiguous site (S542/S543) and six localised sites (T183, S340, S347, S348, S444, and S647) (Figure 3.9A and C). At 4 h, phosphorylation at the T183 and S348 sites was decreased, and phosphorylation was increased at the S444 site. At 24 h, phosphorylation at the S347 site was increased, whilst all other sites

displayed no significant change (Figure 3.9A and C). SLK activity is increased through the autophosphorylation of the T183 activation segment [268,269]. SLK activity is inhibited by S347 and S348 phosphorylation[270]. Phosphorylation of the S444 site has no known function. These findings demonstrate that activity induces temporal phospho-regulation of multiple SLK sites.

In comparison to the TMT discovery screen, the PRM analysis results largely reflected the same direction of phosphosite regulation in T183 and S444 at Pilo 4 h (Figure 3.9B), with different magnitude changes. Phospho-T183 and S444 were both indicated to be significantly regulated in both experiments at 4 h (Figure 3.9B). S340 and S647 had no significant phosphorylation level change at 4 or 24 h using either TMT or PRM (Figure 3.9B and D). Phospho-S347 also reported no significant changes at 4 h in both experiments. At 24 h, the T183 and S347 sites were found to be up regulated in both the TMT and LFQ analyses. However, T183 was only significant in the TMT experiment and S347 was significant in the LFQ analysis. This may be due to full separation of the phospho-S347 and S348 signals in the targeted PRM experiment in comparison to the data-dependent detection used the TMT experiment. In both the LFQ and TMT analysis at 4 and 24 h, there was no change in the underlying SLK protein level (Appendix 16A and B).

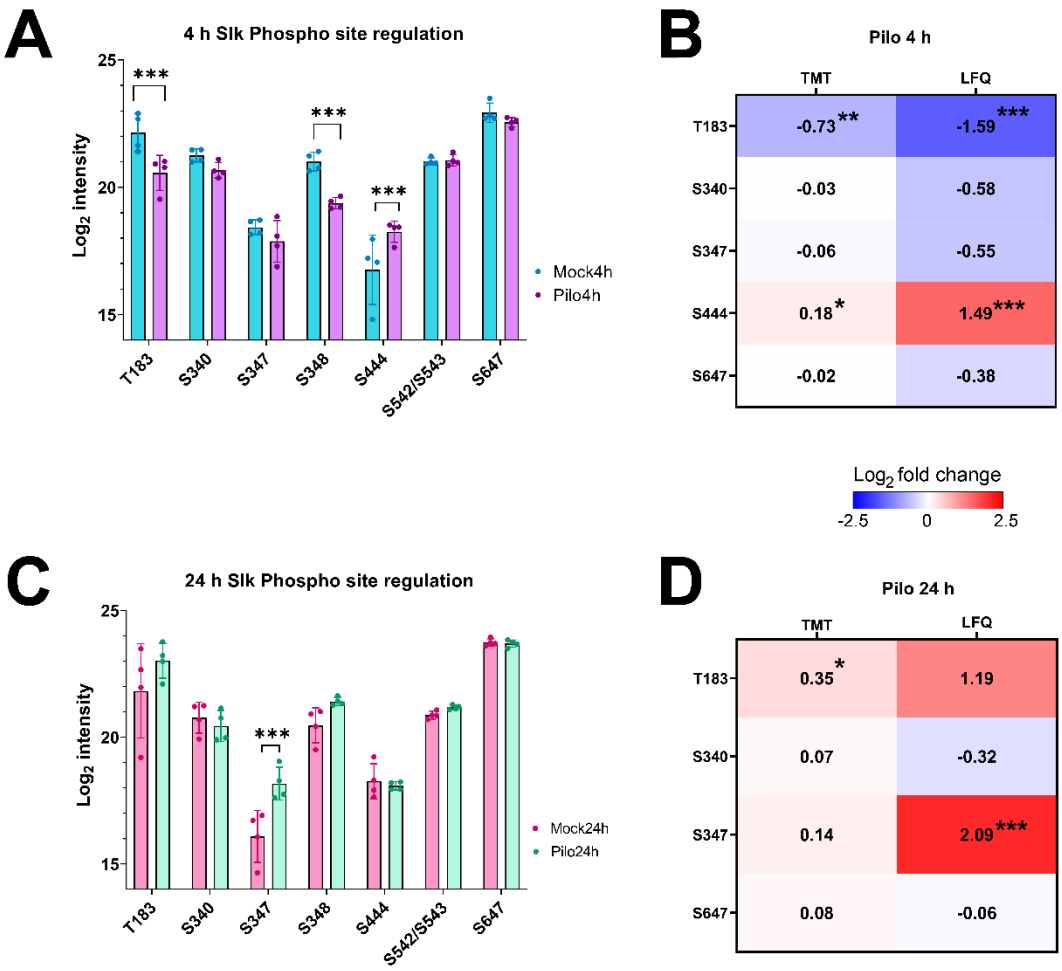

Figure 3.9. Parallel reaction monitoring analysis of activity-modified phosphorylation of SLK. (A and C) Fold change in phosphorylation 4 h (A) and 24 h (B) after pilocarpine induced stimulation using label-free quantitation (LFQ). (B and D) Comparison of quantitative pilocarpine results from the TMT discovery screen and LFQ PRM analysis at 4 h (B) and 24 h (D). *** designates significant level changes (adjusted P value > 0.0006). ** designates significant level changes (adjusted P value > 0.005). * designates significant level changes (adjusted P value > 0.05).

3.8 Discussion of SLK validation

3.8.1 TMT ratio-compression

The SLK phosphopeptide data from the TMT discovery screen and the LFQ PRM at both 4 h and 24 h reflected the same direction of regulation but differed in the magnitude change. This

greater magnitude change in the PRM data was to be expected as TMT reporter ions suffer from 'ratio-compression'[271]. Ratio-compression is an issue unique to isobaric tag labelling experiments, where contaminating background peptide ions are selected for fragmentation alongside target ions due to a wide preset MS isolation windows [272,273]. As quantitation of peptides between samples in a TMT experiment is measured with respect to the ratio of TMT reporter ions, the introduction of contaminating peptides into the MS^2 scan introduces additional reporter ions distorting the TMT reporter ion ratio for the target ion [272,273]. As a result, the measure of relative peptide abundance between TMT labelled samples is underestimated[272,273]. Sample fractionation prior to LC-MSMS can lower the abundance of contaminating peptide ions during MS, however, the ratio-compression effect is not completely eliminated [273]. The addition of a third ion fragmentation event (MS^3) has been shown to almost eliminate the ratio-compression effect completely [273], but this technology was not accessible for the TMT discovery screen. Hence the necessity to perform data validation using LFQ PRM, which is not affected by the same phenomenon.

3.8.2 SE triggers SLK phosphorylation

It was not known if a signalling mechanism linked SLK to electrophysiological activity. Here, we show by PRM analysis that the phosphorylation status of key sites that are known to regulate SLK change in response to the hyperactivity induced by status epilepticus [267], validating our TMT results. A key site was T183, in the activation segment of SLK [268], which was dephosphorylated early after status epilepticus (4 h) and then re-phosphorylated at 24 h. This indicates that SLK may be inactivated by high activity, but eventually recovers. The phosphatases activated by calcium influx have also been shown to return to basal activity after 24 h in a status epilepticus model [274]. Another key site, S348 was also dephosphorylated at 4 h, which is permissive for SLK activity [270]. We note that an adjacent site, S347, which shares

the same function, was also dephosphorylated by application of elevated KCl for 10 s to hippocampal cultured neurons [95]. S347 had increased phosphorylation at 24 h post-status epilepticus. A casein kinase 2 mechanism can provoke an inhibition of SLK activity through S347/S348 phosphorylation[270]. Thus, there was a reversal of this regulatory mechanism from 4 to 24 h. We don't know whether these phosphorylation site changes occurred on the same molecule or in the same cells, potentially opposing each other in regulating SLK activity. These questions will require further work. SLK protein level did not change after high electrophysiological activity. Thus, it is clear that acute electrophysiological activity is mechanistically linked to SLK activity via phospho-signalling and not protein expression.

Chapter 4. Epilepsy in a dish: A follow up study of MTOR signalling in an *in vitro* epileptogenesis model

4.1 Introduction

Mammalian target of rapamycin (MTOR) is a serine/threonine kinase involved in signalling that controls cellular metabolism, growth, proliferation, and survival [275]. MTOR signalling is directed by two distinct protein complexes, MTOR complex 1 (MTORC1) and 2 (MTORC2) [275,276]. MTORC1 is currently thought to modify cellular responses through the regulation of protein synthesis, whilst MTORC2 is associated with cytoskeletal organisation and is thought to moderate MTORC1 activity [170,275,276]. MTORC1 directed protein synthesis is known to be required for the induction of various forms of synaptic plasticity such as synaptic upscaling [53,54] and LTP [277], whilst MTORC2 activity is necessary for LTD [278]. Given the central role of MTOR signalling in the brain, it is unsurprising that the dysregulation of this cascade has been associated with various neurological and neurodevelopmental disorders, such as epilepsy, autism, and Alzheimer's disease [275,276]. Furthermore, increased MTORC1 activity is associated with increased seizure severity in epilepsy models of tuberous sclerosis complex and focal cortical dysplasia [279]. In general, studies pharmaceutically inhibiting MTORC1 by rapamycin indicate some antiepileptogenic effects and have shown success in the reduction of spontaneous seizure activity in some models of epilepsy [130,280-282] with exceptions [129,283]. Everolimus (EvLS), another MTORC1 specific inhibitor has shown similar antiseizure effects in a similar mouse model [284]. Overall, these studies provide indications that perturbed MTORC1 activity may be associated with epileptogenesis.

The phosphoproteomic and proteomic discovery screen of epileptogenesis performed in Chapter 3 of this thesis provided evidence of early MTOR activation. To follow up the results from the discovery screen, we sought to further explore the role of MTOR signalling in

epileptogenesis using bicuculline (Bic) stimulated primary hippocampal cultures as an *in vitro* model of epilepsy. Microelectrode array (MEA) was employed to measure perturbations in neuronal network activity and western blot was used to measure MTORC1 activity, to test our hypothesis that MTORC1 activity is associated with epileptogenesis.

Briefly, MEA analysis constitutes the plating of dissociated neurons in specialised tissue culture plates with embedded microelectrodes to measure the electrical activity of neuronal networks [285]. The plated neurons grow unperturbed on the MEA plates possessing characteristics of *in vivo* neurons, such as a capacity for spontaneous firing and network forming capabilities [286]. The neurons can then be non-invasively stimulated through the introduction of drugs into the media and monitored for changes in electrical activity[287]. Work from the Bradley, et al. [287] group profiled the electrophysiological responses of various types of *in vitro* epilepsy models in rat cortical neurons using MEAs. The group found that Bic stimulated models exhibited responses in burst structure and network synchrony that fit a seizurogenic profile [287]. For this study, the electrophysiological responses from stimulated neurons were monitored with MEAs to observe the increased firing and burst rate described by the Bradley, et al. [287] group. The MTORC1 inhibitor EvLS [288] was used. The activity of MTOR signalling was assessed through western blot, monitoring the relative protein and phosphorylated protein levels of p70 S6 kinase, a downstream effector of MTOR signalling. The aim of this follow-up study was to functionally characterise the involvement of MTOR signalling in early epileptogenesis.

4.2 Results

4.2.1 Optimisation of cell seeding density for *in vitro* model

To explore the ideal cell seeding conditions for MEA experiments, dissociated neuron cultures were grown in 24 well MEA plates for the optimisation of an *in vitro* epilepsy model (Figure 4.1A). Two biological replicates were used for the optimisation experiments, using one MEA plate for replicate one and two MEA plates for replicate two, due to tissue availability. The seeding density for the microelectrodes was optimised through the plating of various densities (90K, 70K, 50K and 30K cells per well) and tested by measurement of the spikes generated per second from each well (Figure 4.1B). Two different electrode seeding techniques were also tested, denoted "whole well seeding" and "electrode seeding" (Figure 4.1B and C). The electrode seeding technique detected activity in only 2-4 wells in the 70K cell seeding density from 12 wells tested. Little to no activity was detected in the 90K, 50K and 30K cell densities at days *in vitro* (DIV)14-16 (Figure 4.1B). The whole well seeding technique yielded activity for 2-5 wells from the 6 wells tested at every seeding density. To test the time taken for neurons to become active and reach a stable firing rate, plated neurons were taken for 10-minute MEA recordings without stimulation from DIV7 and measured every two to three days until DIV16 (Figure 4.1B). Based on reliability of seeing any signal, the whole well seeding technique was employed for subsequent experiments (Figure 4.1B). Wells seeded with 70K cells produced the strongest electrophysiological activity between DIV14-16 (Figure 4.1B) and this density was used thereafter.

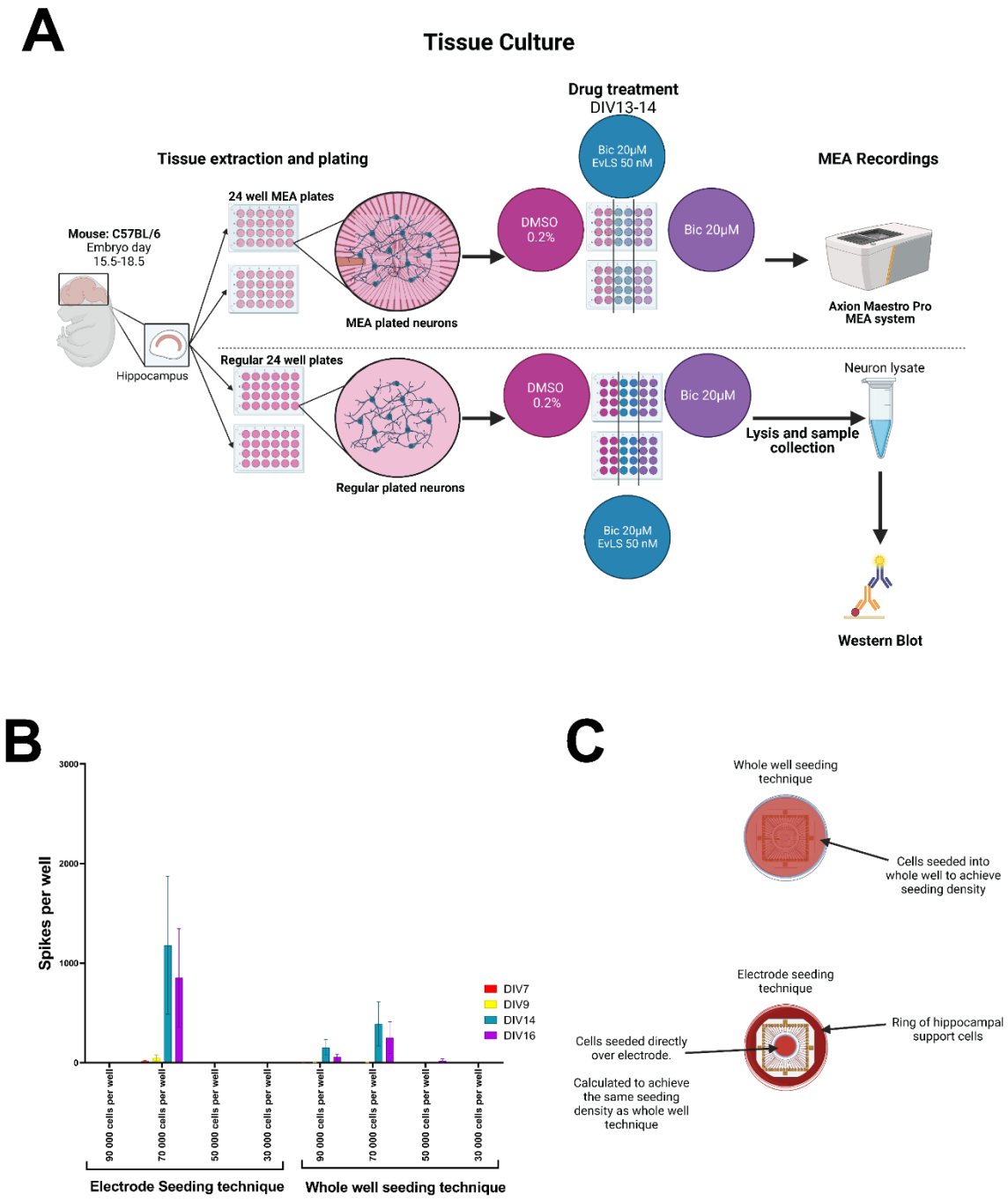

Figure 4.1. Experimental overview of MTOR signalling in an *in vitro* epileptogenesis model. (A) The hippocampus was harvested from embryonic mice at E15.5-E18.5. The hippocampal tissue was dissociated and plated in both regular and MEA 24 well plates and grown until DIV13-14 for use in experiments. One biological replicate constituted two 24 well MEA plates and one regular 24 well plate. On each plate 8 wells were stimulated with either Bic 20µM, Bic 20µM + EvLS 50nM or DMSO 0.2% control. Neurons on regular plates were lysed and harvested 6 h following stimulation for western blot experiments. MEA experiments required a 5 min baseline MEA recording prior to stimulation followed by MEA readings at 30

min, 1 h, 2 h, 6 h, 24 h and 48 h following stimulation. (B) Bar graph of average detected spikes per well for each seeding density colour indicated for DIV7 (red), DIV9 (yellow), DIV14 (blue) and DIV16 (purple). The seeding technique is indicated below corresponding data as "Electrode seeding technique" or "Whole well seeding technique". The ± SEM is indicated as error bars. (C) An illustration of the two different seeding techniques used. Created with BioRender.com.

4.2.2 Electrophysiological and physiological analysis of bicuculline stimulated neurons

Increased MTORC1 activity is associated with hyperexcitable neuronal activity[170] and the pilocarpine induced phosphoproteome changes implicated MTOR. To explore the role of MTOR signalling in early epileptogenesis, Bic stimulated neurons were used to induced seizure-like activity in hippocampal neuronal cultures and MTORC1 was inhibited using EvLS[288]. For each 24 well plate, eight wells were stimulated with either 0.2% DMSO (Control), 20 μM Bic, or a combination of 20 μM Bic and 50 nM EvLS (Figure 4.1A). For the 24 well MEA plates, control, Bic and Bic/EvLS stimulated cultures were subjected to 5-minute MEA recordings prior to stimulation to obtain a baseline reading for data normalisation (Figure 4.1A). To track changes in firing rates and number of bursts, a 10-minute MEA recording was also performed at 5 min, 30 min, 1 h, 2 h, 6 h, 24 h and 48 h following stimulation.

To account for differences in detected well activity on individual MEA plates, the raw MEA output was analysed as described in Chapter 2 Section 2.4.3.1. From the three biological replicates the normalised data was averaged and plotted to display the mean firing rate and number of bursts across all timepoints for each treatment as shown in Figure 4.2E and F, respectively.

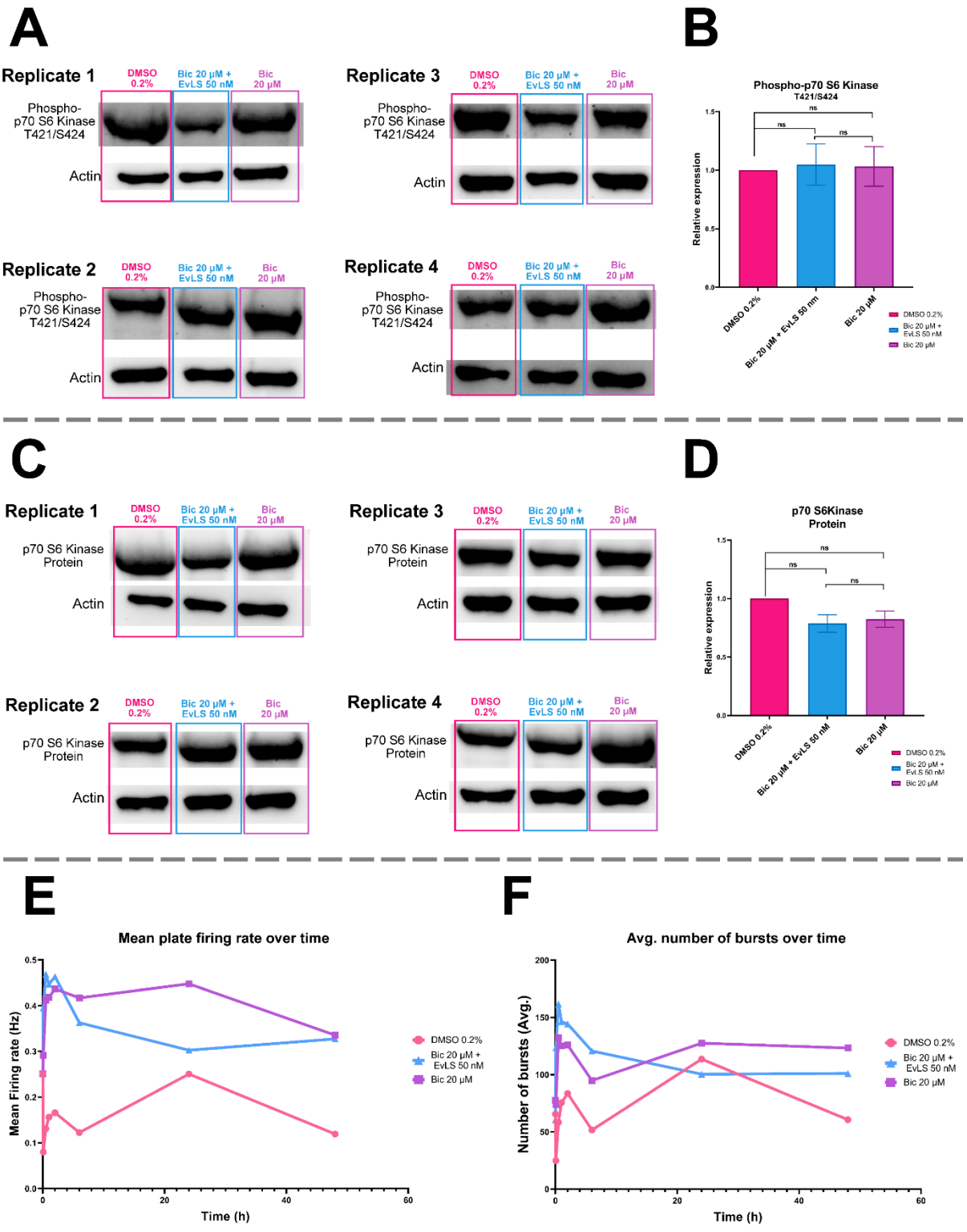

Figure 4.2. Western blot and MEA analysis of MTOR activation in Bic stimulated neurons. (A) Western blots of phospho-p70 S6 kinase for each replicate with the corresponding actin loading control. The lanes are colour coded to indicate the DMSO (pink),

Bic/EvLS (blue) and Bic (purple) treatments respectively. (B) The average relative expression level of phospho-p70 S6 kinase is represented in a bar graph. The lanes are colour coded to indicate the DMSO (pink), Bic/EvLS (blue) and Bic (purple) relative expression. An unpaired, two-tailed t-test with welch correction was conducted with no significance determined. The comparisons conducted were DMSO vs Bic (p val = 0.86), DMSO vs Bic/EvLS (p val = 0.81) and Bic vs Bic/EvLS (p val = 0.95), as indicated in the graph. (C) Western blots of p70 S6 kinase protein for each replicate with the corresponding actin loading control. The lanes are colour coded to indicate the DMSO (pink), Bic/EvLS (blue) and Bic (purple) treatments respectively. (D) The average relative expression level of p70 S6 kinase protein is represented in a bar graph. The lanes are colour coded to indicate the DMSO (pink), Bic/EvLS (blue) and Bic (purple) relative expression. An unpaired, two-tailed t-test with welch correction was conducted with no significance determined. The comparisons conducted were DMSO vs Bic (p val = 0.09), DMSO vs Bic/EvLS (p val = 0.07) and Bic vs Bic/EvLS (p val = 0.73), as indicated in the graph. The average (E) mean firing rate and (F) number of bursts from the normalised MEA replicate data is plotted for all timepoints. The average treatment values for the mean firing rate and number of bursts is colour coded to indicate the DMSO (pink), Bic/EvLS (blue) and Bic (purple) well values.

To gauge MTOR activity under each of the respective treatment conditions, cell lysates were harvested from the regular 24 well plates 6 h following stimulation. There were four biological replicates used for the analysis. Proteins from the neuronal lysate were blotted with anti-phospho-protein p70 S6 kinase (T421/S424) and anti-p70 S6 kinase, as well as anti-actin for a loading control (Figure 4.2A and C, Appendix 17 and 18). Densitometry analysis was performed for the actin, p70 S6 kinase protein and phospho-p70 S6 kinase blots to obtain a relative expression value for the Bic and Bic/EvLS treatments with respect to the DMSO control for each replicate. The relative protein expression levels from the western blot analysis were normalised as described in Chapter 2 Section 2.5.1.4. The average relative protein expression is plotted in bar graphs for phospho- and protein S6 kinase, shown in Figure 4.2B and D.

4.2.3 No difference in relative p70 S6 kinase protein and phospho-protein expression

The MEA data for both the mean firing rate and number of bursts for both Bic and Bic/EvLS treatments indicated that the neurons were being highly stimulated (Figure 4.2E and F). The DMSO control had a lower mean firing rate and number of bursts. As only 3 replicates were used for the MEA analysis, more repetitions will be required before any conclusions can be made. The western blot analysis indicated no significant difference in relative protein expression between the DMSO, Bic and Bic/EvLS treatments for both the phospho- and protein S6 kinase blots.

4.3 Discussion

4.3.1 Bicuculline stimulation does not engage MTOR signalling pathway

In measuring the activity of Bic treated neurons, I expected that the network activity might drop to below the level of the DMSO control, as others have observed with a stronger picrotoxin treatment [289]. In general, the activity was above or similar to the control at late time points (24-48 h). Further repetition of the experiment may have clarified whether Bic stimulation results in a different background network activity level. When applying the MTORC1 inhibitor, the activity could have changed or stayed the same depending on the role of MTORC1 in the time course examined, which we have not yet established. The the activity with and without the MTORC1 inhibitor was similar, from a qualitative perspective. Thus, we find no indication of a role for MTORC1 in this model. This experiment is somewhat preliminary and would be improved by greater repetition.

Chapter 5. Proteomic and phosphoproteomic study of synaptic downscaling

5.1 Introduction

Homeostatic regulation of synaptic activity prevents the establishment of neuronal networks that tend to reach extremes of high or low activity[2]. An increasing number of studies have implicated the connection between dysregulated homeostatic mechanisms and various neurological disorders such as schizophrenia[30], Rett syndrome[75], autism[290] and epilepsy[177]. Whilst other studies have demonstrated the therapeutic potential of pharmaceutically targeting homeostatic mechanisms, such as tropomyosin receptor kinase B signalling for mood disorders[291-293]. Examining the overlap of homeostatic mechanisms with neurological disorders may yield a better understanding of these conditions and open an avenue for drug discovery.

Proteomic studies of synaptic scaling by Schanzenbacher et al. investigated the identity of newly synthesised proteins in response to perturbed activity[37,38]. The group found that the largest functional groups of newly synthesised proteins were kinases and phosphatases followed by ubiquitin-proteosome pathway proteins, implicating protein translation, degradation and posttranslational modifications as mechanisms for homeostatic regulation [37,38]. Other differentially expressed proteins were members of the pre- and postsynaptic terminal associated with neurotransmitter receptors, ion channels and synaptic-vesicle release [37,38]. A follow up analysis of the phosphoproteome found that identified phosphoproteins were involved in cytoskeletal reorganisation and were mainly located at synapses[39].

The proteomic studies by Schanzenbacher et al. only explored synaptic proteomic changes at 2 and 24 h during up- and downscaling. A phosphoproteomic study by Desch, et al. [39], which was completed during the course of my investigation, focused only on the 5 min, 15 min and

24 h timepoints. The limited timepoints explored meant that many time-dependent processes may be being overlooked, as newly synthesised proteins would become more apparent after hours, rather than minutes, of stimulation and the full strength of synaptic scaling mechanisms can take up to 48 h to manifest[2,146]. They used the Kinase–Substrate Enrichment Analysis (KSEA) tool to perform kinase activity predictions and produced limited results, since KSEA relies heavily on known kinase substrates[294].

In this study, the aim was to provide a broader temporal landscape of proteomic and phosphoproteomic alterations occurring during synaptic downscaling across seven timepoints. Here a large-scale study of phospho-signalling during synaptic downscaling is presented, tracking 15,439 phosphopeptides changes across early (5 and 30 min), mid (1, 2 and 6 h) and late timepoints (24 and 48 h). The 7,278 protein changes across all seven timepoints is also detailed. Increased persistent phosphorylation targeting the regulation of translation was observed. Both persistent and varied temporal patterns of synaptic protein dephosphorylation was observed. Using software to infer protein kinase activity, p90RSK was predicted to have high activity and CDK5 was predicted to have low activity. The data generated from this study was validated against the results generated from the Desch et al. group. Furthermore, the results of this synaptic downscaling study were contrasted with the results from the early epileptogenesis study (Chapter 3) to reveal specific differences. Collectively, this study serves as a valuable resource to understand the phosphorylation-based mechanisms underlying synaptic downscaling.

5.2 Results

The hippocampus was extracted from E15.5-E18.5 C57/Bl6 mice and cultured *in vitro* for 14-16 days (Figure 5.1A and Chapter 2, Section 2.4.1.1). Two 12-well plates were required to generate samples for the eight time points. To commence the experiment, 0 min control wells were lysed and collected and all other wells were stimulated with 20 µM Bicuculline (Bic). At the respective 5 min, 30 min, 1 h, 2 h, 6 h, 24 h and 48 h timepoints, the samples were lysed and collected for analysis (Figure 5.1A and Chapter 2, Section 2.4.1.1). Approximately 50 µg of protein from the eight samples was reserved for western blot. Collaborators used western blot of phosphoERK to confirm that Bic stimulated the neurons (Figure 5.1A, Appendix 19), since increased phosphoERK is a known consequence of elevated activity [39,289]. Proteins were extracted from the remaining sample lysate, digested with trypsin and TMT labelled in a scheme involving two 17-plex sets (Appendix 20A, Chapter 2, Section 2.5.2). Phosphopeptides were enriched and fractionated using the TiSH protocol[103]. Multi- and mono-phosphorylated peptide enriched fractions were analysed by LC-MS/MS to explore the downscaled phosphoproteome (Figure 5.1A). The phosphopeptide-depleted samples were also fractionated to establish proteomic alterations induced by Bic stimulation (Figure 5.1A).

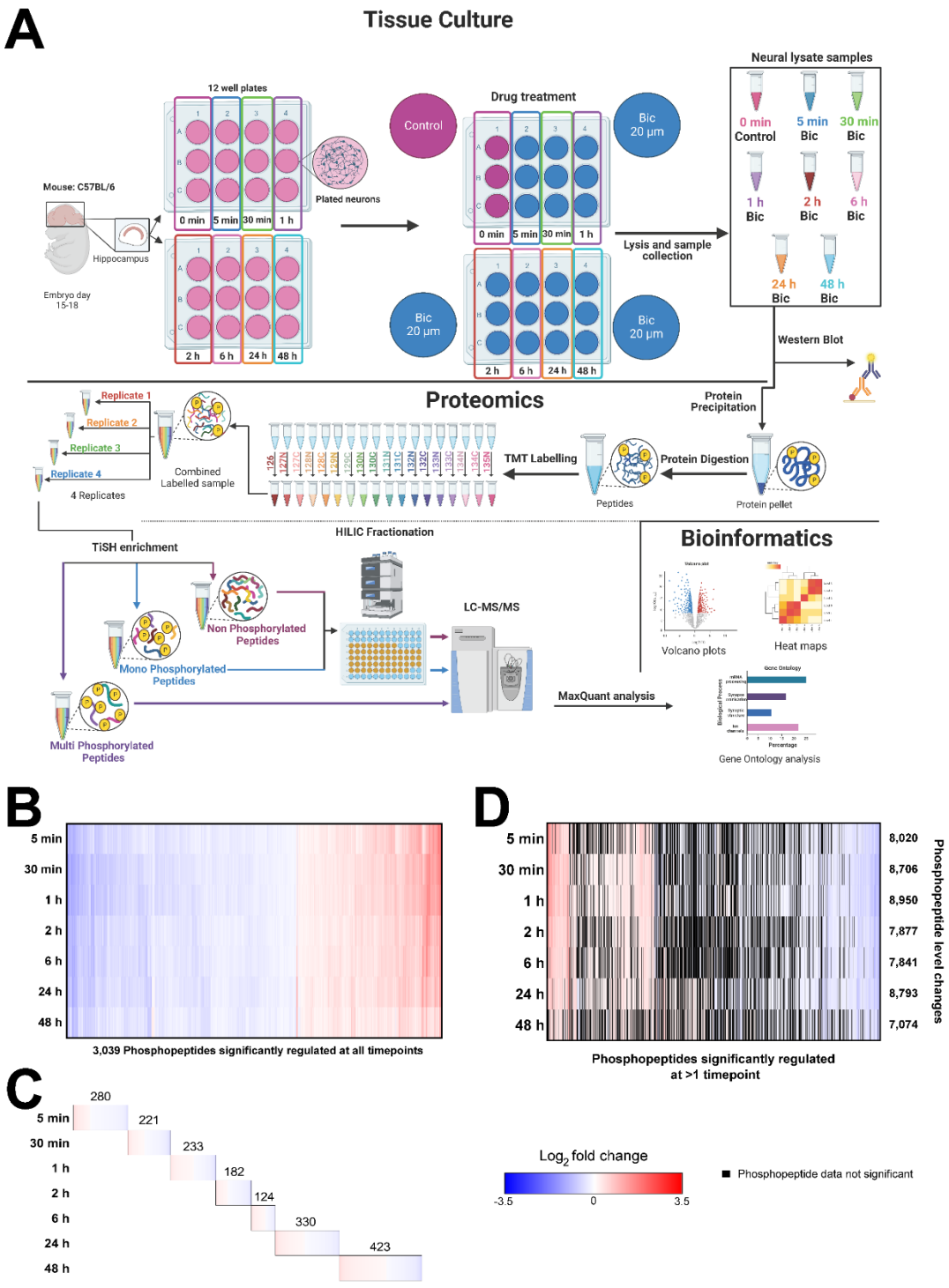

Figure 5.1. Experimental overview and bicuculline induced temporal regulation of the phosphoproteome. (A) Cultured hippocampal neurons were stimulated with 20 µM Bic to induce synaptic downscaling. An unstimulated 0 min control served as a comparison to 5 min, 30 min, 1 h, 2 h, 6 h, 24 h and 48 h timepoints. Samples were lysed and collected at respective timepoints and proteins were subsequently digested and TMT labelled. Labelled samples were

enriched for phosphopeptides and multi-, mono- and non-phosphorylated fractions were analysed by LC-MS/MS. The MS data output was processed to analysis the phosphoproteome and proteome. Heatmaps of log2 fold change values for B) significant phosphopeptides across all timepoints, C) significant phosphopeptides at only one timepoint and D) phosphopeptides significant in at least two timepoints with non-significant values excluded. Heatmaps (B) and (D) are hierarchically clustered. A scale bar of the log_2 fold change is shown.

The raw mass spectrometry data was first processed with MaxQuant to attain raw tables. To obtain highly curated tables and quality control figures, the raw tables were processed down a custom bioinformatics pipeline, involving normalisation and removal of unwanted variation (Chapter 2, Section 2.6.2). One measure of quality control is a principal component analysis (PCA) of the replicate intensities. The PCA was performed to determine both the similarity between sample replicates and the differences between each time point (Appendix18B and C). Following normalisation, individual phosphopeptide sample replicates appeared to cluster in accordance with their respective time points (Appendix 20B). The 0 min control samples appeared to cluster away from the Bic stimulated time course on both components in the phosphopeptide PCA plot (Appendix 20B). In the protein PCA plot, the early to mid Bic stimulated time points (5 min, 30 min, 1 h, 2 h and 6 h) and 0 min controls were clustered on the first component and separated from the late 24 and 48 h samples (Appendix 20C). This may indicate that substantial alterations to the proteome are not manifested until the later time points. The average TMT reporter ion intensities for each time point were then log_2 transformed prior to statistical analysis. The log_2 fold change was calculated by comparison of each Bic-stimulated time point to the 0 min control (as the log of the ratio or the difference of logs, which are mathematically equivalent). These comparisons are abbreviated to simply 5 min, 30 min, 1 h, 2 h, 6 h, 24 h and 48 h. For the purposes of the analysis, early timepoints are 5 and 30 min,

mid timepoints are 1, 2 and 6 h, and late timepoints are 24 and 48 h. The raw phosphoproteome and proteome data is supplied as tables in Appendix 21 and 22 respectively.

5.2.1 Temporal phosphoproteomic profile of synaptic downscaling

The phosphopeptide data was processed as described in (Chapter 2, Section 2.6.2). Following data processing, 15,439 phosphopeptides with quantitative information across all time points was obtained. 3,039 phosphopeptides showed significant regulation at every time point (Figure 5.1B). Some phosphopeptides demonstrated significance at only one time point (Figure 5.1C), with the lowest number of uniquely significant phosphorylation events occurring at 6 h (124 phosphopeptides) and the largest number occurring at 48 h (423 phosphopeptides). Further analysis indicated that over 7,000 phosphopeptides were significantly regulated in at least two or more time points (Figure 5.1D).

5.2.2 Gene ontology enrichment of synaptic downscaling and general data analysis approach

To gain an understanding of the cellular processes and functions influenced by phosphorylation events across the Bic stimulation time course, a GO term enrichment analysis was performed (Appendix 23). The same GO enrichment approach described in Chapter 3 Section 3.3 was used. The GO enrichment was performed separately for significantly up- and downregulated phosphorylation events.

To generate heatmaps of the protein phosphorylation events contributing to the enriched GO terms, gene lists associated with chosen GO terms were extracted using QuickGO[295] or ComPath[296], since the gProfiler output contains only a limited list of ranked genes. The phosphorylated peptide rank, limited to either up or down-regulation, as described in Chapter 3 section 3.3, was used to create a new combined rank for the timepoints in which the GO term

was enriched. The top 30 phosphorylated proteins were determined based on the combined rank to create the heat map.

5.2.3 RNA processing proteins were phosphorylated following Bic stimulation

Enriched GO terms for upregulated phosphorylation site changes are presented in Figure 5.2A-D. Most molecular function, biological process and WikiPathways GO terms were significantly enriched in the early to mid time points (Figure 5.2A, B and D). These included the terms dendrite development, nucleoside-triphosphatase regulator activity and mRNA processing (Figure 5.2A, B and D). The list of genes corresponding to the dendrite development, nucleoside-triphosphatase regulator activity and RNA processing terms were compared to significantly up regulated phosphorylation sites. The top ranked 30 genes were extracted and are presented in a hierarchically clustered heatmap (Figure 5.2E-G). The protein phosphosite fold changes of select proteins associated with the top ranked 30 genes shown in the heatmaps (Figure 5.2E-G) were extracted and presented as XY scatters in Figure 5.2H-K.

In the heatmap of genes corresponding to the wiki pathway term mRNA processing (Figure 5.2D), RNA binding and processing proteins appeared to become increasingly phosphorylated in distinct time windows. The RNA binding proteins which increased phosphorylation at the early to mid-timepoints were pumilio homolog 1 (encoded by *Pum1*), nucleolin (encoded by *Ncl*), and RNA-binding protein FUS (encoded by *Fus*) (Figure 5.2G and I). Other RNA binding proteins were phosphorylated at late timepoints, these included splicing factor, proline- and glutamine-rich (encoded by *Sfpq*), and polyadenylate-binding protein 1 (encoded by *Pabpc1*) (Figure 5.2G). The exception was the mRNA processing protein apoptotic chromatin

condensation inducer in the nucleus (encoded by *Acin1*) which was persistently phosphorylated across all timepoints (Figure 5.2G).

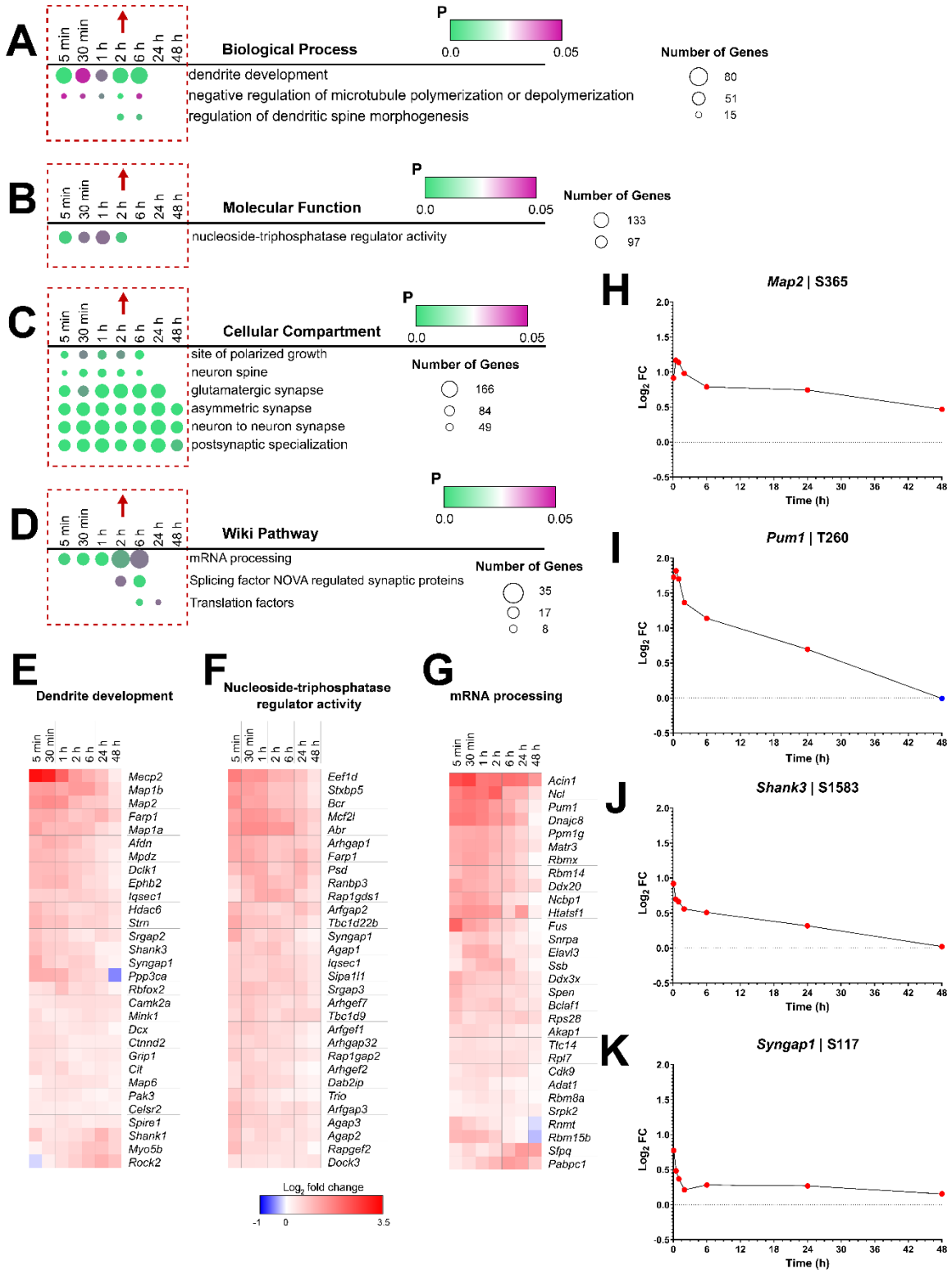

Figure 5.2. Gene ontology term enrichment analysis of temporally up regulated phosphorylation. Enriched GO terms for up regulated phosphosites across all timepoints from (A) Biological Process, (B) Molecular Function, (C) Cellular Component and (D)

WikiPathway sources. A scale bar for probability is shown. The size of the circle represents the number of genes enriched for each term. A heatmap of the top 30 ranked phosphopeptide signals, represented by the associated gene name, for the biological process term (E) dendrite development, molecular function term (F) nucleoside-triphosphatase regulator activity, and WikiPathway term (G) mRNA Processing are hierarchically clustered. A scale bar of the log_2 fold change is shown for all heatmaps. Proteins were required to have a significant change at one or more time points. Scatter plots of the (H) MAP2 S365, (I) PUM1 T260, (J) SHANK3 S1583 and (K) synGAP1 S117 top ranked phosphorylation sites are shown with values for the seven timepoints indicated as dots. The dots are coloured either red or blue to indicate values above or below 0, respectively.

From the RNA binding molecules identified, the proteins encoded by *Sfpq*, *Pum1* and *Fus* are known to play important roles in the alternative splicing of neurotransmitter receptors, Ras/Rap GTPase-activating protein synGAP and Tau [219,297-300](Figure 5.2G and I). These time-specific patterns of RNA binding protein phosphorylation indicates that carefully coordinated posttranscriptional regulation, including alternative splicing, may be activated by protein kinases and play a mechanistic role in synaptic downscaling.

Further supporting a role of translation was the enrichment of the translation factors term at mid-late times. The phosphorylated transcription factors included proteins encoded by *Eif4g1*, *Eif4b*, *Eif3c*, *Eif3a* and *Eef1d* (Appendix 21). Included in this group was the phosphorylation of S422 on eukaryotic translation initiation factor 4B (EIF4B), which causes increased translation and can be phosphorylated by either p90RSK in a MAPK-dependent pathway or by p70S6K via an MTOR-dependent pathway [301].

5.2.4 GTPase regulatory proteins were bidirectionally phospho-regulated

GTPase proteins are involved in spine morphogenesis and synapse development through targeted molecular interactions[302]. In this analysis, members from a parent molecular function

term nucleoside-triphosphatase regulator activity were found to be phosphorylated in the early to mid time points (Figure 5.2B). Whilst members from the daughter molecular function term, GTPase regulator activity were found to be dephosphorylated across the time course (Figure 5.3B).

Members of the nucleoside-triphosphatase regulator activity term included various Rho GTPase activating protein families with increased phosphorylation at early timepoints. These included ADP-ribosylation factor GTPase-activating protein family (ARFGAPs), Rho GTPase-activating protein family (ARHGAPs) and Arf-GAP with GTPase, ANK repeat and PH domain-containing protein (AGAP) family proteins (Figure 5.2F). Notably synGAP, a GTPase regulator and mediator of NMDAR signalling in the postsynaptic density (PSD) was also upregulated at early time points[78] (Figure 5.2F and K).

The molecular function term GTPase regulator activity had members which were strongly dephosphorylated in the 30 min to 1 h interval (Figure 5.3F). Notable dephosphorylated proteins in this group were the ARHGAPs and Rho guanine nucleotide exchange factor TIAM1, which is known to be involved in synaptogenesis (Figure 5.3H) [303]. Overall, Bicuculline stimulation induced both increased and decreased phosphorylation of GTPase regulatory proteins. In general, GTPase regulatory proteins were similar to the synapse-related proteins, which they often regulate, in the way they were represented by both increased and decreased phosphorylation.

5.2.5 Dendrite and synapse related GO terms enriched in both up- and downregulated phosphorylation events

The biological process terms associated with increased phosphorylation (Figure 5.2A) were related to microtubule polymerisation and dendrite morphogenesis. The highly ranked genes

associated with dendrite development (Figure 5.2E) were microtubule and cytoskeletal proteins. Thus, postsynaptic cytoskeletal proteins appear to be major substrates of phosphorylation. For example, the postsynaptic cytoskeletal proteins microtubule associated protein (MAP) 1A and MAP2 had increased phosphorylation in the early to mid-time points (Figure 5.2E and H). Presynaptic MAP1B was also upregulated in the early to mid-time points; however, the dephosphorylation of MAP1B sites was also highly ranked (Figure 5.3D and G). The postsynaptic scaffold proteins SHANK1 and 3 had highly ranked increased phosphorylation, but with different patterns across the time course (Figure 5.2E and J). Dephosphorylation of SHANK1 and 3 sites were also highly ranked (Figure 5.3D and I). From the GO term enrichment of significantly downregulated phosphorylation events, there were dendrite, cytoskeletal and synapse-related terms (Figure 5.3A and B). For example, the synapse organisation biological process term (Figure 5.3A and D) included upper layer PSD scaffolding proteins PSD95 (encoded by *Dlg4*), PSD93 (encoded by *Dlg2*) and SPAR (encoded by *Sipa1l1*)(Figure 5.3D). The strongest fold change was seen in the early 30 min to 1 h interval (Figure 5.3D). The vesicle-mediated transport in synapse biological process term comprised of proteins from the presynaptic terminal associated with the active zone, endocytosis, exocytosis and vesicle tethering. This included dynamin 1 (encoded by *Dnm1*), piccolo (encoded by *Pclo*) and bassoon (encoded by *Bsn*). Proteins involved in synaptic vesicle endocytosis and cell junctions were dephosphorylated early according to the enriched biological process terms (Figure 5.3A), but such trends were driven by subsets of proteins, rather than by all protein members of the enriched term. Overall, Bic stimulation induced dephosphorylation of cell junction, vesicle-associated and postsynaptic scaffold proteins.

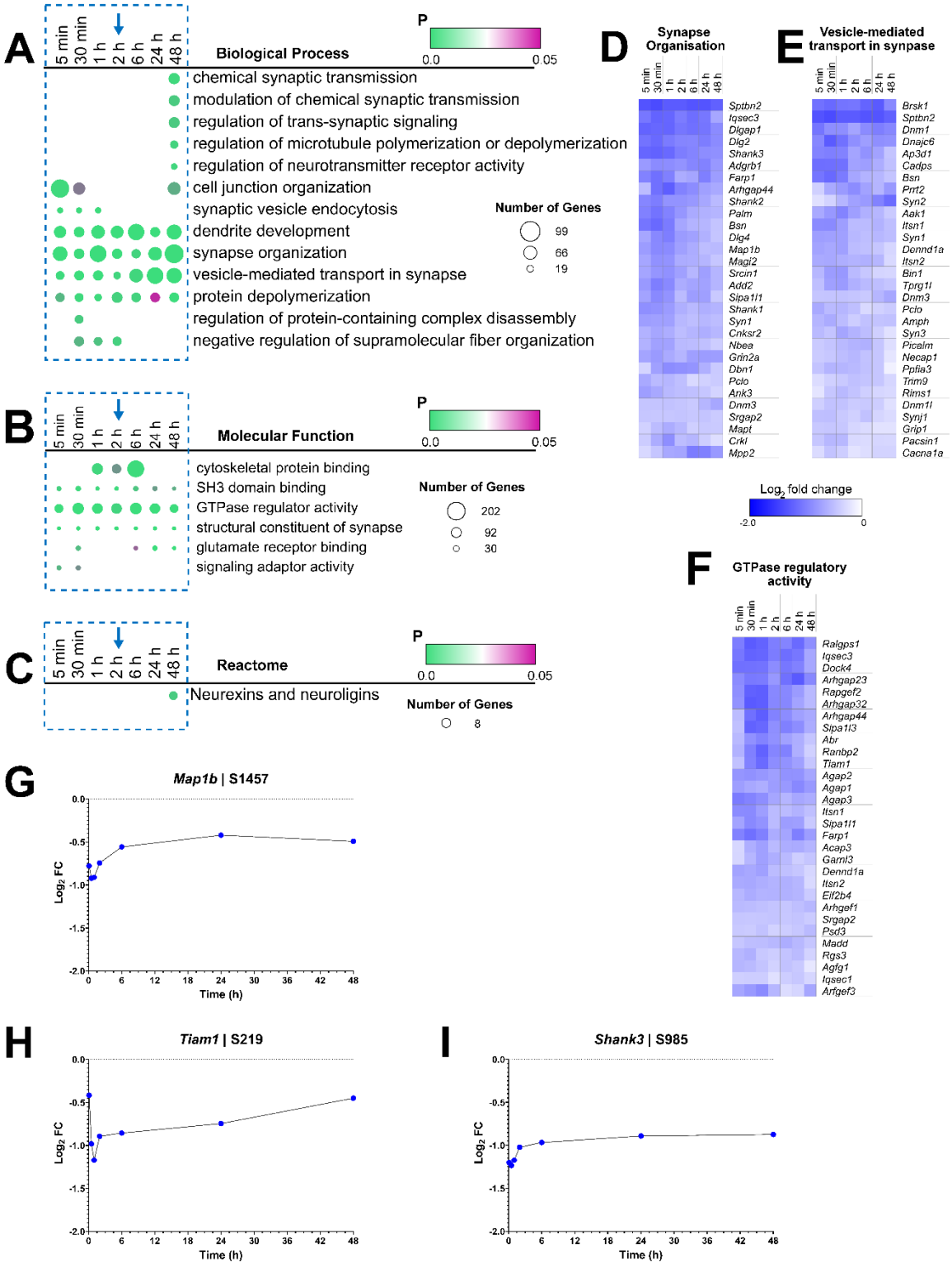

Figure 5.3. Gene ontology term enrichment analysis of temporally down regulated phosphorylation. Enriched GO terms for down regulated phosphosites across all timepoints from (A) Biological Process, (B) Molecular Function and (C) Reactome sources. A scale bar for probability is shown. The size of the circle represents the number of genes enriched for each term. A heatmap of the top 30 ranked phosphopeptide signals, represented by the

associated gene name, for the biological process terms (D) synapse organisation, (E) vesicle-mediated transport in synapse and molecular function term (F) GTPase regulator activity are hierarchically clustered. A scale bar of the log_2 fold change is shown. Proteins were required to have a significant change at one or more time points. Scatter plots of the (G) MAP1B S1457, (H) TIAM1 S219 and (I) SHANK3 S985 top ranked phosphorylation sites are shown with values for the seven timepoints indicated as dots. The dots are coloured either red or blue to indicate values above or below 0, respectively.

5.2.6 Presynaptic proteins predominantly dephosphorylated

To simplify the data and thereby obtain an "overall" direction of phosphorylation, the median phosphorylation log_2 fold change was calculated for core pre- and postsynaptic proteins. The median was calculated for all time points using the phosphopeptides that had at least one significant change at any time point (Appendix 21). The median and site-level phosphopeptide log_2 fold changes for core presynaptic and postsynaptic proteins are presented as heatmaps in Figures 5.4 and 5.5, respectively. Ambiguous patterns of phosphorylation and supplementary figures of presynaptic and postsynaptic protein phosphorylation are presented in Appendix 25 and Appendix 26, respectively. A phosphorylation state summary of presynaptic and postsynaptic proteins at the synapse are presented in Figure 5.6 and 5.7.

An analysis of the median phosphorylation state of presynaptic proteins provided a different perspective to the maximum up/down regulation in the GO term analysis. I found that most proteins tended toward an overall state of dephosphorylation (Figure 5.4, Appendix 24).

These included endocytosis, exocytosis, active zone and SNARE (Soluble N-ethylmaleimide-sensitive factor activating protein receptor) proteins. Many key proteins within these groups were strongly dephosphorylated at every timepoint. For instance, bassoon (Figure 5.4A, Appendix 24A), piccolo (Figure 5.4A, Appendix 24B) and Munc-13 (Figure 5.4A, Appendix 24C) active zone proteins were strongly dephosphorylated at every time point, as was the

SNARE protein syntaxin 1A (Figure 5.4A, Appendix 24F), the complexin 1 (Figure 5.4A and C, Appendix 24H) exocytosis protein, the endocytosis proteins dynamin 1 (Figure 5.4A and E, Appendix 24I), epsin 1 (Figure 5.4A, Appendix 24N), AP2-associated protein kinase 1 (AAK1; Figure 5.4A, Appendix 24M), AP2 complex subunit μ encoded by *Ap2m1* (Figure 5.4A, Appendix 24J), synaptojanin 1 (Figure 5.4A, Appendix 24K) and syndapin 1 (Figure 5.4A, Appendix 24L). Notably, I found a key RIM1 site S1045 was dephosphorylated across all timepoints (Appendix 21), which is known to induce upscaling through mediating the release of synaptic vesicles when phosphorylated [304]. Overall, presynaptic protein groups tended towards a state of dephosphorylation following Bic stimulation.

5.2.1 Bicuculline induces phosphorylation of a select minority of presynaptic proteins

Some members of presynaptic protein groups defied the group trend and had persistent or temporarily increased phosphorylation. For example, some core endocytosis proteins were dephosphorylated at early timepoints and showed a late increase in phosphorylation, such as the clathrin coat assembly protein AP180 (Figure 5.4A and F, Appendix 25Q). Phosphorylation sites from other endocytosis proteins, such as amphiphysin (Figure 5.4A, Appendix 25R) and the single site detected for AP2 complex member encoded by *Ap2α2* (Figure 5.4A and B, Appendix 25T) had persistently increased phosphorylation (Figure 5.6A-C), defying the trend of median decreased phosphorylation for endocytic proteins.

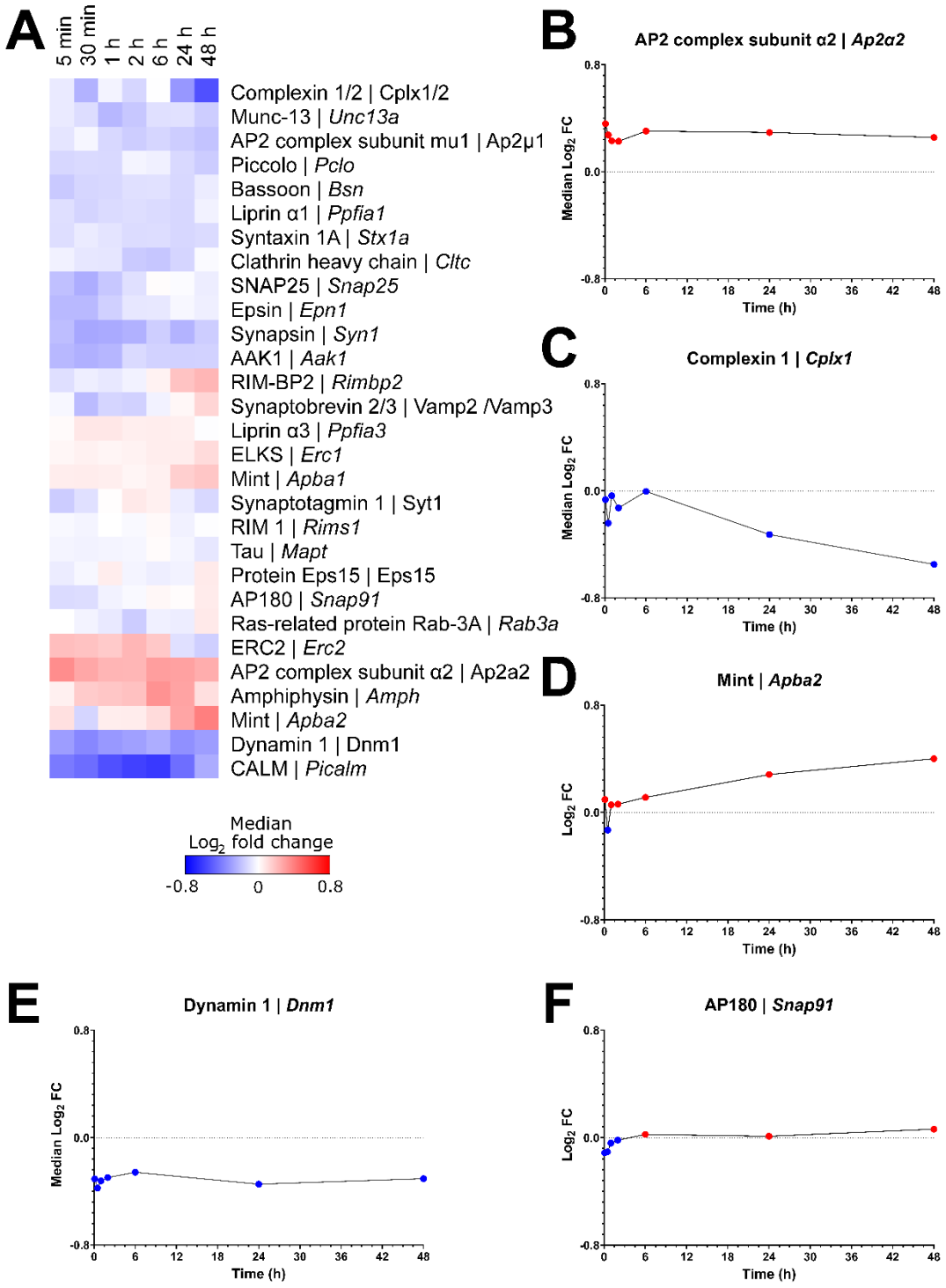

Figure 5.4. Median phosphorylation changes of key presynaptic proteins induced by Bicuculline stimulation. Hierarchically clustered heatmap of the median phosphopeptide $\log_2$ fold changes at every time point for key presynaptic proteins. A scale bar of the $\log_2$ fold change is shown. Scatter plots of median $\log_2$ phosphopeptide fold changes for (B) Ap2 complex subunit α2, (C) Complexin 1, (D) Mint encoded by *Apba2*, (E) Dynamin 1 and (F) AP180

proteins are shown for all timepoints indicated as dots. The dots are coloured either red or blue to indicate values above or below 0, respectively.

These patterns of either time specific or persistent phosphorylation were seen amongst the members of the active zone, SNARE and exocytosis proteins (Figure 5.4 and 5.6A-C, Appendix 24 and 25). Persistently phosphorylated active zone proteins were Liprin α3 encoded by *Ppfia3* (Figure 5.4A, Appendix 24P), ELKS (encoded by *Erc1*) (Figure 5.4, Appendix 24Q), and ERC protein 2 (encoded by *Erc2*) (Figure 5.4A, Appendix 25X). These proteins perform scaffold and adapter protein binding roles in the active zone, thereby regulating the exocytosis of synaptic vesicles[305-307]. Mint, encoded by *Apba1* (Figure 5.4A, Appendix 24S), and *Apba2* (Figure 5.4A and D, Appendix 25W), is a non-core member of the active zone and was overall phosphorylated. Notably, liprin α3, ELKS, ERC protein 2 and mint all had increased phosphorylation and have close association with transsynaptic membrane proteins. Exocytosis protein Munc-18 (Figure 5.4A, Appendix 25U) was also phosphorylated and dephosphorylated at varying time points.

5.2.2 Bicuculline induces dephosphorylation of upper layer PSD proteins and phosphorylation of lower layer proteins

Calculation of the median phosphorylation status of postsynaptic proteins supported the GO term analysis in showing that postsynaptic scaffolding proteins were mostly dephosphorylated (Figure 5.7A-C). Focusing on the PSD, these included upper layer PSD93/95 (Figure 5.5A and F, Appendix 26D and E), disks large-associated protein 1 (DLGAP1; Figure 5.5A, Appendix 26J) and SPAR (Figure 5.5A, Appendix 26F).

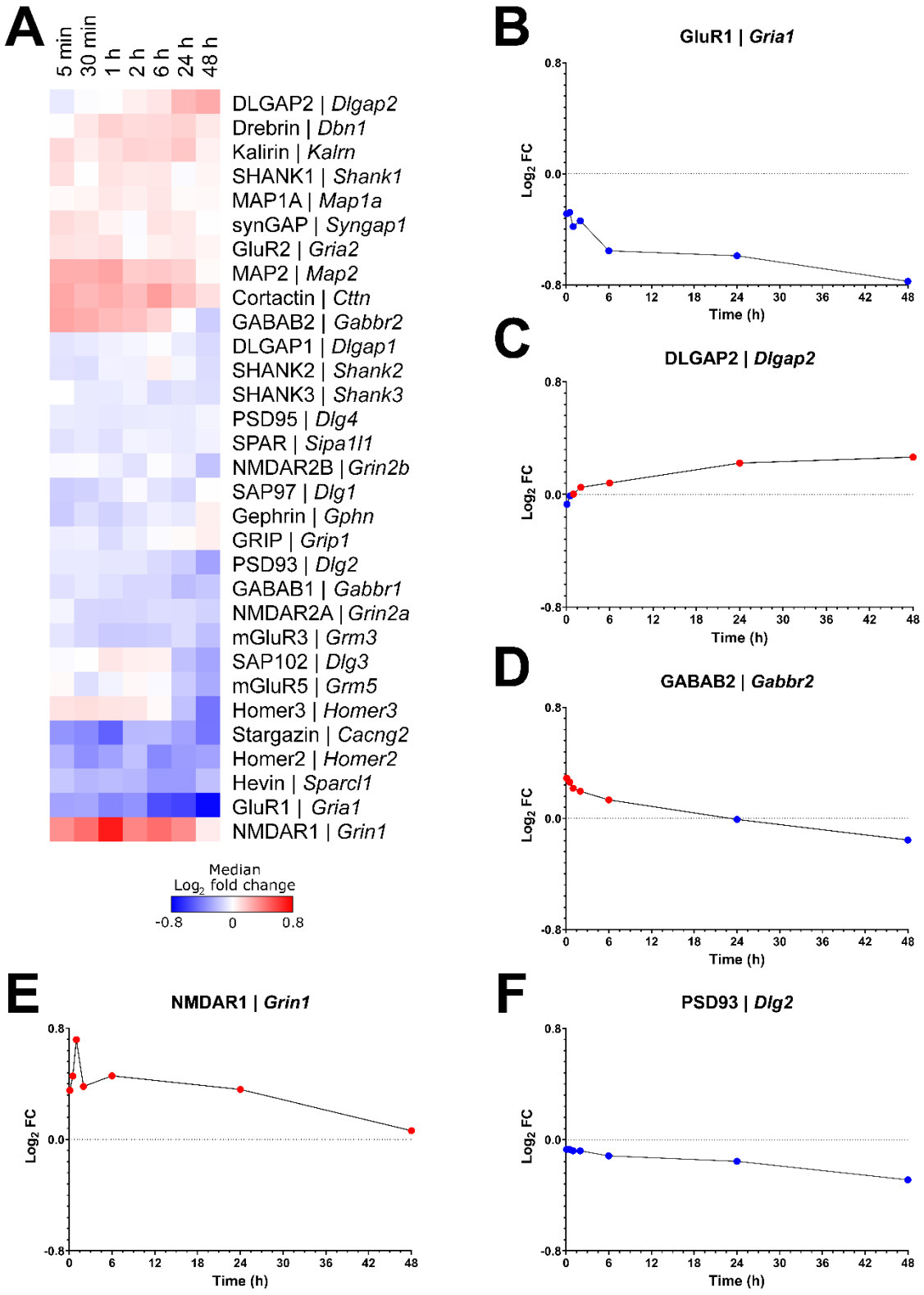

Figure 5.5. Median phosphorylation changes of key postsynaptic density proteins induced by Bicuculline stimulation. (A) Hierarchically clustered heatmap of the median phosphopeptide $\log_2$ fold changes at every time point for key PSD proteins. A scale bar of the $\log_2$ fold change is shown. Scatter plots of median $\log_2$ phosphopeptide fold changes for (B)

GluR1, (C) DLGAP2, (D) GABAB2, (E) NMDAR1 and (F) PSD93 proteins are shown for all timepoints indicated as dots. The dots are coloured either red or blue to indicate values above or below 0, respectively.

Both excitatory and inhibitory PSD scaffolding proteins also showed persistent dephosphorylation, such as stargazin (Figure 5.5A, Appendix 26B), gephyrin (Figure 5.5A, Appendix 26L) and GRIP1 (Figure 5.5A, Appendix 27C). In contrast many lower layer PSD proteins showed persistent phosphorylation. These included actin and microtubule binding proteins like MAP (Figure 5.5A, Appendix 26T and U), SHANK1 (Figure 5.5A, Appendix 26S), SHANK3 (Figure 5.5A, Appendix 26I), cortactin (Figure 5.5A, Appendix 26R) and drebrin (Figure 5.5A, Appendix 26Q). The S142 site on drebrin was found to be dephosphorylated. Phosphorylation of the site by CDK5 is known facilitate F-actin binding and microtubule capture[308]. Other PSD proteins found to be persistently phosphorylated were DLGAP2 and 4 (Figure 5.5A and C, Appendix 27 K and L), kalarin (Figure 5.5A, Appendix 26V), and synGAP (Figure 5.5A, Appendix 26W). Overall, the Bic stimulation induced a dephosphorylation trend of upper layer PSD proteins, with increased phosphorylation of lower layer PSD proteins (Figure 5.7A-C). This is a similar trend to that which was noted following pilocarpine stimulation in the early epileptogenesis analysis (See Chapter 3 Section 3.3 and Figure 3.2Q).

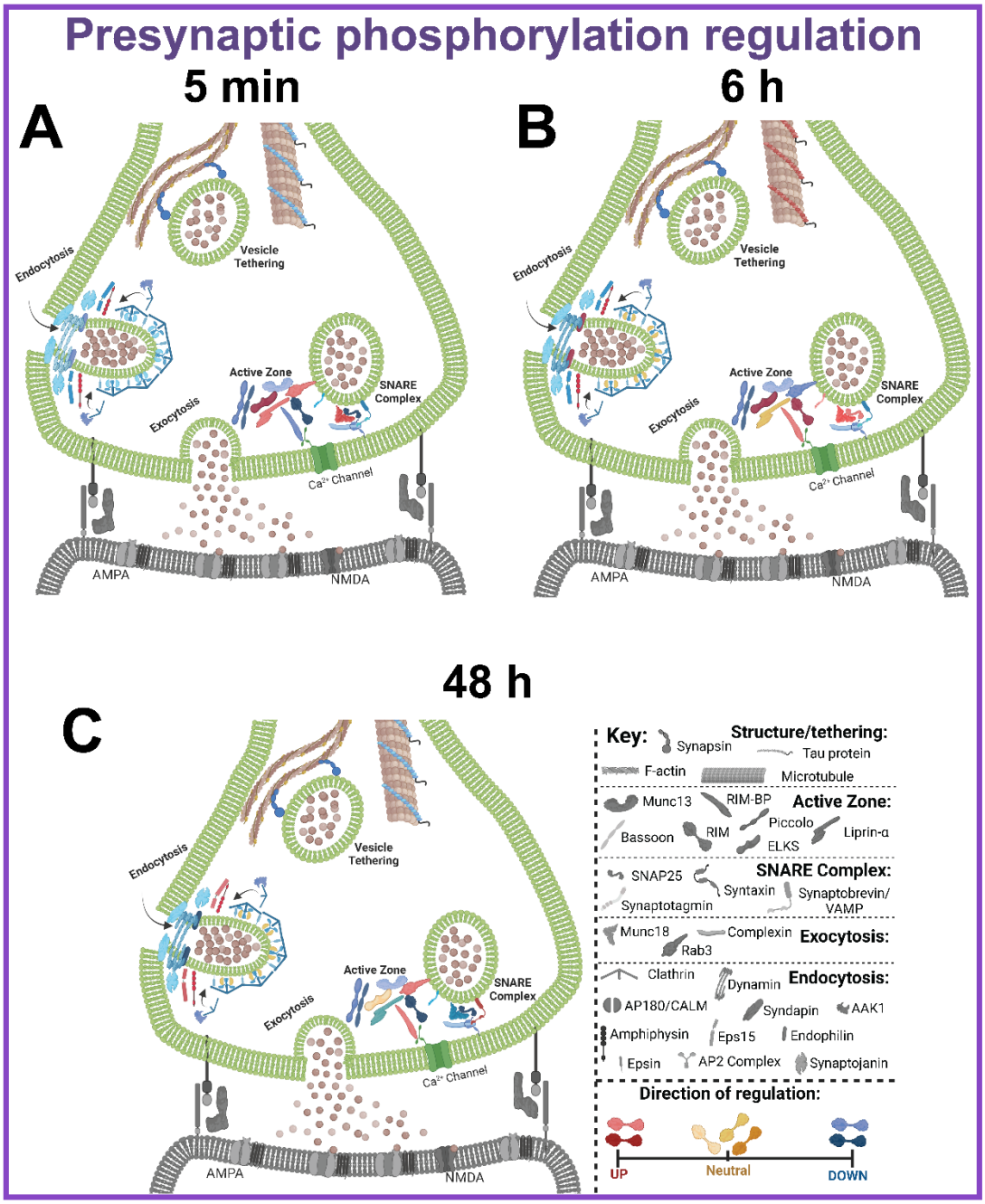

Figure 5.6. Schematic of the presynaptic terminal indicating the overall direction of protein phosphorylation for core proteins involved in neurotransmission. The presynaptic compartments indicate the key phosphorylation events occurring at (A) 5 min, (B) 6 h and (C) 48 h. Members of the active zone, SNARE complex, tethering, endo- and exocytosis proteins are shown with the corresponding key identifying each protein by shape. All proteins are coloured to reflect the overall increased (red), neutral (yellow) or decreased (blue) phosphorylation. Created with BioRender.com

5.2.1 Bicuculline induces phosphorylation of select neurotransmitter receptor subunits

An analysis of the overall phosphorylation status of various neurotransmitter receptors indicated that most protein subunits were dephosphorylated (Figure 5.5 and 5.7, Appendix 26 and 27). These included the $GABA_B$ subunit encoded by *Gabbr1* (Figure 5.5A, Appendix 26K), mGluR subunit encoded by *Grm5* (Figure 5.5A, Appendix 27F), NMDAR subunits GluN2A (Figure 5.5A, Appendix 26N) and GluN2B (Figure 5.5A, Appendix 27D), and the single sites detected for AMPAR subunit GluR1 (Figure 5.5A and B, Appendix 26M), mGluR subunit encoded by *Grm3* (Figure 5.5A, Appendix 26O) and glycine receptor subunit encoded by *Glrb* (Appendix 27E). Further examination indicated that only select receptor subunits were being persistently or bidirectionally phospho-regulated, irrespective of excitatory or inhibitory function (Figure 5.5A and Appendix 26 and 25). Receptors which were persistently phosphorylated were $GABA_B$ subunit encoded by *Gabbr2* (Figure 5.5A and D, Appendix 26X), AMPAR subunit encoded by *Gria2* (Figure 5.5A, Appendix 26Z) and NMDAR subunit encoded by *Grin1* (Figure 5.5A and E, Appendix 26AA). The mGluR subunit encoded by *Grm1* (Figure 5.5A, Appendix 27I) increased in phosphorylation at the early to mid-time points and was dephosphorylated from 6 h and into the late time points.

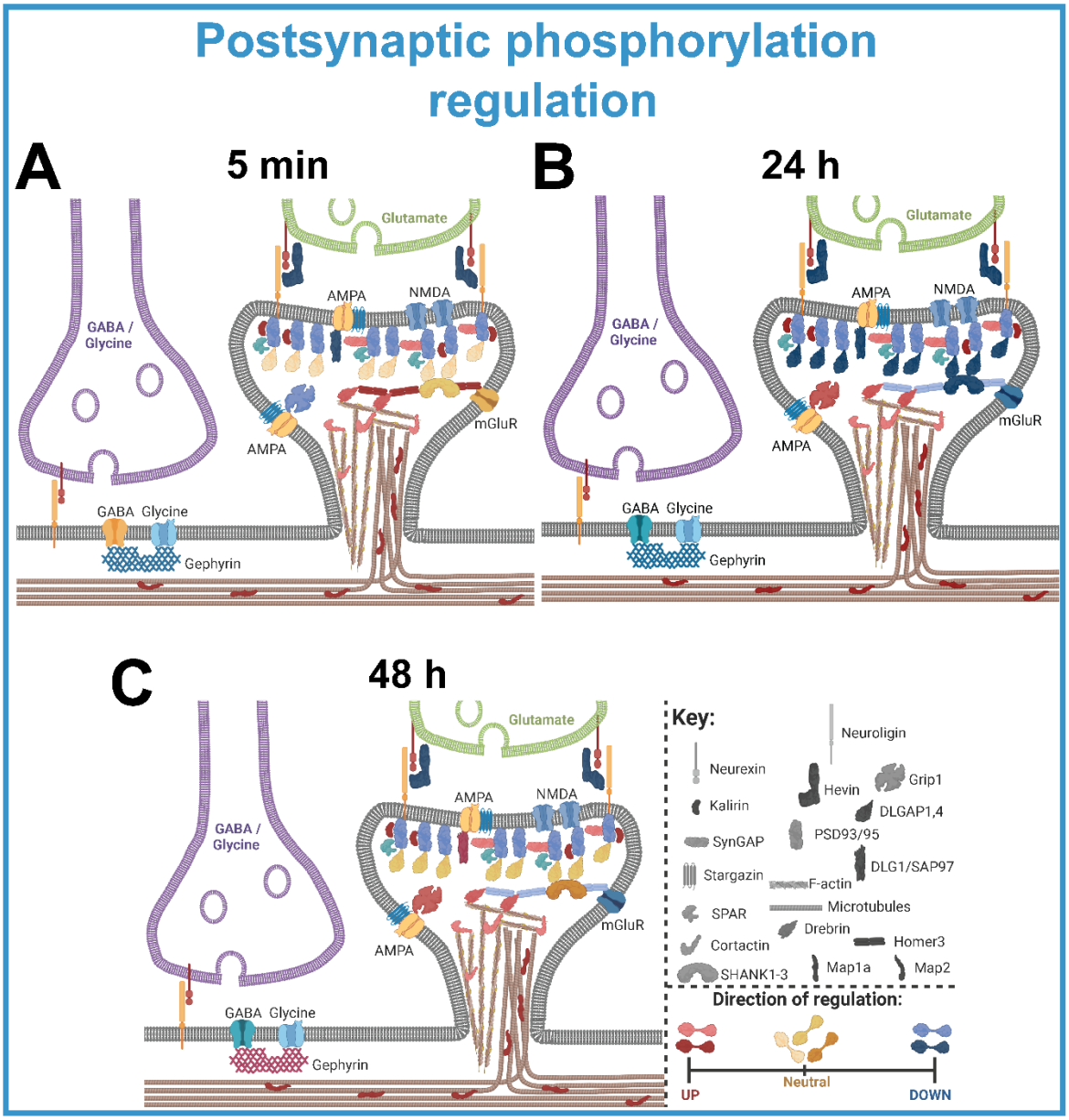

Figure 5.7. Schematic of the postsynaptic terminal indicating the overall direction of protein phosphorylation for core proteins involved in neurotransmission. The postsynaptic compartments indicates the key phosphorylation events occurring at (A) 5 min, (B) 24 h and (C) 48 h. Members of the PSD are indicated in scaffold layers with the corresponding key identifying each protein by shape. All proteins are coloured to reflect the overall increased (red), neutral (yellow) or decreased (blue) phosphorylation. Created with BioRender.com

5.2.2 Temporal analysis of protein kinase substrate motifs

Using the same process as for Chapter 3 Section 3.3, I determined the average log_2 fold change for the phosphopeptides containing known substrate sites for protein kinases. A minimum of four substrate matches was required for a protein kinase to be included in the analysis, these kinase substrate matches are shown in Figure 5.8A and B. For this analysis I separated the kinases that met the minimum criteria of substrate matches across all time points (Figure 5.8A) from kinases which met the criteria only at specific timepoints (Figure 5.8B).

Using KinSwing software[95], the quantitative phosphopeptide data was analysed to infer the activity of protein kinases with known substrate motifs for each timepoint (Appendix 27). From the kinases matched in Figure 5.8A and B, a heatmap was created corresponding to the predicted protein kinase activity. The kinases that met the minimum criteria of substrate matches across all time points (Figure 5.8A) are shown with the corresponding predicted kinase activity in Figure 5.8C. The kinases which met the minimum substrate criteria only at specific timepoints are displayed in Figure 5.8D. To assess the similarity between the substrate average log_2 fold change data and KinSwing analysis, a scatter plot was generated for each time point (Figure 5.9A-G). The bubbles were included to represent the number of matched protein kinase substrates from the phosphopeptide data. The two analyses agreed that several protein kinases had either elevated or inhibited activity and will be discussed below.

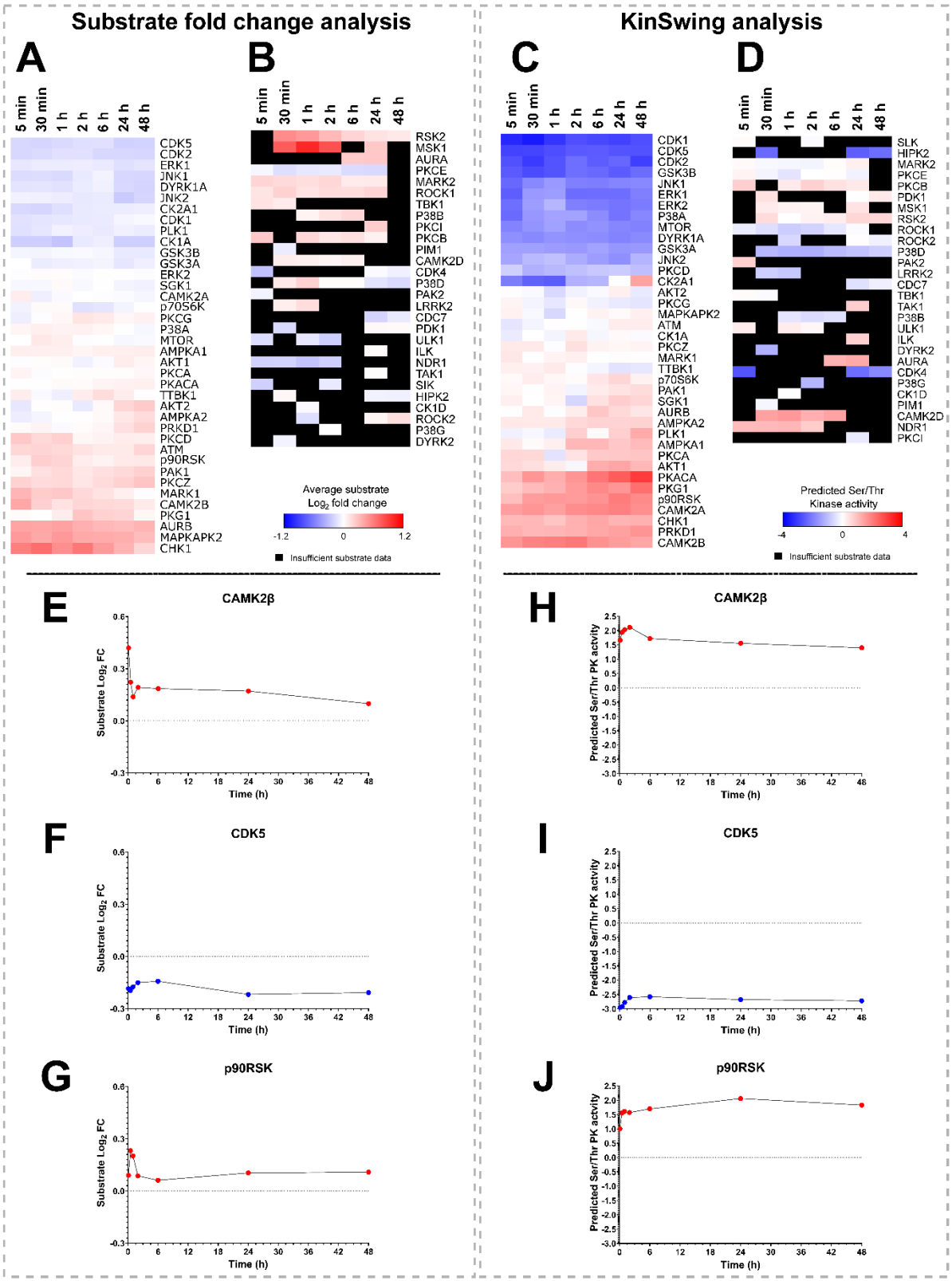

Figure 5.8. Temporal regulation of known substrates following Bicuculline stimulation and inferred kinase activity across timecourse. A heatmap of the average substrate fold change was plotted indicating kinases with four significantly regulated substrate matches (A) across all timepoints or (B) in at least one timepoint. A heatmap of the KinSwing predicted

protein kinase activity score was plotted indicating kinases with significantly regulated substrate matches (C) across all timepoints or (D) at least one timepoint. Heatmaps are hierarchically clustered. A scale bar of the log_2 fold change or predicted protein activity is shown for the respective heatmaps. Scatter plots of the average substrate log_2 fold changes for (E) CAMK2β, (F) CDK5 and (G) p90RSK kinases are shown for all timepoints indicated as dots. Scatter plots of the predicted kinase activity for (H) CAMK2β, (I) CDK5 and (J) p90RSK kinases are shown for all timepoints indicated as dots. The dots are coloured either red or blue to indicate values above or below 0, respectively.

5.2.1 Predicted increased activity of p90RSK and decreased cyclin-dependent kinase activity were major features of the temporal kinase profile

Cyclin dependent kinases (CDK) members and dual specificity tyrosine-phosphorylation-regulated kinase 1A (DYRK1A) were predicted to have reduced activity following Bic stimulation. CDK1, CDK2, CDK5 and DYRK1A showed negative substrate regulation and low activity at every time point (Figure 5.8A, C, F and I, Figure 5.9). At 5 min, and the late time points, CDK4 also had negative substrate regulation and low predicted activity. Members of the extracellular-signal regulated kinase (ERK) and c-Jun N-terminal kinase (JNK) pathways [309,310] had many associated substrates with negative regulation and were predicted to have low activity. These included ERK1 (MAPK3), ERK2 (MAPK1), JNK1 and JNK2, (Figure 5.8 A, C and 5.9A-G). However, MAPK1 and 3 activities are known to be up-regulated by electrophysiological activity[289]; so the predictions might be wrong, and instead are reflective of CDK activity because of the inability to distinguish between CDK and MAPK family substrate motifs.

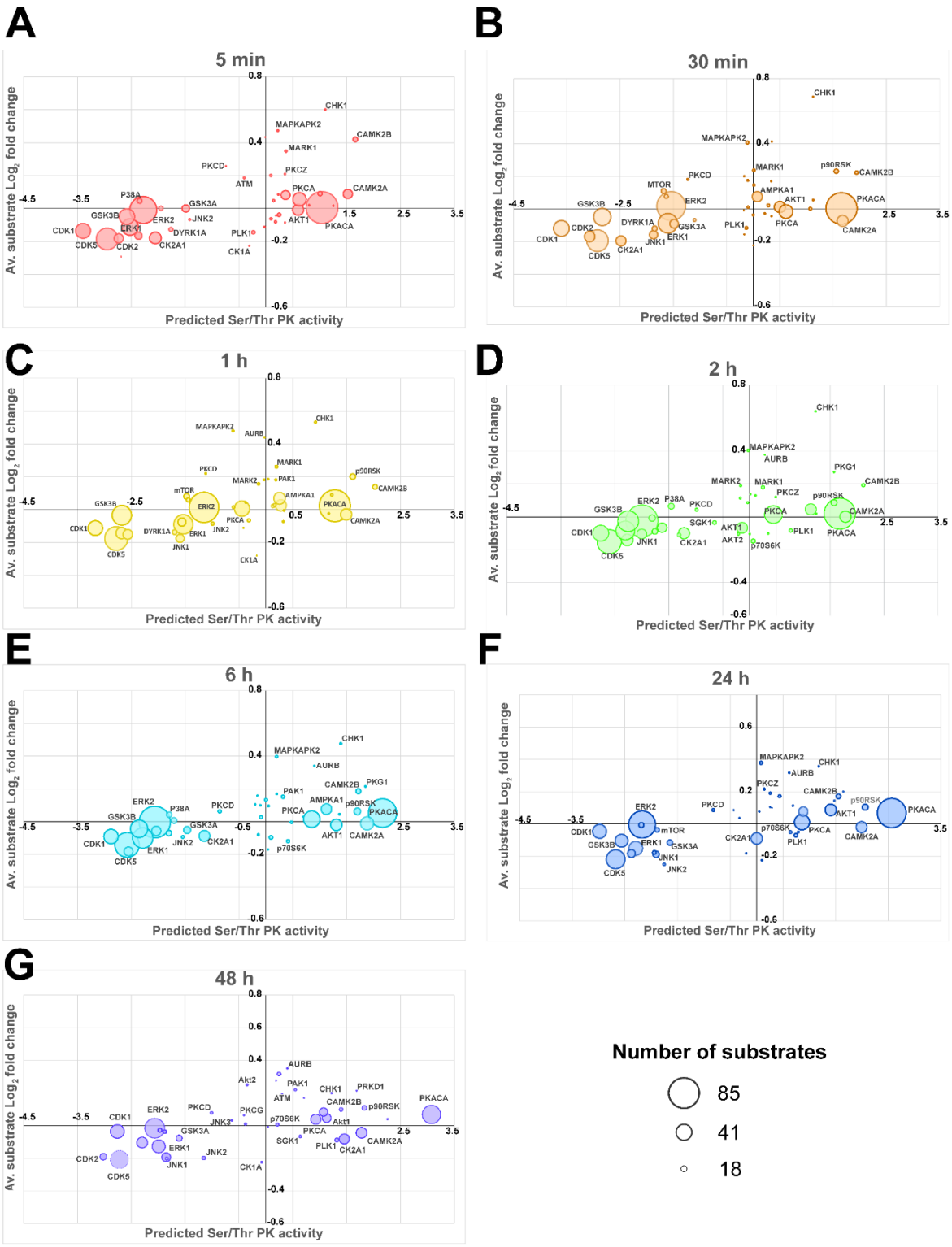

Figure 5.9. Bubble plot of the temporal substrate regulation against the KinSwing predicted protein kinase activity. A bubble plot of the average substrate log2 fold change for known substrates of protein kinases versus the KinSwing predicted protein kinase activity following Bicuculline stimulation at (A) 5 min, (B) 30 min, (C) 1 h, (D) 2 h, (E) 6 h, (F) 24 h and (G) 48 h. A minimum of four substrate matches was required for a protein kinase to be

included in the analysis. The size of each bubble is scaled to the number of substrates found in the data.

The mammalian target of rapamycin (MTOR) was predicted to have low activity, whilst the MTOR downstream target p70 RSK (S6K) was predicted to have slight activity (Figure 5.8C and 5.9A-G)[311]. MTOR substrates were positively regulated in the early time points and were negatively regulated in the late time points (Figure 5.8A and Figure 5.9B, C and F), whilst S6K substrates were mainly negatively regulated across most time points and dropped to neutral at 48 h (Figure 5.8A and 5.9D-F).

P90RSK is downstream of both MAPK1/3 and 3-phosphoinositide-dependent protein kinase 1 (PDK1) and the latter kinase was predicted to be upregulated (Figure 5.8 C), with known substrates particularly up-regulated late (Figure 5.8A). P90RSK was predicted to have both high activity and upregulation of known substrates (Figure 5.8A, C, G and J, 5.9A-G)[312].

Across all timepoints, the kinase activity of CAMK2β was predicted to be active and the average substrate $\log_2$ fold change was positive, although dropping closer to neutral at late times (Figure 5.8A and E, 5.9A-G). The kinase activity of CAMK2α was predicted by KinSwing to have been high (Figure 5.8C and H); however, substrates of CAMK2α showed early increased phosphorylation followed by dephosphorylation in the mid to late time points (Figure 5.8A and 5.9A). PKG substrates were found to have positive regulation from the mid to late time points and was predicted to have high activity over the time course (Figure 5.8A and C).

5.2.2 The temporal proteomic profile of Bicuculline induced synaptic downscaling

The proteomic screen detected 7,278 protein groups with quantitative information across all seven timepoints (Appendix 22). At least 6 proteins were significantly regulated in two or more timepoints (Figure 5.10A). The time points with the largest number of protein level changes were 24 and 48 h with 1,212 and 1,340 protein changes, respectively (Figure 5.10A). Some proteins demonstrated significance at only one timepoint (Figure 5.10B), ranging from 1 protein at 5 min to 1,073 unique protein changes at 48 h. To understand the biological functions of the significantly regulated proteins, a GO term enrichment analysis was performed and is presented in Figures 5.11A-E and 5.12A-C.

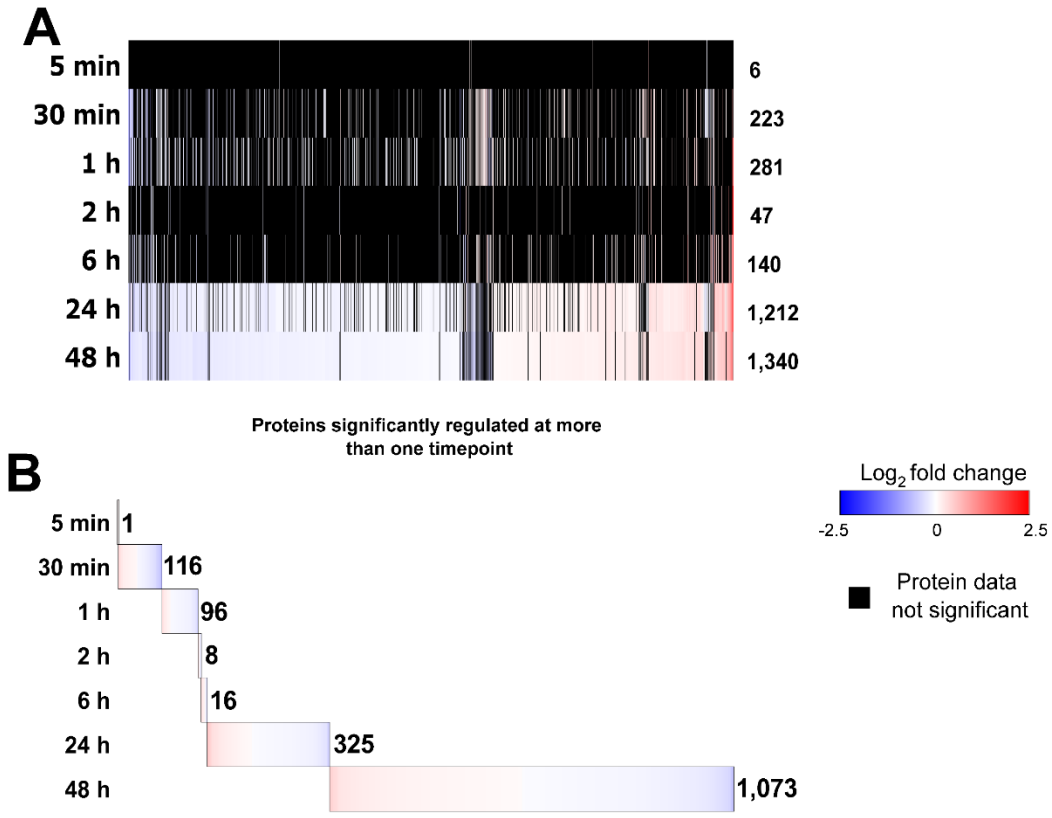

Figure 5.10. Temporal alterations to the proteome following Bicuculline stimulation. Heatmaps of log2 fold change values for A) significant phosphopeptides across one or more timepoints with non-significant values excluded and B) significant phosphopeptides at only

one timepoint. Heatmap (A) is hierarchically clustered. A scale bar of the log_2 fold change is shown.

5.2.3 Proteins associated with the presynaptic terminal are downregulated following bicucline stimulation

Following the same GO enrichment procedure implemented to analyse significantly regulated phosphopeptides. The same GO analysis was performed on significantly up and down regulated protein groups across all timepoints (Figure 5.11A-C and 5.12A-C). The top 30 ranked proteins corresponding to the GO term gene list were hierarchically clustered in heatmaps in the same manner used for the phosphopeptide analysis (Figure 5.11D-E and 5.12F). There were instances where there were less than 30 ranked proteins associated with the GO term (Figure 5.12D and E). In these instances, all ranked proteins were hierarchically clustered. A schematic representation of the changes to core pre- and postsynaptic proteins involved in neurotransmission is shown in Figure 5.13.

Many presynaptic proteins had decreased abundance (Figure 5.11D and 5.13A-B). The downregulated proteins were associated with the core endocytosis, exocytosis, active zone and SNARE protein groups. Including endocytosis proteins such as AP2 complex subunit σ (encoded by *Ap2s1*), endophilin A1/3 (encoded by *Sh3gl2* and *Sh3gl3*), active zone protein ERC protein 2 (encoded by *Erc2*) tethering protein synapsin 2 (encoded by *Syn2*), exocytosis proteins complexin 1 and 2 (encoded by *Cplx1* and *Cplx2*), SNARE proteins synaptotagmin 1/5/12 (encoded by *Syt1*, *Syt5* and *Syt12*) and syntaxin 1B (encoded by *Stx1b*) (Figure 5.11D). A subset of presynaptic proteins were upregulated in the early and mid timepoints and then downregulated in later timepoints (Figure 5.11D and G, 5.13A-B). These included endocytosis proteins dynamin 3 (encoded by *Dnm3*), amphiphysin 1 (encoded by *Amph*) and auxilin (encoded by *Dnajc6*); and active zone protein piccolo (encoded by *Pclo*; Figure 5.11G).

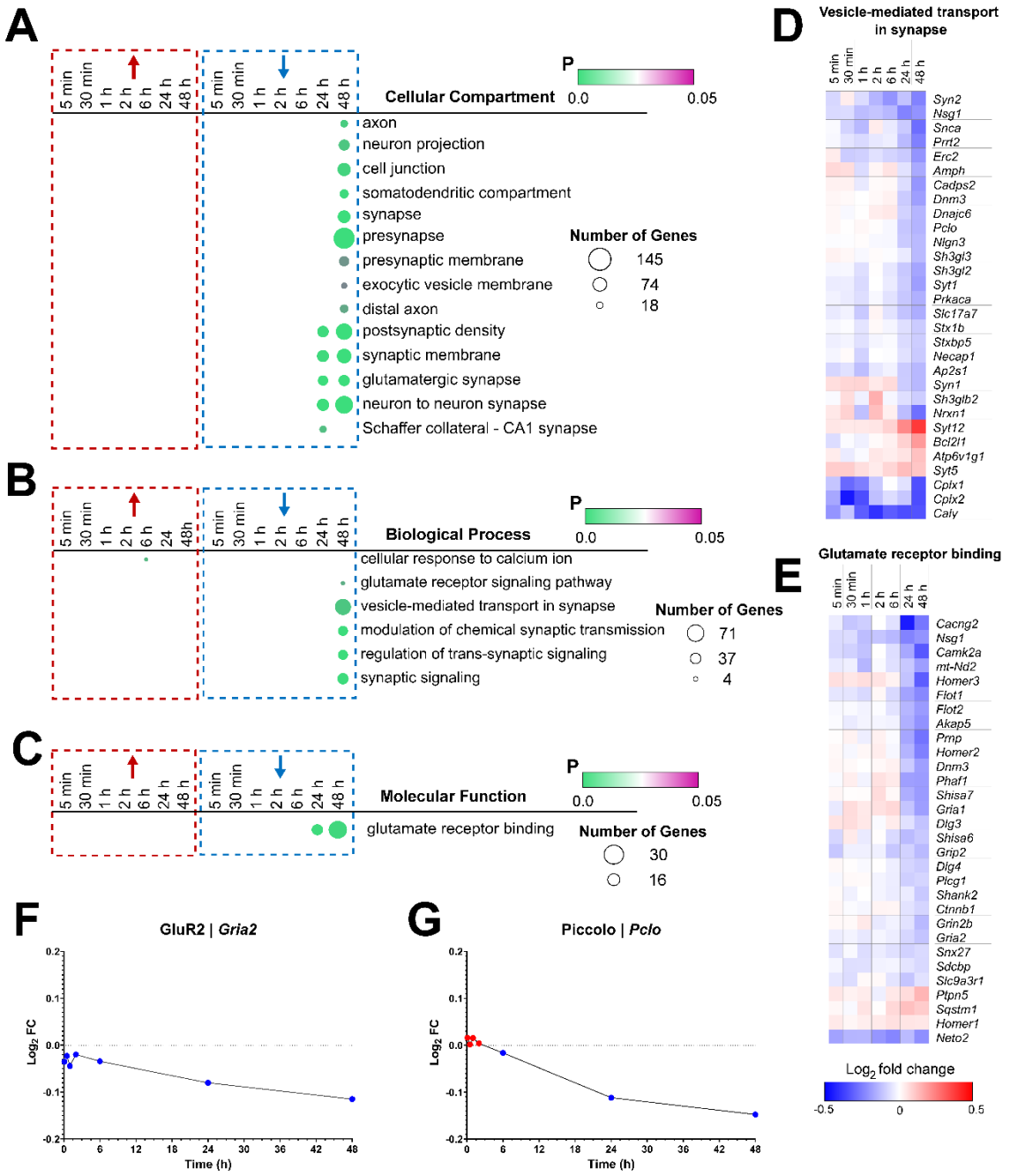

Figure 5.11. Gene Ontology analysis of significantly regulated cellular component, biological process and molecular function proteome terms following Bicuculline stimulation. Enriched GO terms for significantly up and down regulated proteins across all timepoints from (A) Cellular Component, (B) Biological Process and (C) Molecular Function. A scale bar for probability is shown. The size of the circle represents the number of genes enriched for each term. A heatmap of the top 30 ranked genes for the biological process term, (D) vesicle-mediated transport in synapse and molecular function term (F) glutamate receptor

binding are hierarchically clustered. A scale bar of the log_2 fold change is shown. Scatter plots of the log_2 protein fold changes for (F) GluR2 and (G) Piccolo proteins are shown for all timepoints indicated as dots. The dots are coloured either red or blue to indicate values above or below 0, respectively.

5.2.1 Excitatory receptors and receptor binding proteins had reduced abundance at 24 and 48h

The top ranked 30 genes belonging to the molecular function term glutamate receptor binding were plotted in a heat map (Figure 5.11E). Many of the significantly regulated proteins associated with this term were excitatory receptors which were down regulated at the late time points (Figure 5.11E and 5.13D-E). These proteins include NMDAR subunit GluN2B (encoded by *Grin2b*) and AMPAR subunit GluR1 (encoded by *Gria1*). The AMPAR subunit, GluR2, encoded by *Gria2* was downregulated across all timepoints (Figure 5.11E and F). The receptor binding proteins stargazin (encoded by *Cacng2*) and GRIP1/2 (encoded by *Grip1* and *Grip2*) were also downregulated across all timepoints (Figure 5.11E and 5.13D-E).

Receptor binding associated proteins in the upper layer of the PSD were found to be initially upregulated and subsequently downregulated at the late timepoints (Figure 5.11E and 5.13C-D). These include homer family proteins (encoded by *Homer2* and *Homer3*), SHANK2 (encoded by *Shank2*) and SAP102 (encoded by *Dlg3*). PSD95 (encoded by *Dlg4*) was downregulated across all timepoints (Figure 5.11E and 5.13C-D). Homer1 was upregulated at all timepoints (Figure 5.11E). In general, the Bic stimulation resulted in the late downregulation of excitatory receptors and their respective binding partners in the upper layer of the PSD, as depicted in as a schematic in Figure 5.13 and a supplementary heatmap in Appendix 28.

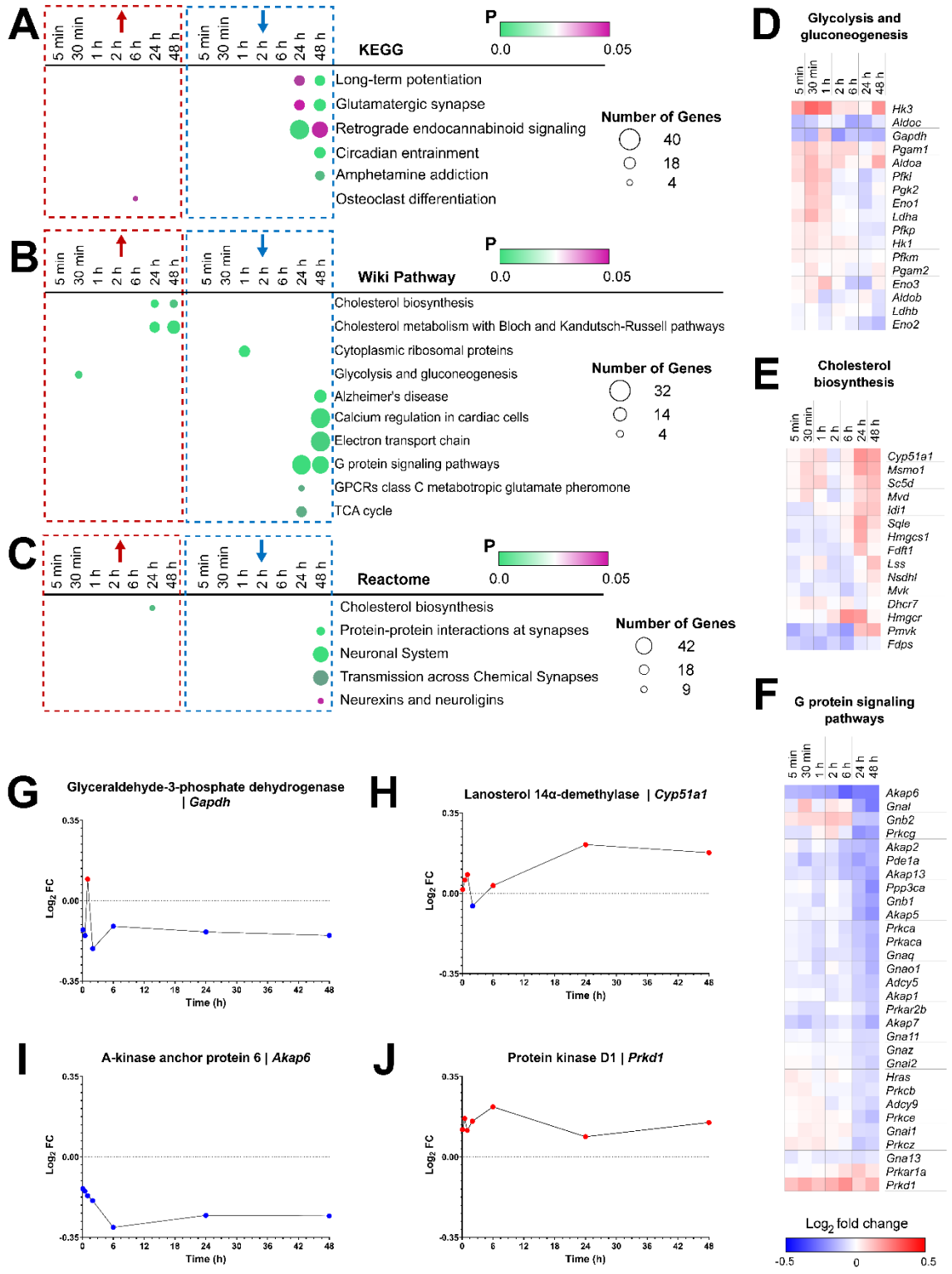

Figure 5.12. Gene Ontology analysis of significantly regulated KEGG, WikiPathway and Reactome proteome terms following Bicuculline stimulation. Enriched GO terms for significantly up and down regulated proteins across all timepoints from (A) KEGG, (B) WikiPathway and (C) Reactome. A scale bar for probability is shown. The size of the circle represents the number of genes enriched for each term. A heatmap of the genes for the

WikiPathway terms, (E) Glycolysis and gluconeogenesis, (F) G protein signalling pathways and the Reactome term (G) Cholesterol biosynthesis are hierarchically clustered. The top 30 ranked genes are shown for (F). A scale bar of the log_2 fold change is shown. Scatter plots of the log_2 protein fold changes for (G) Glyceraldehyde-3-phosphate dehydrogenase, (H) lanosterol 14α-demethylase, (I) A-kinase anchor protein 6 and (J) Protein kinase D1 proteins are shown for all timepoints indicated as dots. The dots are coloured either red or blue to indicate values above or below 0, respectively.

5.2.1 G-protein signalling proteins had reduced abundance at 24 and 48h s

Various members of the G-protein signalling pathway were down regulated including multiple members of the Guanine nucleotide-binding protein Gi/o family, such as the proteins encoded by *Gnaq*, *Gna11*, *Gna13*, *Gnb1* and *Gnao1* (Figure 5.12F). Multiple A-kinase anchoring proteins encoded by *Akap1*, *Akap5*, *Akap6*, *Akap7*, *Akap13*, and the adenylate cyclase family member protein encoded by *Adcy5* (Figure 5.12F and I). Multiple protein kinase A (PKA) and C (PKC) family members encoded by *Prkaca*, *Prkar2b*, *Prkca*, *Prkcb*, *Prkce*, *Prkcg* and *Prkcz* were also downregulated (Figure 5.12F). The PKA and protein kinase D family members encoded by *Prkd1* and *Prkar1a* were upregulated (Figure 5.12F and J).

5.2.2 Metabolic enzymes had increased abundance at specific times following Bicuclline stimulation

Enzymes involved in cholesterol biosynthesis had increased abundance at late timepoints (Figure 5.12E). These include lanosterol 14α-demethylase (encoded by *Cyp51a1*; Figure 5.12H), methylsterol monooxygenase 1 (encoded by *Msmo1*), diphosphomevalonate decarboxylase (encoded by *Mvd*), and lanosterol synthase (encoded by *Lss*).

Key enzymes involved in the glycolysis and gluconeogenesis pathways had rapidly increased abundance at 30 min post-Bic stimulation (Figure 5.12D). These enzymes included enolases

(encoded by *Eno1*, *Eno2* and *Eno3*), aldolases (encoded by *Aldoca*, *Aldob* and *Aldoc*), hexokinases (encoded by *Hk1*and *Hk3*) and glyceraldehyde 3-phosphate dehydrogenase (encoded by *Gapdh*; Figure 5.12G).

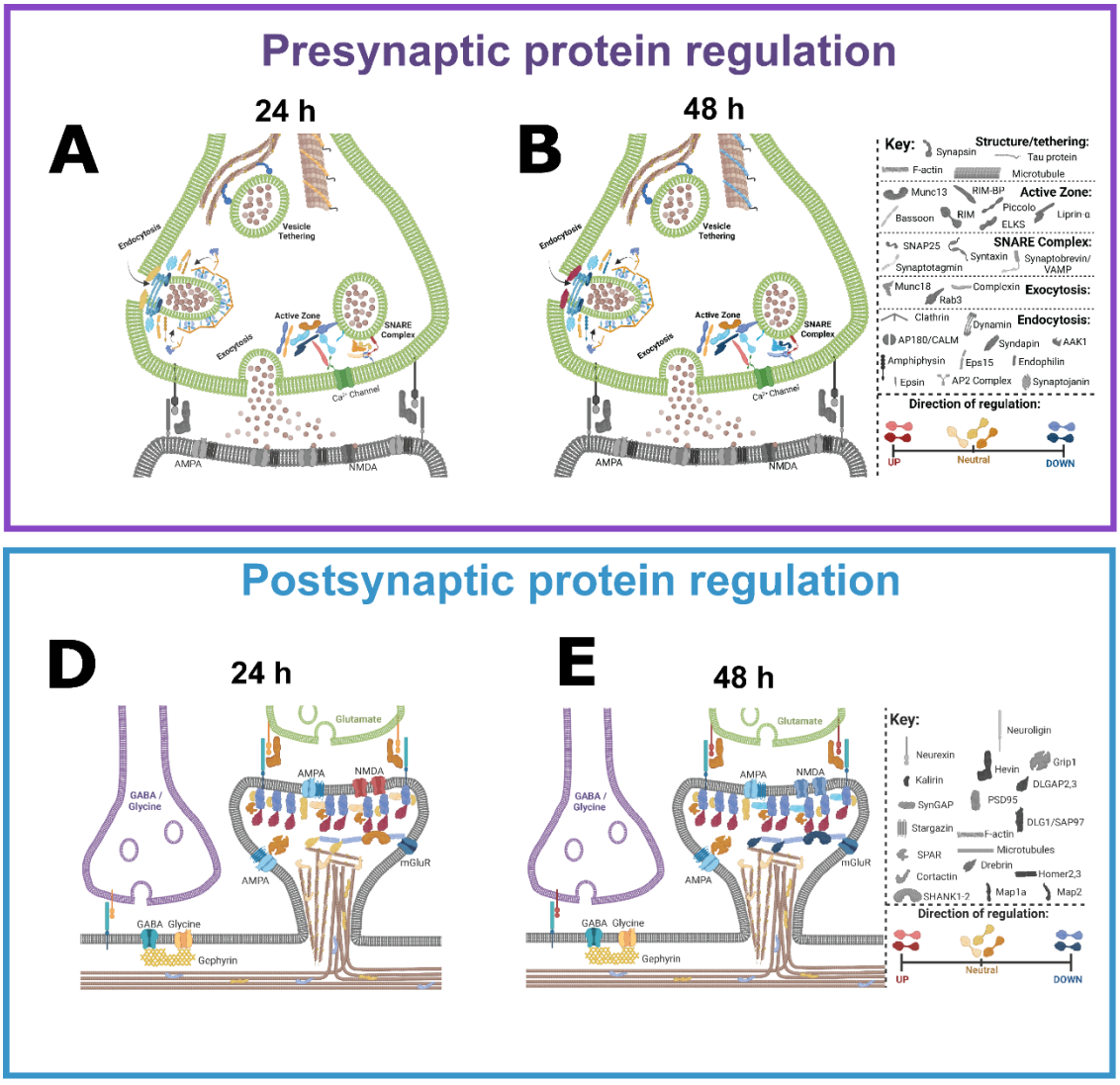

Figure 5.13. Schematic of the pre- and postsynaptic terminal indicating the overall direction of protein regulation. Drawings of the pre- and postsynaptic compartments showing the core proteins groups. The presynaptic compartments indicate the overall late protein regulation at (A) 24 h and (B) 48 h. Members of the active zone, SNARE complex, tethering, endo- and exocytosis proteins are shown with the corresponding key identifying each protein by shape. The postsynaptic compartments indicates overall protein regulation occurring at (C) 24 h and (F) 48 h. Members of the PSD are indicated in scaffold layers with the corresponding

key identifying each protein by shape. All proteins are coloured to reflect the overall increased (red), neutral (yellow) or decreased (blue) phosphorylation. Created with BioRender.com

5.2.3 Evidence of alternatively spliced proteins across the Bic stimulation time course

Sixteen alternatively spliced protein variants (encoded by *Dgkb, Ndrg4, Nectin2, Gria2, Prkcb, Syn2, Hmgn3, Dnajb6, Mapt, Tac1, Guk1, Slc3a2, Pkm, Rundc3a, Ubap2l and Cltb*) were detected with altered abundance at 30 min, 1 h, 6 h, 24 h and 48 h, respectively (Figure 5.14). This may be related to the increased phosphorylation of proteins involved in RNA processing (Figure 5.2D and G), including those with RNA splicing functions.

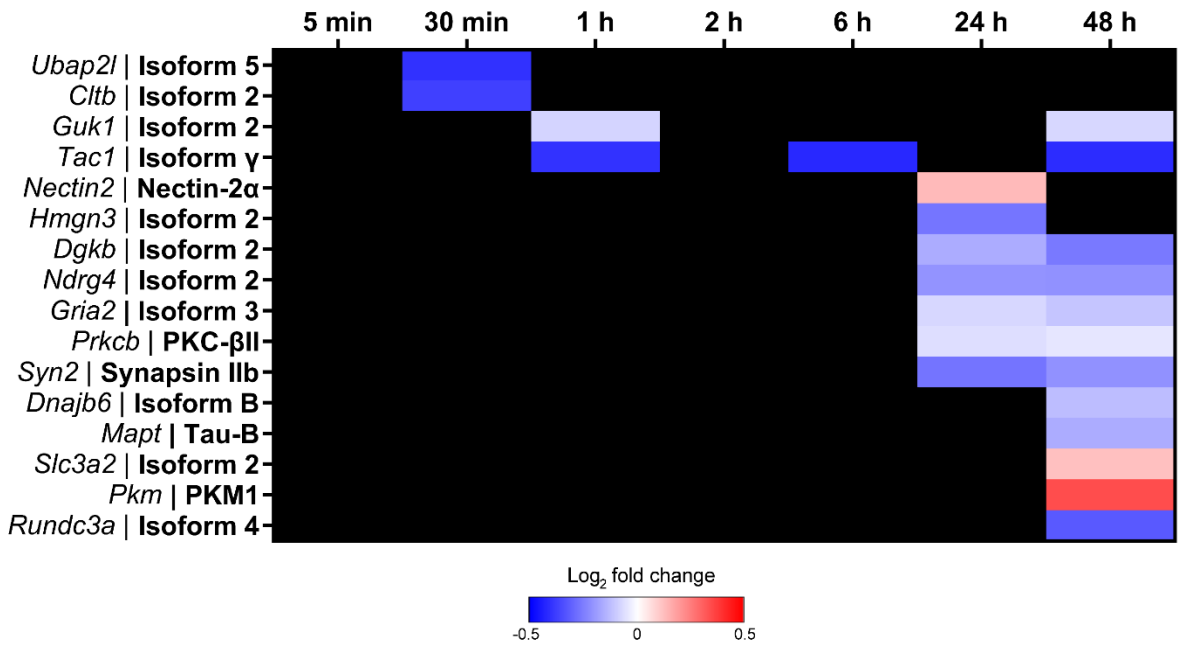

Figure 5.14. Protein evidence of splice variants induced by Bicuculline stimulation. Heatmaps of log2 fold change values for significantly regulated protein splice variants. The isoform protein name is indicated where possible otherwise the UniProt isoform number is given. A scale bar of the log_2 fold change is shown.

5.2.4 Comparison of synaptic downscaling phosphoproteome and proteome data with previous work

A comparison of the phosphoproteomic and proteomic data generated by Desch, et al. [39] was made to validate the results from this synaptic downscaling study. The MaxQuant output from the Desch et al. group was passed through our workflow to facilitate the comparison. Subtle differences to the downscaled mouse phosphoproteome and proteome were anticipated as the Desch et al. group analysed downscaled hippocampal neurons sourced from post-natal rats and used a label-free quantification (LFQ) MS method. To ensure phosphorylation sites were being compared between both datasets, phosphopeptides were matched based on a ± 7 amino acid residue sequence window and were required to have an identical gene name. The $\log_2$ fold change at the 5 min and 24 h phosphopeptides from Desch et al. was compared to my work (Figure 5.15A-B).

Since protein samples in this experiment were TMT labelled (Figure 5.1A), we expect they were affected by TMT ratio compression, which is a phenomenon where interfering ions coelute, fragment with the target peptide and distort the TMT reporter ion intensities used for quantitation[271,272,313]. As the Desch et al. group performed their analysis using LFQ, the protein and phosphopeptide fold change detected in our analysis would reflect the same direction of change but not the magnitude due to this ratio compression. To measure the strength and direction of the relationship between both data sets, a Pearson correlation was applied to only the significantly regulated phosphopeptides and proteins detected in both analyses and is indicated in Figure 5.15.

There was an approximate 25% phosphopeptide data overlap with the Desch et al. data across both timepoints. In the 5 min and 24 h timepoint comparisons, 310 and 396 phosphopeptides were significant in both datasets, respectively (Figure 5.15A-B). For the Desch et al. data at the 5 min and 24 h timepoint comparisons, 146 and 216 phosphopeptides were uniquely

significantly regulated, respectively (Figure 5.15A-B). In the 5 min and 24 h timepoint comparisons 681 and 673 phosphopeptides were uniquely significant in this study, respectively (Figure 5.15A-C). With Pearson coefficients greater than 0.7, the analysis indicated that significantly regulated phosphosites in both datasets were highly correlated in a positive direction (Figure 5.15A-C).

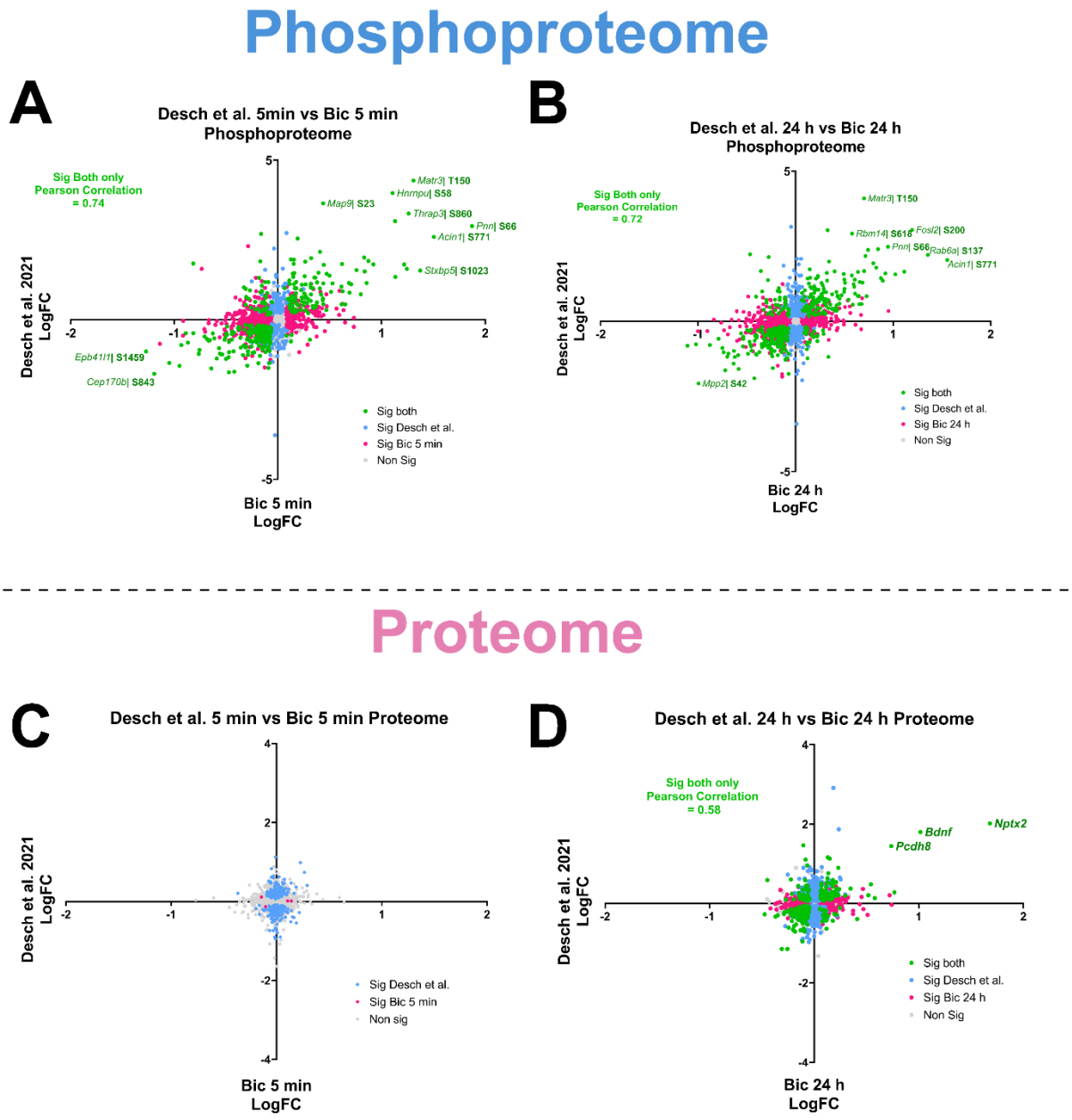

Figure 5.15. Comparison of phosphoproteomic and proteomic analysis to Desch et al. Phosphopeptide log2 fold change data from the bic stimulation analysis is presented in an XY scatter plot comparing the (A) 5 min and (B) 24 h timepoints to the respective 5 min and 24 h

phosphopeptide data from Desch et al. Protein log2 fold change data from the bic stimulation analysis is presented in an XY scatter plot comparing the (C) 5 min and (D) 24 h timepoint to the 5 min and 24 h protein data presented in Desch et al. Dots are colour coded to indicate significant datapoints from both datasets (green), significant only in Desch et al. (pink) and significant in Bicuculline dataset only (blue). Other data points are non-significant (grey). Pearson coefficient for significantly regulated phosphosites and proteins indicated on relevant plots.

Over 88% of the proteomic data reported in Desch et al. overlapped the proteome data. There was no overlap in significantly regulated proteins detected at 5 mins, which is a point of differentiation between this study and the Desch et al. data (Figure 5.15C). Protein expression and degradation can occur rapidly on a time scale of minutes, but more often requires hours [314]. There were 286 significantly regulated proteins at 5 min for Desch et al., whilst only 4 proteins showed significant regulation in this analysis (Figure 5.15C). At 24 h, 304 proteins were significantly regulated in both datasets, 678 were only significantly regulated in my Bic 24 h data and 700 were only significantly regulated in the Desch et al. data. A Pearson correlation at 24 h indicated a moderate positive correlation with a coefficient of 0.58 (Figure 5.15D).

5.2.5 Comparison of the early epileptogenesis and synaptic downscaling measured phosphoproteomes and proteomes

The phosphoproteome at Pilo4h and Pilo24h was compared to the Bic 2, 6 and 24h phosphopeptide data respectively (Figure 5.16A-C). A Pearson correlation of the significantly regulated phosphopeptides and proteins in both data sets was completed for all comparisons and is presented in Figure 5.16A-D.

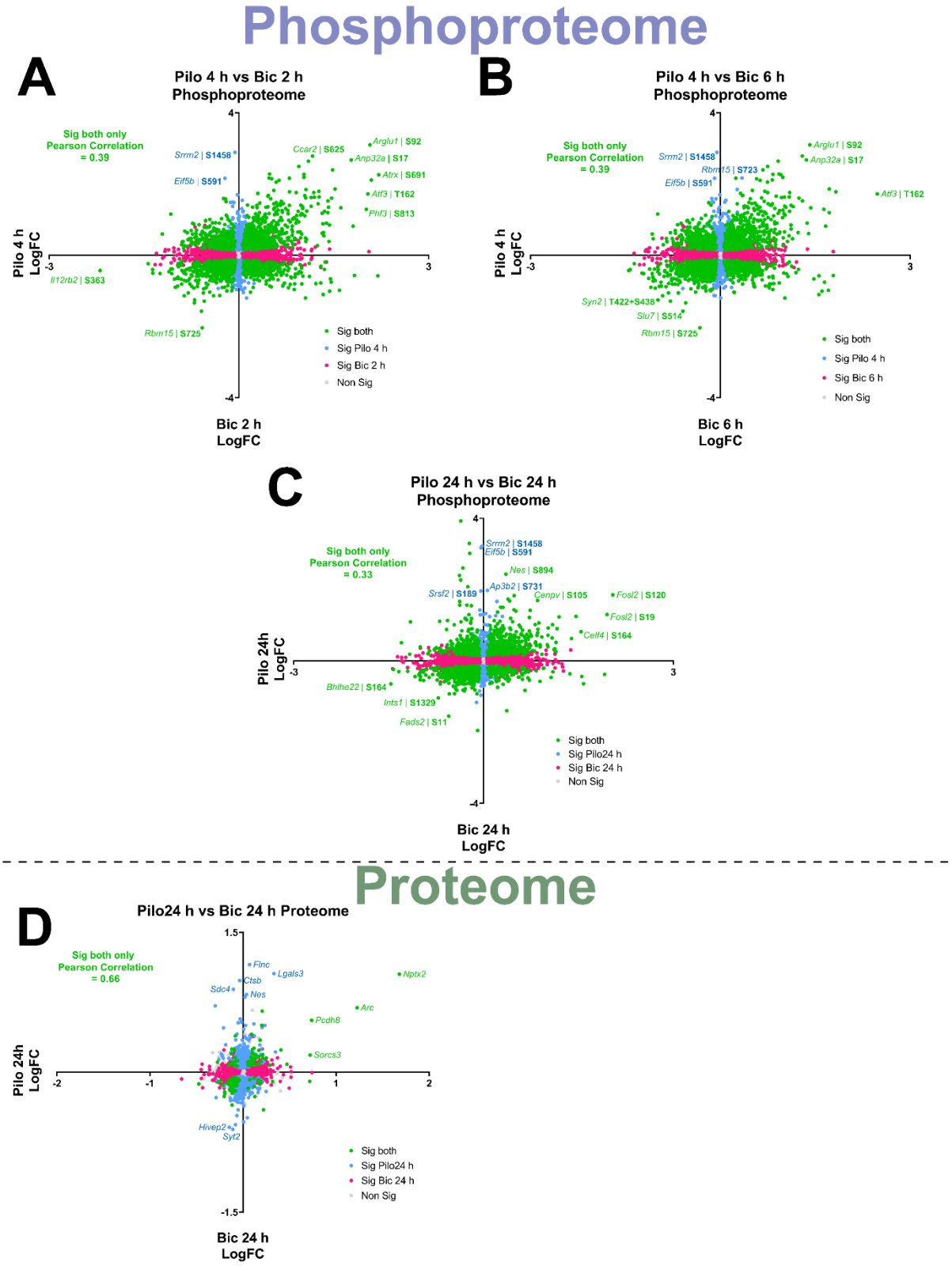

Figure 5.16. Comparison of phosphoproteomic and proteomic alterations in epileptogenesis and synaptic downscaling. Phosphopeptide $\log_2$ fold change data from the Bic stimulation analysis is presented in an XY scatter plot comparing the Pilo4h phosphopeptide data against the (A) 2 h and (B) 6 h Bic stimulation data. The Pilo24h

phosphopeptide data is presented in an XY scatter plot against the (C) 24 h Bic stimulation data. Protein log_2 fold change data from the Bic stimulation analysis is presented in an XY scatter plot comparing the (D) 24 h timepoint to the Pilo24h protein data. Dots are colour coded to indicate significant datapoints from both datasets (green), significant only in Pilo4 or 24h. (pink) and significant in Bicuculline dataset only (blue). Other data points are non-significant (grey). Pearson coefficient is indicated on each plot.

5.2.6 Pilocarpine stimulated phosphoproteome is low to moderately correlated with Bicuculline stimulated phosphoproteome

Approximately 60% phosphopeptide data from the Bic phosphoproteome had matching phosphorylation site sequences with the Pilo4h data across all timepoints. In the 2, 6 and 24 h timepoint comparisons 1918, 1914 and 1376 phosphopeptides were significant in both datasets, respectively (Figure 5.16A-C). For the Pilo4h data at the 2 and 6 h timepoint comparisons, 1079 and 1915 phosphopeptides were uniquely significantly regulated, respectively (Figure 5.16A-B). There were 607 phosphopeptides uniquely significantly regulated in the Pilo24h comparison (Figure 5.16C). For the 2, 6 and 24 h timepoint comparisons 3391, 3380 and 4345 phosphopeptides were significant in this study, respectively (Figure 5.16A-C). In comparing the 2, 6 and 24 h phosphoproteome data to the Pilo4h and 24h data. The analysis indicated that significantly regulated phosphosites from the 2 and 6 h datasets were low to moderately correlated with the significantly regulated phosphosites in the Pilo4h data. The data was correlated in a positive direction with Pearson coefficients of 0.39 (Figure 5.16A and B). The significantly regulated phosphosites from both the Bic 24 h and the Pilo24h had a low correlation in a positive direction with a Pearson coefficient of 0.33 (Figure 5.16C). Overall, the analysis indicated that the Bic and pilocarpine induce a phosphoproteome with low-moderate similarity.

The effect of the Pilo24h and the Bic 24 h proteome was compared by plotting the respective log_2 fold changes in an XY scatter (Figure 5.16D). Over 86% of proteins detected in the Pilo24h data were detected in the Bic 24h data. 326 proteins were significantly regulated in both datasets, 833 were only significantly regulated in the Bic 24 h data and 880 were only significantly regulated in the Pilo24h data. A Pearson correlation of the significantly regulated proteins in both datasets indicated a moderate positive correlation with a coefficient of 0.66 (Figure 5.16D). Thus, there are moderate similarities between the protein level changes induced by Bic and pilocarpine in these samples.

5.2.7 Early pilocarpine induced and Bic induced predicted kinase activity is different

The KinSwing predicted kinase activity at Pilo4h and Pilo24h was compared to the Bic 2, 6 and 24h predicted kinase activities respectively and a Pearson correlation was performed (Figure 5.17A-C). The kinases predicted with activity in the Pilo4h data matched 146 kinases in the Bic 2 and 6 h data. Only the p90RSK kinase was significantly regulated in both datasets at Bic 2 and Pilo4h (Figure 5.17A). Fourteen kinases were only significantly regulated in the Pilo4h data (Figure 5.17A and B). Fifteen and seventeen kinases were only significantly regulated at Bic 2 and 6 h, respectively. MTOR and other MAPK family kinases were prominent negatively-correlated kinases. A Pearson correlation of the Pilo4h with Bic 2 h predicted kinase activity indicated a low correlation in a negative direction with a coefficient of -0.32 (Figure 5.17A).

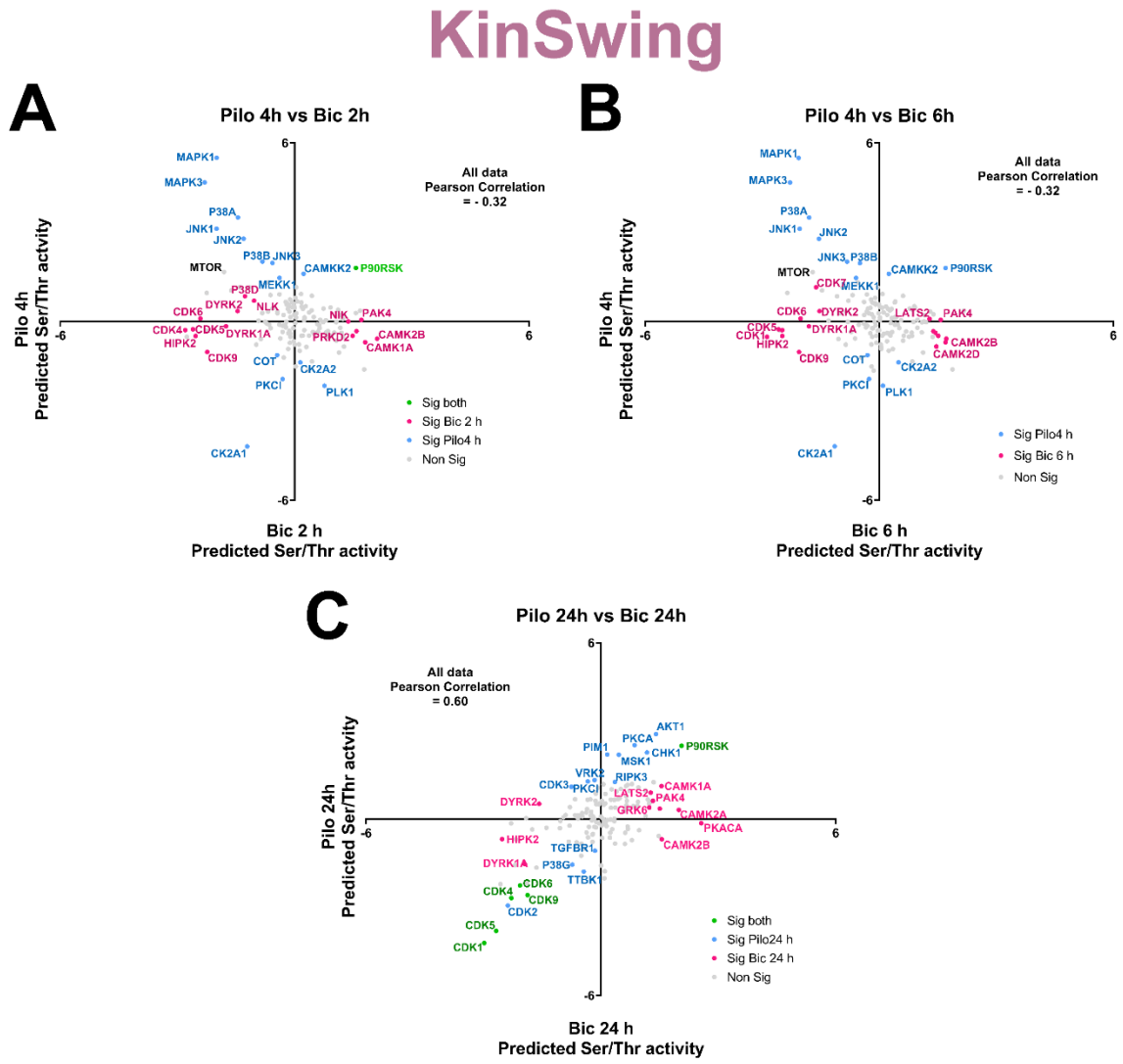

Figure 5.17. Comparison of kinase activity epileptogenesis and synaptic downscaling. Predicted Pilo4h kinase activity is presented in an XY scatter plot against the (A) 2 h and (B) 6 h Bic stimulation data. The predicted Pilo24h kinase activity is presented in an XY scatter plot against the (C) 24 h Bic stimulation data. Dots are colour coded to indicate significant datapoints from both datasets (green), significant only in Pilo 4 or 24h. (pink) and significant in Bicuculline dataset only (blue). Other data points are non-significant (grey). Pearson coefficient is indicated on each plot.

Likewise, the Pilo4h and Bic 6h Pearson correlation indicated a low correlation in a negative direction with a coefficient of – 0.32 (Figure 5.17B). Thus, Pilo4h has distinctive higher early kinase activity for the MAPK family.

The kinases predicted with activity in the Pilo24h data matched 146 kinases in the Bic 24 h data. Five downregulated CDKs and upregulated p90RSK were significantly regulated in both datasets, eleven were only significantly regulated in the Bic 24 h data and thirteen were only significantly regulated in the Pilo24h data. A Pearson correlation of the Pilo24h with the Bic 24 h predicted kinase activity indicated that the predicted kinase activity had a moderate positive correlation with a coefficient of 0.60 (Figure 5.17C).

5.3 Discussion

In this study, the signalling cascades initiated by Bic stimulation in hippocampal neuronal cell cultures caused the phosphorylation of mRNA processing proteins and translation factors. Bic also induced the dephosphorylation of presynaptic proteins and layer-specific postsynaptic density proteins. Most of these same presynaptic and postsynaptic proteins had reduced abundance at 24-48 h. Increased p90RSK and reduced CDK5 activity was implicated. The results of this analysis support a phosphatase-mediated deactivation and decrease of abundance of presynaptic and postsynaptic proteins alongside activation of posttranscriptional regulation and translation. A comparison with the pilocarpine omics analysis identified key differences.

5.3.1 Synaptic downscaling triggers broad synaptic dephosphorylation and reduced protein expression

Across the pre- and postsynaptic terminal, many core proteins involved in neurotransmission had a median log_2 fold change that indicated overall dephosphorylation. Calcium sensitive protein phosphatase 2B (PP2B/calcineurin) [315] and the downstream protein phosphatase 1 (PP1) are likely candidates as the responsible phosphatases [316]. At the presynaptic terminal, PP2B has a clear role opposing CDK5 activity [71]. CDK5 was predicted to be consistently reduced across the time course. PP1 activity is a suspected facilitator of synaptic downscaling and is activated by the dephosphorylation of the PP1 inhibitor 1 protein by PP2B[227,317,318]. In support of increased PP1 activity, inhibitor 1 (encoded by *Ppp1r1a*) T35 was dephosphorylated. Although direct evidence for phosphatase activity is difficult to obtain from this type of study, several known PP1 substrates were dephosphorylated. For example, NMDAR subunit GluN2B (encoded by *Grin2b*) was dephosphorylated at S1303 across all timepoints[319,320]. Gephryin S188 was dephosphorylated across all timepoints [321]. Gephyrin dephosphorylation promotes increased clustering of gephyrin [321], which supports a stabilisation and strengthening of inhibitory synapses. However, gephyrin S188 phosphorylation is also required for binding of inhibitory glycine receptor subunit B [322]. The dephosphorylation of stargazin S235 in this study, is likely to be mediated by PP1 [234,323]. Stargazin dephosphorylation promotes AMPAR endocytosis in a mechanism of synaptic downscaling [323]. GluN2B S1303 is both a CAMK2α and PP1 substrate which facilitates Ca^{2+} influx through NMDAR when phosphorylated[319,320,324]. The functional implications of PP1 dephosphorylation at these sites is the promotion of inhibitory function and reduced excitatory transmission. Thus, calcineurin and PP1 activity are further implicated in synaptic downscaling by this study, and likely work in concert with an extended network of phosphatases [38], to cause the observed general trend of dephosphorylation of synaptic proteins.

Dephosphorylation of synaptic proteins occurred throughout the time course and was followed by reduced abundance of synaptic proteins at 24-48 h. Reduced abundance would require activation of degradation pathways. Molecular signatures for activation of the proteosome were not enriched but may be present in the data.

Not all synaptic proteins were dephosphorylated and had reduced abundance. For the PSD, the dephosphorylation was layer specific. Most lower layer scaffold proteins had increased phosphorylation. Substrates of CAMK2 such as DLAGPs and SHANKs were among those phosphorylated proteins[238,325]. CAMK2α and β had either predicted neutral or increased activity and may be responsible for the increased phosphorylation. At the presynaptic terminal, some active zone core and non-core proteins had increased phosphorylation. These phosphorylated proteins had a closer association with transsynaptic proteins, which may indicate similar regulation of these proteins by kinases and phosphatases.

Dephosphorylation of synaptic proteins was ongoing throughout the time course and at 24-48 h there was a decreased abundance of synaptic proteins. Similar to the dephosphorylation pattern, PSD proteins and neurotransmitter receptors in the upper two layers were the main proteins with decreased abundance; however, there were exceptions such as middle layer DLGAP2 and 3, which were increased at 24-48 h. G-protein signalling proteins were targeted as a group for decreased expression or degradation which would stifle signalling downstream of G-protein coupled receptors (GPCRs), which includes many of neurotransmitter receptors. Substrates of PKA and PKC, which are downstream of GPCRs would be affected and there was some evidence that the activity of these kinases was restricted to early time points only. The overall dephosphorylation and decreased abundance of synaptic proteins would likely serve the purpose of downscaling by reducing synaptic strength via molecular changes at the synapse.

5.3.2 Activation of translation and alternative splicing is a feature of synaptic downscaling

RNA processing proteins, mainly in the early to mid time points, and translation factors, in the mid-late time points, had increased phosphorylation levels. Many RNA binding proteins of these proteins have been reported to have posttranscriptional control of neurotransmitter receptors. These included proteins encoded by *Hnrnpr*, *Cpeb4*, *Pum1*, *Pum2*, *Stau1* and *Stau2* which were differentially regulated at mid to late timepoints in the proteome data[219]. Notably, staufen 2 depletion is reported to decrease the number of dendritic spines, alter synaptic morphology and reduce excitatory current amplitude [326]. Various RNA processing proteins were phospho-regulated at different time points. For example, most RNA processing proteins were phosphorylated early, but the protein encoded by *Sfpq* was phosphorylated late in the time course.

The effects on protein expression following activity-dependent phospho-regulation of mRNA processing has not been well studied. Transcriptomics and targeted experiments knocking down/out specific posttranscriptional regulators and phosphosites will likely be required. However, it is notable that sixteen alternatively spliced protein isoforms had altered abundance in the proteome data, particularly at 24-48 h. Many affected splice variants were synaptic proteins and had decreased expression, indicating that changes to protein isoforms is a pathway to downscaling initiated by phospho-signalling, as shown previously [73].

The predicted increase in activity of p90RSK, supported by phosphorylation of known substrates, offers a likely pathway for regulation of mRNA processing proteins. P90RSK is known to be a regulator of translation and is activated by PDK1 And MAPK1/3. Although MAPK1/3 were predicted to be down-regulated, this was likely due to the difficulty in

assigning substrates correctly to the many proline-directed protein kinases. The activation sites of MAPK1/3 had increased phosphorylation across the entire time course proving the prediction was likely false. P90RSK is not yet explicitly linked with down-scaling. Thus, MAPK1/3 and PDK1 activation of p90RSK to regulate translation during downscaling is a new hypothesis arising from this work.

5.3.3 Similarities and differences between synaptic downscaling and early epileptogenesis

A Pearson correlation analysis of protein abundance changes showed some similar changes in the direction of protein expression and phosphorylation following both types of chemical stimulation. There were overlapping changes in the dephosphorylation of upper layer PSD scaffolding proteins and neurotransmitter receptors, such as PSD93, PSD95, DLGAP1, homer2, mGluR5 and GluR1 (Appendix 29). Protein expression of GluR5 and homer2 was also decreased in both datasets, which supports the concept that mechanisms involved in synaptic downscaling are a feature of the response to pilocarpine treatment. There were some exceptions such as Bic induced phosphorylation of SHANK2 S648, SHANK3 S897, and increased DLGAP2 and $GABA_A$ protein expression. Following pilocarpine, postsynaptic proteins were more uniformly dephosphorylated and presynaptic proteins had very little regulation. Likely, differences in stimulation strength, electrophysiological activation mechanism and the live animal versus cell culture environment accounts for these differences.

A comparison of the kinase activity prediction between Bic and pilocarpine at mid time points revealed that the kinase activity was negatively correlated with low to moderate correlation. This implied that the phospho-signalling was being driven by different kinases. Notably, a broader set of MAPK pathway kinases such as p38 and MSK were activated after pilocarpine

and MTOR activation was also specific to pilocarpine stimulation. Activation of this broader set of kinases involved in translation may also explain why a much larger (~3 times) set of posttranscriptional regulatory proteins were phosphorylated following pilocarpine, compared to after Bic stimulation. Nevertheless, the activation of MAPK1/3 and p90RSK predicted after Bic stimulation is enough to be pathogenic [327]. Thus, the relatively weak Bic stimulation may also be considered a weak model of epilepsy[287] that has pathogenic features. The many features of the data and hypotheses generated will require targeted analysis.

Activation of ribosomes and the proteasome was another a feature of pilocarpine stimulation that was not seen after Bic. This activation of proteostasis has been identified as a possible pathogenic mechanism that is associate to some seizure types [328]. The comparison of downscaling and early epileptogenesis may allow easier identification of the features of epileptogenesis which may be pathogenic or simply neuroprotective.

5.3.4 Comparison to other synaptic downscaling analysis

To provide validation of the data generated in this study, the phosphoproteomic and proteomic output was compared to the Desch et al. data. A Pearson correlation between the phosphoproteomic and proteomic data from both analyses showed a moderate to high positive correlation. In general, the results from this analysis were supported by the Desch et al. study.

Chapter 6. General discussion and concluding remarks

Synaptic scaling is a negative feedback mechanism that enables synaptic inputs to counteract extreme shifts in neuronal activity ensuring transmission strength and activity are maintained at a setpoint [4]. Epileptic seizures are defined as neuronal activity which is abnormally excessive or highly synchronised [111]. At a superficial level, epileptic seizure activity would appear to be the antithesis of synaptic activity that is being homeostatically regulated. In this study, I examined epilepsy through the lens of a failed homeostatic mechanism.

In Chapter 3 of this thesis, I performed a discovery screen to profile the early phosphoproteomic and proteomic changes occurring during epileptogenesis. It was apparent that neurotransmitter receptors and proteins in the upper two scaffolding layers of the PSD were mainly dephosphorylated whilst lower layer PSD proteins had increased phosphorylation. Based on the phosphorylation site data, predicted kinase activity and known functions in the literature[227,244,246], CAMK2α and protein phosphatase 2B (PP2B) were the likely key upstream phospho-signalling regulators. PP2B probably activated other protein phosphatases, such as PP1, and phosphatases were mainly predicted to target CDK5 substrates for dephosphorylation. Some of this dephosphorylation is likely to be neuroprotective, but some may be pathogenic and contribute to synapse loss, in which case, PP2B could be reconsidered as a target for antiepileptogenesis treatment.

Rho GTPases and guanyl-nucleotide exchange factor sites were phosphorylated following pilocarpine. Since these proteins are associated with synapse morphogenesis and cell growth[257], they have a potential role in excitatory synapse biogenesis. The exact protein kinase substrates involved are not clear, but they could be determined by predictive methods along with systematic use of multiple protein kinase inhibitors.

Posttranscriptional regulatory proteins were primary targets of increased phosphorylation in the epileptogenesis study. Amongst detected phosphorylation sites were those belonging to the RNA binding proteins encoded by *Sfpq*, *Nova2*, *Celf4*, *Pum1*, *Pum2*, *Eif4enif1* and *Cpeb4* which are involved in neurotransmitter mRNA processing[219]. Many regulators of alternative splicing were phosphorylated and twelve alternatively spliced protein variants were also detected. More work will be required, using transcriptomics, to understand the extent of alternative splicing.

There was evidence to support the activation of MAPK family members and MTOR as key drivers of increased phosphorylation of the posttranscriptional regulatory proteins. MAPK and MTOR signalling has been proposed to be important in epileptogenesis by targeting RNA binding proteins[170,219]. This work supports this hypothesis and provides mechanistic hypotheses to pursue. For example, inhibition of MAPKs and MTOR could be performed to confirm which posttranscriptional regulators are direct or indirect substrates. Phosphorylation sites on posttranscriptional regulators could be mutated to make them "phospho-mimetic" and "phospho-deficient" and a comparison of the transcriptome, neuronal morphology and electrophysiology arising from the different mutants could be performed to determine the mechanisms that contribute to an epileptogenic phenotype. Suitable kinase inhibitors could be tested in epilepsy animal models to determine if the onset of seizures is delayed or prevented.

In a preliminary study, I used Bic to stimulate neurons in an *in vitro* epilepsy model to functionally characterise the role of MTOR activity. My analysis did not provide evidence supporting the connection between MTOR signalling and the generation of seizurogenic activity in hippocampal neurons. The interpretation was hindered by a lack of repetition. More importantly, the results of the phosphoproteomics study on Bic stimulated neurons showed that MTOR has low or no involvement in Bic stimulated electrophysiological activity. Thus, to gain a better understanding of MTOR inhibition on seizure activity it would also be necessary to

determine which *in vitro* model of epilepsy is most like the animal model of epilepsy. Bradley, et al. [287] outlined how each chemical stimulation produces seizure-like electrophysiological signals via MEA; however, the underlying mechanisms for these functional readouts have not been determined. Our work will allow the use of biomarkers, such as MTOR substrates, to test for the presence of these underlying mechanisms, paving the way to high throughput drug screens.

Inflammation is suspected to have a role in the early stages of epileptogenesis, but there were only minor indicators of inflammation in the epileptogenesis study. Cytokines are difficult to detect by mass spectrometry due to their low abundance and so a subset of the proteins were probably underrepresented. Another aspect of the epileptogenesis data was increased production of protein synthesis machinery and proteasome proteins. These proteins have opposing functions. Recently, overactive synthesis and degradation, known as excessive proteostasis, has been identified as a pathological feature of fragile X and linked to audiogenic seizures [328]. Future work could focus on inhibiting these mechanisms to show whether they are pathogenic in epilepsy models.

To enable a comparison of epileptogenesis and synaptic downscaling mechanisms, I performed a deep temporal profile of the phosphoproteome and proteome following Bic stimulation in Chapter 5. The phosphorylation pattern had some similarities to the epileptogenesis study. Both studies had downregulated phosphorylation of neurotransmitter receptors, dephosphorylation of the two upper layers of scaffolding proteins in the PSD and increased phosphorylation of lower layer PSD proteins. Similarly, this signalling appeared to result in the reduced protein expression of the same proteins that were dephosphorylated. There were more exceptions to this trend in the Bic stimulation data, such as the increased phosphorylation of DLGAP2 and $GABA_A$ protein expression. An examination of how different types and strengths of stimulation leads to different phosphorylation levels for neurotransmitter receptors and PSD proteins may

help to differentiate between pathogenic and neuroprotective mechanisms. In my analysis, I highlighted different phosphosites and proteins with regulation specific to the pilocarpine stimulation. These signalling mechanisms and proteins could be drug targets or potential biomarkers of epileptogenesis, following further validation.

Similar to the data in the early epileptogenesis discovery screen, downscaling involved phosphorylation of posttranscriptional regulatory proteins and translation factors. For example, the proteins encoded by *Sfpq* and *Pum1* were phosphorylated in both studies. Analysis of kinase activity for downscaling indicated that p90RSK, downstream of MAPK1/3 and PDK1, had the most support as an activated protein kinase and is known as a driver of translation. An inhibitor of p90RSK in combination with transcriptomic, proteomic and functional analysis could be used to determine whether p90RSK has a major role in synaptic downscaling.

A Pearson correlation analysis of the predicted kinase activity in both epileptogenesis and synaptic downscaling indicated that the kinase activation was distinct. P90RSK was activated in both studies, but MAPK family members and MTOR were activated specifically following pilocarpine. This finding may lend support to the idea that the pilocarpine stimulation is stronger than Bic and leads to additional pathogenic activation of the MAPK family of protein kinases and additional downstream kinases.

The data generated in Chapter 3, was validated by performing a label free quantitative analysis of Ste20-like kinase (SLK) peptides, which matched the direction of the $\log_2$ fold change in the discovery screen data. The data also corroborated many previously observed biomarkers found in epileptogenesis models. The results generated in Chapter 5 were compared to the phosphoproteomic and proteomic data provided by Desch, et al. [39], finding that both datasets were moderately to highly correlated.

Overall, this thesis provides mechanistic insights into epileptogenesis and synaptic downscaling that advances neurobiology and might be exploited for drug targets and biomarkers.

Chapter 7. References

1 Hebb, D. O. *The organization of behavior: a neuropsychological theory*. 99 edn, (John Wiley & Sons, 1949).

2 Turrigiano, G. G., Leslie, K. R., Desai, N. S., Rutherford, L. C. & Nelson, S. B. Activity-dependent scaling of quantal amplitude in neocortical neurons. *Nature* **391**, 892-896, doi:10.1038/36103 (1998).

3 Fisher, R. S. *et al.* Epileptic seizures and epilepsy: definitions proposed by the International League Against Epilepsy (ILAE) and the International Bureau for Epilepsy (IBE). *Epilepsia* **46**, 470-472, doi:10.1111/j.0013-9580.2005.66104.x (2005).

4 Turrigiano, G. Homeostatic synaptic plasticity: local and global mechanisms for stabilizing neuronal function. *Cold Spring Harb Perspect Biol* **4**, a005736, doi:10.1101/cshperspect.a005736 (2012).

5 Styr, B. & Slutsky, I. Imbalance between firing homeostasis and synaptic plasticity drives early-phase Alzheimer's disease. *Nature neuroscience* **21**, 463-473, doi:10.1038/s41593-018-0080-x (2018).

6 Jarero-Basulto, J. J. *et al.* Interactions Between Epilepsy and Plasticity. *Pharmaceuticals (Basel)* **11**, 17, doi:10.3390/ph11010017 (2018).

7 Wang, J. *et al.* Epilepsy-associated genes. *Seizure* **44**, 11-20, doi:10.1016/j.seizure.2016.11.030 (2017).

8 Wondolowski, J. & Dickman, D. Emerging links between homeostatic synaptic plasticity and neurological disease. *Frontiers in cellular neuroscience* **7**, 223, doi:10.3389/fncel.2013.00223 (2013).

9 Roeper, J. Closing gaps in brain disease-from overlapping genetic architecture to common motifs of synapse dysfunction. *Current opinion in neurobiology* **48**, 45-51, doi:10.1016/j.conb.2017.09.007 (2018).

10 Li, J., Park, E., Zhong, L. R. & Chen, L. Homeostatic synaptic plasticity as a metaplasticity mechanism - a molecular and cellular perspective. *Current opinion in neurobiology* **54**, 44-53, doi:10.1016/j.conb.2018.08.010 (2019).

11 Glasgow, S. D., McPhedrain, R., Madranges, J. F., Kennedy, T. E. & Ruthazer, E. S. Approaches and Limitations in the Investigation of Synaptic Transmission and Plasticity. *Frontiers in synaptic neuroscience* **11**, 20, doi:10.3389/fnsyn.2019.00020 (2019).

12 Abbott, L. F. & Regehr, W. G. Synaptic computation. *Nature* **431**, 796-803, doi:10.1038/nature03010 (2004).

13 Vizi, E. S. Presynaptic modulation of neurochemical transmission. *Progress in neurobiology* **12**, 181-290, doi:10.1016/0301-0082(79)90011-x (1979).

14 McCormick, D. A. in *From Molecules to Networks* (eds John H. Byrne, Ruth Heidelberger, & M. Neal Waxham) 351-376 (Academic Press, 2014).

15 Pereda, A. E. Electrical synapses and their functional interactions with chemical synapses. *Nature reviews. Neuroscience* **15**, 250-263, doi:10.1038/nrn3708 (2014).

16 Pereda, A. E. Developmental functions of electrical synapses. *The Journal of physiology* **594**, 2561-2562, doi:10.1113/JP272361 (2016).

17 Connors, B. W. & Long, M. A. Electrical synapses in the mammalian brain. *Annual review of neuroscience* **27**, 393-418, doi:10.1146/annurev.neuro.26.041002.131128 (2004).

18 Hyman, S. E. Neurotransmitters. *Current biology : CB* **15**, R154-158, doi:10.1016/j.cub.2005.02.037 (2005).

19 Collingridge, G. L., Isaac, J. T. & Wang, Y. T. Receptor trafficking and synaptic plasticity. *Nature reviews. Neuroscience* **5**, 952-962, doi:10.1038/nrn1556 (2004).

20 Kuriyama, K., Hirouchi, M. & Nakayasu, H. Structure and function of cerebral GABAA and GABAB receptors. *Neuroscience research* **17**, 91-99, doi:10.1016/0168-0102(93)90087-7 (1993).

21 Twomey, E. C. & Sobolevsky, A. I. Structural Mechanisms of Gating in Ionotropic Glutamate Receptors. *Biochemistry* **57**, 267-276, doi:10.1021/acs.biochem.7b00891 (2018).

22 Suh, Y. H. *et al.* Regulation of metabotropic glutamate receptor 7 (mGluR7) internalization and surface expression by Ser/Thr protein phosphatase 1. *The Journal of biological chemistry* **288**, 17544-17551, doi:10.1074/jbc.M112.439513 (2013).

23 Kennedy, M. B. Signal-processing machines at the postsynaptic density. *Science* **290**, 750-754, doi:10.1126/science.290.5492.750 (2000).

24 Fernandes, D. & Carvalho, A. L. Mechanisms of homeostatic plasticity in the excitatory synapse. *J Neurochem* **139**, 973-996, doi:10.1111/jnc.13687 (2016).

25 Vitureira, N. & Goda, Y. Cell biology in neuroscience: the interplay between Hebbian and homeostatic synaptic plasticity. *The Journal of cell biology* **203**, 175-186, doi:10.1083/jcb.201306030 (2013).

26 Yin, J. & Yuan, Q. Structural homeostasis in the nervous system: a balancing act for wiring plasticity and stability. *Frontiers in cellular neuroscience* **8**, 439, doi:10.3389/fncel.2014.00439 (2014).

27 Turrigiano, G. G. & Nelson, S. B. Hebb and homeostasis in neuronal plasticity. *Current opinion in neurobiology* **10**, 358-364, doi:10.1016/s0959-4388(00)00091-x (2000).

28 Burrone, J. & Murthy, V. N. Synaptic gain control and homeostasis. *Current opinion in neurobiology* **13**, 560-567, doi:10.1016/j.conb.2003.09.007 (2003).

29 Swann, J. W. & Rho, J. M. How is homeostatic plasticity important in epilepsy? *Advances in experimental medicine and biology* **813**, 123-131, doi:10.1007/978-94-017-8914-1_10 (2014).

30 Dickman, D. K. & Davis, G. W. The schizophrenia susceptibility gene dysbindin controls synaptic homeostasis. *Science* **326**, 1127-1130, doi:10.1126/science.1179685 (2009).

31 Davis, G. W. & Muller, M. Homeostatic control of presynaptic neurotransmitter release. *Annual review of physiology* **77**, 251-270, doi:10.1146/annurev-physiol-021014-071740 (2015).

32 Turrigiano, G. G. The dialectic of Hebb and homeostasis. *Philosophical transactions of the Royal Society of London. Series B, Biological sciences* **372**, 20160258, doi:10.1098/rstb.2016.0258 (2017).

33 Pribiag, H. & Stellwagen, D. Neuroimmune regulation of homeostatic synaptic plasticity. *Neuropharmacology* **78**, 13-22, doi:10.1016/j.neuropharm.2013.06.008 (2014).

34 Lee, K. F., Soares, C. & Beique, J. C. Tuning into diversity of homeostatic synaptic plasticity. *Neuropharmacology* **78**, 31-37, doi:10.1016/j.neuropharm.2013.03.016 (2014).

35 Joseph, A. & Turrigiano, G. G. All for One But Not One for All: Excitatory Synaptic Scaling and Intrinsic Excitability Are Coregulated by CaMKIV, Whereas Inhibitory Synaptic Scaling Is Under Independent Control. *The Journal of neuroscience : the official journal of the Society for Neuroscience* **37**, 6778-6785, doi:10.1523/JNEUROSCI.0618-17.2017 (2017).

36 O'Brien, R. J. *et al.* Activity-dependent modulation of synaptic AMPA receptor accumulation. *Neuron* **21**, 1067-1078, doi:10.1016/s0896-6273(00)80624-8 (1998).

37 Schanzenbacher, C. T., Sambandan, S., Langer, J. D. & Schuman, E. M. Nascent Proteome Remodeling following Homeostatic Scaling at Hippocampal Synapses. *Neuron* **92**, 358-371, doi:10.1016/j.neuron.2016.09.058 (2016).

38 Schanzenbacher, C. T., Langer, J. D. & Schuman, E. M. Time- and polarity-dependent proteomic changes associated with homeostatic scaling at central synapses. *eLife* **7**, doi:10.7554/eLife.33322 (2018).

39 Desch, K., Langer, J. D. & Schuman, E. M. Dynamic bi-directional phosphorylation events associated with the reciprocal regulation of synapses during homeostatic up- and down-scaling. *Cell reports* **36**, 109583, doi:10.1016/j.celrep.2021.109583 (2021).

40 Perry, S. W., Dewhurst, S., Bellizzi, M. J. & Gelbard, H. A. Tumor necrosis factor-alpha in normal and diseased brain: Conflicting effects via intraneuronal receptor crosstalk? *J Neurovirol* **8**, 611-624, doi:10.1080/13550280290101021 (2002).

41 Heir, R. & Stellwagen, D. TNF-Mediated Homeostatic Synaptic Plasticity: From in vitro to in vivo Models. *Frontiers in cellular neuroscience* **14**, 565841, doi:10.3389/fncel.2020.565841 (2020).

42 Stellwagen, D. & Malenka, R. C. Synaptic scaling mediated by glial TNF-alpha. *Nature* **440**, 1054-1059, doi:10.1038/nature04671 (2006).

43 Steinmetz, C. C. & Turrigiano, G. G. Tumor necrosis factor-alpha signaling maintains the ability of cortical synapses to express synaptic scaling. *The Journal of neuroscience : the official journal of the Society for Neuroscience* **30**, 14685-14690, doi:10.1523/JNEUROSCI.2210-10.2010 (2010).

44 Kaneko, M., Stellwagen, D., Malenka, R. C. & Stryker, M. P. Tumor necrosis factor-alpha mediates one component of competitive, experience-dependent plasticity in developing visual cortex. *Neuron* **58**, 673-680, doi:10.1016/j.neuron.2008.04.023 (2008).

45 Aivaliotis, M. *et al.* Large-scale identification of N-terminal peptides in the halophilic archaea Halobacterium salinarum and Natronomonas pharaonis. *J Proteome Res* **6**, 2195-2204, doi:10.1021/pr0700347 (2007).

46 Frank, C. A., Kennedy, M. J., Goold, C. P., Marek, K. W. & Davis, G. W. Mechanisms underlying the rapid induction and sustained expression of synaptic homeostasis. *Neuron* **52**, 663-677, doi:10.1016/j.neuron.2006.09.029 (2006).

47 Frank, C. A., Pielage, J. & Davis, G. W. A presynaptic homeostatic signaling system composed of the Eph receptor, ephexin, Cdc42, and CaV2.1 calcium channels. *Neuron* **61**, 556-569, doi:10.1016/j.neuron.2008.12.028 (2009).

48 Hu, J. H. *et al.* Homeostatic scaling requires group I mGluR activation mediated by Homer1a. *Neuron* **68**, 1128-1142, doi:10.1016/j.neuron.2010.11.008 (2010).

49 Diering, G. H. *et al.* Homer1a drives homeostatic scaling-down of excitatory synapses during sleep. *Science* **355**, 511-515, doi:10.1126/science.aai8355 (2017).

50 Ghiani, C. A. *et al.* The dysbindin-containing complex (BLOC-1) in brain: developmental regulation, interaction with SNARE proteins and role in neurite outgrowth. *Mol Psychiatry* **15**, 115, 204-115, doi:10.1038/mp.2009.58 (2010).

51 Dickman, D. K., Tong, A. & Davis, G. W. Snapin is critical for presynaptic homeostatic plasticity. *The Journal of neuroscience : the official journal of the Society for Neuroscience* **32**, 8716-8724, doi:10.1523/JNEUROSCI.5465-11.2012 (2012).

52 Takei, N. & Nawa, H. mTOR signaling and its roles in normal and abnormal brain development. *Frontiers in molecular neuroscience* **7**, 28, doi:10.3389/fnmol.2014.00028 (2014).

53 Henry, F. E. *et al.* Retrograde changes in presynaptic function driven by dendritic mTORC1. *The Journal of neuroscience : the official journal of the Society for Neuroscience* **32**, 17128-17142, doi:10.1523/JNEUROSCI.2149-12.2012 (2012).

54 Henry, F. E. *et al.* A Unique Homeostatic Signaling Pathway Links Synaptic Inactivity to Postsynaptic mTORC1. *The Journal of neuroscience : the official journal of the Society for Neuroscience* **38**, 2207-2225, doi:10.1523/JNEUROSCI.1843-17.2017 (2018).

55 Robison, A. J. Emerging role of CaMKII in neuropsychiatric disease. *Trends Neurosci* **37**, 653-662, doi:10.1016/j.tins.2014.07.001 (2014).

56 Thiagarajan, T. C., Piedras-Renteria, E. S. & Tsien, R. W. alpha- and betaCaMKII. Inverse regulation by neuronal activity and opposing effects on synaptic strength. *Neuron* **36**, 1103-1114, doi:10.1016/s0896-6273(02)01049-8 (2002).

57 Groth, R. D., Lindskog, M., Thiagarajan, T. C., Li, L. & Tsien, R. W. Beta Ca2+/CaM-dependent kinase type II triggers upregulation of GluA1 to coordinate adaptation to synaptic inactivity in hippocampal neurons. *Proc Natl Acad Sci U S A* **108**, 828-833, doi:10.1073/pnas.1018022108 (2011).

58 Zech, M. *et al.* A unique de novo gain-of-function variant in CAMK4 associated with intellectual disability and hyperkinetic movement disorder. *Cold Spring Harb Mol Case Stud* **4**, a003293, doi:10.1101/mcs.a003293 (2018).

59 Ibata, K., Sun, Q. & Turrigiano, G. G. Rapid synaptic scaling induced by changes in postsynaptic firing. *Neuron* **57**, 819-826, doi:10.1016/j.neuron.2008.02.031 (2008).

60 Lima Giacobbo, B. *et al.* Brain-Derived Neurotrophic Factor in Brain Disorders: Focus on Neuroinflammation. *Molecular neurobiology* **56**, 3295-3312, doi:10.1007/s12035-018-1283-6 (2019).

61 Rutherford, L. C., DeWan, A., Lauer, H. M. & Turrigiano, G. G. Brain-derived neurotrophic factor mediates the activity-dependent regulation of inhibition in neocortical cultures. *The Journal of neuroscience : the official journal of the Society for Neuroscience* **17**, 4527-4535, doi:10.1523/jneurosci.17-12-04527.1997 (1997).

62 Rutherford, L. C., Nelson, S. B. & Turrigiano, G. G. BDNF Has Opposite Effects on the Quantal Amplitude of Pyramidal Neuron and Interneuron Excitatory Synapses. *Neuron* **21**, 521-530, doi:10.1016/s0896-6273(00)80563-2 (1998).

63 Reimers, J. M., Loweth, J. A. & Wolf, M. E. BDNF contributes to both rapid and homeostatic alterations in AMPA receptor surface expression in nucleus accumbens medium spiny neurons. *Eur J Neurosci* **39**, 1159-1169, doi:10.1111/ejn.12422 (2014).

64 Wu, X. & Reddy, D. S. Integrins as receptor targets for neurological disorders. *Pharmacology & therapeutics* **134**, 68-81, doi:10.1016/j.pharmthera.2011.12.008 (2012).

65 Cingolani, L. A. & Goda, Y. Differential involvement of beta3 integrin in pre- and postsynaptic forms of adaptation to chronic activity deprivation. *Neuron Glia Biol* **4**, 179-187, doi:10.1017/S1740925X0999024X (2008).

66 Cingolani, L. A. *et al.* Activity-dependent regulation of synaptic AMPA receptor composition and abundance by beta3 integrins. *Neuron* **58**, 749-762, doi:10.1016/j.neuron.2008.04.011 (2008).

67 Saraf, J. *et al.* A Friend or Foe: Calcineurin across the Gamut of Neurological Disorders. *ACS Central Science* **4**, 805-819, doi:10.1021/acscentsci.8b00230 (2018).

68 Pao, P. C. & Tsai, L. H. Three decades of Cdk5. *J Biomed Sci* **28**, 79, doi:10.1186/s12929-021-00774-y (2021).

69 Aroor, A. & Brewster, A. L. Getting Excited Through Cyclin: A Role for Endothelial Cdk5 Signaling in Hippocampal Hyperexcitability. *Epilepsy currents* **20**, 396-398, doi:10.1177/1535759720958418 (2020).

70 Kim, S. H. & Ryan, T. A. CDK5 serves as a major control point in neurotransmitter release. *Neuron* **67**, 797-809, doi:10.1016/j.neuron.2010.08.003 (2010).

71 Kim, S. H. & Ryan, T. A. Balance of calcineurin Aalpha and CDK5 activities sets release probability at nerve terminals. *The Journal of neuroscience : the official journal of the Society for Neuroscience* **33**, 8937-8950, doi:10.1523/JNEUROSCI.4288-12.2013 (2013).

72 Nussbacher, J. K., Tabet, R., Yeo, G. W. & Lagier-Tourenne, C. Disruption of RNA Metabolism in Neurological Diseases and Emerging Therapeutic Interventions. *Neuron* **102**, 294-320, doi:10.1016/j.neuron.2019.03.014 (2019).

73 Li, B. *et al.* Neuronal Inactivity Co-opts LTP Machinery to Drive Potassium Channel Splicing and Homeostatic Spike Widening. *Cell* **181**, 1547-1565 e1515, doi:10.1016/j.cell.2020.05.013 (2020).

74 Gold, W. A., Krishnarajy, R., Ellaway, C. & Christodoulou, J. Rett Syndrome: A Genetic Update and Clinical Review Focusing on Comorbidities. *ACS chemical neuroscience* **9**, 167-176, doi:10.1021/acschemneuro.7b00346 (2018).

75 Qiu, Z. *et al.* The Rett syndrome protein MeCP2 regulates synaptic scaling. *The Journal of neuroscience : the official journal of the Society for Neuroscience* **32**, 989-994, doi:10.1523/JNEUROSCI.0175-11.2012 (2012).

76 Blackman, M. P., Djukic, B., Nelson, S. B. & Turrigiano, G. G. A critical and cell-autonomous role for MeCP2 in synaptic scaling up. *The Journal of neuroscience : the official journal of the Society for Neuroscience* **32**, 13529-13536, doi:10.1523/JNEUROSCI.3077-12.2012 (2012).

77 Gamache, T. R., Araki, Y. & Huganir, R. L. Twenty Years of SynGAP Research: From Synapses to Cognition. *The Journal of neuroscience : the official journal of the Society for Neuroscience* **40**, 1596-1605, doi:10.1523/JNEUROSCI.0420-19.2020 (2020).

78 Wang, C. C., Held, R. G. & Hall, B. J. SynGAP regulates protein synthesis and homeostatic synaptic plasticity in developing cortical networks. *PLoS One* **8**, e83941, doi:10.1371/journal.pone.0083941 (2013).

79 Lane, M. A. & Bailey, S. J. Role of retinoid signalling in the adult brain. *Progress in neurobiology* **75**, 275-293, doi:10.1016/j.pneurobio.2005.03.002 (2005).

80 Aoto, J., Nam, C. I., Poon, M. M., Ting, P. & Chen, L. Synaptic signaling by all-trans retinoic acid in homeostatic synaptic plasticity. *Neuron* **60**, 308-320, doi:10.1016/j.neuron.2008.08.012 (2008).

81 Sarti, F., Schroeder, J., Aoto, J. & Chen, L. Conditional RARalpha knockout mice reveal acute requirement for retinoic acid and RARalpha in homeostatic plasticity. *Frontiers in molecular neuroscience* **5**, 16, doi:10.3389/fnmol.2012.00016 (2012).

82 Chen, N. & Napoli, J. L. All-trans-retinoic acid stimulates translation and induces spine formation in hippocampal neurons through a membrane-associated RARalpha. *FASEB journal : official publication of the Federation of American Societies for Experimental Biology* **22**, 236-245, doi:10.1096/fj.07-8739com (2008).

83 Arendt, K. L. *et al.* Retinoic Acid and LTP Recruit Postsynaptic AMPA Receptors Using Distinct SNARE-Dependent Mechanisms. *Neuron* **86**, 442-456, doi:10.1016/j.neuron.2015.03.009 (2015).

84 Epstein, I. & Finkbeiner, S. The Arc of cognition: Signaling cascades regulating Arc and implications for cognitive function and disease. *Semin Cell Dev Biol* **77**, 63-72, doi:10.1016/j.semcdb.2017.09.023 (2018).

85 Shepherd, J. D. *et al.* Arc/Arg3.1 mediates homeostatic synaptic scaling of AMPA receptors. *Neuron* **52**, 475-484, doi:10.1016/j.neuron.2006.08.034 (2006).

86 Gao, M. *et al.* A specific requirement of Arc/Arg3.1 for visual experience-induced homeostatic synaptic plasticity in mouse primary visual cortex. *The Journal of neuroscience : the official journal of the Society for Neuroscience* **30**, 7168-7178, doi:10.1523/JNEUROSCI.1067-10.2010 (2010).

87 Needham, E. J., Parker, B. L., Burykin, T., James, D. E. & Humphrey, S. J. Illuminating the dark phosphoproteome. *Science signaling* **12**, doi:10.1126/scisignal.aau8645 (2019).

88 Nishi, H., Demir, E. & Panchenko, A. R. Crosstalk between signaling pathways provided by single and multiple protein phosphorylation sites. *J Mol Biol* **427**, 511-520, doi:10.1016/j.jmb.2014.11.001 (2015).

89 Kim, M. J. *et al.* Synaptic accumulation of PSD-95 and synaptic function regulated by phosphorylation of serine-295 of PSD-95. *Neuron* **56**, 488-502, doi:10.1016/j.neuron.2007.09.007 (2007).

90 Tao, J. *et al.* Phosphorylation of MeCP2 at Serine 80 regulates its chromatin association and neurological function. *Proc Natl Acad Sci U S A* **106**, 4882-4887, doi:10.1073/pnas.0811648106 (2009).

91 Bhullar, K. S. *et al.* Kinase-targeted cancer therapies: progress, challenges and future directions. *Mol Cancer* **17**, 48, doi:10.1186/s12943-018-0804-2 (2018).

92 Loscher, W., Gillard, M., Sands, Z. A., Kaminski, R. M. & Klitgaard, H. Synaptic Vesicle Glycoprotein 2A Ligands in the Treatment of Epilepsy and Beyond. *CNS Drugs* **30**, 1055-1077, doi:10.1007/s40263-016-0384-x (2016).

93 Xue-Ping, W., Hai-Jiao, W., Li-Na, Z., Xu, D. & Ling, L. Risk factors for drug-resistant epilepsy: A systematic review and meta-analysis. *Medicine (Baltimore)* **98**, e16402, doi:10.1097/MD.0000000000016402 (2019).

94 Liu, G., Kotloski, R. J. & McNamara, J. O. Antiseizure effects of TrkB kinase inhibition. *Epilepsia* **55**, 1264-1273, doi:10.1111/epi.12671 (2014).

95 Engholm-Keller, K. *et al.* The temporal profile of activity-dependent presynaptic phospho-signalling reveals long-lasting patterns of poststimulus regulation. *PLoS biology* **17**, e3000170, doi:10.1371/journal.pbio.3000170 (2019).

96 Aebersold, R. & Mann, M. Mass-spectrometric exploration of proteome structure and function. *Nature* **537**, 347-355, doi:10.1038/nature19949 (2016).

97 Riley, N. M. & Coon, J. J. Phosphoproteomics in the Age of Rapid and Deep Proteome Profiling. *Anal Chem* **88**, 74-94, doi:10.1021/acs.analchem.5b04123 (2016).

98 Andersson, L. & Porath, J. Isolation of phosphoproteins by immobilized metal (Fe3+) affinity chromatography. *Anal Biochem* **154**, 250-254, doi:10.1016/0003-2697(86)90523-3 (1986).

99 Ikeguchi, Y. & Nakamura, H. Determination of organic phosphates by column-switching high performance anion-exchange chromatography using on-line preconcentration on titania. *Analytical Sciences* **13**, 479-483, doi:DOI 10.2116/analsci.13.479 (1997).

100 Jensen, S. S. & Larsen, M. R. Evaluation of the impact of some experimental procedures on different phosphopeptide enrichment techniques. *Rapid communications in mass spectrometry : RCM* **21**, 3635-3645, doi:10.1002/rcm.3254 (2007).

101 Thingholm, T. E., Jensen, O. N., Robinson, P. J. & Larsen, M. R. SIMAC (sequential elution from IMAC), a phosphoproteomics strategy for the rapid separation of monophosphorylated from multiply phosphorylated peptides. *Molecular & cellular proteomics : MCP* **7**, 661-671, doi:10.1074/mcp.M700362-MCP200 (2008).

102 Engholm-Keller, K. *et al.* TiSH--a robust and sensitive global phosphoproteomics strategy employing a combination of TiO2, SIMAC, and HILIC. *J Proteomics* **75**, 5749-5761, doi:10.1016/j.jprot.2012.08.007 (2012).

103 Engholm-Keller, K. & Larsen, M. R. Improving the Phosphoproteome Coverage for Limited Sample Amounts Using TiO2-SIMAC-HILIC (TiSH) Phosphopeptide Enrichment and Fractionation. *Methods in molecular biology* **1355**, 161-177, doi:10.1007/978-1-4939-3049-4_11 (2016).

104 Hoffman, N. J. *et al.* Global Phosphoproteomic Analysis of Human Skeletal Muscle Reveals a Network of Exercise-Regulated Kinases and AMPK Substrates. *Cell Metab* **22**, 922-935, doi:10.1016/j.cmet.2015.09.001 (2015).

105 Batth, T. S. *et al.* Large-Scale Phosphoproteomics Reveals Shp-2 Phosphatase-Dependent Regulators of Pdgf Receptor Signaling. *Cell reports* **22**, 2784-2796, doi:10.1016/j.celrep.2018.02.038 (2018).

106 Batth, T. S. & Olsen, J. V. Offline High pH Reversed-Phase Peptide Fractionation for Deep Phosphoproteome Coverage. *Methods in molecular biology* **1355**, 179-192, doi:10.1007/978-1-4939-3049-4_12 (2016).

107 Sharma, K. *et al.* Ultradeep human phosphoproteome reveals a distinct regulatory nature of Tyr and Ser/Thr-based signaling. *Cell reports* **8**, 1583-1594, doi:10.1016/j.celrep.2014.07.036 (2014).

108 Beghi, E. *et al.* Global, regional, and national burden of epilepsy, 1990–2016: a systematic analysis for the Global Burden of Disease Study 2016. *The Lancet Neurology* **18**, 357-375, doi:10.1016/s1474-4422(18)30454-x (2019).

109 Devinsky, O. *et al.* Epilepsy. *Nat Rev Dis Primers* **4**, 18024, doi:10.1038/nrdp.2018.24 (2018).

110 Group, G. B. D. N. D. C. Global, regional, and national burden of neurological disorders during 1990-2015: a systematic analysis for the Global Burden of Disease Study 2015. *The Lancet. Neurology* **16**, 877-897, doi:10.1016/S1474-4422(17)30299-5 (2017).

111 Fisher, R. S. *et al.* ILAE official report: a practical clinical definition of epilepsy. *Epilepsia* **55**, 475-482, doi:10.1111/epi.12550 (2014).

112 Kwan, P. *et al.* Definition of drug resistant epilepsy: consensus proposal by the ad hoc Task Force of the ILAE Commission on Therapeutic Strategies. *Epilepsia* **51**, 1069-1077, doi:10.1111/j.1528-1167.2009.02397.x (2010).

113 Levesque, M., Avoli, M. & Bernard, C. Animal models of temporal lobe epilepsy following systemic chemoconvulsant administration. *Journal of neuroscience methods* **260**, 45-52, doi:10.1016/j.jneumeth.2015.03.009 (2016).

114 Loscher, W. Fit for purpose application of currently existing animal models in the discovery of novel epilepsy therapies. *Epilepsy research* **126**, 157-184, doi:10.1016/j.eplepsyres.2016.05.016 (2016).

115 Oliver, K. L. *et al.* Genes4Epilepsy: An epilepsy gene resource. *Epilepsia* **64**, 1368-1375, doi:10.1111/epi.17547 (2023).

116 van Loo, K. M. J. & Becker, A. J. Transcriptional Regulation of Channelopathies in Genetic and Acquired Epilepsies. *Frontiers in cellular neuroscience* **13**, 587, doi:10.3389/fncel.2019.00587 (2019).

117 Carvill, G. L., Dulla, C. G., Lowenstein, D. H. & Brooks-Kayal, A. R. The path from scientific discovery to cures for epilepsy. *Neuropharmacology* **167**, 107702, doi:10.1016/j.neuropharm.2019.107702 (2020).

118 Bertram, E. H. in *Neurobiology of disease* Vol. 2 *Paroxysmal Disorders* (eds S. L. Moshe, M. Johnston, H. Jr Adams, & A. Fatemi) Ch. Temporal Lobe Epilepsy, 289-293 (Oxford University Press, 2016).

119 Tatum, W. O. t. Mesial temporal lobe epilepsy. *J Clin Neurophysiol* **29**, 356-365, doi:10.1097/WNP.0b013e31826b3ab7 (2012).

120 Englot, D. J., Morgan, V. L. & Chang, C. Impaired vigilance networks in temporal lobe epilepsy: Mechanisms and clinical implications. *Epilepsia* **61**, 189-202, doi:10.1111/epi.16423 (2020).

121 Sendrowski, K. & Sobaniec, W. Hippocampus, hippocampal sclerosis and epilepsy. *Pharmacol Rep* **65**, 555-565, doi:10.1016/s1734-1140(13)71033-8 (2013).

122 Scharfman, H. E. The Dentate Gyrus and Temporal Lobe Epilepsy: An "Exciting" Era. *Epilepsy currents* **19**, 249-255, doi:10.1177/1535759719855952 (2019).

123 Parkin, A. J. Human memory: The hippocampus is the key. *Current Biology* **6**, 1583-1585, doi:10.1016/s0960-9822(02)70778-1 (1996).

124 Thom, M. Review: Hippocampal sclerosis in epilepsy: a neuropathology review. *Neuropathol Appl Neurobiol* **40**, 520-543, doi:10.1111/nan.12150 (2014).

125 Kempermann, G., Song, H. & Gage, F. H. Neurogenesis in the Adult Hippocampus. *Cold Spring Harb Perspect Biol* **7**, a018812, doi:10.1101/cshperspect.a018812 (2015).

126 Scharfman, H. E. Advances in understanding hilar mossy cells of the dentate gyrus. *Cell Tissue Res* **373**, 643-652, doi:10.1007/s00441-017-2750-5 (2018).

127 Koyama, R. & Ikegaya, Y. The Molecular and Cellular Mechanisms of Axon Guidance in Mossy Fiber Sprouting. *Frontiers in neurology* **9**, 382, doi:10.3389/fneur.2018.00382 (2018).

128 Toda, T., Parylak, S. L., Linker, S. B. & Gage, F. H. The role of adult hippocampal neurogenesis in brain health and disease. *Mol Psychiatry* **24**, 67-87, doi:10.1038/s41380-018-0036-2 (2019).

129 Heng, K., Haney, M. M. & Buckmaster, P. S. High-dose rapamycin blocks mossy fiber sprouting but not seizures in a mouse model of temporal lobe epilepsy. *Epilepsia* **54**, 1535-1541, doi:10.1111/epi.12246 (2013).

130 Zeng, L. H., Rensing, N. R. & Wong, M. The mammalian target of rapamycin signaling pathway mediates epileptogenesis in a model of temporal lobe epilepsy. *The Journal of neuroscience : the official journal of the Society for Neuroscience* **29**, 6964-6972, doi:10.1523/JNEUROSCI.0066-09.2009 (2009).

131 Zhang, X. *et al.* Relations between Brain Pathology and Temporal Lobe Epilepsy. *The Journal of Neuroscience* **22**, 6052-6061, doi:10.1523/jneurosci.22-14-06052.2002 (2002).

132 Patel, D. C., Tewari, B. P., Chaunsali, L. & Sontheimer, H. Neuron-glia interactions in the pathophysiology of epilepsy. *Nature reviews. Neuroscience* **20**, 282-297, doi:10.1038/s41583-019-0126-4 (2019).

133 Sofroniew, M. V. Astrogliosis. *Cold Spring Harb Perspect Biol* **7**, a020420, doi:10.1101/cshperspect.a020420 (2014).

134 Pitkanen, A. & Engel, J., Jr. Past and present definitions of epileptogenesis and its biomarkers. *Neurotherapeutics : the journal of the American Society for Experimental NeuroTherapeutics* **11**, 231-241, doi:10.1007/s13311-014-0257-2 (2014).

135 Mathern, G. W., David Adelson, P., Cahan, L. D. & Leite, J. P. 237-251 (Elsevier, 2002).

136 Liu, R. S. *et al.* Progressive neocortical damage in epilepsy. *Ann Neurol* **53**, 312-324, doi:10.1002/ana.10463 (2003).

137 Coan, A. C., Appenzeller, S., Bonilha, L., Li, L. M. & Cendes, F. Seizure frequency and lateralization affect progression of atrophy in temporal lobe epilepsy. *Neurology* **73**, 834-842, doi:10.1212/WNL.0b013e3181b783dd (2009).

138 Rapport, R. L., 2nd & Penry, J. K. Pharmacoligic prophylaxis of posttraumatic epilepsy. A review. *Epilepsia* **13**, 295-304, doi:10.1111/j.1528-1157.1972.tb05264.x (1972).

139 Loscher, W. & Brandt, C. Prevention or modification of epileptogenesis after brain insults: experimental approaches and translational research. *Pharmacol Rev* **62**, 668-700, doi:10.1124/pr.110.003046 (2010).

140 Weaver, D. F. Epileptogenesis, ictogenesis and the design of future antiepileptic drugs. *Can J Neurol Sci* **30**, 4-7, doi:10.1017/s0317167100002353 (2003).

141 Loscher, W. The holy grail of epilepsy prevention: Preclinical approaches to antiepileptogenic treatments. *Neuropharmacology* **167**, 107605, doi:10.1016/j.neuropharm.2019.04.011 (2020).

142 Reddy, D. S. Role of hormones and neurosteroids in epileptogenesis. *Frontiers in cellular neuroscience* **7**, 115, doi:10.3389/fncel.2013.00115 (2013).

143 Maguire, J. Epileptogenesis: More Than Just the Latent Period. *Epilepsy currents* **16**, 31-33, doi:10.5698/1535-7597-16.1.31 (2016).

144 Loscher, W., Hirsch, L. J. & Schmidt, D. The enigma of the latent period in the development of symptomatic acquired epilepsy - Traditional view versus new concepts. *Epilepsy Behav* **52**, 78-92, doi:10.1016/j.yebeh.2015.08.037 (2015).

145 Gowers, W. R. *Epilepsy and other chronic convulsive diseases their causes, symptoms, & treatment*. (J & A Churchill, 1881).

146 Pitkanen, A., Lukasiuk, K., Dudek, F. E. & Staley, K. J. Epileptogenesis. *Cold Spring Harb Perspect Med* **5**, a022822, doi:10.1101/cshperspect.a022822 (2015).

147 Giblin, K. A. & Blumenfeld, H. Is epilepsy a preventable disorder? New evidence from animal models. *Neuroscientist* **16**, 253-275, doi:10.1177/1073858409354385 (2010).

148 Ben-Ari, Y. & Dudek, F. E. Primary and secondary mechanisms of epileptogenesis in the temporal lobe: there is a before and an after. *Epilepsy currents* **10**, 118-125, doi:10.1111/j.1535-7511.2010.01376.x (2010).

149 Pitkanen, A., Immonen, R. J., Grohn, O. H. & Kharatishvili, I. From traumatic brain injury to posttraumatic epilepsy: what animal models tell us about the process and treatment options. *Epilepsia* **50 Suppl 2**, 21-29, doi:10.1111/j.1528-1167.2008.02007.x (2009).

150 Younus, I. & Reddy, D. S. Epigenetic interventions for epileptogenesis: A new frontier for curing epilepsy. *Pharmacology & therapeutics* **177**, 108-122, doi:10.1016/j.pharmthera.2017.03.002 (2017).

151 Kandratavicius, L. *et al.* Animal models of epilepsy: use and limitations. *Neuropsychiatric disease and treatment* **10**, 1693-1705, doi:10.2147/NDT.S50371 (2014).

152 Hellier, J. L. & Dudek, F. E. Chemoconvulsant model of chronic spontaneous seizures. *Curr Protoc Neurosci* **Chapter 9**, Unit 9 19, doi:10.1002/0471142301.ns0919s31 (2005).

153 Thodeson, D. M., Brulet, R. & Hsieh, J. Neural stem cells and epilepsy: functional roles and disease-in-a-dish models. *Cell Tissue Res* **371**, 47-54, doi:10.1007/s00441-017-2675-z (2018).

154 Antonio, L. L. *et al.* In vitro seizure like events and changes in ionic concentration. *Journal of neuroscience methods* **260**, 33-44, doi:10.1016/j.jneumeth.2015.08.014 (2016).

155 Avoli, M. & Jefferys, J. G. Models of drug-induced epileptiform synchronization in vitro. *Journal of neuroscience methods* **260**, 26-32, doi:10.1016/j.jneumeth.2015.10.006 (2016).

156 Raimondo, J. V. *et al.* Methodological standards for in vitro models of epilepsy and epileptic seizures. A TASK1-WG4 report of the AES/ILAE Translational Task Force of the ILAE. *Epilepsia* **58 Suppl 4**, 40-52, doi:10.1111/epi.13901 (2017).

157 Greene, N. D. *et al.* Proteome changes associated with hippocampal MRI abnormalities in the lithium pilocarpine-induced model of convulsive status epilepticus. *Proteomics* **7**, 1336-1344, doi:10.1002/pmic.200601027 (2007).

158 Kirschstein, T. *et al.* The 27-kDa heat shock protein (HSP27) is a reliable hippocampal marker of full development of pilocarpine-induced status epilepticus. *Epilepsy research* **98**, 35-43, doi:10.1016/j.eplepsyres.2011.08.015 (2012).

159 Li, A. *et al.* Proteomic profiling of the epileptic dentate gyrus. *Brain Pathol* **20**, 1077-1089, doi:10.1111/j.1750-3639.2010.00414.x (2010).

160 Liu, X. Y. *et al.* Comparative proteomics and correlated signaling network of rat hippocampus in the pilocarpine model of temporal lobe epilepsy. *Proteomics* **8**, 582-603, doi:10.1002/pmic.200700514 (2008).

161 Marques-Carneiro, J. E. *et al.* Hippocampal Proteome of Rats Subjected to the Li-Pilocarpine Epilepsy Model and the Effect of Carisbamate Treatment. *Pharmaceuticals (Basel)* **10**, 67, doi:10.3390/ph10030067 (2017).

162 Sadeghi, L. *et al.* Hippocampal asymmetry: differences in the left and right hippocampus proteome in the rat model of temporal lobe epilepsy. *J Proteomics* **154**, 22-29, doi:10.1016/j.jprot.2016.11.023 (2017).

163 Wu, L. *et al.* Characterization, using comparative proteomics, of differentially expressed proteins in the hippocampus of the mesial temporal lobe of epileptic rats following treatment with valproate. *Amino Acids* **40**, 221-238, doi:10.1007/s00726-010-0638-8 (2011).

164 Wu, L., Zhang, C. & Yin, F. Dynamic changes in the proteomic profile of mesial temporal lobe epilepsy at different disease stages in an immature rat model. *Protein Pept Lett* **22**, 180-192, doi:10.2174/0929866521666141028214244 (2015).

165 Keck, M. *et al.* Proteomic profiling of epileptogenesis in a rat model: Focus on cell stress, extracellular matrix and angiogenesis. *Neurobiology of disease* **112**, 119-135, doi:10.1016/j.nbd.2018.01.013 (2018).

166 Keck, M. *et al.* A systems level analysis of epileptogenesis-associated proteome alterations. *Neurobiology of disease* **105**, 164-178, doi:10.1016/j.nbd.2017.05.017 (2017).

167 Bitsika, V. *et al.* High-Throughput LC-MS/MS Proteomic Analysis of a Mouse Model of Mesiotemporal Lobe Epilepsy Predicts Microglial Activation Underlying Disease Development. *J Proteome Res* **15**, 1546-1562, doi:10.1021/acs.jproteome.6b00003 (2016).

168 Canto, A. M. *et al.* Benchmarking the proteomic profile of animal models of mesial temporal epilepsy. *Ann Clin Transl Neurol* **9**, 454-467, doi:10.1002/acn3.51533 (2022).

169 Canto, A. M. *et al.* Multi-omics analysis suggests enhanced epileptogenesis in the Cornu Ammonis 3 of the pilocarpine model of mesial temporal lobe epilepsy. *Hippocampus* **31**, 122-139, doi:10.1002/hipo.23268 (2021).

170 Pernice, H. F., Schieweck, R., Kiebler, M. A. & Popper, B. mTOR and MAPK: from localized translation control to epilepsy. *BMC neuroscience* **17**, 73, doi:10.1186/s12868-016-0308-1 (2016).

171 Pitkanen, A. & Lukasiuk, K. Mechanisms of epileptogenesis and potential treatment targets. *The Lancet. Neurology* **10**, 173-186, doi:10.1016/S1474-4422(10)70310-0 (2011).

172 Arulsamy, A. & Shaikh, M. F. Tumor Necrosis Factor-alpha, the Pathological Key to Post-Traumatic Epilepsy: A Comprehensive Systematic Review. *ACS chemical neuroscience* **11**, 1900-1908, doi:10.1021/acschemneuro.0c00301 (2020).

173 Friedman, A. & Dingledine, R. Molecular cascades that mediate the influence of inflammation on epilepsy. *Epilepsia* **52 Suppl 3**, 33-39, doi:10.1111/j.1528-1167.2011.03034.x (2011).

174 Vezzani, A., Balosso, S. & Ravizza, T. Neuroinflammatory pathways as treatment targets and biomarkers in epilepsy. *Nat Rev Neurol* **15**, 459-472, doi:10.1038/s41582-019-0217-x (2019).

175 Lindskog, M. *et al.* Postsynaptic GluA1 enables acute retrograde enhancement of presynaptic function to coordinate adaptation to synaptic inactivity. *Proc Natl Acad Sci U S A* **107**, 21806-21811, doi:10.1073/pnas.1016399107 (2010).

176 Jakawich, S. K. *et al.* Local presynaptic activity gates homeostatic changes in presynaptic function driven by dendritic BDNF synthesis. *Neuron* **68**, 1143-1158, doi:10.1016/j.neuron.2010.11.034 (2010).

177 Lignani, G., Baldelli, P. & Marra, V. Homeostatic Plasticity in Epilepsy. *Frontiers in cellular neuroscience* **14**, 197, doi:10.3389/fncel.2020.00197 (2020).

178 Du, W. *et al.* Calcium-sensitive potassium channelopathy in human epilepsy and paroxysmal movement disorder. *Nature genetics* **37**, 733-738, doi:10.1038/ng1585 (2005).

179 Fath, T., Ke, Y. D., Gunning, P., Gotz, J. & Ittner, L. M. Primary support cultures of hippocampal and substantia nigra neurons. *Nat Protoc* **4**, 78-85, doi:10.1038/nprot.2008.199 (2009).

180 Wessel, D. & Flugge, U. I. A method for the quantitative recovery of protein in dilute solution in the presence of detergents and lipids. *Anal Biochem* **138**, 141-143, doi:10.1016/0003-2697(84)90782-6 (1984).

181 Farrah, T. *et al.* PASSEL: the PeptideAtlas SRMexperiment library. *Proteomics* **12**, 1170-1175, doi:10.1002/pmic.201100515 (2012).

182 Lange, V., Picotti, P., Domon, B. & Aebersold, R. Selected reaction monitoring for quantitative proteomics: a tutorial. *Molecular systems biology* **4**, 222, doi:10.1038/msb.2008.61 (2008).

183 Kim, H. J. *et al.* PhosR enables processing and functional analysis of phosphoproteomic data. *Cell reports* **34**, 108771, doi:10.1016/j.celrep.2021.108771 (2021).

184 Kim, H. J., Kim, T., Xiao, D. & Yang, P. Protocol for the processing and downstream analysis of phosphoproteomic data with PhosR. *STAR Protoc* **2**, 100585, doi:10.1016/j.xpro.2021.100585 (2021).

185 Tyanova, S., Temu, T. & Cox, J. The MaxQuant computational platform for mass spectrometry-based shotgun proteomics. *Nat Protoc* **11**, 2301-2319, doi:10.1038/nprot.2016.136 (2016).

186 Gagnon-Bartsch, J. A. & Speed, T. P. Using control genes to correct for unwanted variation in microarray data. *Biostatistics* **13**, 539-552, doi:10.1093/biostatistics/kxr034 (2012).

187 Molania, R., Gagnon-Bartsch, J. A., Dobrovic, A. & Speed, T. P. A new normalization for Nanostring nCounter gene expression data. *Nucleic Acids Res* **47**, 6073-6083, doi:10.1093/nar/gkz433 (2019).

188 Ritchie, M. E. *et al.* limma powers differential expression analyses for RNA-sequencing and microarray studies. *Nucleic Acids Res* **43**, e47, doi:10.1093/nar/gkv007 (2015).

189 Storey, J. D. A direct approach to false discovery rates. *Journal of the Royal Statistical Society: Series B (Statistical Methodology)* **64**, 479-498, doi:10.1111/1467-9868.00346 (2002).

190 Fisher, R. A. *Statistical methods for research workers*. (Springer, 1992).

191 Perez-Riverol, Y. *et al.* The PRIDE database resources in 2022: a hub for mass spectrometry-based proteomics evidences. *Nucleic Acids Res* **50**, D543-D552, doi:10.1093/nar/gkab1038 (2022).

192 Raudvere, U. *et al.* g:Profiler: a web server for functional enrichment analysis and conversions of gene lists (2019 update). *Nucleic Acids Res* **47**, W191-W198, doi:10.1093/nar/gkz369 (2019).

193 Reimand, J., Kull, M., Peterson, H., Hansen, J. & Vilo, J. g:Profiler--a web-based toolset for functional profiling of gene lists from large-scale experiments. *Nucleic Acids Res* **35**, W193-200, doi:10.1093/nar/gkm226 (2007).

194 Scharfman, H. E. Epilepsy as an example of neural plasticity. *Neuroscientist* **8**, 154-173, doi:10.1177/107385840200800211 (2002).

195 Jeans, A. F., van Heusden, F. C., Al-Mubarak, B., Padamsey, Z. & Emptage, N. J. Homeostatic Presynaptic Plasticity Is Specifically Regulated by P/Q-type Ca(2+) Channels at Mammalian Hippocampal Synapses. *Cell reports* **21**, 341-350, doi:10.1016/j.celrep.2017.09.061 (2017).

196 Trinka, E. *et al.* A definition and classification of status epilepticus--Report of the ILAE Task Force on Classification of Status Epilepticus. *Epilepsia* **56**, 1515-1523, doi:10.1111/epi.13121 (2015).

197 Guidelines for epidemiologic studies on epilepsy. Commission on Epidemiology and Prognosis, International League Against Epilepsy. *Epilepsia* **34**, 592-596, doi:10.1111/j.1528-1157.1993.tb00433.x (1993).

198 Shi, T. *et al.* Advances in targeted proteomics and applications to biomedical research. *Proteomics* **16**, 2160-2182, doi:10.1002/pmic.201500449 (2016).

199 van Bentum, M. & Selbach, M. An Introduction to Advanced Targeted Acquisition Methods. *Molecular & cellular proteomics : MCP* **20**, 100165, doi:10.1016/j.mcpro.2021.100165 (2021).

200 Schoch, S. *et al.* Ste20-like Kinase Is Critical for Inhibitory Synapse Maintenance and Its Deficiency Confers a Developmental Dendritopathy. *The Journal of neuroscience : the official journal of the Society for Neuroscience* **41**, 8111-8125, doi:10.1523/JNEUROSCI.0352-21.2021 (2021).

201 Becker, A. J. Review: Animal models of acquired epilepsy: insights into mechanisms of human epileptogenesis. *Neuropathol Appl Neurobiol* **44**, 112-129, doi:10.1111/nan.12451 (2018).

202 Shao, L. R. & Dudek, F. E. Changes in mIPSCs and sIPSCs after kainate treatment: evidence for loss of inhibitory input to dentate granule cells and possible compensatory responses. *Journal of neurophysiology* **94**, 952-960, doi:10.1152/jn.01342.2004 (2005).

203 Tauck, D. L. & Nadler, J. V. Evidence of functional mossy fiber sprouting in hippocampal formation of kainic acid-treated rats. *The Journal of neuroscience : the*

official journal of the Society for Neuroscience **5**, 1016-1022, doi:10.1523/JNEUROSCI.05-04-01016.1985 (1985).

204 Hendricks, W. D., Westbrook, G. L. & Schnell, E. Early detonation by sprouted mossy fibers enables aberrant dentate network activity. *Proc Natl Acad Sci U S A* **116**, 10994-10999, doi:10.1073/pnas.1821227116 (2019).

205 Qian, X. *et al.* Proteomic Analysis Reveals the Vital Role of Synaptic Plasticity in the Pathogenesis of Temporal Lobe Epilepsy. *Neural Plast* **2022**, 8511066, doi:10.1155/2022/8511066 (2022).

206 Xiao, W. *et al.* iTRAQ-Based Proteomic Analysis of Dentate Gyrus in Temporal Lobe Epilepsy With Hippocampal Sclerosis. *Frontiers in neurology* **11**, 626013, doi:10.3389/fneur.2020.626013 (2020).

207 Pires, G. *et al.* Proteomic differences in the hippocampus and cortex of epilepsy brain tissue. *Brain Commun* **3**, fcab021, doi:10.1093/braincomms/fcab021 (2021).

208 Okamoto, O. K. *et al.* Whole transcriptome analysis of the hippocampus: toward a molecular portrait of epileptogenesis. *BMC Genomics* **11**, 230, doi:10.1186/1471-2164-11-230 (2010).

209 Kalozoumi, G. *et al.* Glial responses during epileptogenesis in Mus musculus point to potential therapeutic targets. *PLoS One* **13**, e0201742, doi:10.1371/journal.pone.0201742 (2018).

210 Beaumont, T. L., Yao, B., Shah, A., Kapatos, G. & Loeb, J. A. Layer-specific CREB target gene induction in human neocortical epilepsy. *The Journal of neuroscience : the official journal of the Society for Neuroscience* **32**, 14389-14401, doi:10.1523/JNEUROSCI.3408-12.2012 (2012).

211 Dingledine, R. *et al.* Transcriptional profile of hippocampal dentate granule cells in four rat epilepsy models. *Scientific data* **4**, 170061, doi:10.1038/sdata.2017.61 (2017).

212 Hansen, K. F., Sakamoto, K., Pelz, C., Impey, S. & Obrietan, K. Profiling status epilepticus-induced changes in hippocampal RNA expression using high-throughput RNA sequencing. *Sci Rep* **4**, 6930, doi:10.1038/srep06930 (2014).

213 Lee, T. S. *et al.* Gene expression in the epileptic (EL) mouse hippocampus. *Neurobiology of disease* **147**, 105152, doi:10.1016/j.nbd.2020.105152 (2021).

214 Arion, D. *et al.* Correlation of transcriptome profile with electrical activity in temporal lobe epilepsy. *Neurobiology of disease* **22**, 374-387, doi:10.1016/j.nbd.2005.12.012 (2006).

215 Bungenberg, J. *et al.* Gene expression variance in hippocampal tissue of temporal lobe epilepsy patients corresponds to differential memory performance. *Neurobiology of disease* **86**, 121-130, doi:10.1016/j.nbd.2015.11.011 (2016).

216 Pitsch, J. *et al.* Functional role of mGluR1 and mGluR4 in pilocarpine-induced temporal lobe epilepsy. *Neurobiology of disease* **26**, 623-633, doi:10.1016/j.nbd.2007.03.003 (2007).

217 Pitsch, J. *et al.* The presynaptic active zone protein RIM1alpha controls epileptogenesis following status epilepticus. *The Journal of neuroscience : the official journal of the Society for Neuroscience* **32**, 12384-12395, doi:10.1523/JNEUROSCI.0223-12.2012 (2012).

218 Sheng, M. & Hoogenraad, C. C. The postsynaptic architecture of excitatory synapses: a more quantitative view. *Annu Rev Biochem* **76**, 823-847, doi:10.1146/annurev.biochem.76.060805.160029 (2007).

219 Schieweck, R., Ninkovic, J. & Kiebler, M. A. RNA-binding proteins balance brain function in health and disease. *Physiological reviews* **101**, 1309-1370, doi:10.1152/physrev.00047.2019 (2021).

220 Hornbeck, P. V. *et al.* PhosphoSitePlus, 2014: mutations, PTMs and recalibrations. *Nucleic Acids Res* **43**, D512-520, doi:10.1093/nar/gku1267 (2015).

221 Zhang, B. *et al.* Integrated systems approach identifies genetic nodes and networks in late-onset Alzheimer's disease. *Cell* **153**, 707-720, doi:10.1016/j.cell.2013.03.030 (2013).

222 Schubert, S. *et al.* beta2-Syntrophin is a Cdk5 substrate that restrains the motility of insulin secretory granules. *PLoS One* **5**, e12929, doi:10.1371/journal.pone.0012929 (2010).

223 Turrigiano, G. G. & Nelson, S. B. Homeostatic plasticity in the developing nervous system. *Nature reviews. Neuroscience* **5**, 97-107, doi:10.1038/nrn1327 (2004).

224 Postnikova, T. Y. *et al.* Impairments of Long-Term Synaptic Plasticity in the Hippocampus of Young Rats during the Latent Phase of the Lithium-Pilocarpine Model of Temporal Lobe Epilepsy. *International journal of molecular sciences* **22**, 13355, doi:10.3390/ijms222413355 (2021).

225 Kryukov, K. A., Kim, K. K., Magazanik, L. G. & Zaitsev, A. V. Status epilepticus alters hippocampal long-term synaptic potentiation in a rat lithium-pilocarpine model. *Neuroreport* **27**, 1191-1195, doi:10.1097/WNR.0000000000000656 (2016).

226 Shavit-Stein, E. *et al.* Modulation of the Thrombin Pathway Restores LTP in a Pilocarpine Mice Model of Status Epilepticus. *Frontiers in cellular neuroscience* **16**, 900925, doi:10.3389/fncel.2022.900925 (2022).

227 Mulkey, R. M., Endo, S., Shenolikar, S. & Malenka, R. C. Involvement of a calcineurin/inhibitor-1 phosphatase cascade in hippocampal long-term depression. *Nature* **369**, 486-488, doi:10.1038/369486a0 (1994).

228 Guo, W., Ceolin, L., Collins, K. A., Perroy, J. & Huber, K. M. Elevated CaMKIIalpha and Hyperphosphorylation of Homer Mediate Circuit Dysfunction in a Fragile X Syndrome Mouse Model. *Cell reports* **13**, 2297-2311, doi:10.1016/j.celrep.2015.11.013 (2015).

229 Quintana, A. R., Wang, D., Forbes, J. E. & Waxham, M. N. Kinetics of calmodulin binding to calcineurin. *Biochemical and biophysical research communications* **334**, 674-680, doi:10.1016/j.bbrc.2005.06.152 (2005).

230 Hashimoto, Y., King, M. M. & Soderling, T. R. Regulatory interactions of calmodulin-binding proteins: phosphorylation of calcineurin by autophosphorylated Ca2+/calmodulin-dependent protein kinase II. *Proc Natl Acad Sci U S A* **85**, 7001-7005, doi:10.1073/pnas.85.18.7001 (1988).

231 Hashimoto, Y. & Soderling, T. R. Regulation of calcineurin by phosphorylation. Identification of the regulatory site phosphorylated by Ca2+/calmodulin-dependent protein kinase II and protein kinase C. *The Journal of biological chemistry* **264**, 16524-16529 (1989).

232 Park, K. S., Mohapatra, D. P., Misonou, H. & Trimmer, J. S. Graded regulation of the Kv2.1 potassium channel by variable phosphorylation. *Science* **313**, 976-979, doi:10.1126/science.1124254 (2006).

233 Sanderson, J. L., Gorski, J. A. & Dell'Acqua, M. L. NMDA Receptor-Dependent LTD Requires Transient Synaptic Incorporation of Ca(2)(+)-Permeable AMPARs Mediated by AKAP150-Anchored PKA and Calcineurin. *Neuron* **89**, 1000-1015, doi:10.1016/j.neuron.2016.01.043 (2016).

234 Tomita, S., Stein, V., Stocker, T. J., Nicoll, R. A. & Bredt, D. S. Bidirectional synaptic plasticity regulated by phosphorylation of stargazin-like TARPs. *Neuron* **45**, 269-277, doi:10.1016/j.neuron.2005.01.009 (2005).

235 Lai, K. O. *et al.* TrkB phosphorylation by Cdk5 is required for activity-dependent structural plasticity and spatial memory. *Nature neuroscience* **15**, 1506-1515, doi:10.1038/nn.3237 (2012).

236 McCamphill, P. K., Farah, C. A., Anadolu, M. N., Hoque, S. & Sossin, W. S. Bidirectional regulation of eEF2 phosphorylation controls synaptic plasticity by decoding neuronal activity patterns. *The Journal of neuroscience : the official journal of the Society for Neuroscience* **35**, 4403-4417, doi:10.1523/JNEUROSCI.2376-14.2015 (2015).

237 Shin, S. M. *et al.* GKAP orchestrates activity-dependent postsynaptic protein remodeling and homeostatic scaling. *Nature neuroscience* **15**, 1655-1666, doi:10.1038/nn.3259 (2012).

238 Rasmussen, A. H., Rasmussen, H. B. & Silahtaroglu, A. The DLGAP family: neuronal expression, function and role in brain disorders. *Mol Brain* **10**, 43, doi:10.1186/s13041-017-0324-9 (2017).

239 Lee, K. J. *et al.* Requirement for Plk2 in orchestrated ras and rap signaling, homeostatic structural plasticity, and memory. *Neuron* **69**, 957-973, doi:10.1016/j.neuron.2011.02.004 (2011).

240 Fu, A. K. *et al.* APC(Cdh1) mediates EphA4-dependent downregulation of AMPA receptors in homeostatic plasticity. *Nature neuroscience* **14**, 181-189, doi:10.1038/nn.2715 (2011).

241 Eom, T. *et al.* NOVA-dependent regulation of cryptic NMD exons controls synaptic protein levels after seizure. *eLife* **2**, e00178, doi:10.7554/eLife.00178 (2013).

242 Lin, Y. C. & Koleske, A. J. Mechanisms of synapse and dendrite maintenance and their disruption in psychiatric and neurodegenerative disorders. *Annual review of neuroscience* **33**, 349-378, doi:10.1146/annurev-neuro-060909-153204 (2010).

243 Wang, L., Liu, Y. H., Huang, Y. G. & Chen, L. W. Time-course of neuronal death in the mouse pilocarpine model of chronic epilepsy using Fluoro-Jade C staining. *Brain research* **1241**, 157-167, doi:10.1016/j.brainres.2008.07.097 (2008).

244 Kurz, J. E., Moore, B. J., Henderson, S. C., Campbell, J. N. & Churn, S. B. A cellular mechanism for dendritic spine loss in the pilocarpine model of status epilepticus. *Epilepsia* **49**, 1696-1710, doi:10.1111/j.1528-1167.2008.01616.x (2008).

245 Monteiro, P. & Feng, G. SHANK proteins: roles at the synapse and in autism spectrum disorder. *Nature reviews. Neuroscience* **18**, 147-157, doi:10.1038/nrn.2016.183 (2017).

246 Freire-Cobo, C., Sierra-Paredes, G., Freire, M. & Sierra-Marcuno, G. The calcineurin inhibitor Ascomicin interferes with the early stage of the epileptogenic process induced by Latrunculin A microperfusion in rat hippocampus. *J Neuroimmune Pharmacol* **9**, 654-667, doi:10.1007/s11481-014-9558-9 (2014).

247 Lively, S. & Brown, I. R. The extracellular matrix protein SC1/hevin localizes to excitatory synapses following status epilepticus in the rat lithium-pilocarpine seizure model. *Journal of neuroscience research* **86**, 2895-2905, doi:10.1002/jnr.21735 (2008).

248 Arstikaitis, P. *et al.* Paralemmin-1, a modulator of filopodia induction is required for spine maturation. *Mol Biol Cell* **19**, 2026-2038, doi:10.1091/mbc.e07-08-0802 (2008).

249 Yap, E. L. & Greenberg, M. E. Activity-Regulated Transcription: Bridging the Gap between Neural Activity and Behavior. *Neuron* **100**, 330-348, doi:10.1016/j.neuron.2018.10.013 (2018).

250 Pitkanen, A. *et al.* Gender issues in antiepileptogenic treatments. *Neurobiology of disease* **72 Pt B**, 224-232, doi:10.1016/j.nbd.2014.05.037 (2014).

251 Mauger, O. & Scheiffele, P. Beyond proteome diversity: alternative splicing as a regulator of neuronal transcript dynamics. *Current opinion in neurobiology* **45**, 162-168, doi:10.1016/j.conb.2017.05.012 (2017).

252 Siemen, H., Colas, D., Heller, H. C., Brustle, O. & Pera, R. A. Pumilio-2 function in the mouse nervous system. *PLoS One* **6**, e25932, doi:10.1371/journal.pone.0025932 (2011).

253 Gonatopoulos-Pournatzis, T. *et al.* Autism-Misregulated eIF4G Microexons Control Synaptic Translation and Higher Order Cognitive Functions. *Molecular cell* **77**, 1176-1192 e1116, doi:10.1016/j.molcel.2020.01.006 (2020).

254 Engel, T. *et al.* Spatiotemporal progression of ubiquitin-proteasome system inhibition after status epilepticus suggests protective adaptation against hippocampal injury. *Mol Neurodegener* **12**, 21, doi:10.1186/s13024-017-0163-2 (2017).

255 Lee, S. H., Park, Y., Yoon, S. K. & Yoon, J. B. Osmotic stress inhibits proteasome by p38 MAPK-dependent phosphorylation. *The Journal of biological chemistry* **285**, 41280-41289, doi:10.1074/jbc.M110.182188 (2010).

256 Naujokat, C. & Hoffmann, S. Role and function of the 26S proteasome in proliferation and apoptosis. *Lab Invest* **82**, 965-980, doi:10.1097/01.lab.0000022226.23741.37 (2002).

257 Govek, E. E., Newey, S. E. & Van Aelst, L. The role of the Rho GTPases in neuronal development. *Genes Dev* **19**, 1-49, doi:10.1101/gad.1256405 (2005).

258 Lee, H. K., Takamiya, K., He, K., Song, L. & Huganir, R. L. Specific roles of AMPA receptor subunit GluR1 (GluA1) phosphorylation sites in regulating synaptic plasticity in the CA1 region of hippocampus. *Journal of neurophysiology* **103**, 479-489, doi:10.1152/jn.00835.2009 (2010).

259 Lee, K. J. *et al.* Mossy fiber-CA3 synapses mediate homeostatic plasticity in mature hippocampal neurons. *Neuron* **77**, 99-114, doi:10.1016/j.neuron.2012.10.033 (2013).

260 Bridi, M. C. D. *et al.* Two distinct mechanisms for experience-dependent homeostasis. *Nature neuroscience* **21**, 843-850, doi:10.1038/s41593-018-0150-0 (2018).

261 Bolstad, B. M., Irizarry, R. A., Astrand, M. & Speed, T. P. A comparison of normalization methods for high density oligonucleotide array data based on variance and bias. *Bioinformatics* **19**, 185-193, doi:10.1093/bioinformatics/19.2.185 (2003).

262 Troyanskaya, O. *et al.* Missing value estimation methods for DNA microarrays. *Bioinformatics* **17**, 520-525, doi:10.1093/bioinformatics/17.6.520 (2001).

263 Leek, J. T., Johnson, W. E., Parker, H. S., Jaffe, A. E. & Storey, J. D. The sva package for removing batch effects and other unwanted variation in high-throughput experiments. *Bioinformatics* **28**, 882-883, doi:10.1093/bioinformatics/bts034 (2012).

264 Coombes, K. R. *et al.* Quality control and peak finding for proteomics data collected from nipple aspirate fluid by surface-enhanced laser desorption and ionization. *Clinical chemistry* **49**, 1615-1623, doi:10.1373/49.10.1615 (2003).

265 Benjamini, Y. & Hochberg, Y. Controlling the False Discovery Rate - a Practical and Powerful Approach to Multiple Testing. *Journal of the Royal Statistical Society Series B-Statistical Methodology* **57**, 289-300, doi:DOI 10.1111/j.2517-6161.1995.tb02031.x (1995).

266 Supek, F., Bosnjak, M., Skunca, N. & Smuc, T. REVIGO summarizes and visualizes long lists of gene ontology terms. *PLoS One* **6**, e21800, doi:10.1371/journal.pone.0021800 (2011).

267 Royero, P. *et al.* Circuit-selective cell-autonomous regulation of inhibition in pyramidal neurons by Ste20-like kinase. *Cell reports* **41**, 111757, doi:10.1016/j.celrep.2022.111757 (2022).

268 Luhovy, A. Y., Jaberi, A., Papillon, J., Guillemette, J. & Cybulsky, A. V. Regulation of the Ste20-like kinase, SLK: involvement of activation segment phosphorylation. *The Journal of biological chemistry* **287**, 5446-5458, doi:10.1074/jbc.M111.302018 (2012).

269 Cybulsky, A. V., Guillemette, J., Papillon, J. & Abouelazm, N. T. Regulation of Ste20-like kinase, SLK, activity: Dimerization and activation segment phosphorylation. *PLoS One* **12**, e0177226, doi:10.1371/journal.pone.0177226 (2017).

270 Chaar, Z., O'Reilly, P., Gelman, I. & Sabourin, L. A. v-Src-dependent down-regulation of the Ste20-like kinase SLK by casein kinase II. *The Journal of biological chemistry* **281**, 28193-28199, doi:10.1074/jbc.M605665200 (2006).

271 Hogrebe, A. *et al.* Benchmarking common quantification strategies for large-scale phosphoproteomics. *Nature communications* **9**, 1045, doi:10.1038/s41467-018-03309-6 (2018).

272 Savitski, M. M. *et al.* Measuring and managing ratio compression for accurate iTRAQ/TMT quantification. *J Proteome Res* **12**, 3586-3598, doi:10.1021/pr400098r (2013).

273 Ting, L., Rad, R., Gygi, S. P. & Haas, W. MS3 eliminates ratio distortion in isobaric multiplexed quantitative proteomics. *Nat Methods* **8**, 937-940, doi:10.1038/nmeth.1714 (2011).

274 Wang, A., Chi, Z., Wang, S., Wang, S. & Sun, Q. Calcineurin-mediated GABA(A) receptor dephosphorylation in rats after kainic acid-induced status epilepticus. *Seizure* **18**, 519-523, doi:10.1016/j.seizure.2009.05.001 (2009).

275 Moloney, P. B., Cavalleri, G. L. & Delanty, N. Epilepsy in the mTORopathies: opportunities for precision medicine. *Brain Commun* **3**, fcab222, doi:10.1093/braincomms/fcab222 (2021).

276 Hoeffer, C. A. & Klann, E. mTOR signaling: at the crossroads of plasticity, memory and disease. *Trends Neurosci* **33**, 67-75, doi:10.1016/j.tins.2009.11.003 (2010).

277 Henry, F. E., Hockeimer, W., Chen, A., Mysore, S. P. & Sutton, M. A. Mechanistic target of rapamycin is necessary for changes in dendritic spine morphology associated with long-term potentiation. *Mol Brain* **10**, 50, doi:10.1186/s13041-017-0330-y (2017).

278 Zhu, P. J., Chen, C. J., Mays, J., Stoica, L. & Costa-Mattioli, M. mTORC2, but not mTORC1, is required for hippocampal mGluR-LTD and associated behaviors. *Nature neuroscience* **21**, 799-802, doi:10.1038/s41593-018-0156-7 (2018).

279 Nguyen, L. H., Mahadeo, T. & Bordey, A. mTOR Hyperactivity Levels Influence the Severity of Epilepsy and Associated Neuropathology in an Experimental Model of Tuberous Sclerosis Complex and Focal Cortical Dysplasia. *The Journal of neuroscience : the official journal of the Society for Neuroscience* **39**, 2762-2773, doi:10.1523/JNEUROSCI.2260-18.2019 (2019).

280 Huang, X. *et al.* Pharmacological inhibition of the mammalian target of rapamycin pathway suppresses acquired epilepsy. *Neurobiology of disease* **40**, 193-199, doi:10.1016/j.nbd.2010.05.024 (2010).

281 Zhao, W. *et al.* Advances in the mTOR signaling pathway and its inhibitor rapamycin in epilepsy. *Brain Behav* **13**, e2995, doi:10.1002/brb3.2995 (2023).

282 Zeng, L. H., Xu, L., Gutmann, D. H. & Wong, M. Rapamycin prevents epilepsy in a mouse model of tuberous sclerosis complex. *Ann Neurol* **63**, 444-453, doi:10.1002/ana.21331 (2008).

283 Buckmaster, P. S. & Lew, F. H. Rapamycin suppresses mossy fiber sprouting but not seizure frequency in a mouse model of temporal lobe epilepsy. *The Journal of neuroscience : the official journal of the Society for Neuroscience* **31**, 2337-2347, doi:10.1523/JNEUROSCI.4852-10.2011 (2011).

284 Yang, M. T., Lin, Y. C., Ho, W. H., Liu, C. L. & Lee, W. T. Everolimus is better than rapamycin in attenuating neuroinflammation in kainic acid-induced seizures. *J Neuroinflammation* **14**, 15, doi:10.1186/s12974-017-0797-6 (2017).

285 Miccoli, B. *et al.* High-Density Electrical Recording and Impedance Imaging With a Multi-Modal CMOS Multi-Electrode Array Chip. *Frontiers in neuroscience* **13**, 641, doi:10.3389/fnins.2019.00641 (2019).

286 Robinette, B. L., Harrill, J. A., Mundy, W. R. & Shafer, T. J. In vitro assessment of developmental neurotoxicity: use of microelectrode arrays to measure functional changes in neuronal network ontogeny. *Frontiers in neuroengineering* **4**, 1, doi:10.3389/fneng.2011.00001 (2011).

287 Bradley, J. A., Luithardt, H. H., Metea, M. R. & Strock, C. J. In Vitro Screening for Seizure Liability Using Microelectrode Array Technology. *Toxicol Sci* **163**, 240-253, doi:10.1093/toxsci/kfy029 (2018).

288 Kurdi, A. *et al.* Continuous administration of the mTORC1 inhibitor everolimus induces tolerance and decreases autophagy in mice. *Br J Pharmacol* **173**, 3359-3371, doi:10.1111/bph.13626 (2016).

289 Bateup, H. S., Denefrio, C. L., Johnson, C. A., Saulnier, J. L. & Sabatini, B. L. Temporal dynamics of a homeostatic pathway controlling neural network activity. *Frontiers in molecular neuroscience* **6**, 28, doi:10.3389/fnmol.2013.00028 (2013).

290 Nelson, S. B. & Valakh, V. Excitatory/Inhibitory Balance and Circuit Homeostasis in Autism Spectrum Disorders. *Neuron* **87**, 684-698, doi:10.1016/j.neuron.2015.07.033 (2015).

291 Gideons, E. S., Kavalali, E. T. & Monteggia, L. M. Mechanisms underlying differential effectiveness of memantine and ketamine in rapid antidepressant responses. *Proc Natl Acad Sci U S A* **111**, 8649-8654, doi:10.1073/pnas.1323920111 (2014).

292 Gideons, E. S., Lin, P. Y., Mahgoub, M., Kavalali, E. T. & Monteggia, L. M. Chronic lithium treatment elicits its antimanic effects via BDNF-TrkB dependent synaptic downscaling. *eLife* **6**, doi:10.7554/eLife.25480 (2017).

293 Lin, P. Y., Ma, Z. Z., Mahgoub, M., Kavalali, E. T. & Monteggia, L. M. A synaptic locus for TrkB signaling underlying ketamine rapid antidepressant action. *Cell reports* **36**, 109513, doi:10.1016/j.celrep.2021.109513 (2021).

294 Wiredja, D. D., Koyuturk, M. & Chance, M. R. The KSEA App: a web-based tool for kinase activity inference from quantitative phosphoproteomics. *Bioinformatics* **33**, 3489-3491, doi:10.1093/bioinformatics/btx415 (2017).

295 Huntley, R. P. *et al.* The GOA database: gene Ontology annotation updates for 2015. *Nucleic Acids Res* **43**, D1057-1063, doi:10.1093/nar/gku1113 (2015).

296 Domingo-Fernandez, D., Hoyt, C. T., Bobis-Alvarez, C., Marin-Llao, J. & Hofmann-Apitius, M. ComPath: an ecosystem for exploring, analyzing, and curating mappings across pathway databases. *NPJ systems biology and applications* **5**, 3, doi:10.1038/s41540-018-0078-8 (2019).

297 Dai, J., Aoto, J. & Sudhof, T. C. Alternative Splicing of Presynaptic Neurexins Differentially Controls Postsynaptic NMDA and AMPA Receptor Responses. *Neuron* **102**, 993-1008 e1005, doi:10.1016/j.neuron.2019.03.032 (2019).

298 Lim, Y. W., James, D., Huang, J. & Lee, M. The Emerging Role of the RNA-Binding Protein SFPQ in Neuronal Function and Neurodegeneration. *International journal of molecular sciences* **21**, 7151, doi:10.3390/ijms21197151 (2020).

299 Udagawa, T. *et al.* FUS regulates AMPA receptor function and FTLD/ALS-associated behaviour via GluA1 mRNA stabilization. *Nature communications* **6**, 7098, doi:10.1038/ncomms8098 (2015).

300 Yokoi, S. *et al.* 3'UTR Length-Dependent Control of SynGAP Isoform alpha2 mRNA by FUS and ELAV-like Proteins Promotes Dendritic Spine Maturation and Cognitive Function. *Cell reports* **20**, 3071-3084, doi:10.1016/j.celrep.2017.08.100 (2017).

301 Shahbazian, D. *et al.* The mTOR/PI3K and MAPK pathways converge on eIF4B to control its phosphorylation and activity. *EMBO J* **25**, 2781-2791, doi:10.1038/sj.emboj.7601166 (2006).

302 Tolias, K. F., Duman, J. G. & Um, K. Control of synapse development and plasticity by Rho GTPase regulatory proteins. *Progress in neurobiology* **94**, 133-148, doi:10.1016/j.pneurobio.2011.04.011 (2011).

303 Um, K. *et al.* Dynamic control of excitatory synapse development by a Rac1 GEF/GAP regulatory complex. *Developmental cell* **29**, 701-715, doi:10.1016/j.devcel.2014.05.011 (2014).

304 Muller, J. A. *et al.* A presynaptic phosphosignaling hub for lasting homeostatic plasticity. *Cell reports* **39**, 110696, doi:10.1016/j.celrep.2022.110696 (2022).

305 Emperador-Melero, J. *et al.* PKC-phosphorylation of Liprin-alpha3 triggers phase separation and controls presynaptic active zone structure. *Nature communications* **12**, 3057, doi:10.1038/s41467-021-23116-w (2021).

306 Held, R. G., Liu, C. & Kaeser, P. S. ELKS controls the pool of readily releasable vesicles at excitatory synapses through its N-terminal coiled-coil domains. *eLife* **5**, doi:10.7554/eLife.14862 (2016).

307 Stryker, E. & Johnson, K. G. LAR, liprin alpha and the regulation of active zone morphogenesis. *Journal of cell science* **120**, 3723-3728, doi:10.1242/jcs.03491 (2007).

308 Worth, D. C., Daly, C. N., Geraldo, S., Oozeer, F. & Gordon-Weeks, P. R. Drebrin contains a cryptic F-actin-bundling activity regulated by Cdk5 phosphorylation. *The Journal of cell biology* **202**, 793-806, doi:10.1083/jcb.201303005 (2013).

309 Sweatt, J. D. Mitogen-activated protein kinases in synaptic plasticity and memory. *Current opinion in neurobiology* **14**, 311-317, doi:10.1016/j.conb.2004.04.001 (2004).

310 Coffey, E. T. Nuclear and cytosolic JNK signalling in neurons. *Nature reviews. Neuroscience* **15**, 285-299, doi:10.1038/nrn3729 (2014).

311 Biever, A., Valjent, E. & Puighermanal, E. Ribosomal Protein S6 Phosphorylation in the Nervous System: From Regulation to Function. *Frontiers in molecular neuroscience* **8**, 75, doi:10.3389/fnmol.2015.00075 (2015).

312 Romeo, Y., Zhang, X. & Roux, P. P. Regulation and function of the RSK family of protein kinases. *The Biochemical journal* **441**, 553-569, doi:10.1042/BJ20110289 (2012).

313 McAlister, G. C. *et al.* MultiNotch MS3 enables accurate, sensitive, and multiplexed detection of differential expression across cancer cell line proteomes. *Anal Chem* **86**, 7150-7158, doi:10.1021/ac502040v (2014).

314 Shamir, M., Bar-On, Y., Phillips, R. & Milo, R. SnapShot: Timescales in Cell Biology. *Cell* **164**, 1302-1302 e1301, doi:10.1016/j.cell.2016.02.058 (2016).

315 Kim, S. & Ziff, E. B. Calcineurin mediates synaptic scaling via synaptic trafficking of Ca2+-permeable AMPA receptors. *PLoS biology* **12**, e1001900, doi:10.1371/journal.pbio.1001900 (2014).

316 Winder, D. G. & Sweatt, J. D. Roles of serine/threonine phosphatases in hippocampal synaptic plasticity. *Nature reviews. Neuroscience* **2**, 461-474, doi:10.1038/35081514 (2001).

317 Lisman, J. A mechanism for the Hebb and the anti-Hebb processes underlying learning and memory. *Proc Natl Acad Sci U S A* **86**, 9574-9578, doi:10.1073/pnas.86.23.9574 (1989).

318 Siddoway, B., Hou, H. & Xia, H. Molecular mechanisms of homeostatic synaptic downscaling. *Neuropharmacology* **78**, 38-44, doi:10.1016/j.neuropharm.2013.07.009 (2014).

319 Raveendran, R. *et al.* Phosphorylation status of the NR2B subunit of NMDA receptor regulates its interaction with calcium/calmodulin-dependent protein kinase II. *J Neurochem* **110**, 92-105, doi:10.1111/j.1471-4159.2009.06108.x (2009).

320 Prabhu Ramya, R., Suma Priya, S., Mayadevi, M. & Omkumar, R. V. Regulation of phosphorylation at Ser(1303) of GluN2B receptor in the postsynaptic density. *Neurochem Int* **61**, 981-985, doi:10.1016/j.neuint.2012.08.016 (2012).

321 Bausen, M., Weltzien, F., Betz, H. & O'Sullivan, G. A. Regulation of postsynaptic gephyrin cluster size by protein phosphatase 1. *Molecular and cellular neurosciences* **44**, 201-209, doi:10.1016/j.mcn.2010.02.007 (2010).

322 Zita, M. M. *et al.* Post-phosphorylation prolyl isomerisation of gephyrin represents a mechanism to modulate glycine receptors function. *EMBO J* **26**, 1761-1771, doi:10.1038/sj.emboj.7601625 (2007).

323 Louros, S. R., Caldeira, G. L. & Carvalho, A. L. Stargazin Dephosphorylation Mediates Homeostatic Synaptic Downscaling of Excitatory Synapses. *Frontiers in molecular neuroscience* **11**, 328, doi:10.3389/fnmol.2018.00328 (2018).

324 Tavalin, S. J. & Colbran, R. J. CaMKII-mediated phosphorylation of GluN2B regulates recombinant NMDA receptor currents in a chloride-dependent manner. *Molecular and cellular neurosciences* **79**, 45-52, doi:10.1016/j.mcn.2016.12.002 (2017).

325 Yasuda, R., Hayashi, Y. & Hell, J. W. CaMKII: a central molecular organizer of synaptic plasticity, learning and memory. *Nature reviews. Neuroscience* **23**, 666-682, doi:10.1038/s41583-022-00624-2 (2022).

326 Goetze, B. *et al.* The brain-specific double-stranded RNA-binding protein Staufen2 is required for dendritic spine morphogenesis. *The Journal of cell biology* **172**, 221-231, doi:10.1083/jcb.200509035 (2006).

327 Sawicka, K., Pyronneau, A., Chao, M., Bennett, M. V. & Zukin, R. S. Elevated ERK/p90 ribosomal S6 kinase activity underlies audiogenic seizure susceptibility in fragile X mice. *Proc Natl Acad Sci U S A* **113**, E6290-E6297, doi:10.1073/pnas.1610812113 (2016).

328 Louros, S. R. *et al.* Excessive proteostasis contributes to pathology in fragile X syndrome. *Neuron* **111**, 508-525 e507, doi:10.1016/j.neuron.2022.11.012 (2023).